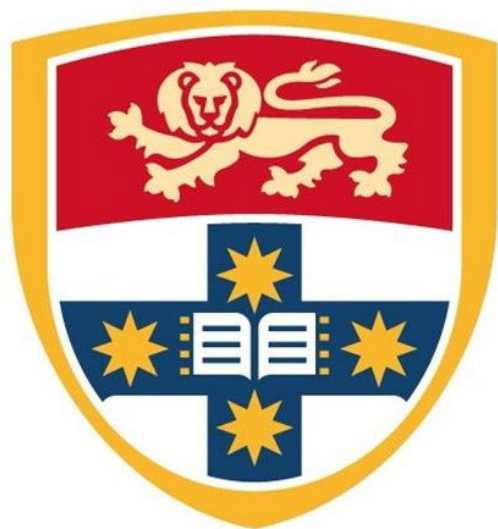# The role of LDL-cholesterol and annexin A6 for cancer cell growth and progression

Mohamed Wahba
School of Pharmacy
Faculty of Medicine and Health
The University of Sydney

A thesis submitted to fulfil requirements for the degree of Doctor of Philosophy

28th June 2023

Table of Contents

5

Abstract

The increased demand for cholesterol to support cancer growth and progression is often associated with elevated uptake of cholesterol from low density lipoproteins (LDL). Once endocytosed, LDL-cholesterol then needs to be delivered from late endosomes/lysosomes (LE/Lys) to other cellular sites to promote proliferation and metastatic behaviour. Yet, in oncogenic settings, the cholesterol transporters and molecular machinery in LE/Lys that endorse this process are not fully understood.

In Chapter 1, the impact of inhibiting late endosomal cholesterol export on aggressive cancer cell behaviour was addressed. Therefore, we depleted the major cholesterol transporter in LE/Lys (Niemann Pick Type C1, NPC1) with stable siRNA-mediated gene knockdown in human A431 squamous epithelial cells, a well-established cancer model with metastatic features. The NPC1-depleted A431 cell line displayed strong cholesterol accumulation in LE/Lys similar to recognized NPC1 mutant cell lines and were suitable for experiments assessing motility and invasive behaviour. Indeed, cholesterol accumulation in NPC1-depleted A431 cells correlated with significantly reduced cell migration in wound healing assays. Moreover, after tail vein injection, the number of tumors in the lung derived from NPC1-depleted A431 cells were strongly reduced, suggesting that inability to distribute late endosomal cholesterol interferes with the invasive potential of A431 cells *in vivo*.

In Chapter 2, we collated expression patterns and overall patient survival data on the scaffold protein ANXA6 in cancers linked to de-regulated cholesterol homeostasis or increased responsiveness to oversupply with dietary cholesterol. The Grewal group extensively studied this protein, which is a potential tumor suppressor that upon upregulation, induces an NPC1-mutant like phenotype that is associated with reduced growth, migration, and invasion. In contrast, ANXA6 depletion improved cholesterol export from LE/Lys to focal adhesions and lipid droplets to promote cancer cell growth and motility independent of NPC1, requiring RAB7 activation and another cholesterol transporter in LE/Lys, STARD3. In prostate cancer, a significant downregulation of ANXA6 expression during the progression from localized to metastatic prostate cancer was observed. Furthermore, low ANXA6 levels were associated with reduced overall survival in triple-negative breast cancers as well as pancreatic cancers. These findings may indicate

an improved ability of cancers with low ANXA6 levels to effectively utilize incoming cholesterol for growth and progression advantage.

In Chapters 3 and 4, we aimed to identify ANXA6-related gene network associations in cholesterol-sensitive cancers by co-analyzing the expression patterns of ANXA6 in combination with genes from its interactome in LE/Lys, consisting of LDL receptor (LDLR), cholesterol transporters (NPC1, STARD3) and regulatory proteins (RAB7A, TBC1D5, TBC1D15). A negative association between ANXA6 and LDLR, NPC1 and RAB7 was made in several cancers, in particular ER-negative and triple-negative breast cancer, but also several prostate and colon cancer cohorts, which point at improved LDL-cholesterol utilization when ANXA6 levels are low, and relevant for cancer aggressiveness, progression and treatment outcome. On the other hand, ANXA6 and STARD3 levels were positively associated in most cancer cohorts, including breast, prostate, colon, pancreas, and liver, indicating that ANXA6 is indeed a gatekeeper that limits the involvement of STARD3 in cholesterol export from LE/Lys, as proposed by Grewal and colleagues in recent studies.

In Chapter 4, we observed low ANXA6 levels to strongly reduce the survival probability in patients with high LDLR or high RAB7 or high STARD3 levels. Although sample numbers were low, this supports ANXA6 downregulation to improve LDL-cholesterol distribution via RAB7- and STARD3-dependent cholesterol routes in breast cancer subgroups, which are ER-negative and/or EGFR-related (triple-negative). On the other hand, high ANXA6 levels were associated with longer patient survival probability in breast cancer samples with high/low LDLR and NPC1, high STARD3, RAB7, TBC1D5 and TBC1D15, suggesting elevated ANXA6 levels to counteract efficient LDL-cholesterol distribution in these breast cancers. In several metastatic prostate cancers, reduced ANXA6 levels coincided with high RAB7A levels, which may indicate ANXA6-related gene networks that allow competent utilization of LDL-derived cholesterol in order to gain growth and progression advantages. The results from other cancer cohorts (liver, pancreas, colon) are also described and discussed in detail.

Authorship attribution statement

All of Chapter1 and section from Chapter 2-4 of this thesis has been published as referenced below. I contributed to the design, conducted, and analysed experiments and along with the co-authors, took part in the preparation of figures and writing of both manuscripts.

Jose J, Hoque M, Engel J, Beevi SS, **Wahba M**, Georgieva MI, Murphy KJ, Hughes WE, Cochran BJ, Lu A, Tebar F, Hoy AJ, Timpson P, Rye KA, Enrich C, Rentero C, Grewal T. Annexin A6 and NPC1 regulate LDL-inducible cell migration and distribution of focal adhesions. Sci Rep. 2022 Jan 12;12(1):596. doi: 10.1038/s41598-021-04584-y. PMID: 35022465

Nguyen MKL, Jose J, **Wahba M**, Bernaus-Esqué M. Hoy AJ, Enrich C, Rentero C, Grewal T. Linking late endosomal cholesterol with cancer progression and anticancer drug resistance. Int J Mol Sci. 2022 Jun 29;23(13):7206. doi: 10.3390/ijms23137206. PMID: 35806209

Grewal T, Hoque M, Conway JRW, Reverter M, **Wahba M**, Beevi SS, Timpson P, Enrich C, Rentero C. Annexin A6-A multifunctional scaffold in cell motility. Cell Adh Migr. 2017 May 4;11(3):288-304. doi: 10.1080/19336918.2016.1268318. PMID: 28060548

In addition to the statement above, in cases where I am not the corresponding author of a published item, permission to include the published material has been granted by the corresponding author.

Mohamed Wahba

28/06/2022

As supervisor for the candidature upon which this thesis is based, I can confirm that the authorship attribution statements above are correct.

Thomas Grewal

 28/06/2022

Statement of originality

I certify that to the best of my knowledge, the content of this thesis is my own work, unless otherwise specified. All assistances provided for the completion of this thesis and other sources have been referenced appropriately. This thesis has not been submitted in whole or in part for any degree or other purposes in this, or any other University.

Mohamed Wahba

June 2022

Published works by the author that are relevant and forms part of this thesis

Chapters 1-4

Jose J, Hoque M, Engel J, Beevi SS, **Wahba M**, Georgieva MI, Murphy KJ, Hughes WE, Cochran BJ, Lu A, Tebar F, Hoy AJ, Timpson P, Rye KA, Enrich C, Rentero C, Grewal T. Annexin A6 and NPC1 regulate LDL-inducible cell migration and distribution of focal adhesions. Sci Rep. 2022 Jan 12;12(1):596. doi: 10.1038/s41598-021-04584-y. PMID: 35022465

Nguyen MKL, Jose J, **Wahba M**, Bernaus-Esqué M. Hoy AJ, Enrich C, Rentero C, Grewal T. Linking late endosomal cholesterol with cancer progression and anticancer drug resistance. Int J Mol Sci. 2022 Jun 29;23(13):7206. doi: 10.3390/ijms23137206. PMID: 35806209

Grewal T, Hoque M, Conway JRW, Reverter M, **Wahba M**, Beevi SS, Timpson P, Enrich C, Rentero C. Annexin A6-A multifunctional scaffold in cell motility. Cell Adh Migr. 2017 May 4;11(3):288-304. doi: 10.1080/19336918.2016.1268318. PMID: 28060548

Published works by the author that are relevant but does not form part of this thesis

Grewal T, Rentero C, Enrich C, **Wahba M**, Raabe CA, Rescher U. Annexin Animal Models- From Fundamental Principles to Translational Research. Int J Mol Sci. 2021 Mar 26;22(7):3439. doi: 10.3390/ijms22073439.PMID: 33810523

Alvarez-Guaita A, Blanco-Muñoz P, Meneses-Salas E, **Wahba M**, Pollock AH, Jose J, Casado M, Bosch M, Artuch R, Gaus K, Lu A, Pol A, Tebar F, Moss SE, Grewal T, Enrich C, Rentero C. Annexin A6 Is Critical to Maintain Glucose Homeostasis and Survival During Liver Regeneration in Mice. Hepatology. 2020 Dec;72(6):2149-2164. doi: 10.1002/hep.31232. PMID: 32170749.

Meneses-Salas E, Garcia-Forn M, Castany-Pladevall C, Lu A, Fajardo A, Jose J, **Wahba M**, Bosch M, Pol A, Tebar F, Klein AD, Zanlungo S, Pérez-Navarro E, Grewal T, Enrich C, Rentero C. Lack of Annexin A6 Exacerbates Liver Dysfunction and Reduces Lifespan of Niemann-Pick Type C Protein-Deficient Mice. Am J Pathol. 2021 Mar;191(3):475-486. doi: 10.1016/j.ajpath.2020.12.009. Epub 2020 Dec 17. Erratum in: Am J Pathol. 2021 Jul;191(7):1325. PMID: 33345999.

Conference presentations given by the author

Jose J, Hoque M, Engel J, Beevi SS, **Wahba M**, Georgieva MI, Enrich C, Rentero C, Grewal T. Annexin A6 and NPC1 regulate LDL-inducible cell migration and distribution of focal adhesions. 2021. Oral presentation. *Annexins 2021 International Digital Conference*, online, 14-15 June 2021.

Jose J, Hoque M, Engel J, Beevi SS, **Wahba M**, Georgieva MI, Enrich C, Rentero C, Grewal T. Blocking cholesterol export from late endosomes inhibits LDL-inducible cell migration. 2020. Oral presentation. *The School of Pharmacy AAPS HDR Postgraduate Conference 2020*, online, 4-5 November 2020.

Grewal T, Meneses-Salas E, Garcia-Melero A, Hoque M**, Wahba M**, Beevi S, Rentero C, Enrich C. Annexin A6 recruits TBC1D15 to regulate RAB7-dependent delivery of late endosomal cholesterol required for cell migration. Hunter Cell Biology Meeting, Hunter Valley, Australia, 3-7 April 2017.

Grewal T, Meneses-Salas E, Garcia-Melero A, Hoque M**, Wahba M**, Beevi S, Rentero C, Enrich C. Annexin A6 recruits TBC1D15 to regulate RAB7-dependent delivery of late endosomal cholesterol for cell migration. 2nd Australian Cancer and Metabolism Meeting, Melbourne, Australia, 15-17 May 2017.

Grewal T, Meneses-Salas E, Garcia-Melero A, Hoque M, **Wahba M**, Beevi S, Rentero C, Enrich C. Annexin A6-mediated recruitment of TBC1D15 regulates RAB7-dependent cholesterol egress

from late endosomes in NPC1 mutant cells. 40th European Lipoprotein Club (ELC) Meeting. Tutzing, Germany, 4-7 September 2017.

Grewal T, Meneses-Salas E, Garcia-Melero A, Hoque M, **Wahba M**, Beevi S, Rentero C, Enrich C. Annexin A6-mediated recruitment of TBC1D15 regulates RAB7-dependent cholesterol egress from late endosomes in NPC1 mutant cells. **Selected for oral presentation.** 58th International Conference on the Bioscience of Lipids (ICBL). Lipids in health and disease. Zuerich, Switzerland, 10-14 September 2017.

Hoque M, Conway JR, Elmaghrabi Y, **Wahba M**, Rentero C, Timpson P, Enrich C, Grewal T. Annexin A6 expressing cancer cells have increased sensitivity towards EGFR inhibitors. Poster presentation. 2016 Sydney Cancer Conference (SCC2016), Sydney, Australia, 22-23 Sept 2016.

Beevi SS, Hoque M, **Wahba M**, Rentero C, Enrich C, Grewal T. Annexin A6 recruits TBC1D15 to regulate RAB7-dependent delivery of late endosomal cholesterol required for cell migration. 8th Garvan Signalling Symposium, Sydney, Australia, 31 Oct - 1 Nov 2016.

Statement of contribution by others to the thesis as a whole

Prof. Paul Timpson and Dr. David Gallego-Ortega (Cancer Research Program, Garvan Institute of Medical Research and Kinghorn Cancer Centre, St. Vincent's Clinical School, Faculty of Medicine, University of New South Wales, Sydney, Australia) provided technical support regarding the tail vein injection of NPC1-depleted A431 cells and lung tumor analysis in mice. Fluorescence microscopy was conducted under the supervision of Dr. William Hughes at the Children's Medical Research Institute, University of Sydney, Westmead (Sydney, Australia). Wound healing (scratch) assays that assessed cell migration of NPC1-depleted A431 cells was conducted in-house with the assistance of Dr. Sayeeda Sultan Beevi, a visiting postdoctoral researcher in the Grewal group. Dr. Zeyad Nassar (Adelaide Medical School, University of Adelaide, SA, Australia) and Dr. Erdahl Teber (Bioinformatics Unit, Children's Medical Research Institute, University of Sydney, Westmead, New South Wales, Australia) provided technical guidance and support on the analysis of gene expression patterns in publicly available cancer cohorts. Associate Professor Thomas Grewal provided the initial experimental training, supervised the project, contributed to its conception and design, and revised the drafts of this thesis.

Acknowledgment

List of Figures

List of Tables

24

List of Abbreviations

ACAT	Acetyl-CoA-acetyltransferase
ACAT1	Acetyl-CoA cholesteryl acyltransferase 1
AML	Acute myeloid leukemia
ANXA6	Annexin A6
ANXA6-KO	ANXA6 knockout
ATCC	American Type Culture collection
BSA	Bovine serum albumin
CCP	Clathrin-coated pit
CE	Cholesteryl Esters
CGN/TGN	Cis/trans-Golgi-network
CHO	Chinese hamster ovary
CHO-M12	NPC1 mutant CHO cells
CMT2B	Charcot-Marie-Tooth type 2B
cPLA2	Cytoplasmic phospholipase A2
CPTAC	Clinical Proteomic Tumor Analysis Consortium
CRPC	Castration-resistant prostate cancer
DTT	Dithiothreitol
DMEM	Dulbecco's Modified Eagle Medium
EDTA	Ethylenediaminetetraacedic acid
EGF	Epidermal growth factor
EGFR	Epidermal growth factor receptor
ER	Endoplasmic Reticulum
ERBB2	V-erb-b2 avian erythroblastic leukemia viral oncogene homolog 2
ESCRT	Endosomal sorting complexes required for transport

FAK	Focal adhesion kinase
FBS	Fetal bovine serum
FN	Fibronectin
GAP	GTPase-activating protein
GEF	Guanine-nucleotide exchange factor
GEPIA	Gene Expression Profiling Interactive Analysis
GTEx	Genotype-Tissue Expression
HCC	Hepatocellular carcinoma
Her2	Human epidermal growth factor receptor 2 (Erbb2)
HMG-CoA	3-hydroxy-3-methylglutaryl-CoA
HPA	The Human Protein Atlas
LAMP2	Lysosomal associated membrane protein 2
LDL	Low Density Lipoprotein
LDLR	Low density lipoprotein receptor
LE	Late Endosomes
LIMP2	Lysosomal integral membrane protein 2, also named SCARB2
LPDS	Lipoprotein-deficient serum
LSB	Laemmli sample buffer
Lys	Lysosomes
MAPK	Mitogen-activated protein kinase
MβCD	Methyl-β-cyclodextrin
MCS	Membrane contact sites
MEF	Mouse embryo fibroblast
MLN64	Metastatic lymph node 64
MMP	Matrix metalloprotease

MSKCC – PCOG	Memorial Sloan Kettering Cancer Center - Prostate Cancer Oncogenome Group
MT1-MMP	Membrane type 1 matrix metalloproteases
mTORC1	Mammalian target of rapamycin complex 1
MVBs	Multivesicular bodies
NPC	Neuroendocrine Prostate Cancer
NPC1	Niemann-Pick type C1
NPC2	Niemann-Pick type C2
ORP	Oxysterol binding protein
ORP1L	OSBPL1A Gene - Oxysterol Binding Protein Like 1A
ORP2	OSBPL2 Gene - Oxysterol Binding Protein Like 2
OSBP	Oxysterol binding protein
P53	Tumor Protein P53, TP53
PBS	Phosphate buffered saline
PCSK9	Proprotein convertase subtilisin/kexin type 9
PDAC	Pancreatic ductal adenocarcinoma
PDGFR	Platelet-derived growth factor receptor
PFA	Paraformaldehyde
PKCα	Protein kinase Cα
PMSF	Phenylmethylsulfonyl fluoride
PTEN	Phosphatase And Tensin-Like Protein
PVDF	poly-vinyl-D-fluoride
QCMG	Queensland Centre for Medical Genomics
Rab11	Ras-Related Protein Rab-11a
RAB7	Ras-Related Protein Rab-7a
RAB7-GAP	RAB7-GTPase activating protein

Rab8	Ras-Related Protein Rab-8a
Rab9	Ras-Related Protein Rab-9a
Rab-GAPs	Rab-GTPase activating proteins
Rab-GEFs	Rab guanine nucleotide exchange factors
Rac1	Ras-Related C3 Botulinum Toxin Substrate 1
RasGRF2	Ras protein specific guanine nucleotide exchange factor
RE	Recycling Endosomes
RWD	Relative wound density
SCC	Squamous cell carcinoma
SDS	Sodium Dodecyl Sulfate
SMMU	Second Military Medical University
SNAP23	Synaptosome Associated Protein 23
SNARE	Soluble N-ethylmaleimide sensitive factor attachment protein receptor
StAR	Steriodogenic acute regulatory
STARD3	StAR-related lipid transfer domain containing 3
STARD3NL	STARD3 N-terminal like
Stx4	Syntaxin 4
Su2C/PCF	Stand Up to Cancer Prostate/Prostate Cancer Foundation
TBC	Tre2-Bub2-Cdc16
TBC1D15	Tre-2/Bub2/Cdc16 domain family member 15, TBC1 domain family member 15
TBC1D5	Tre-2/Bub2/Cdc16 domain family member 5, TBC1 domain family member 5
TCA	Tricarboxylic acid cycle
TCGA	The Cancer Genome Atlas
TGN	Trans-Golgi network
TMBCP	The Metastatic Breast Cancer Project

TNBC	Triple-negative breast cancer
Tris	Tris(hydroxymethyl)aminomethane
t-SNARE	Target membrane soluble NSF attachment protein receptor
UALCAN	University of ALabama at Birmingham CANcer data analysis portal
VAMP	Vesicle-associated membrane protein or synaptobrevin
VEGF	Vascular endothelial growth factor
VLDL	Very Low-Density Lipoproteins
v-SNARE	Vesicular soluble NSF attachment protein receptor
WT	Wild type

Chapter 1

The role of NPC1 in cancer cell migration and invasion

1.1. Introduction

1.1.1. Cholesterol homeostasis

Besides proteins and carbohydrates, lipids are essential for proper cell functioning, determining cell viability, growth, differentiation, and cell motility (1, 2). Lipids fulfill numerous important cellular functions, such as the provision of building blocks for membrane growth during cell division and differentiation, energy storage in lipid droplets, precursors for steroid hormones and vitamins, as well as serving as signalling molecules to respond to changes in the extracellular environment. Hence, cellular lipid homeostasis requires a tight control and coordination. This is achieved by a complex network of regulatory mechanisms, often involving feedback control of ana- and catabolic pathways and mediated by signalling proteins and transcription factors. Altogether, this ensures that nutrient availability remains in synchronization with cellular energy status and homeostasis, tissue functioning and overall body physiology. Pathological changes in chronic diseases such as cancer commonly display alterations in cell metabolism. This not only includes drastic changes how cells metabolize glucose ('Warburg effect'), but also lipids, such as cholesterol. However, the current understanding on the underlying molecular mechanisms how this supports cancer growth and progression is still incomplete (1-3).

Lipids comprise a plethora of different biomolecules that include fatty acids, triglycerides, phospho-, sphingo- and glycolipids. In addition, cholesterol and its sterol backbone serve as precursors for many other sterol derivatives and vitamins. Over the last decades, it has become clear that cholesterol and its derivatives control many aspects of cellular homeostasis. In particular, cholesterol is indispensable for membrane integrity at the cell surface, compartmentalization of specific functions within organelles, proper membrane transport and exchange of biomolecules and information between organelles, ligand internalization and cell surface receptor signalling. In addition, cholesterol is the precursor for bile acids and steroid hormones, while the cholesterol biosynthesis intermediate 7-dehydrocholesterol serves to generate vitamin D (4). Altogether, this positions cholesterol at the centre of numerous biological processes ensuring proper cellular functioning. Hence, dysregulation of cholesterol homeostasis can have significant consequences

for cell and tissue functions, leading to pathophysiology in many chronic diseases beyond cardiovascular disease and metabolic disorders, including cancer (4).

Despite most mammalian cells being able to synthesize cholesterol, cholesterol synthesis mainly occurs in the liver. In hepatocytes, *de novo* cholesterol biosynthesis takes place in the endoplasmic reticulum (ER), with tricarboxylic acid cycle (TCA)-derived citrate generating acetyl-CoA. Several enzymatic reactions, including the 3-hydroxy-3-methylglutaryl-CoA (HMG-CoA) reductase -mediated and rate-limiting conversion of HMG-CoA to mevalonate lead to the generation of cholesterol. Elevated plasma and low density lipoprotein (LDL) -derived cholesterol levels are a prominent risk factor in cardiovascular disease and the abovementioned enzymatic step is inhibited by statins, the most common cholesterol-lowering medication for cardiovascular disease worldwide (5). As outlined below, given the prominent roles for cholesterol in cancer cell growth and motility, this has also led to the use of statins in cancer, with promising results in many, but not all cell and animal studies and clinical trials (1, 2, 5).

In hepatocytes, for *de novo* cellular cholesterol to reach the circulation, newly synthesized cholesterol is assembled together with triglycerides in very low-density lipoproteins (VLDL) in the Golgi apparatus and then released into the circulation. Once in plasma, several lipases remove fatty acids from these triglyceride-rich VLDL particles to generate LDL, which contains predominantly cholesteryl esters. Cellular LDL uptake then serves as the major source for cholesterol in peripheral tissues. As the *de novo* synthesis of cholesterol requires ATP, complex feedback control mechanisms are in place to monitor energy-consuming cholesterol biosynthesis. Cells are capable to sense cholesterol levels in the ER, and when cellular cholesterol levels are high, cholesterol synthesis is repressed, and most cells acquire cholesterol via LDL uptake (2, 4).

For dietary cholesterol to enter the circulation and be made available to cells, it is first incorporated into micelles in the intestine and then taken up by enterocytes. Next, internalized cholesterol is integrated into triglyceride-rich chylomicrons and released into the lymph to reach the circulation. After lipoprotein lipase -mediated removal of fatty acids from chylomicrons, so-called chylomicron remnants are then taken up by the liver through chylomicron remnant receptors (6). In hepatocytes, after internalization and subsequent degradation of remnant particles, cholesterol is esterified and alike newly synthesized cholesterol, either stored in lipid droplets or re-assembled into VLDL particles, which as described above, are then released from the liver into the circulation. After removal of fatty acids in VLDL for storage in adipocyte and muscle tissue

(7), the resulting and cholesteryl ester-rich LDL particles can bind to the LDL receptor (LDLR) in non-hepatic cells, and endocytosis of the LDL/LDLR complex effectively covers the cellular demand for cholesterol in peripheral cells, continuously downregulating the activity of the cholesterol synthesis pathway (8). In addition, hepatocytes remove excess LDL from plasma via LDLR-mediated endocytosis. In fact, this route is most effective and can remove >70% of LDL-cholesterol from plasma for secretion of cholesterol into bile (6, 8).

1.1.2. The cellular fate of LDL-derived cholesterol

Endocytosed LDL first reaches early endosomes (Figure 1.1) and is then delivered to late endosomes/lysosomes (LE/Lys). Along this route, the pH in the endosomal compartment becomes acidic, ultimately leading to the dissociation of LDL from LDLR in sorting endosomes. This enables the sorting of LDLR into tubular endosomal structures (recycling endosomes) that traffic the LDLR back to the cell surface for another round of LDL internalization (9). The LDL particle on the other hand undergoes a different fate, with lysosomal lipases hydrolyzing LDL-associated cholesteryl esters within multivesicular bodies (MVBs) of the LE/Lys compartment to generate free cholesterol. This pool of free cholesterol in LE/Lys is then delivered to other cellular sites, such as the plasma membrane, ER, Golgi and mitochondria via late endosomal cholesterol transporters, in particular Niemann-Pick type C1/2 (NPC1/2) proteins (10). Ultimately, LDL-derived cholesterol reaches the ER, which senses increased amounts of incoming cholesterol to effectively downregulate the cholesterol biosynthesis pathway. Figure 1.1 depicts the various cellular transport pathways of LDL-derived cholesterol, which clearly identifies the LE/Lys compartment as a central hub for the distribution of LDL-derived cholesterol in cells.
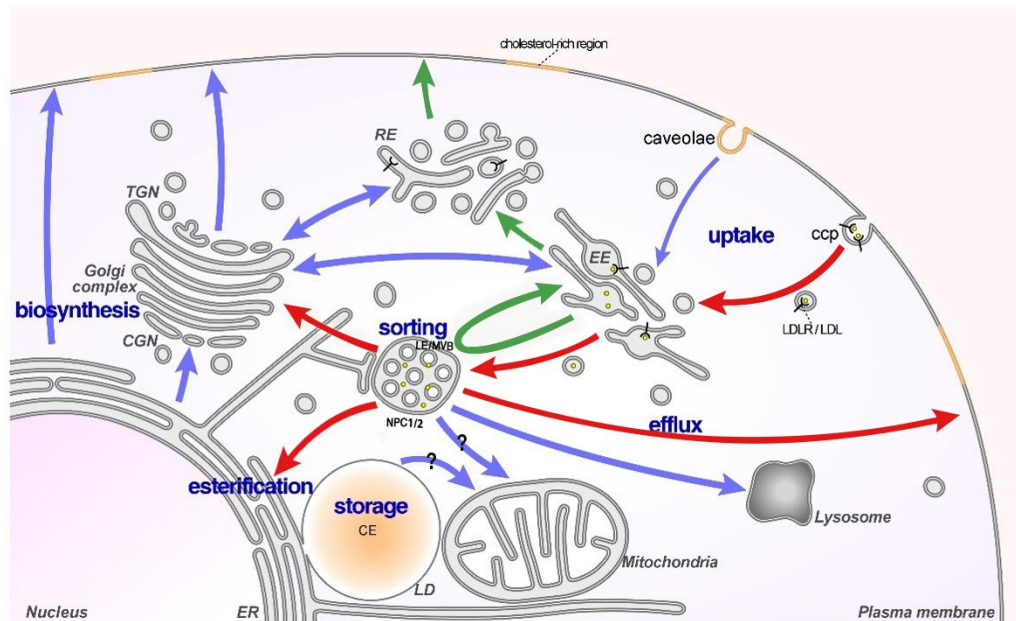
Figure 1.1: Late endosomes (LE) facilitate the cellular distribution of Low-Density lipoprotein (LDL)-derived cholesterol. LDL is internalized via LDL receptor (LDLR)-mediated endocytosis to reach early endosomes (EE) and then late endosomes/multivesicular bodies (LE/MVB). In this location, the LDL/LDLR complex dissociates and LDLR is recycled back to the surface via recycling endosomes (RE). LDL-associated cholesteryl esters (CE) in LDL are hydrolyzed to generate free cholesterol. LDL-derived cholesterol is then transported via Niemann-Pick type C1/2 (NPC1/2) proteins and other transporters to the endoplasmic reticulum (ER), mitochondria, Golgi and plasma membrane. Newly synthesized cholesterol in the ER is transported to the plasma membrane directly or via the Golgi complex. In the ER, cholesterol is esterified for storage of CE in lipid droplets (LD). Red arrows indicate the transport routes of LDL-derived cholesterol. Green arrows highlight the recycling route of the LDL receptor. Abbreviations: ccp, clathrin-coated pit; CGN/TGN: cis/trans-Golgi-network. Taken from (11).

1.1.3. Cholesterol transporters in the LE/Lys compartment

1.1.3.1. NPC1/2

As mentioned above, NPC1/2 proteins are considered the main transporters to export cholesterol form the LE/Lys compartment (12, 13). NPC2 is located in the lumen of LE/Lys to bind incoming cholesterol and transfers cholesterol to NPC1, which resides in the limiting LE/Lys membrane (14, 15) for subsequent transport of cholesterol from LE/Lys to the plasma membrane. The NPC1/2-dependent cellular routes of LDL-derived cholesterol from LE/Lys to other organelles are not well understood, and direct or indirect (via the plasma membrane) transport routes to the ER, Golgi, mitochondria and recycling endosomes seem to exist, most likely requiring supporting actions of neighbouring proteins in the LE/Lys outer membrane (see below) (13, 16-19) . Underscoring the critical role of NPC1/2 proteins for cholesterol export from LE/Lys, NPC1/2 loss-of-function mutations cause NPC disease, a fatal neurodegenerative lysosomal

storage disorder that is characterized by massive LE/Lys-cholesterol accumulation (20). The inability of NPC1/2 mutant cells to deliver cholesterol from LE/Lys to other organelles ultimately causes a cellular cholesterol imbalance that interferes with membrane trafficking and inter-organelle communication, triggering cellular stress and apoptosis (16-18). Common NPC disease phenotypes include hepatic or neurodegenerative symptoms, including psychiatric symptoms, dementia, ataxia and dystonia (20).

Besides NPC1/2, several other cholesterol transporters in the LE/Lys compartment exist, including the steriodogenic acute regulatory (StAR) -related lipid transfer domain containing 3 (STARD3), STARD3 N-terminal like (STARD3NL), members of the oxysterol-binding protein (OSBP) family, such as OSBP-related proteins (ORP1L, ORP2), and lysosomal membrane proteins (lysosomal associated membrane protein 2 (LAMP2) and lysosomal integral membrane protein 2 (LIMP2)) (16-19). In addition, small Rab GTPases (RAB7, 8, 9 and 11) and members of the annexin protein family participate to ensure cholesterol transport to the plasma membrane, ER, Golgi and mitochondria (16-19) (Figure 1.2). Their key features are described below and their differential roles in cancer growth and progression will be examined in more detail in Chapter 2-4.
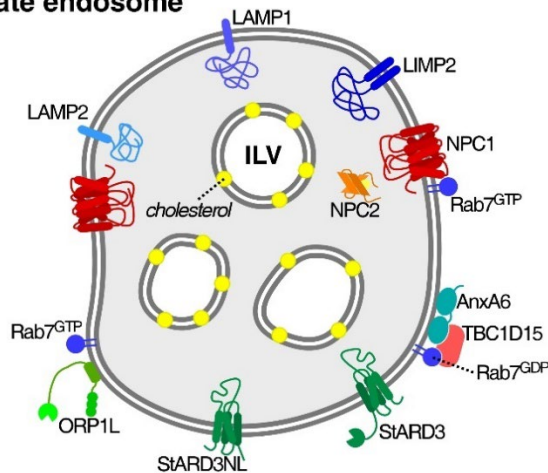
Figure 1.2. Cholesterol transporters and other proteins contributing to cholesterol export from late endosomes. Abbreviations: LAMP1/2, lysosome-associated membrane proteins 1/2; LIMP2, lysosomal integral membrane protein 2; NPC1/2, Niemann-Pick Type C1/2; ANXA6, annexin A6; TBC1D15, Tre-2/Bub2/Cdc16 domain family member 15; ORP1L, OSBP-related protein 1L; STARD3, Steroidogenic acute regulatory (StAR) -related lipid transfer domain containing 3; STARD3NL, STARD3 N-terminal like protein. Taken from (11).

1.1.3.2. STARD3

Like other StARD family members, STARD3 (also called metastatic lymph node 64, MLN64) can bind and transport cholesterol between organelles. STARD3 in LE appears to transfer cholesterol between LE/Lys and the ER via membrane contact sites (MCS) (21). When cellular cholesterol levels are low, STARD3 has been proposed to move cholesterol from the ER or plasma membrane into LE (21-26). Yet, upon cholesterol accumulation in LE/Lys, Grewal and colleagues demonstrated STARD3 to facilitate restoration of late endosomal cholesterol egress to the ER in a RAB7-dependent manner (16, 27) (see below). These findings were obtained from a well-established Chinese hamster fibroblast (CHO) cell line lacking NPC1 (CHO M12). In contrast, STARD3 gain-of function overexpression failed to overcome late endosomal cholesterol accumulation in NPC patient fibroblasts (22, 23) or increase acetyl-CoA cholesteryl acyltransferase 1 (ACAT1) -mediated esterification of cholesterol in the ER in macrophages and fibroblasts (24, 28), indicating differential STARD3 capabilities depending on the cell type analyzed. In addition, in cells lacking NPC1, STARD3 has been described to promote cholesterol transfer into mitochondria (29, 30), which might confer anti-apoptotic properties in cancer cells that can utilize increased cholesterol delivery into mitochondria for steroidogenesis and energy production (31, 32).

1.1.3.3. ORP proteins

The ORP family comprises proteins that can transfer two lipids in opposite directions across MCS, for example between LE/Lys and other organelles (33). OSBP was the first ORP protein identified and transfers one molecule of phosphatidylinositol-4-phosphate from LE/Lys to the ER in exchange for one molecule of cholesterol in the opposite direction. In NPC mutant cells, pharmacological or genetic inhibition of OSBP downregulated mammalian target of rapamycin complex 1 (mTORC1) kinase signalling, the master regulator of cancer cell metabolism and restored autophagy, indicating a role for OSBP in the hyperactivation of mTORC1 in cancer settings with low NPC1 levels (34).

ORP1L represents another ORP family member and in MCS, simultaneously interacts with proteins in LE/Lys and the ER. ORP1L-containining protein complexes comprised the late endosomal small GTPase RAB7, the RAB7 effector RAB7-interacting lysosomal protein (RILP) and ER-associated vesicle-associated membrane (VAMP) proteins. These interactions support

MCS formation between LE/Lys and the ER, but also control cholesterol-sensitive LE motility (35-38) and trafficking of autophagic vesicles (39). Possibly related to these findings, ORP1L can transfer cholesterol from the ER to LE/Lys when cells are deprived of incoming LDL-cholesterol (40, 41).

As ORP1L depletion caused cholesterol accumulation in LE/Lys and was accompanied with reduced cholesterol esterification and increased *de novo* cholesterol synthesis (42), this may indicate that ORP1L can also deliver cholesterol from LE/Lys to the ER. This may occur through stimulation of MCS formation, as an ORP1L deletion mutant lacking the sterol-binding domain reduced accumulation of cholesterol in LE/Lys in NPC1 mutant cells (30). In support of these findings, the adenoviral RIDα protein stimulates late endosomal LDL-cholesterol export, cholesterol esterification and cholesteryl ester storage in lipid droplets in an ORP1L-dependent manner (43). Hence, the direction of ORP1L-mediated cholesterol transfer between LE/Lys and the ER may depend on cholesterol levels in the various compartments, the presence or absence of viruses, and the expression levels of NPC1 and other cholesterol transporters.

In addition, the ORP member ORP2 is responsible for the exchange of LDL-derived cholesterol and phosphatidylinositol-4,5-biphosphate between LE and recycling endosomes. This ORP2-dependent route to deliver cholesterol to the cell periphery was a driver for the activation of focal adhesion kinase (FAK), increasing focal adhesion dynamics and cancer cell motility (44). In hepatocytes, these mechanisms may contribute to the reduced growth and migratory behaviour upon ORP2 depletion (45). Furthermore, interaction of ORP5 with NPC1 may support cholesterol export from LE/Lys to the ER (46). However, ORP5 may also indirectly influence cholesterol egress from LE/Lys due to its role in delivering phosphatidylserine to the plasma membrane, which influences cholesterol transport to and from the plasma membrane (33, 47). Taken together, several ORPs connect cholesterol export from LE/Lys with molecular events that contribute to cancer growth and aggressiveness (see also Chapter 3).

1.1.3.4. LAMP-2 and LIMP-2

Besides NPC1 and members of the StARD and ORP family described above (1.1.3.1-1.1.3.3.), two other cholesterol-binding proteins in lysosomes exist (19). Lysosome-associated membrane proteins 1/2 (LAMP-1/2) are prominent type 1 transmembrane proteins in LE/Lys and their luminal domains can bind cholesterol with high affinity. LAMP-2 is believed to support transfer of NPC2-

bound cholesterol in the lumen of LE/Lys vesicles onto NPC1 within the LE/Lys limiting membrane, thereby contributing to cholesterol egress from LE/Lys (48).

The second abundant integral membrane protein in LE/Lys is Lysosome Integral Membrane Protein 2 (LIMP-2; also named SCARB2). The recently deciphered structure of LIMP-2 revealed a hydrophobic tunnel, which has been proposed to work alongside NPC1 to export cholesterol from the LE/Lys (49).

Several roles and upregulated expression for LAMP-2 and LIMP-2 in cancer have been reported, some of those related to cholesterol-sensitive lysosomal functions, such as autophagy (50).

1.1.3.5. Rab proteins

Rab proteins are key players in the regulation of membrane transport and directional trafficking of vesicles between organelles. Alike all other members of the superfamily of small Ras GTPases, guanine-nucleotide exchange factors (GEFs) and GTPase-activating proteins (GAPs) balance the amounts of active (GTP-bound) and inactive (GDP-bound) Rab proteins (51). In addition, the prenylation of active Rabs ensures their association with membranes in specific cellular locations, while inactive Rabs (GDP-bound) are released into the cytosol. The Rab-dependent directional movement of vesicles requires a plethora of regulators and effectors that ensure organelle-specific functioning for each Rab protein. Out of the Rab family, several Rabs have been linked to cholesterol transport in the LE/Lys compartment, in particular RAB7, the master regulator of the LE/Lys compartment (51).

The recruitment of several effectors enable active RAB7-GTP to safeguard not only the distinct multilamellar morphology of LE/Lys, but also ascertain the proper functioning of many different processes in the LE/Lys compartment that require LE vesicle movement and/or directional membrane transport such as autophagy (16, 18, 51, 52). Most relevant here is the critical role for RAB7 in the final steps of the lysosomal targeting of LDL along the endocytic pathway for degradation (53) and the requirement of RAB7 for effective LDL-cholesterol distribution from LE/Lys to other cellular sites (16, 18). In NPC1 mutant cells, cholesterol accumulation compromised RAB7 activity and led to reduced LE/Lys motility (52). Vice versa, RAB7 inhibition resulted in an enlarged and cholesterol-loaded LE/Lys compartment with reduced capacity to export LDL-derived cholesterol (16, 27, 54). In contrast, overexpression of RAB7 overcame

cholesterol accumulation in NPC1 mutant cells (16, 54, 55), and as shown by Grewal and coworkers, enabled LDL to induce cancer cell migration and invasion (56). The Ikonen group recently reported the transfer of LDL-cholesterol from LE to recycling endosomes in the cell periphery, possibly requiring RAB7, and stimulating Rab8-dependent integrin recycling and FAK signaling in cancer cells (44, 57). In addition, the Grewal group and others reported active RAB7 to stimulate cholesterol transfer via NPC1, STARD3 or ORP1L from LE/Lys across MCS to the ER. The latter route could ultimately supply cholesterol for storage in lipid droplets or the plasma membrane to support oncogenic growth and motility (16, 18, 35, 36, 38, 55, 58)

Rab9 is another Rab protein affected by NPC1 deficiency and cholesterol accumulation and was found inactive and sequestered on LE/Lys membranes, causing defects in membrane trafficking from LE/Lys to the trans-Golgi network (TGN) (58). Alike RAB7, overexpression of Rab9 restored cholesterol export in NPC mutant cells, stimulating its delivery to the TGN (58-60). Similarly, cholesterol accumulation in cells lacking NPC1 was rescued by Rab8 overexpression (61), promoting the delivery of cholesterol from LE/Lys to the cell surface to increase focal adhesions turnover and migratory abilities of A431 carcinoma cells (44, 57). Finally, Rab11 was proposed to control LE/Lys-Chol transport routes towards the cell surface. Although Rab11 controls $\beta1$ integrin recycling (62, 63), a link to Rab8-dependent LDL-cholesterol delivery to recycling endosomes and focal adhesion dynamics could not be established (57).

Interestingly, up- and downregulation of several endosomal Rab GTPases have been observed in cancer and linked to oncogenic features in cancer cell behaviour (64-66). Hence, expression levels of the abovementioned Rab proteins could alter the efficacy of how cancer cells utilize incoming cholesterol to support growth and progression. On the other hand, the cholesterol content in membrane microdomains that contain Rab proteins could alter Rab-GTPase activity (52, 58-61). This liaison between Rab activity and dietary cholesterol could be relevant for cancer growth and progression and will be examined in more detail for RAB7 in Chapters 3-4.

1.1.3.6. Annexin A6

Annexin A6 (ANXA6) belongs to the conserved annexin protein family, which is characterized by their calcium (Ca^{2+})-dependent binding to phospholipids and membranes. ANXA6 consists of an N-terminal leader sequence and a C-terminal core domain with eight Ca^{2+}-binding 'Annexin repeats', the latter facilitating transient and Ca^{2+}-inducible association with cellular membranes.

which are organized in two tetrads connected by a hydrophobic linker (containing a rare tryptophan) allowing for both calcium-dependent (transient) and hydrophobic binding to membrane lipids. This dynamic behaviour, together with the interaction of ANXA6 with a variety of proteins and lipids, allows scaffolding functions relevant for cell proliferation and motility, such as stabilizing protein complex assembly for transient signaling events, supporting membrane-cytoskeleton dynamics and recruiting proteins from the cytosol to specific membrane microdomains at the plasma membrane or LE/Lys (67, 68). All these features are also important for membrane microdomain formation, membrane transport, as well as controlling the formation of MCS for cholesterol transfer (67-71).

Ca^{2+}-dependent binding of ANXA6 to negatively charged phospholipids is probably relevant in clathrin-coated pits at the cell surface, enabling ANXA6 to interact with epidermal growth factor receptor (EGFR) and H-Ras GTPase, and recruit protein kinase Cα (PKCα) for EGFR inactivation and the GTPase activating protein p120GAP to downregulate H-Ras and mitogen-activated protein kinase pathway signaling (72-74), reducing their oncogenic growth potential. Furthermore, ANXA6 binds to members of the Src kinase family with prominent roles in many molecular events that affect cell viability and motility. Extracellular ANXA6 activities have also been reported, with consequences for focal adhesion dynamics, metastatic behaviour, and response to therapy in several cancers. Grewal and colleagues have summarized these cancer-relevant findings in several review articles (67-71, 75, 76).

In relation to cholesterol homeostasis, a role for ANXA6 in LDL endocytosis and subsequent delivery of LDL to the lysosomal compartment was initially described by Grewal and coworkers as well as others (74, 77-79). In follow-up studies, the Grewal group revealed the translocation of ANXA6 to LE/Lys upon LDL loading or genetic/pharmacological NPC1 inhibition (77, 79, 80). The association of ANXA6 with LE/Lys did not require Ca^{2+}, but appeared cholesterol-dependent, a novel property within the annexin family that was confirmed by others *in vitro* (81). Most importantly, when overexpressed, ANXA6 induced an NPC1-like phenotype, with cholesterol accumulating in LE/Lys, causing major trafficking defects in transport routes to the cell surface.

For example, NPC1 inhibition as well as ANXA6 overexpression blocked cytoplasmic phospholipase A2-dependent transport of caveolin-1 to the cell surface, leading to reduced numbers of cholesterol-rich caveolae at the cell surface. Also, the soluble NSF attachment protein receptor (SNARE) proteins syntaxin 4 (Stx4), soluble N-ethylmaleimide-sensitive fusion protein

23 (SNAP23) and Stx6 were mislocalized and failed to support fibronectin secretion and integrin recycling (82-86). Thus, NPC1 inhibition or ANXA6 overexpression effectively compromised the ability of LDL-cholesterol to stimulate migration and invasion in several cancer cell lines (27, 56, 87).

Based on these findings, the Grewal group and colleagues then performed ANXA6 knockdown experiments in NPC1 mutant cells. Most strikingly, this approach restored cholesterol efflux from LE/Lys in NPC1 mutant cells (55). Mechanistically, late endsomal cholesterol accumulation leads to elevated ANXA6 levels and increased translocation of ANXA6 to LE/Lys (55, 80). ANXA6 located in LE/Lys recruits the RAB7-GTPase activating protein (RAB7-GAP) TBC1D15 to downregulate RAB7-GTP levels. Hence, loss of the ANXA6 scaffold did not permit recruitment of TBC1D15 to LE/Lys in order to downregulate RAB7-GTP levels in ANXA6-depleted NPC1 mutant cells. Consequently, elevated RAB7-GTP levels increased MCS between LE/Lys and ER and facilitated a STARD3-mediated cholesterol transfer to the ER, followed by ACAT1-dependent cholesterol esterification for storage in lipid droplets. Restoration of cholesterol export in ANXA6-depleted NPC1 mutant cells also enabled cholesterol delivery to focal adhesions, thereby improving migratory activities (56). These mechanisms also appear to be in place in NPC1 expressing cells, as A431 carcinoma cells, which lack endogenous ANXA6, and mouse embryo fibroblasts (MEFs) from ANXA6-KO mice also displayed elevated RAB7-GTP levels (55).

Taken together, high, and low expression levels of ANXA6 seem to control NPC1-dependent and -independent cholesterol export routes from LE/Lys to multiple locations inside cells. This gatekeeper function of late endosomal ANXA6 has consequences for cells to grow or move forward and invade (55, 69, 87) and its potential to influence cancer progression and prognosis, possibly in a cholesterol-related manner, will be addressed in Chapters 2-4.

1.1.4. LDL-derived cholesterol is a risk factor for cancer growth and progression

Due to the increased demand for cholesterol in cancer growth and progression, alterations in the way human cancer cells metabolize cholesterol to support tumorigenesis are common, often also supporting the development of drug resistance (1, 88-91). A shared feature of many cancer cells is the upregulation of *de novo* cholesterol synthesis or the elevation of serum cholesterol levels. Both adaptations elevate the readiness of cholesterol to support cancer growth and progression. Hence, many cancers display cholesterol accumulation in the form of cholesteryl ester

storage in lipid droplets (92, 93). Examples for elevated plasma cholesterol levels as risk factor include lung, pancreatic, breast and prostate cancer (94). Higher prostate cancer risk and progression and hypercholesterolemia was also linked to a more rapid development of castrate-resistant prostate cancer (89, 95). Furthermore, lipid-rich diets and obesity have been linked with the development of cholesterol-rich environments that are considered risk factors for tumor initiation and progression. In line with this, administration of a high-fat diet in mouse models enhanced the onset, incidence, and frequency of breast cancers (96).

The upregulation of LDLR-mediated endocytosis is a shared feature of many cancer cells, driving many oncogenic adaptations that require cholesterol to foster tumor development and expansion. This has been reviewed in detail (2, 92, 93, 97), identifying many additional mechanisms beyond its role in proliferation as a critical element for the building of membranes. In particular, cholesterol provides the foundation to establish specialized membrane microdomains at the cell surface, secretory and endocytic routes that trigger oncogenic signaling events (lipid rafts) and promote adhesion, migration, and invasion (focal adhesions). In addition, several cell surface receptors (e.g. smoothened receptor (98)), scaffolding proteins (PDZ domain-containing proteins) (99), membrane transport regulators (SNAREs) (17)) or regulators of mTORC1 kinase (100), directly bind cholesterol. All these interactions contribute to modulate proliferation, invasion, and metastasis. Also, the ability of mitochondria to provide ATP and synthesize steroid hormones to nurture energy and hormonal needs for oncogenic, but also contribute to chemoresistance greatly benefits from increased cholesterol levels in mitochondria (101).

Hence, enabling enhanced LDL uptake, overexpression of LDLR can be observed in lymphoma (102) and leukemia (103), but also many solid tumors such as pancreatic ductal adenocarcinoma (PDAC) (104) (105), breast cancer (106, 107), hepatocellular carcinoma (HCC) (108), lung adenocarcinoma (109, 110), colorectal carcinoma (69, 111), nasopharyngeal carcinoma (112), glioblastoma (113), and renal cell carcinoma (114) (Table 1.1). In these settings, enhanced LDL-cholesterol uptake could explain the often reduced plasma LDL-cholesterol levels in cancer patients (115) as well as hypocholesterolemia in acute myeloid leukemia (AML) (116, 117), prostate, lung, bowel, head and neck cancers (118-121). Similarly, LDL-cholesterol also seems to support metastatic behavior, as prostate and lung cancer progression was associated with increased LDL clearance (122, 123). However, it should be noted that some findings did not support elevated LDLR levels to drive cancer growth and progression, as low LDLR expression was related to poor

prognosis and clinical outcomes in several studies (123-125), although an increased dependence on cholesterol synthesized *de novo* in these cohorts (HCC, prostate, cervical) cannot be ruled out (123-125) . The findings on LDLR expression in oncogenic settings are summarized in Table 1.1.

LDLR and tumor characteristics	Cancer types
Elevated expression	breast cancer (106, 126, 127), colorectal cancer (69, 111), glioblastoma (113), HCC (108), lung cancer (109, 110), leukemia (103, 128), lymphoma (102), nasopharyngeal carcinoma (112), renal cancer (114), PDAC (104, 105)
Increased proliferation, migration and invasion	breast cancer (129), colorectal cancer (115), nasopharyngeal cancer (112), PDAC (105), prostate cancer (130-132)
Poor prognosis and clinical outcomes	AML (133), breast cancer (129), cervical cancer (125), HCC (123), PDAC (134, 135), Prostate cancer (124)
Chemoresistance	breast cancer (129), ovarian cancer (136), PDAC (105)

Table 1.1: Tumor characteristics associated with elevated LDLR expression. Abbreviations: AML, acute myeloid leukemia HCC, hepatocellular carcinoma; PDAC, pancreatic ductal adenocarcinoma. Adapted from (11).

Studies using cell and animal models have supported the association of LDLR upregulation and various aspects of oncogenesis. LDLR gene knockdown or antibody-mediated LDLR inhibition compromised growth in pancreatic (105), prostate (133), nasopharyngeal (112), colon (69), and breast cancer models (133). In contrast, elevated LDLR expression and consequently, increased LDL uptake, were supportive of growth in models for breast (129), prostate (131), and colorectal cancer (69). Furthermore, elevated ACAT1 levels, which esterifies incoming cholesterol in the ER, (106), leading to increased storage of LDL-derived cholesteryl esters in lipid droplets, supported tumor growth and progression in prostate and pancreatic cancer cell lines and tissues (89, 137, 138). Pointing at this transport route as a therapeutic target, pharmacological inhibition of ACAT1 reduced LDL-inducible proliferation and motility, and re-established feedback mechanisms in the ER responsible for LDLR downregulation (89, 138).

As summarized in Table 1.1, these observations extend to LDLR expression levels having potential to predict clinical outcomes. In hyperlipidemic mice, upregulated LDLR activity accelerated growth of breast cancer xenografts (115). In cell models for ovarian cancer and leukemia, elevated LDLR levels caused resistance to platinum-based anticancer treatments. Vice

versa, cisplatin and gemcitabine treatment was more efficient in LDLR-depleted epithelial ovarian carcinomas (138) and pancreatic cancer cells (93) (Table 1.1). This appears to translate to relevance in human cancer, as increased risk of recurrence of PDAC (92, 93) and AML (135) correlated with LDLR upregulation, while overall and recurrence-free survival in PDAC (130, 138), AML (135), breast cancer (115) was increased in patients with low LDLR levels.

1.1.5. Aims

As outlined above (1.1.4.), cancer cell adaptations to support growth and metastasis include upregulation of LDL uptake. In addition, studies identifying increased cholesterol esterification in the ER and cholesteryl ester storage in LD in PDAC and prostate cancer models (89, 137, 138), implicate that mechanisms in cancer cells are in place that ensure increased distribution of internalized and LDL-derived cholesterol in LE/Lys to promote cancer cell proliferation and migratory behaviour. Indeed, as outlined above, the Grewal group identified pharmacological or genetic NPC1 inhibition or ANXA6 overexpression and the resulting cellular cholesterol imbalance to interfere with many aspects relevant for cancer cell migration (27, 55, 56, 82, 83, 85, 87).

NPC1 mutant CHO cells (139), the pharmacological NPC1 inhibitor U18666A (139, 140) or ANXA6 overexpression served to demonstrate the requirement of late endosomal cholesterol for cell motility. However, to better address the impact of late endosomal cholesterol accumulation on aggressive cancer cell behaviour, a more appropriate human cancer cell model lacking NPC1 would be desirable. However, while transient NPC1 depletion in cancer models has been described (57, 141), stable NPC1 gene knockdown approaches in cancer cell lines are still lacking in the field, indicating that continuous NPC1 deficiency interferes with cell viability. The A431 squamous epithelial cell line is a well-established cell line with characteristic features of aggressive behaviour as judged by their high potential to migrate, invade, and metastasize (142-144).

Moreover, A431 cells express substantial amounts of LDLR (57, 145, 146), ensuring efficient LDL uptake. In A431 cells, stable ANXA6 overexpression triggered a NPC1-mutant-like phenotype characterized by late endosomal cholesterol accumulation. This cell line, as well as U18666A treatment, showed reduced migratory and invasive behaviour (86, 87, 147), indicating the suitability of the A431 cell line for stable NPC1 gene depletion and cholesterol-related studies in the context of cancer cell motility. Hence, the aim of this chapter was to generate a stable NPC1-

deficient cell line that would display cholesterol accumulation and reduced migratory and invasive behaviour.

1.2. Materials and methods

1.2.1 Cell line and tissue culture

The epidermoid carcinoma A431 cell line was obtained from American Type Culture Collection (ATCC) (72, 74). A431 wildtype (wt) and a stable A431 cell line lacking NPC1 (A431-NPC1KD) were maintained in Dulbecco's Modified Eagle Medium (DMEM; low glucose with Glutamax), supplemented with 10% (v/v) fetal bovine serum (FBS; Hyclone; Logan, UT, USA), penicillin (100 units/mL) and streptomycin (100μg/mL; GIBCO) at 37°C, 5% CO_2.

1.2.1.1. Generation of a NPC1-deficient A431 cell line

For the generation of the A431 cell line with stable NPC1 knockdown, 1-2x10^5 cells were transfected with different combinations of four NPC1 gene-specific (human) shRNA plasmids (*SureSilencing*, QIAGEN) targeting human NPC1 (accession number: NM_000271.5) at positions 3869-3889 (clone 1), 1483-1503 (clone 2), 3061-3081 (clone 3) and 3030-3050 (clone 4), respectively, together with Lipofectamine 2000 (Invitrogen), according to the manufacturer instructions (56). A431 cells stably transfected with scramble shRNA served as control. Each plasmid carries a shRNA under the control of the Ul promoter and a puromycin resistance gene for selection of plasmid expressing cells. 48-72 hours after transfection, cells were selected with 1.5μg/ml puromycin. After 2 weeks, puromycin-resistant and NPC1-depleted colonies were identified. The shRNA sequences of the four clones are shown in Table 1.2. After transfection and selection, cell lines were maintained in DMEM and 10% FBS as described above (1.2.1.). Cells were passaged twice weekly (1:10 dilution) and seeded at 1-2x10^5 cells/well in 6-well plates for preparation of cell lysates (1.2.3.), filipin staining (1.2.7.) or migration (scratch) assays (1.2.8.), unless otherwise specified. Cells were discarded after passage 25.

Clone ID	Insert Sequence	NPC1 gene position
1	GGAGCCACTCACGGATTAATA	3869-3889
2	GCACCAGGTTCTTGACTTACA	1483-1503
3	CTGCAATGCTTCAGTGGTTGA	3061-3081
4	GCTGTCGAGTGGACAATATCA	3030-3050
Scramble	ggaatctcattcgatgcatac	

Table 1.2: SureSilencing shRNA plasmids: The shRNA sequences targeting the human NPC1 gene at position 3869-3889 (clone 1), 1483-1503 (clone 2), 3061-3081 (clone 3) and 3030-3050 (clone 4) are shown. The non-targeting scrambled shRNA sequence is also given.

1.2.2. Recombinant DNA techniques

1.2.2.1. Transformation

Competent E. coli cells (HB101; Promega) were transformed using a protocol adapted from Sambrook and colleagues (148). 30 µL cells and approximately 20 ng DNA were combined in a microcentrifuge tube, incubated on ice for 10 minutes before a heat shock for 45-50 sec at 42°C was performed. The cells were then placed on ice for 2 minutes, and 500 µL Luria Broth (LB) medium (Sigma) was added to the cells, which were then incubated for 60 minutes at 37°C on a shaker at 225 rpm. 400 µL of the cell suspension was then plated on agar plates containing ampicillin (100 µg/mL; agar from Sigma-Aldrich; bacterial plates from BD Falcon (Franklin Lakes, NJ, USA); ampicillin from Merck Millipore, Billerica, MA, USA). Cells were incubated overnight at 37°C and the following day, single colonies were harvested with a pipette tip and placed in 2 mL LB medium containing ampicillin (100 µg/mL) and incubated at 225 rpm overnight at 37°C. These cultures were then used for DNA isolation using a Miniprep kit (Sigma; see 2.2.2).

1.2.2.2. Plasmid DNA preparation

For plasmid isolation and preparation, the Miniprep Kit (Sigma) was used. The procedure consisted of 3 basic steps: (i) preparation of bacterial lysates; (ii) adsorption of DNA onto a DNA binding column, (iii) washing and elution of plasmid DNA.

The bacterial lysate was prepared as follows: 5 ml overnight cultures of E. coli grown in LB medium were transferred to a microcentrifuge tube and cells were pelleted at 1,500 rpm for 3 minutes. The supernatant was discarded, and the bacterial pellet was resuspended thoroughly in 200 µl Resuspension Solution. Next, 200 µl Lysis Solution was added and samples were mixed

immediately by gentle inversion (6–8 times) until the mixture became clear and viscous. Cell debris was then precipitated by adding 350 µl Neutralization/Binding Solution and tubes were gently inverted 4–6 times. To pellet the cell debris, samples were centrifuged at 14,000 rpm for 10 minutes and the supernatant was collected. Then a GenEalute Miniprep Binding Column was inserted into a microcentrifuge tube, and 500 µl of the Column Preparation Solution was added to each column before centrifugation at 14,000 rpm for 30-60 seconds. The flow-through was discarded and the clear cell lysate was loaded onto the column. The column was centrifuged at 14,000 rpm for 30-60 seconds and the flow-through was discarded.

Residual salt and other contaminants were removed, 750 µl diluted Wash Solution was added to the column, before centrifugation at 14,000 rpm for 30-60 seconds. The flow-through was discarded and the column was centrifuged at 14,000 rpm for 1-2 minutes to remove excess ethanol. Finally, the column was transferred to a fresh collection tube, before adding 100 µl Elution Solution to the column, followed by centrifugation at 14,000 rpm for 1 minute. The eluted DNA was stored at –20°C. Recovery and DNA purity was determined by spectrophotometric analysis. The ratio of absorbance of DNA samples at 260 nm and 280 nm (A260/A280) was 1.7 - 1.9.

1.2.2.3. Plasmid DNA Transfection

$1x10^5$ A431 cells/well were seeded on a 6-well plate and incubated overnight at 37°C, 5% CO_2. On the following day, 1.5 µg plasmid and 4 µL Lipofectamine 2000® (Invitrogen) were diluted in 250 µL Opti-MEM® each, before mixing them to form the transfection mix. Different combinations of the plasmids were added into each well as illustrated in Table 1.3. The cells were washed twice with phosphate buffered saline (PBS) before adding the corresponding transfection mix into each well with cells growing in 2 ml antibiotic free media and the plate was incubated for 6 hours under the abovementioned conditions.

6 hours later, the media containing the transfection mix was removed and the cells were washed twice with PBS to remove any traces of the transfection mix before adding fresh media supplemented with 10% (v/v) FBS, penicillin (100 units/mL) and streptomycin (100 µg/mL) and incubating at 37°C, 5% CO_2.

Well Number	Clone (Plasmid; shRNA)	μg Plasmid / Well
1	Scramble (Clone 5; -Ve Control)	1.5 μg scrambled shRNA
2	Clone 1 + Clone 2	0.75 μg per clone
3	Clone 3 + Clone 4	0.75 μg per clone
4	Clone 1 + Clone 2 + Clone 3	0.5 μg per clone
5	Clone 1 + Clone 2 + Clone 3 + Clone 4	0.375 μg per clone
6	No transfection	

Table 1.3: shRNA plasmid combinations used for the generation of NPC1-deficient A431 cells. The amount of shRNA plasmid used in each transfection is provided. Scrambled (non-targeting) shRNA plasmid served as negative control. Non-transfected cells served as control for the puromycin selection 48 hours after transfection.

1.2.2.4. Selection of puromycin-resistant A431 cells

48-72 hours after transfection, cells were passaged (1:10 dilution) and selected in 1.5 μg/ml puromycin (Sigma-Aldrich) containing media (DMEM; low glucose with Glutamax, 10% FBS, penicillin (100 units/mL) and streptomycin (100 μg/mL)) at 37°C, 5% CO_2. After 2 weeks, puromycin-resistant and NPC1-depleted colonies were identified by western blotting (1.2.6.) and filipin staining (1.2.7.). The cells were maintained in the puromycin-containing media for another 2 weeks after selection before using the puromycin free media again (72).

1.2.3. Preparation of whole cell lysates

Cell lysates for the analysis of protein expression by western blot analysis (2.5.-2.6.) were prepared as follows. In a 6-well plate, 5×10^5 cells/well were seeded and incubated overnight at 37°C, 5% CO_2. The following day, the cells were lysed by adding 100 μL/well ice-cold lysis buffer [(20 mM Tris-HCl, 2 mM ethylenediaminetetraacedic acid (EDTA), 100 mM NaCl, 5mM $MgCl_2$, 1% v/v Triton X-100, 5 mM NaF, 10% v/v glycerol, 0.5% v/v 2-mercaptoethanol, 0.1 mM Na_3VO_4 (phosphatase inhibitor), 1 mM phenylmethylsulfonyl fluoride (PMSF), 5 μg/mL leupeptin and 2 μg/mL aprotinin (protease inhibitors)]. The cells were then scraped, and the lysates were centrifuged at 14,000 rpm at 4°C for 5 minutes. The supernatant was taken and stored at -20°C (72, 74).

1.2.4. Protein quantification

For the determination of the protein content in each lysate, a Lowry assay was performed as described (149). Samples were prepared by adding 5 µl of each sample to 395 µl of deionised H_2O in duplicate and serial dilutions of bovine serum albumin (BSA) ranging from zero to 50 µg/ml were prepared using stock BSA solution (1 mg/ml) for the standard curve. 1 ml of freshly prepared Lowry solution (solution A: 3% Na_2CO_3, 0.15 M NaOH; solution B: 2% NaK; solution C: 1% $CuSO_4.5H_2O$; in a ratio of 9.7:0.15:0.15, respectively) was added to each sample. After 10 minutes 0.125 ml diluted Folin solution (Folin:H_2O, 1:3; Sigma Aldrich) was added and samples were incubated at room temperature for 30 minutes before measuring the absorbance of each sample at 750 nm. Standard curve readings were used to calculate the concentration of each cell lysate (149).

1.2.5. SDS gel electrophoresis (SDS-PAGE)

Following protein quantification, proteins were separated using polyacrylamide gel electrophoresis. In this method, proteins are denatured by heating them in buffer containing SDS and a thiol-reducing agent such as 2-mercaptoethanol. The resulting denatured proteins were then separated according to their molecular weight. Cellular proteins were denatured with 4 µl of 5X Laemmli Sample Buffer (LSB, 200 mM Tris-HCl pH 6.7, 10% (w/v) SDS, 50% (v/v) glycerol, 0.025% bromophenol blue, 250 mM dithiothreitol (DTT)) were added to each lysate, heated for 5 minutes at 95°C, then cooled on ice for 5 minutes, then centrifuged for 5 minutes at 1,0000 rpm. 25 µg of protein were loaded per lane onto SDS-PAGE composed of a resolving gel containing 8-12% acrylamide (Amresco, Solon, OH, USA) and a stacking gel containing 4% acrylamide. Gels were run using a Bio-Rad Mini-Protean gel apparatus (Bio-Rad Laboratories) with running buffer (25 mM Tris, 192 mM glycine, 0.1% (w/v) SDS) at 200 V for 45-60 minutes. PageRuler® prestained protein ladder (Fermentas, Thermo Fisher Scientific) was used to visualise separation of proteins and to determine molecular weight of proteins (150).

1.2.6. Western blotting

Proteins were transferred onto poly-vinyl-D-fluoride (PVDF) membranes (0.2 µm pore size, Merck Millipore, USA), which were prepared by washing the membranes in methanol for 30 seconds, deionised H_2O for 1 minute and then transfer buffer (15 mM Tris, 120 mM glycine, 20% (v/v) methanol) for another 60 seconds. Transfer was performed in the Bio-Rad Mini-Protean wet

transfer system (Bio-Rad Laboratories) for 2 hours at 70 V, at 4°C (151). Following the transfer, membranes were blocked in 5% (w/v) BSA in PBS with 0.1% (v/v) Tween- 20 (PBS-Tween) for 15 minutes at room temperature, then incubated with primary antibody (1:500) in 1% (w/v) BSA in PBS-Tween, overnight at 4°C on a roller mixer or shaker. Membranes were then washed with PBS-Tween (3x5 minutes) and incubated with horseradish-peroxidase (HRP)-conjugated secondary antibody (1:10000) in 1% (w/v) BSA at room temperature for 1 hour. Subsequently, membranes were washed with PBS-Tween (3x5 minutes) and then proteins were visualised using Western Lightning® Plus-ECL substrates (Perkin Elmer) according to manufacturer instructions (77). Membranes incubated in ECL were visualised using ChemiDoc™ Touch Imaging System (Life Sciences Research, Bio-Rad). The densitometry was carried out using Image J (1.47v).

1.2.7. Filipin staining

1×10^5 cells/well of the A431 scramble and A431 NPC1 KD cell lines were seeded onto sterile coverslips, and incubated overnight at 37°C, 5% CO_2. 24 hours later, cells were fixed for fluorescence microscopy. For fixation, cells were washed with PBS, fixed with 4% (w/v) paraformaldehyde (PFA) for 20 minutes, washed and permeabilized with 0.1% saponin for 10 minutes, washed extensively with PBS (4x5 minutes), then blocked with 1% (w/v) BSA/PBS for 20 minutes at room temperature. Cells were washed with PBS twice before incubation with 5 µg/mL filipin (Sigma Aldrich) for 1 hour in the dark. Cells were subsequently washed with PBS (3x5 minutes) and coverslips were then dipped in deionised water, dried and mounted onto microscope slides with 5-15 µL Mowiol® (Sigma Aldrich) and left in a 37°C oven to dry overnight. Confocal microscopy was carried out at the Advanced Microscopy Facility in the Bosch Institute, University of Sydney, with a Leica Spe-II confocal microscope consisting of four solid-state lasers (405nm, 488nm, 532nm and 635nm) and one spectral detector. APO 63x and 100x oil immersion objective lenses were used. Images were collected using Leica LAS AF software. Image analysis was performed with ImageJ software (v1.47) (83).

1.2.8. Scratch assays using Incucyte

Scratch assays were conducted in 96-well plates. 1×10^4 cells/well were seeded into a 96-well plate and left to settle overnight. 24 hours later, a single scratch was made in each well using the 96-pinblock WoundmakerTM (Essen Bioscience) according to manufacturer instructions. Wells were washed with PBS to remove cell debris and treatment media replenished. Images were acquired using 10X objective on the IncuCyte ZOOM® (EssenBioscience) at regular time intervals and the wound area (area of the scratch) was used to calculate the Relative Wound Density (RWD%) at each time point as follows:

$$ RWD\ (\%) = \left(\frac{\Delta\ \text{Scratch Area}}{Scratch\ Area\ t = 0} \right) x100 $$

where Δ Scratch Area = Scratch Area$_{t=0}$ – Scratch Area$_{t=n}$ and n = test time point.

In some experiments, cells were treated with epidermal growth factor (EGF), LDL and lipoprotein-deficient serum (LPDS). For this, 2×10^5 cells/well were seeded into a 6-well plate and left to settle overnight at 37°C, 5% CO_2. Cells were then incubated overnight in growth media supplemented with 10% (v/v) LPDS at 37°C, 5% CO_2. Cells were then treated with LDL (50 µg/mL) and incubated overnight. 24 hours later, some of the cells were washed twice with PBS and media has been changed to an FBS-free media and incubated for 2 hours before adding EGF (10 ng/ml). Following these incubations, cells were analysed for wound healing (1.2.8.), lysed for western blot analysis (1.2.6.), or fixed for fluorescence microscopy (1.2.7.).

1.2.9. Analysis of lung metastasis *in vivo*

Lung metastasis in mice injected with A431 scramble and A431-NPC1KD cells was examined with the help of Dr. David Gallego-Ortega at the Garvan Institute of Medical Research (The Kinghorn Cancer Centre), Darlinghurst, New South Wales, Australia. Mice were maintained following the Australian code of practice and experiments were approved by the Garvan Institute of Medical Research/St. Vincent's Hospital Animal Ethics Committee (AEC# 14/27). Female NSG mice, a highly immunodeficient mouse strain commonly used for cancer xenograft modelling, were housed in pathogenic-free conditions in a 12-hour:12-hour light:dark cycle and given food and water ad libitum. Tumor engraftment in female NSG mice is well known to be more efficient

compared to their male counterparts. Therefore, 8 weeks old female NSG mice were injected into the tail vein with 250,000 A431 scramble (n=9) or A431-NPC1KD cells (n = 5) using a 100 μl injection into the dorsal tail vein. Mice were sacrificed 2 weeks after tumor cell inoculation. At the end of the experiment, mice were euthanized with CO_2 asphyxiation and the lungs were harvested and fixed for 4 hours in 10% buffered formalin at room temperature. After fixation, lungs were sectioned, stained with hematoxylin and eosin for histochemistry as per the manufacturer's instructions and the number of lung tumors were quantified.

1.3. Results

1.3.1. Identification of NPC1-deficient A431 cells

The Grewal group previously demonstrated that inhibition of cholesterol export from late endosomes reduced migratory and invasive cell behaviour (17, 86, 152) of mutant Chinese Hamster Ovary (CHO) (139) cells lacking NPC1. Alternatively, overexpression of the scaffold protein annexin A6 (68, 147) or the pharmacological NPC1 inhibitor U18666A (139, 140) was utilized to demonstrate that cholesterol accumulation in late endosomes inhibits cell migration and invasion (86, 87, 147). As outlined in the Aims (1.1.7.), to study aggressive cancer cell behaviour, more suitable cell models rather than CHO fibroblasts are still needed. The A431 squamous epithelial cell line is a well-established cell line with characteristic features of aggressive behaviour as judged by their high potential to migrate, invade and metastasize (142-144) and the Grewal group used ANXA6 overexpression or U18666A treatment to demonstrate reduced A431 cell migration/invasion in these settings (86, 87, 147).

We therefore aimed to establish a stable A431 cell line lacking NPC1 in order to study the effect of NPC1 deficiency on cancer cell motility, we aimed to establish a stable A431 cell line lacking NPC1. A431 wildtype cells were therefore transfected with different combinations of four NPC1 gene-specific (human) shRNA plasmids (see 1.2.2.3.). After 48 hours, cells were selected with 1.5 µg/mL puromycin and after 2 weeks, puromycin-resistant cells colonies were identified. For the confirmation of NPC1 knockdown in these colonies, cell lysates were prepared (1.2.3.), separated using SDS-PAGE and western blotting using an anti-NPC1 antibody was performed (1.2.5. – 1.2.6.). Extracts from CHO wildtype (CHO-WT) and NPC1-deficient CHO cells (CHO M12) served as positive and negative control, respectively. Western blots using an antibody against β-actin served as a loading control. The results are shown in Figure 1.3 (56).

As predicted, CHO-WT express substantial amounts of NPC1 (approximately 150 kDa), while the mutation in the NPC1 gene of CHO M12 cells leads to NPC1 deficiency. A431 cells transfected with shRNA plasmid mixtures 1-4, 1-3, 1+3 and 1+2 led to an approximately 40-60% reduction in NPC1 expression levels compared to puromycin-resistant A431 control cells. In these experiments, it should be noted that the detergent TX100 was used for the preparation of cell lysates. TX100 is widely used amongst researchers world-wide to lyse cells and extract proteins. Although the treatment of cells with TX100 generates a non-soluble pellet containing cytoskeletal elements and some membrane-associated proteins, this procedure very effectively solubilizes membrane

proteins, such as NPC1, and is commonly accepted to serve as a tool to compare protein levels by western blot analysis in cell models with high and low NPC1 (56-61) and other cholesterol transporters (22-33, 35-50).
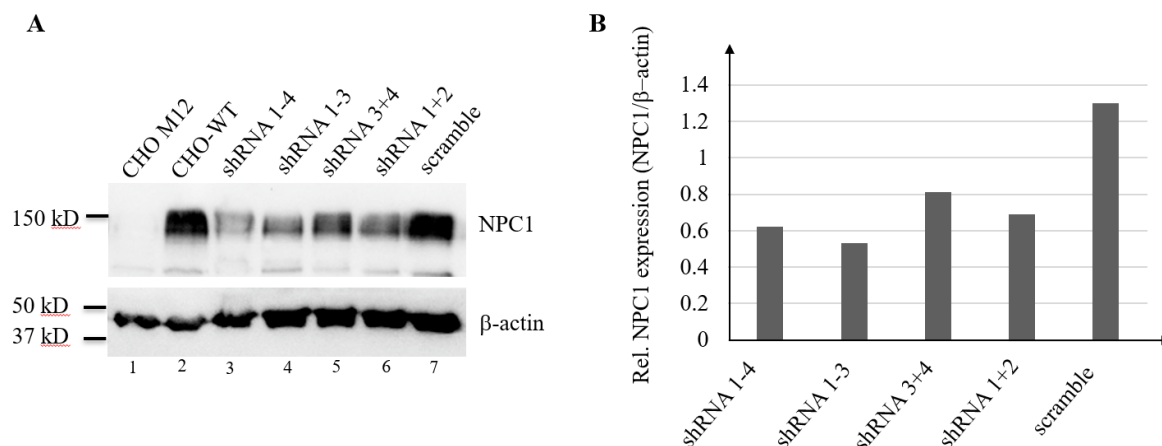
Figure 1.3: Western blot analysis of cell lysates from CHO M12, CHO-WT and A431 cells transfected with NPC1-targeting shRNAs. (A) Western blots are shown of cellular extracts from CHO M12, CHO-WT cells (lanes 1-2), A431 cells transfected with different combinations of shRNA plasmids targeting human NPC1 (shRNA1-4; lanes 3-6) and control shRNA plasmid (scramble; lane 7) as indicated. Cell extracts from CHO-wildtype (WT) and NPC1-deficient CHO M12 cells served as control for the NPC1 antibody. A431 cell extracts were prepared 72 hours after transfection, and 30 μg cell protein was separated by 10% SDS-PAGE and analyzed for NPC1 and β-actin by immunoblotting. The position of molecular weight markers is shown **(B)** Relative NPC1 expression levels in A431 cells (lanes 3-7) were normalized to β-actin (56). The A431 cell line (shRNA 1-4), which was characterized by at least a 50-55% reduction in NPC1 levels, was selected for further studies.

1.3.2. Cholesterol accumulation in NPC1-deficient A431 cells

Ever since the initial studies Liscum and coworkers (153), many researchers including the Grewal group, have demonstrated that NPC1 deficiency results in cholesterol accumulation in late endosomes due to an inhibition of NPC1-dependent cholesterol export from this compartment. Earlier studies were initially performed in NPC1 mutant CHO cell lines (153) and human NPC1 mutant fibroblasts (154).

In order to visualize cholesterol accumulation, in these studies, and many others (86, 87), the ability of filipin to bind unesterified cholesterol was used in fluorescence microscopy experiments. Therefore, to compare the relative amount and localization of free cholesterol in A431 cells in the presence or absence of NPC1, A431 cells expressing control shRNA (scramble) and NPC1-targeting shRNA 1-4 were fixed and stained with filipin (5 μg/mL) (section 1.2.7.)(56). A431 cells expressing the control shRNA (scramble) showed a normal distribution of cholesterol, which is characterized by filipin staining at the plasma membrane and the perinuclear region (ER/Golgi

apparatus) (see arrows and arrowheads in Figure 1.4A). In striking contrast, NPC1-depleted A431 cells displayed a strong filipin staining in an increased number of enlarged perinuclear vesicles (see arrows in panel B), which is comparable to other NPC1 mutant cell lines (56, 86, 153, 154), reflecting a greatly increased amount of free cholesterol accumulating in late endosomes (Figure 1.4B). Hence, based on the accumulation of cholesterol in endocytic compartments upon NPC1 depletion, these cells appeared suitable for further studies examining their motility and metastatic behavior (see below).
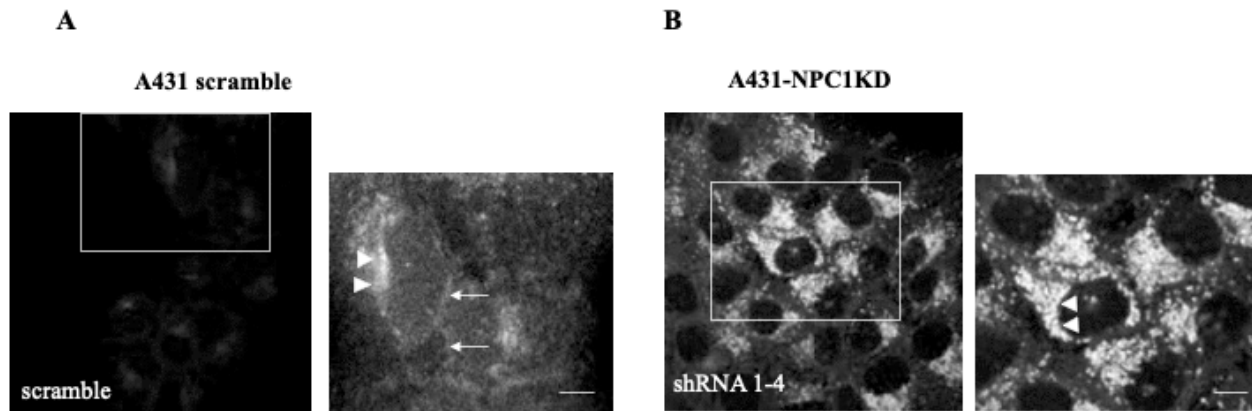
Figure 1.4: Late endosomal cholesterol accumulation in NPC1-depleted A431 cells. Cells were grown in normal media (10% FCS), fixed and then stained with filipin (5 μg/mL). (A) A431 cells expressing control shRNA (scramble). An enlarged section with enhanced filipin staining is shown. Arrows and arrowheads indicate filipin staining at the plasma membrane and the perinuclear region (Endoplasmic Reticulum/Golgi apparatus), respectively. (B) Inhibition of cholesterol export from late endosomes upon NPC1 depletion in A431 cells (A431-NPC1KD, shRNA 1-4) leads to an increased number of enlarged late endosomes that accumulate cholesterol. Arrowheads in the enlarged section highlight cholesterol-enriched late endosomes. Scale bar, 10 μm (56).

1.3.3. Reduced migration of A431 cells lacking NPC1

Cell migration is not only fundamental for the organization and maintenance of multicellular organisms but is also a critical feature of metastatic cancer cells, enabling the formation of secondary tumors (147). Forward movement of cells requires sufficient amounts of cholesterol embedded in the plasma membrane (17) and in the Grewal group, it was demonstrated that the function of cholesterol as a membrane constituent comprises several decisive features relevant for the spatiotemporal coordination of signalling and trafficking events during cellular movement (147). Based on the previous studies from Grewal and co-workers (86, 87, 147, 152), we hypothesized that cholesterol accumulation in A431 cells due to NPC1 deficiency would compromise cell motility.
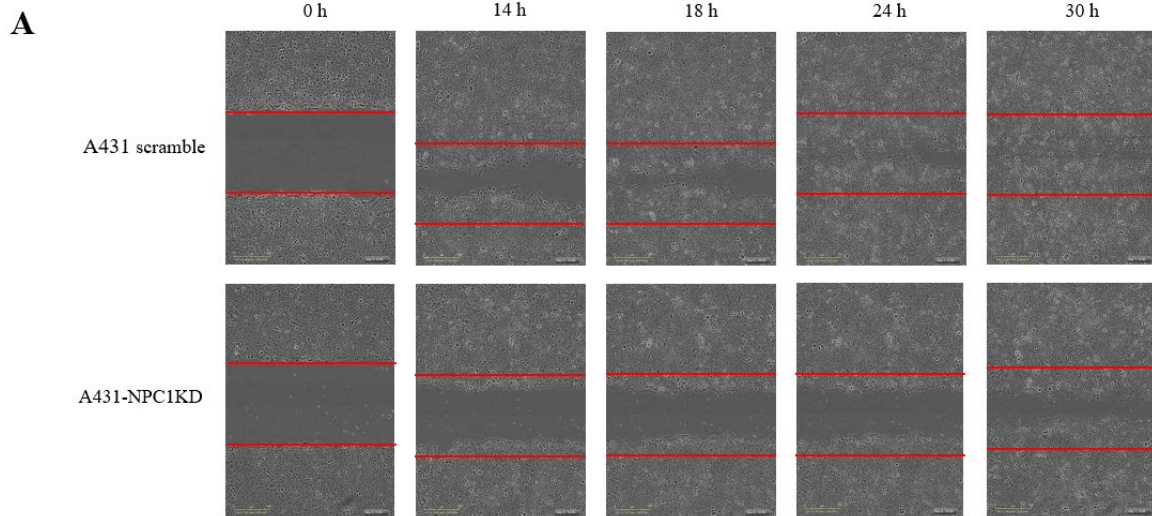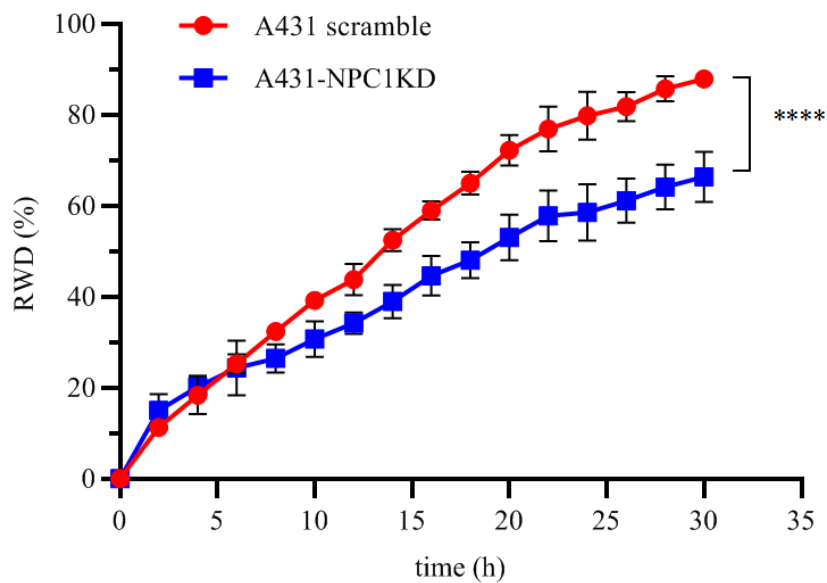
Figure 1.5: NPC1 depletion reduces A431 cell migration. **(A)** A431 cells stably expressing scrambled shRNA or shRNA targeting NPC1 were seeded in 96-well plates, grown until 90% confluency in 10% FCS containing media and then wound healing assays were performed as described in Methods (see chapter 2). Representative images at t = 0, 14, 18, 24 and 30 hours are shown. **(B)** The relative wound density (RWD %) at 2-hour intervals from 3 independent experiments with duplicate samples (Mean ± SD) was calculated using ImageJ. (***p < 0.001, Student's t-test) (56).

For further validation of this hypothesis, we selected our NPC1-depleted A431 cells (A431-NPC1KD) to study the migration behaviour of these cells. Therefore, A431 cells stably expressing scrambled shRNA (scramble) or shRNA targeting NPC1 were seeded in 96-well plates, grown until 90% confluency in 10% FCS-containing media and then wound healing assays were

performed as described (1.2.8.). The relative wound density (RWD %) at 2 hours intervals from 3 independent experiments with duplicate samples (Mean ± SD) was calculated using ImageJ (*** p < 0.001). Results are shown in Figure 1.5B.

As predicted, rapid migration of A431 control cells into the wound area led to approximately 50% wound closure after 12 hours and was completed (>90%) within 30 hours. In contrast, the migratory behaviour of A431-NPC1KD cells was comparable only in the initial 6 hours after the scratch. At later time points (14-30 hours post-scratch), A431-NPC1KD cell migration was approximately 20-25% slower compared to controls, never reaching complete wound closure at 30 hours (Figure 3.3A). Thus, loss of NPC1 expression and consequently, cholesterol accumulation in late endosomes, leading to reduced cholesterol levels at the plasma membrane and an overall unbalanced cholesterol distribution throughout the cell, is coupled to strongly reduced A431 cell migration (56).

1.3.4. EGF- and LDL-inducible A431 cell migration is not altered by NPC1 deficiency

Cholesterol is considered indispensible for cell migration. In fact, cholesterol depletion at the cell surface disrupts the integrity and dynamics of focal adhesion (dis-) assembly, caveolae formation, the recruitment and recycling of integrins, fibronectin-dependent cell migration, and Rac/Rho GTPase activation (87, 147, 152), all critical for forward cellular movement. Most of the cells generally acquire cholesterol through LDL receptor-mediated endocytosis, rather than synthesizing cholesterol *de novo* (10, 152).

EGF is a potent mitogenic factor that plays an important role in the growth, proliferation, and differentiation of numerous cell types (155, 156). In addition, EGF also stimulates integrin-mediated signalling to regulate cell spreading and motility functions and proven to accelerate cell migration (157). In addition, A431 cells express approximately 1-3 x 10^6 EGF receptors (EGFRs) on the cell surface, making this cell line a common and suitable model to investigate oncogenic features of EGFR overexpressing cancer cells, which is relevant for more than 30% of human cancers (27, 72, 73).

Given that many cancer cells, including A431 cells, show elevated LDLR levels and increased LDL uptake (152, 158, 159), along with the positive effect of EGF on cancer cell migration (156, 157), we investigated the impact of LDL and EGF on the migratory behaviour of A431 cells lacking NPC1. Therefore, A431 control and A431-NPC1KD cells were plated on 96-wells, grown

to 90% confluency, placed in 10% lipoprotein-deficient serum for 24 hours, followed by treatment with LDL (50 µg/ml), EGF (10 ng/ml) or both, prior to the wound healing assay (1.2.8).
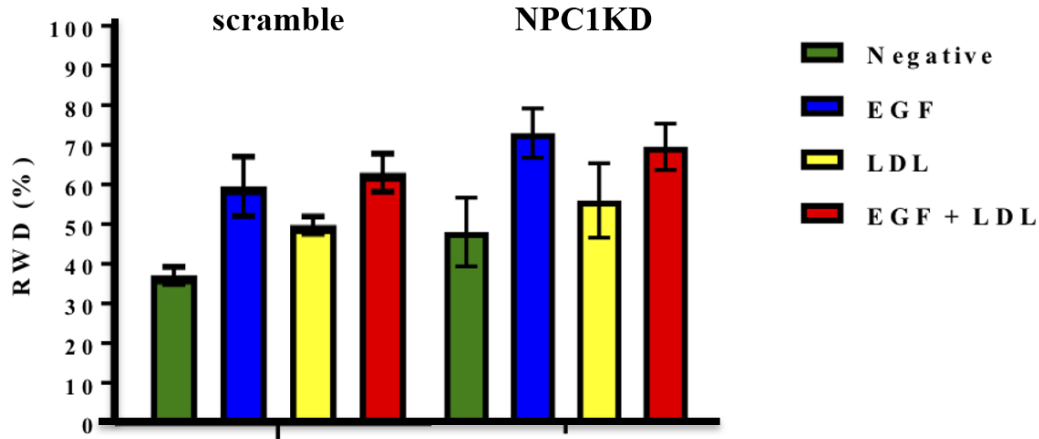
Figure 1.6: NPC1 depletion does not interfere with EGF-induced A431 cell migration. A431 cells stably expressing scrambled shRNA or shRNA targeting NPC1 were seeded in 96-well plates and grown until 90% confluency. Then wound healing assays ± 10ng/ml EGF and/or 50µg/ml LDL were performed as indicated (see Methods for details) and the relative wound density (RWD % ± SD) at 22h from triplicate samples (Mean ± SD) was calculated using ImageJ.

As described previously (27), EGF increased migration of A431 control cells by more than 15% (58.8 ± 7.4% vs 36.7 ± 2.2% at 22 hours) compared to the control. Likewise, incubation of A431 scramble control cells with LDL led to an increase (>10%; 47.2 ± 2.1% vs 36.7 ± 2.2% at 22 hours) compared to the control. Co-incubation of A431 control cells with EGF and LDL stimulated migration comparable to the EGF alone, indicating that both ligands were not capable of cooperatively stimulating A431 cell migration. In striking contrast to the significantly reduced migration of A431-NPC1KD observed in previous experiments (Figure 1.5), cell migration in A431-NPC1KD controls as well as after EGF and/or LDL treatment were similar. These unexpected findings are difficult to explain and could indicate that EGF signaling in NPC1-depleted A431 cell is not compromised, leading to a strong stimulation of NPC1KD cell migration upon EGF incubation. Based on our previous research (17, 86, 87, 147, 152), we hypothesized that loss of LDL-cholesterol distribution inside cells due to NPC1 deficiency would result in a loss of LDL-inducible migration (160). Also, loss of the shRNA-mediated NPC1 knockdown in these cells during the number of passages cannot be excluded and further experiments, ideally with stable NPC1 gene depletion using CRISPR technology (161) could clarify these findings.

1.3.5. Reduced lung metastasis of NPC1-deficient A431 cells *in vivo*

Tumor cells must efficiently generate energy and biomass components in order to expand and disseminate. Highly proliferative cancer cells show a strong lipid and cholesterol avidity, which they satisfy by either increasing the uptake of exogenous (or dietary) lipids and lipoproteins or over activating their endogenous lipid synthesis (160). Along these lines, A431 are established models to study aggressive migratory behavior. They express high LDLR and scavenger receptor BI (SR-BI) levels (152), deliver LDL-cholesterol to focal adhesions (44, 56, 57). and, like other highly invasive cancer cells, show enhanced α5β1 integrin recycling and FAK signaling (145).

As described above, LDL-derived cholesterol is crucial for cell migration using Niemann Pick Type C1 (NPC1) mutant CHO cells (86) as well as CHO and A431 cells overexpressing annexin A6, which display an NPC1-mutant-like phenotype (87). Progressing from the two-dimensional wound healing assays to experiments addressing the invasive potential of these cells, Grewal and co-workers then also demonstrated that CHO cells lacking NPC1, but also CHO as well as A431 overexpressing annexin A6, displayed reduced invasion in transwell migration and matrigel invasion chambers (86, 87). Moreover, in *in vivo* like settings using three-dimensional organotypic matrices that more closely recapitulate a tumor stromal environment, CHO and A431 control cells moved into organotypic matrices in much higher numbers compared to CHO cells lacking NPC1, or CHO and A431 cells overexpressing annexin A6 (86, 87). Taken together, these cell-based assays strongly indicated that blocking cellular distribution of LDL-derived cholesterol from late endosomes also reduced the invasive behaviour of cancer cells.

Hence, to investigate if loss of NPC1 in aggressive cancer cells would reduce their potential to metastasize, and we therefore performed *in vivo* experiments in collaboration with Dr. David Gallego-Ortega (Garvan Institute of Medical Research, Sydney, Australia) and investigated the metastatic behaviour of A431-NPC1KD cells. Therefore, A431 scramble and A431-NPC1KD cells were injected into the tail vein of 8 weeks old immunodeficient mice and 2 weeks after tumour cell inoculation, mice were sacrificed, and the lungs were harvested, fixed in formalin, sectioned and stained with hematoxylin and eosin for histochemistry (1.2.9.). In this experiment, 5 animals per group were analyzed and as predicted, the A431 scramble cells showed strong metastatic behaviour, with plenty of tumors being present in the lungs of animals already 2 weeks after tumor cell injection (Figure 1.7A). In striking contrast, the number of tumors in the stained lung sections analysed and derived from the A431-NPC1KD cells were reduced by approximately 50% (Figure

1.7A, for quantification see 1.7B). In a second and independent experiment, these striking differences between A431 scramble and A431-NPC1KD cells could not be confirmed, probably due to the infection of animals, compromising their overall health after tumor inoculation, requiring earlier sacrifice and limited tumor formation in the control group. Hence, despite the lack of statistical significance when analyzing 2 independent experiments (p=0.11), the findings from the initial experiment strongly suggest that the inability of NPC1-depleted A431 cells to distribute late endosomal cholesterol to other compartments, in particular focal adhesions at the plasma membrane, interferes with the invasive potential of A431 cells *in vivo*.
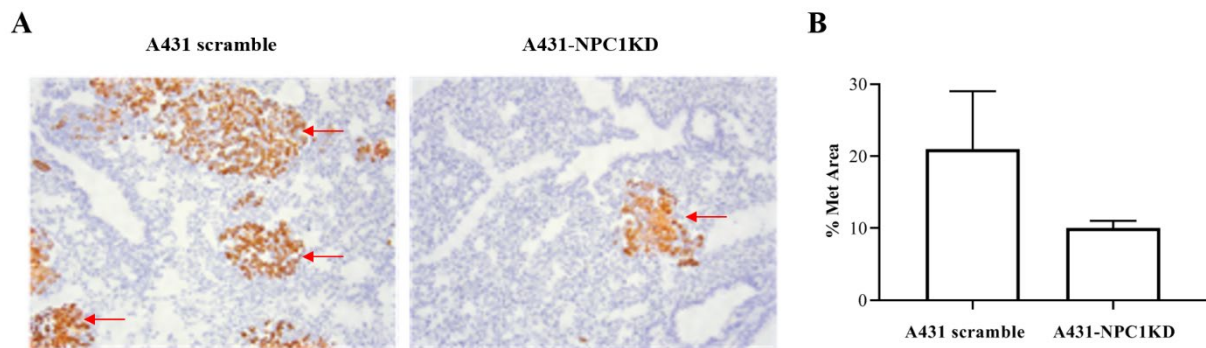
Figure 1.7: NPC1 depletion reduces lung metastasis. (A) 250,000 A431 scramble (n=9) and A431-NPC1KD cells (n = 5) were injected into the tail vein of 8 weeks old immunodeficient mice as indicated. 2 weeks after tumour cell inoculation, mice were sacrificed, and the lungs were harvested, fixed in formalin, sectioned, and stained with hematoxylin and eosin for histochemistry. Arrows indicate metastatic cancer cells. **(B)** Quantification of metastatic tumours in stained lung sections from mice injected with A431 scramble and A431-NPC1KD cells (p = 0.11, Student's t-test).

1.4. Discussion

1.4.1. The potential role of cholesterol export from late endosomes in cancer progression

Metabolic adaptations are now well recognized as additional hallmarks of cancer. This involves an increased demand for lipids, including cholesterol, driving cancer cell growth and metastasis (152). Within this context, numerous studies have focussed on the upregulated cholesterol synthesis pathway commonly observed in many cancer cells (3, 145, 146, 162), providing steroid hormones and other biomolecules that support cellular growth. In addition, despite controversial results from epidemiological studies assessing the potential of elevated LDL levels or statin use to predict risk and succession of certain cancers (e.g. breast, prostate) (3, 145, 146, 162), increased uptake of dietary cholesterol from LDL is also considered to promote cancer aggressiveness. Along these lines, hypercholesterolemia is associated with increased risk and advancement of prostate cancer (163). Moreover, accumulation of LDL-derived cholesteryl esters in lipid droplets promotes prostate cancer progression (138). Hence, blocking cellular uptake of LDL has become a therapeutic target to reduce cancer cell proliferation, and possibly the risk of developing secondary tumours (164). In support of this, inhibiting LDL endocytosis via LDLR depletion improved the performance of anticancer agents in pancreatic adenocarcinoma (105).

Once endocytosed and targeted to LE/Lys, LDL-derived cholesterol is distributed to other cellular compartments via NPC1 or additional cholesterol transporters to fulfill many functions that are related to cell growth, but also cancer cell migration (11). This includes the cholesterol-dependent establishment of caveolae at the cell surface (83), the secretion of extracellular matrix proteins, such as fibronectin (85), and importantly, the recycling of integrins to the cell surface (151) (see also Chapter 1.4.2. for further details). These findings indicate that blocking cholesterol export from late endosomes could improve current anticancer strategies. In line with this, Grewal and co-workers demonstrated that CHO cell lines carrying NPC1 mutations or human fibroblasts from NPC1 patients displayed strongly reduced migration and invasion in 2- and 3-dimensional migration/invasion assays (86). However, these cell types are not considered suitable cancer cell models and as outlined below, limited evidence has yet been provided that loss of NPC1 function could be beneficial to inhibit cancer aggressiveness.

1.4.2 The association of NPC1/2 with cancer

In recent years, accumulating evidence links elevated NPC1 expression levels with cancer incidence, progression, and patient outcome. For instance, elevated NPC1 expression was reported in metastatic estrogen receptor (ER)-negative breast cancer cells (165), and related to an increased risk to develop esophageal cancer (166) and decreased overall survival in glioma (167). Elevated NPC1 levels were also observed in imatinib- and daunorubicin-resistant leukemic cells. In these studies, NPC1 was proposed to support efflux of anticancer drugs and weaken anticancer therapies (168, 169). In esophageal adenocarcinoma, a rare gene fusion of NPC1 with maternal embryonic leucine zipper kinase, which drives proliferation, was found in two biopsies (170). In contrast, transient NPC1 knockdown or overexpression of a NPC1 mutant unable to bind cholesterol, inhibited proliferation, spreading and migration of several common cancer cell lines (56, 57, 86, 141, 152). Yet, NPC1 inhibition may not always protect against cancer development, as accumulation of cholesterol and other lipids can lead to liver injury during chronic inflammation. Hence, liver dysfunction in NPC patients may increase the risk of fibrosis, cirrhosis and ultimately, HCC development (171) (Table 1.4).

NPC1 and tumor characteristics	Cancer types
Cancer risk	esophageal cancer (166, 170), HCC (175)
Proliferation, migration, and invasion	A431 squamous carcinoma (56, 57, 86, 152), cervical cancer (141), ER-negative breast cancer (165), glioma (167)
Poor prognosis	ER-negative breast cancer (165), glioma (167)
Chemoresistance	breast cancer (172), leukemia (57, 169)
Therapeutic target	Itraconazole: basal cell carcinoma (173), non-small cell lung cancer (174), pancreatic cancer (175), prostate cancer (176) Cepharanthine: head and neck cancer (177), prostate cancer (178) Leelamine: metastatic melanoma (179, 180)

Table 1.4: Roles and therapeutic opportunities targeting NPC1 in cancer. Abbreviations: ER, estrogen receptor. Adapted from (56)

Most interestingly, the antifungal agent itraconazole was found to cause late endosomal cholesterol accumulation due to its ability to bind and inhibit NPC1 (173, 176, 181, 182). Moreover, this coincided with itraconazole downregulating the activity of mTORC1 kinase, reducing angiogenesis and tumor progression (174, 181-183). Together with itraconazole

improving cisplatin efficacy (181), this has resulted in Phase I and II clinical trials for non-small cell lung cancer (174), basal cell carcinoma (173), metastatic prostate (176) and pancreatic cancer (175).

Along these approaches to repurpose approved drugs the alkaloid cepharanthine used against acute and chronic diseases and the antihistamine astemizole should also be mentioned. Alike itraconazole, both drugs caused cholesterol accumulation in LE/Lys and inhibited mTORC1 signaling and endothelial growth and motility. Also, efficacy and adverse effects of anticancer drugs were reduced in the presence of these drugs (177, 178, 184). Finally, the lipophilic leelamine, which is a lysosomotropic compound, binds NPC1 and reduced export of cholesterol from LE/Lys. In cell models, this appeared to inhibit apoptosis- and motility- promoting signaling events (179, 180) (Table 1.4). Some of the potentially underlying mechanisms that make NPC1 inhibition a therapeutic target to reduce cancer metastasis are discussed below.

1.4.3. Squamous A431 epithelial cells as a model to study the role of LDL-cholesterol in cell migration

In more than 30% of human cancers, EGFR overexpression contributes to aberrant activation of effector pathways, promoting tumor progression (157, 158). Thus, the human squamous A431 epithelial cell line, with 1-3 x 10^6 EGFRs on the cell surface, has served as a model to investigate oncogenic features of EGFR-overexpressing cancer cells for several decades (121, 122, 142-144). Furthermore, like many other highly invasive cancer cells, A431 cells show enhanced integrin recycling and FAK signaling (145).(100).

Interestingly, cholesterol uptake in cancer cells is often closely linked to the signalling activity of EGFR (123). Additionally, downregulation of the LDLR in EGFR-related cancers reduced tumor growth (124). Likewise, A431 cells express high amounts of LDLR and take up substantial amounts of LDL (72, 113). In these cells, the Ikonen group and studies from our group in CHO cells were able to demonstrate that upon pharmacological NPC1 inhibition, or transient NPC1 depletion using siRNA, that LDL-cholesterol was delivered to focal adhesions at the cell surface in a NPC1-dependent manner to stimulate cell migration (44, 56). Likewise, annexin A6 overexpression in A431 cells, which induces a NPC1-like phenotype, interfered with integrin recycling, consequently reducing A431 cell migration and invasion (87). Similarly, siRNA-

mediated transient NPC1 knockdown reduced migration in the human cervical HeLa cancer cell line and human hepatoma HuH7 cells (141), (125).

Further support to evaluate NPC1 as a potential target for further research came from studies that showed reduced tumor growth upon inhibition of cholesterol export from late endosomes using itraconazole, cepharanthine, astemizole and leelamine (173-181, 183, 184) (see Table 1.4). Likewise, inhibition of acid sphingomyelinase (ASM), which blocks export of sphingosine as well as LDL-derived cholesterol from LE/Lys, showed potential as anticancer agent (180), strongly inhibiting cancer cell growth.

Despite the findings listed above, stable cancer cell lines lacking NPC1, or other cholesterol transporters in this compartment, such as STARD3 or Orp1L, reviewed in (11, 56), have yet not been available in the field to investigate their potential as targets to reduce cancer metastasis. Hence, to establish a model that would allow molecular mechanisms underlying cholesterol export from late endosomes to be developed as a candidate to inhibit aggressive cancer cell behaviour, we aimed to generate a stable A431 cell line lacking NPC1.

1.4.4. NPC1 deficiency reduces migratory A431 cancer cell behaviour

As described in detail in Chapters 1.3.1.-1.3.2., transfection of A431 cells with different combinations of shRNAs targeting NPC1 led to the establishment of several puromycin-resistant cell lines that displayed 40-60% reduced NPC1 protein levels. These cell lines were viable over multiple (>10-20) passages and did not display major defects in cell proliferation and morphology (see also Figure 1.5). This is a remarkable finding, as the pharmacological inhibition of NPC1, using U18666A (140), as well as treatment of cells with leelamine or ASM inhibitors (180-182, 184) induced cell toxicity, leading to cancer cell death. These findings indicate that cells are not viable upon effective/complete inhibition of NPC1 and/or late endosomal function using small molecules. This observation might also explain the lack of stable NPC1-deficient cell lines in the cancer field, as complete loss of NPC1-dependent cholesterol export or overall late endosomal function strongly compromises cell viability. Yet, partial depletion of NPC1 was still sufficient to cause cholesterol accumulation (Figure 1.4), as judged by the strong filipin staining in an increased number of enlarged perinuclear vesicles (1.3.2), matching the filipin staining patterns observed in NPC1 mutant cells observed by many others (139), (16, 18, 98, 99, 153). Hence, this NPC1-

depleted A431 cell line appeared most suitable for wound healing assays assessing the role of late endosomal cholesterol for the migratory behaviour of aggressive cancer cells (Figure 1.5).

As hypothesized, cholesterol accumulation in A431-NPC1KD cells lead to significantly reduced cell migration in wound healing assays (Figure 1.5) (56). Hence, proper functioning of the molecular machinery that distributes cholesterol from the late endosomal compartment is required for normal migratory behaviour of A431 cancer cells. This model is further supported by the ability of LDL to stimulate A431 cell migration (see scramble control in Figure 1.5). Nevertheless, EGF-induced EGFR activation more effectively stimulated migration in A431 cells compared to LDL. Interestingly, although we hypothesized LDL pre-loading to enrich cholesterol in specialized microdomains, such as lipid rafts and caveolae, we did not observe LDL to improve EGF-induced A431 cell migration (Figure 1.6). This observation adds to the controversial literature on the involvement of lipid rafts and caveolae in EGFR signalling (185). In particular in A431 cells, earlier studies investigating unphysiological and vigorous cholesterol depletion, using methyl-β-cyclodextrin (MβCD), caused EGFR hyperphosphorylation, while addition of cholesterol to cells with MβCD-cholesterol reduced EGF binding and EGFR activation (186). The underlying cause of these observations might in-part explain the unexpected ability of EGF to stimulate migration in A431-NPC1KD cells. However, it is important to note that manipulation of cellular cholesterol levels, in particular at the plasma membrane, using non-physiological MβCD or MβCD-cholesterol, are cytotoxic and differ greatly from the trafficking routes of endocytosed LDL-cholesterol. Hence, further studies are required to unravel the role of LDL and NPC1 in EGF-induced A431 cell migration. Overall, based on previous studies from the Grewal group and others (57, 83, 85-87), and data shown here; while lipids, including cholesterol, may activate signal transduction cascades or could be broken down into other bioactive mediators, that promote cell migration (160), it is tempting to speculate that NPC1-depleted A431 cells lack sufficient amounts of cholesterol embedded in the plasma membrane in order to move forward effectively (11, 56, 57, 87, 152).

1.4.5. Multiple migratory defects triggered by NPC1 loss-of-function

LDL-cholesterol from late endosomes reaches the cell surface via direct and indirect trafficking routes. The latter involves exocytic pathways via recycling endosomes or the Golgi apparatus (85-87), both trafficking routes being important for critical features in cell migration. Grewal and co-

workers demonstrated in earlier studies that pharmacological NPC1 inhibition or induction of a NPC1 mutant-like phenotype in A431 cells, using ANXA6 overexpression, inhibited caveolin trafficking from the Golgi apparatus to the cell surface, leading to reduced numbers of caveolae (82). These specialized and cholesterol-rich microdomains at the cell surface regulate integrin internalization during the transition from cell adhesion to cell migration (187). This link between NPC1 dysfunction and caveolin-1 is further highlighted by the upregulation of caveolin-1 in human and mouse NPC1 mutant models and the potential interaction of these two proteins to regulate late endosomal cholesterol export (188).

In addition to caveolin-1, several SNARE proteins within exocytic pathways are de-regulated upon NPC1 inhibition. Cholesterol accumulation in late endosomes caused mislocalization of the t-SNAREs Stx4 and SNAP23, leading to reduced secretion of extracellular matrix proteins (fibronectin) (85). These two SNARE proteins normally cluster in cholesterol-rich domains at the cell surface and one can speculate that other functions of these SNAREs, including integrin recycling (189, 190), Src kinase and FAK trafficking, as well as delivery of metalloproteases (MT1-MMP) to the cell surface, are also compromised (56, 191). Finally, NPC1 deficiency in CHO cells and human fibroblasts caused mislocalization of another SNARE protein, Stx6, which resulted in integrin mislocalization, and strongly reduced migration and invasion in 2- and 3-dimensional environments (86).

One can envisage that the multiple defects triggered by NPC1 loss-of-function or pharmacological NPC1 inhibitors described above, all contribute to the reduced migration observed in the A431-NPC1KD cell line. However, cell migration in this cell line is not completely blocked, and A431-NPC1KD cells still demonstrated a capability to move forward, even upon ~50-55% NPC1 depletion. Hence, future studies will have to clarify potential compensatory mechanisms, such as upregulation of other transporters in the late endosomal compartment, that A431-NPC1KD cells may develop to retain this basic feature of cellular behaviour.

1.4.6. Reduced lung metastasis of NPC1-deficient A431 cells *in vivo*

Although the wound healing assays discussed above revealed a compromised motility of A431-NPC1KD cells, this approach is rather considered a two-dimensional assay with limited implications for later stages of cancer progression *in vivo*. In fact, metastasis is highly complex, as the colonization of secondary organs requires the dissemination of tumour cells to distant sites

within the body. In these sites, cancer cells are required to attach locally, followed by their invasion into surrounding tissue to find a microenvironment that allows secondary tumor growth (192, 193).

These critical steps in invasive cell behaviour were assessed after tail vein injection of cancer cells and subsequent quantification of tumours after lung colonization. We reasoned that this approach would provide a rapid insight into how aberrant cholesterol trafficking in A431-NPC1KD would affect metastatic properties of A431 cells *in vivo*. Indeed, in collaboration with Dr. David Gallego-Ortega (Garvan Institute of Medical Research, Sydney Australia), we identified that 2 weeks after tumour cell inoculation, the histochemical examination of the lung tissue revealed a strongly reduced (~50%) number and size of lung tumours derived from A431-NPC1KD cells compared to the control (figure 3.5). Although these experiments, using 5 and 9 animals per group, respectively, did not reach statistical significance (p=0.11), it strongly supports a model that cellular distribution of late endosomal cholesterol is critical for cancer cell metastasis (56). The underlying causes for the reduced ability of NPC1-depleted A431 cells to effectively colonize lung tissue remain to be determined. NPC1 dysfunction strongly reduces cholesterol levels at the plasma membrane and many reports suggest that this compromises the functioning of lipid rafts as signalling hubs required to establish invasive behaviour (194). Alternatively, NPC1 deficiency interfering with cell surface expression of integrins, but also tetraspanins, could reduce cell attachment and invasion of lung tissue (15, 90). In addition, recent studies from the Grewal group indicate that pharmacological inhibition of LDL-cholesterol export from late endosomes in A431 cells strongly reduces the secretion of metalloproteases (MMPs), such as MMP9 (J. Jose and T. Grewal, unpublished data), which critically influence invasive properties of cancer cells (195, 196). Given the multiple pathways that might be sensitive to the adequate delivery of late endosomal cholesterol for proper functioning, one can envisage that the identification of underlying mechanisms for the reduced invasiveness of A431-NPC1KD cells *in vivo* will be challenging. Thus, rather than using whole animals, future studies in three-dimensional culture models, which closely recapitulate the heterogeneous features of the tumor microenvironment and are highly suitable for experimental manipulation (197, 198), seem appropriate.

Chapter 2

Annexin A6 expression patterns in human cancers

2.1. Introduction

As outlined in Chapter 1.1.3.6., ANXA6 is the largest member of the highly conserved annexin protein family, which is characterized by their Ca^{2+}-dependent binding to cellular membranes. Many cell- and animal-based studies that have been performed over the years established that ANXA6 is predominantly located at the plasma membrane, early and late endosomes, acting as a multifunctional scaffold protein (67, 199-201). Major ANXA6 functions in these locations include the formation of multifactorial protein complexes and the regulation of endo-/exocytic membrane transport, both aspects most relevant for signal transduction, but also cholesterol homeostasis (67, 68, 199-203). Given the various cellular locations and interaction partners, ANXA6 is now well believed to participate in the regulation of cell proliferation, migration, survival, differentiation, and many other cellular activities. Over the last decade, the Grewal group and others identified that some of these ANXA6-related functions are relevant in cancer cell growth, migration and invasion (27, 55, 72-74, 147, 204, 205). Most relevant for cancer cell metabolism, ANXA6 upregulation induced cholesterol accumulation in late endosomes similar to the NPC1 mutant phenotype (55, 68, 82, 83, 202), and was accompanied by reduced growth, but also decreased migratory and invasive behaviour of several cell lines, including A431 cells, the latter representing a classical model for aggressive cancer cell behaviour (27, 55, 73, 74, 147). As described in Chapter 1, inhibition of cellular cholesterol distribution in NPC1-deficient A431 cells also reduced migratory and invasive behaviour (1.3.2.-1.3.5.). Taken together, these findings indicated that ANXA6 levels could be relevant for cancer progression, possibly in cancers that may be linked to de-regulated cholesterol homeostasis and/or increased responsiveness to an oversupply with exogenous cholesterol (55, 147, 152).

The ANXA6 gene is is 68.5 kB long, located on the 151 MB region of human chromosome 5 NC000005.10 and consists of 26 exons. The longest ANXA6 protein isoform of 673 amino acids is about 68kDa and comprises a unique N-terminus and (each eight 68 amino acids repeats separated by a linker sequence between repeats 4 and 5. In fact, ANXA6 is the only annexin with

eight annexin repeats, most likely due to the duplication and fusion of the genes encoding ANXA5 and ANXA10 (67, 206) Due to alternative splicing in exon 21, which is located in the seventh repeat, cells commonly express two isoforms that vary by only 6 amino acids at position 524–529 (VAAEIL) (206, 207). Relatively little is known about the regulation of ANXA6 gene expression. Earlier studies identified several binding sites for the transcription factor SP1 in the human ANXA6 promoter region, which were proposed to be responsible for the high and ubiquitous ANXA6 expression observed in many cell types (208). In addition, epigenetic silencing of ANXA6 expression seems to occur, as the CpG-rich ANXA6 promoter is heavily methylated in several EGFR overexpressing cancer cells and estrogen receptor (ER)-negative breast cancer cells with low ANXA6 levels (74).

Up until recently, overall information about ANXA6 expression levels in humans has been limited. In fact, current knowledge in the annexin field is mainly built on expression studies using human and rodent cell lines as well as tissues from mouse and rat models. Based on these studies, ANXA6 is considered to be highly abundant in endothelial and endocrine cells, hepatocytes, as well as macrophages, but low/undetectable in epithelial cells of the small intestine, colon, and the parathyroid gland (203, 209).

2.2. Aims

Numerous studies have examined ANXA6 expression levels in human cancers (reviewed in (76, 210)). These studies were predominantly based on data sets derived from small and local patient cohorts. In this chapter, we aimed to address if previously established relationships in various cancers between ANXA6 gene expression levels and based on small patient collections could be validated in larger patient cohorts. With the increased availability of larger expression data banks from humans in disease settings such as cancer, we aimed to search publicly available expression data on ANXA6 expression levels in different cancers, including those that are considered cholesterol-sensitive. This approach would provide a more detailed view of the relationships of up- or downregulated ANXA6 expression levels in various cancer and allow a comparison to previously published data on ANXA6 expression levels in relation to different tumors.

For a better appreciation of ANXA6 expression in chronic disease, in Chapter 2.4.1, we first aimed to gather information on ANXA6 expression in normal human tissues. We then collected

ANXA6 expression data in cancer tissues and wherever possible, aimed to compare those findings to normal tissues (Chapter 2.4.2) to possibly establish a relationship between changes in ANXA6 expression levels and tumor onset, occurrence and progression in cholesterol-sensitive cancers, such as breast cancer subtypes and during prostate cancer progression (2.4.3-2.4.4). This is followed by an examination of ANXA6 expression levels in patient survival curves, aiming to possibly identify relationships between high and low/medium ANXA6 expression levels and patient survival probability in cancers that have been shown to be affected by cholesterol availability such as breast, pancreatic, colon, liver and prostate cancers (Chapter 2.5.).

2.3. Methods

In order to investigate ANXA6 expression levels in normal and cancer tissue samples, data was retrieved from the following web-based expression data platforms: The Human Protein Atlas (HPA) (211), Gene Expression Profiling Interactive Analysis (GEPIA) (212) and the University of ALabama at Birmingham CANcer data analysis portal (UALCAN) (213).

2.3.1. The Human Protein Atlas (HPA)

The Human Protein Atlas (HPA) was initially developed in 2003 (211)a web-based interface, using R package to map human protein expression patterns based on multiple technologies including imaging, proteomics, and transcriptomics. *HPAanalyze* is the R-based software that was developed to retrieve and perform exploratory analysis of data from HPA (214) and employed antibody-based tissue micro-array profiling and RNA deep-sequencing. This generated proteomics and transcriptomics data from human non-malignant tissues, cancers, and cell lines with cell type-specific expression patterns via an innovative immunohistochemistry-based approach (214). HPA contains full datasets as downloadable compressed Tab-Separated Value (TSV) or individual entries in Extensible Markup Language (XML), Resource Description Framework (RDF), and TSV formats (214). The *HPAanalyze* package includes *hpaVisTissue* for normal tissue samples, *hpaVisPatho* for pathology/cancer samples, and *hpaVisSubcell* for subcellular localization data, whichcan be easily accessed through the umbrella function *hpaVis* (214).

The Human Protein Atlas consists of twelve separate sections (https://www.proteinatlas.org/), covering (i) protein distribution across 44 normal human tissue types based on antibody profiling using conventional and multiplex immunohistochemistry, (ii) the hierarchical expression

landscape from 13 regions of the brain, (iii) all protein-coding genes in 536 individual cell type clusters corresponding to 15 different cell type groups. based on scRNAseq analysis, (iv) expression of protein-coding genes in human cell types based on bulk RNAseq data, (v) protein levels and survival of cancer patients based on mRNA and protein expression data from 17 different cancers, together with in-house generated immunohistochemically stained tissue sections images and Kaplan-Meier plots showing the correlation between mRNA expression and cancer patient survival, (vi-xii) protein levels in blood, immune cell types, secretome and subcellular locations and cell-line derived expression pattern as well structural and metabolic information.

2.3.2. Gene Expression Profiling Interactive Analysis (GEPIA)

GEPIA was developed using R (version 3.3.2) and Perl (version 5.22.1) (212) and is built by the HTML5 and JavaScript libraries, including jQuery (http://jquery.com), Bootstrap (http://getbootstrap.com/) for the client-side user interface (http://gepia.cancer-pku.cn/). GEPIA has gene expression data from 9736 tumors and 8587 normal samples from the Cancer Genome Atlas (TCGA) and the GTEx databases based on RNA sequencing data. Analysis results cover ~20 000 coding and ~25 000 non-coding genes, as well as ~14 000 pseudogenes and ~400 T-cell receptor segments (212). GEPIA not only provides information on gene expression patterns but can also be utilized for the screening for drug target, oncogenes or suppressor genes, survival analysis and gene correlations analysis in cancer cohorts.

2.3.3. The University of ALabama at Birmingham CANcer data analysis Portal (UALCAN)

UALCAN has been developed by the University of Alabama (Birmingham, USA) profiling genomic, transcriptomic, and proteomic expression data (213) (https://ualcan.path.uab.edu/index.html). UALCAN is based on the TCGA database allowing access to RNA-seq data for approximately 20,000 protein-coding genes in 33 different tumor types (213) for analysis of gene and protein expression and correlation with survival and methylation patterns (213).

2.4. Results

2.4.1. ANXA6 expression in normal tissues

TCGA is one of the most commonly recognized genomics visualization datasets used worldwide by researchers and genomic tool developers. TCGA has produced RNA-Seq data for 9736 tumor samples across 33 cancer types as well as 726 adjacent normal tissues. This imbalance between tumor and normal sample numbers has previously limited efficiency when aiming to identify differential gene expression pattern in cancer vs. normal tissues (212). In contrast, the Genotype-Tissue Expression (GTEx) project aimed to allow comparison ad identify correlations between genetic variation and tissue-specific gene expression in non-diseased individuals, consisting of RNA-Seq data from >8000 normal samples, albeit from unrelated donors (212, 215). The UCSC Xena project then made all the datasets from the different sources within GTEx compatible (212). Altogether, GTEx now allows users to compare TCGA-derived gene expression from tumor samples to corresponding GTEx normal samples (216, 217) (211, 215, 216, 218, 219). Yet, although in line with previously published expression patterns derived from cell lines and animal models (data not shown), all of the abovementioned datasets provided information only on ANXA6 mRNA expression, lacking information on ANXA6 protein levels,

In contrast, the Human Protein Atlas (HPA), has mapped human proteins via multiple technologies including imaging, proteomics and transcriptomic (see Methods) (214), covering not only ANXA6 mRNA data, but also ANXA6 protein levels in various normal tissues and cell types (Figure 2.1-2.2). We therefore examined the ANXA6-related information in this dataset more closely. In support of the earlier studies that were mainly based on rodent tissues (203, 209), highest human ANXA6 mRNA expression levels were found in smooth muscle, adipose tissue, ovary, and appendix. Interestingly, seminal vesicles, which represent the tubular glands close to the urinary bladder that secrete fluid as part of semen, also express high ANXA6 levels. On the other hand, ANXA6 mRNA expression in the liver, considered to be very high in mice and rats, making approximately 0.25% of total liver protein (202, 220), was at medium levels and comparable to ANXA6 levels in numerous other tissues (e.g. tonsil, lymph nodes, spleen, prostate, breast, placenta, gall bladder and others). In support of earlier studies being unable to detect ANXA6 expression in epithelial cells of the parathyroid gland, normalized data from human tissues also revealed only small amounts of ANXA6 mRNA in this tissue. ANXA6 mRNA levels were also very low in salivary gland, duodenum, small intestine and lowest in the pancreas. The

latter finding could indicate a critical regulatory role of ANXA6 in this tissue, requiring a tight control of ANXA6 gene transcription. Indeed, several reports recently proposed therapeutic potential to target ANXA6 in pancreatic cancer (see also Chapter 3-4) (221, 222).
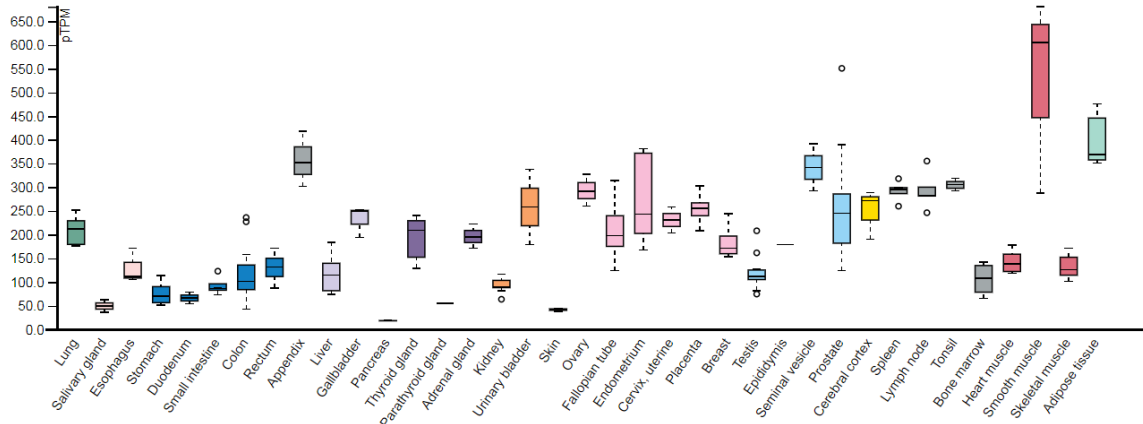
Figure 2.1: ANXA6 mRNA expression in normal tissues (HPA dataset). Individual samples from the HPA dataset and based on multiple RNA sequencing analyses are visualized with box plots shown as median and 25th and 75th percentiles. Outliers that are above or below 1.5 times the interquartile range are also shown.

As mentioned above, the HPA data set also contains information on relative ANXA6 protein expression levels in human tissues (Figure 2.2). This information has been obtained from the relative staining intensity in immunohistochemical studies of tissues, utilizing three different commercial rabbit polyclonal antibodies that were generated on the basis of human ANXA6 protein fragment sequences (211). The staining intensity of two of these three antibodies was consistent with the RNA expression data across 36 tissues, indicating that despite some unspecific signals observed in western blot control experiments (211), findings derived from these antibodies reflect relative ANXA6 protein expression patterns. It should be pointed out that absolute ANXA6 protein levels cannot be obtained from these datasets, as standardisation of signal intensity across different studies utilizing different antibodies and methodologies, together with the lack of standards that would relate to a defined amount of ANXA6 proteins in most proteomic approaches, have made it up to date impossible to precisely define protein levels of ANXA6 (and most other proteins) in a given cell line or tissue. Despite these limitations of the HPA dataset, the overall information gained from these studies is still very insightful. Thus, ANXA6 protein levels in the

HPA dataset are scored as high, medium, low, or not detectable. In line with the ANXA6 mRNA expression data (Figure 2.1), ANXA6 protein levels in smooth muscle were considered high. Also, in agreement with the ANXA6 mRNA expression data (see Figure 2.1), ANXA6 protein levels appeared non detectable in several tissues, including the salivary gland, duodenum, and small intestine. Yet, several tissues with moderate (cerebellum, adrenal gland, testis, placenta, lymph node, tonsils) to low ANXA6 mRNA levels (pancreas) were also scored as containing high ANXA6 protein levels.

In addition, several other differences were observed when comparing the ANXA6 mRNA and protein expression patterns. A large number of tissues, including those with high ANXA6 mRNA levels, such as adipose tissue, ovary, and appendix, expressed medium ANXA6 protein levels. On the other hand, some tissues with high-medium ANXA6 mRNA levels, such as prostate and skeletal muscle, contained low ANXA6 protein levels according to the HPA dataset. The latter is somewhat surprising, as other studies in the field implicated significant amounts of ANXA6 not only in smooth muscle, but also skeletal muscle (223, 224).

As mentioned above, the differences between ANXA6 mRNA and protein levels in a given tissue were most apparent in the pancreas. HPA, GTEx, FANTOM5, but also the TCGA databases all listed pancreas as the tissue with the lowest ANXA6 mRNA levels (211, 212, 215, 218, 219, 225-227). However, pancreas was among the organs with the highest relative ANXA6 protein levels. Within the pancreatic tissue, relative ANXA6 protein levels were particularly scored very high in the islets of Langerhans cells (211, 218, 219).
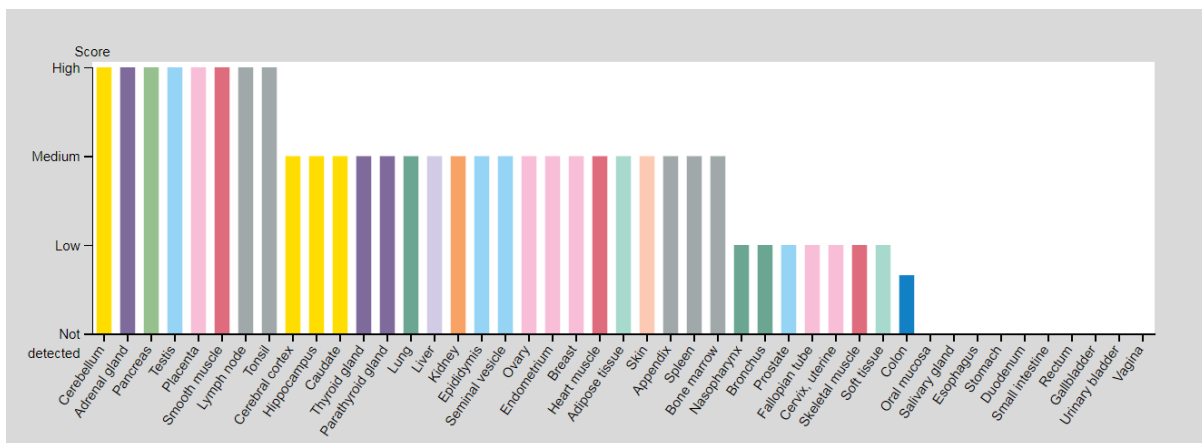
Figure 2.2: Annexin A6 protein expression in normal tissues (HPA dataset) . Relative ANXA6 protein expression levels from 44 tissues were scored as high, medium, low, or not detectable as indicated. Color-coding is based on tissue groups in the same location and/or with common functional features.

Taken together, despite many researchers in the field still considering ANXA6 and other annexins to be ubiquitously expressed, the analysis of ANXA6 protein levels in normal tissues revealed a substantial number of tissues with low to non-detectable ANXA6 protein amounts. On the other hand, at least in rodents, ANXA6 is considered to represent 0.25% of total liver protein, and we speculate that all human tissues scored with high-medium ANXA6 protein levels, represent tissues with substantial amounts of ANXA6 protein.

Interestingly, for many tissues, high ANXA6 mRNA expression did not correlate with high ANXA6 protein levels, and vice versa, low ANXA6 mRNA did not always reflect lack of ANXA6 protein expression. Thus, tissue-specific regulatory mechanisms are likely in place, possibly influencing ANXA6 mRNA transcription, as well as post-transcriptional or post-translational processes that could explain the diversity observed in ANXA6 expression levels in the various normal human tissues. In cancer and other chronic diseases, one post-transcriptional aspect that is increasingly considered relevant to explain differential mRNA and protein levels of a given gene, is the role of micro-RNAs (miRNAs). These short non-coding single-stranded RNAs can bind to the 3′ (and less often to the 5') untranslated regions or coding regions of their mRNA targets, which are subsequently degraded or translationally repressed. While little is yet known about miRNAs targeting ANXA6 in human cancer (228, 229) This might contribute to differential ANXA6 mRNA and protein expression patterns in cancer, which will be examined and discussed in the following chapters (2.4.2.-2.4.3.).

2.4.2. Expression patterns of ANXA6 in cancer tissues
2.4.2.1. Overview and current knowledge

Over the years, increasing evidence points at ANXA6 being either a tumor suppressor or tumor promoter depending on the cell- or animal model analyzed (76, 147, 199, 205, 210). As described in the Introduction (Chapter 1.1.1.6), the involvement of ANXA6 in tumor progression is complex, but may predominantly involve Ca^{2+}-dependent scaffolding functions that alter the activity of signaling complexes and/or the ability of ANXA6 to influence cholesterol metabolism in cancer cells, with consequences for cell proliferation, motility and differentiation (71, 76, 147, 199, 205).

While the underlying mechanisms in the various tumor models are still not fully understood (see Introduction), it is generally believed that changes in ANXA6 expression levels critically contribute to either promote or inhibit cancer cell growth and aggressiveness.

The Grewal group initially focussed on cancer models with low ANXA6 expression. In these cell and animal models, low ANXA6 levels were linked to elevated activity of the EGFR/Ras pathway, which drives oncogenic behaviour in many human cancers (199, 205). This includes A431 cells, a vulval squamous epithelial carcinoma cell line, which overexpresses the EGFR and shows elevated Ras/MAPK activity but lacks endogenous ANXA6 (72, 230). Overexpression of ANXA6 in A431 cells reduced EGFR and Ras/MAPK signalling, which coincided with reduced tumor growth in cell culture and *in vivo* (27, 73, 143). Follow-up studies from Grewal and co-workers then identified ANXA6 downregulation in EGFR overexpressing and ER-negative breast cancer cell lines (73, 74), findings that were later supported and extended to tumor patient samples by others (201, 204, 231). Over the years, ANXA6 has also been found downregulated in the highly malignant forms of gastric cancer (232), hepatocellular carcinomas (233), cervical cancer (234, 235) and the progression of melanomas (236). On the other hand, ANXA6 levels were upregulated in the progression of ovarian carcinomas (237), thyroid cancer (238), polycystic ovarian syndrome (239), pancreatic cancer (221, 222), oesophageal adenocarcinoma (240) and acute lymphoblastic leukemia (241). The various studies implicating ANXA6 tumor suppressor and tumor functions are summarized in Table 2.1.

Proposed ANXA6 functions in cancer	Cancer types
Tumor suppressor	EGFR overexpression: A431, MDA-MB-468 (breast), Fadu (head and neck); ER-negative breast cancer cell lines (73, 74, 201, 204, 231), gastric cancer (232), hepatocellular carcinomas (233), cervical cancer (234, 235) melanoma progression (236).
Tumor promoter	progression of ovarian carcinomas (237), thyroid cancer (238), polycystic ovarian syndrome (239), pancreatic cancer (221, 222), oesophageal adenocarcinoma (240) and acute lymphoblastic leukemia (241).

Table 2.1: Potential ANXA6 tumor suppressor and promoter functions. Abbreviations: EGFR, epidermal growth factor receptor; ER, estrogen receptor. Adapted from (11).

Thus, the determination of ANXA6 levels may provide diagnostic, prognostic, and therapeutic potential in cancer progression, such as treatment efficacy, recurrence, and overall survival in triple-negative breast cancers (76, 210). Yet, the studies and conclusions listed above are

commonly based on the analysis of a single cohort, often with a limited number of samples. For example, only 57 tumor samples were analyzed by O'Sullivan and co-workers (221), proposing ANXA6 as a therapeutic target in pancreatic cancer, and 34 samples by Noreen *et al* (242), implicating ANXA6 as a biomarker in ovarian cancers, respectively. Alternatively, potential tumor suppressor or promoter functions of ANXA6 mainly reflected the interpretation of studies using cell- or animal tumor models (67, 73, 74, 201, 204, 210, 211, 227).

2.4.2.2. ANXA6 expression patterns derived from larger cancer datasets

A more unbiased approach was performed next, and we examined if ANXA6 expression levels collected in larger data sets would also correlate with cancer incidence, we next compared ANXA6 expression levels in 18 different human cancers available in the Gene Expression Profiling Interactive Analysis (GEPIA) dataset, focussing on cancers that have been linked to cholesterol homeostasis and/or been reported to exhibit ANXA6 up- or downregulation. This collection of expression data is based on normalized TCGA and GTEx datasets (212) (Figure 2.3).
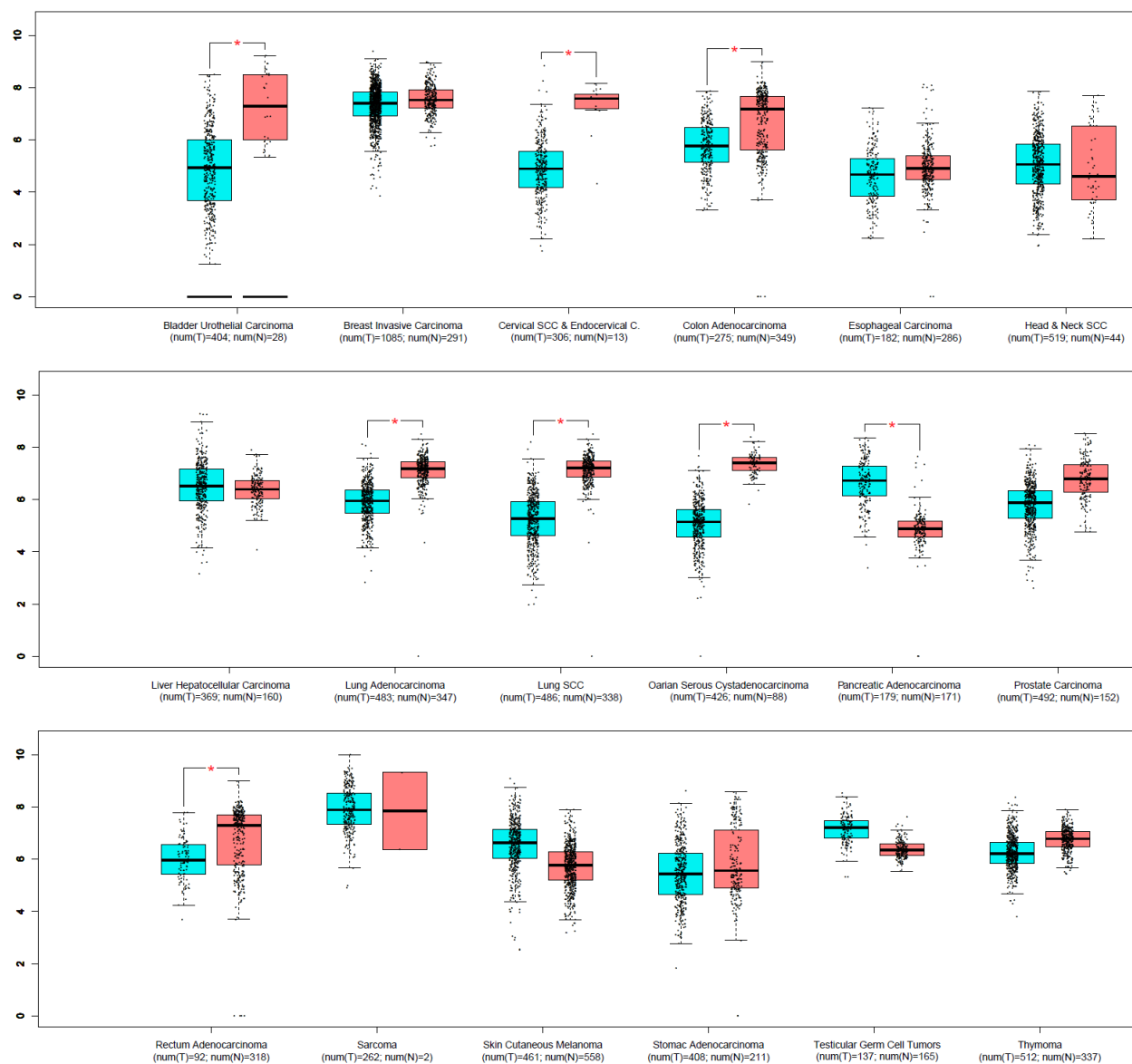
Figure 2.3: Relative Annexin A6 mRNA levels in normal (pink) and malignant tissues (cyan) (212). The origin of different cancers and the total tumor (T) and normal (N) sample numbers based on the GEPIA dataset are given. Individual data points and median box plots are provided (*, $p < 0.05$).

Several cancers, including bladder, cervical, non-small cell lung carcinoma, as well as adenocarcinoma in colon, lung, ovarian, rectum and prostate carcinoma displayed in part significantly reduced ANXA6 levels compared to normal tissues, supporting some (234, 235), but not all of the previously published studies, such as data from ovarian-related cancers (237, 239). ANXA6 levels remained rather unchanged in breast invasive carcinoma, esophageal carcinoma,

head and neck cancers, liver hepatocellular carcinoma, skin cutaneous melanoma, stomach adenocarcinoma and thymoma. Yet, samples from pancreatic adenocarcinoma revealed a significant increase of ANXA6 levels, which is in line with studies reporting elevated ANXA6 in pancreatic cancers (221, 222). On the other hand, ANXA6 downregulation observed in several studies, including those from the Grewal group, in EGFR overexpressing squamous epithelial carcinoma (72, 230), EGFR overexpressing and ER-negative breast cancer (73, 74) , (201, 204, 231), EGFR overexpressing head and neck cancers (74), as well as gastric cancer (232), hepatocellular carcinomas (233), and melanomas (236) were not evident in the GEPIA dataset.

Taken together, previously published correlations between ANXA6 levels and cancer incidence and progression (232-236, 238-242) do not fully reflect data available from the TCGA and GTEx databases. This strongly indicates a greater diversity with multiple subtypes within cancers from a particular tissue. This also suggests that ANXA6 expression levels reported to be altered in some, often small, cohorts published previously, may reflect ANXA6 expression patterns in a specific cancer subtype that is easily overlooked when datasets from diverse cancer subtypes within cohorts are pooled.

2.4.2.3. ANXA6 expression levels in prostate cancer progression

Based on the findings derived from breast cancer subtypes (73, 74, 201, 204, 231), we reasoned that possibly only certain subtypes in other cancers may reveal correlations between ANXA6 expression levels and disease incidence and progression.

As described above and based on the GEPIA dataset (Figure 2.3, middle panel, far right), ANXA6 levels appeared slightly, but not significantly, decreased in prostate carcinoma. In addition, accumulating evidence suggests a role for cholesterol in prostate cancer, as hypercholesterolemia is linked to increased prostate cancer risk and progression (163, 243, 244) and the accumulation of LDL-derived cholesteryl esters has potential as a biomarker for advanced prostate cancer and aggressiveness (138, 239, 245).

Given the role of ANXA6 in LDL-cholesterol uptake and distribution (55, 67, 68, 82, 83, 147, 152, 199), we speculated that high and/or low ANXA6 levels might be linked to prostate cancer progression, which is a multistep process (246-248). In early localized stages, growth of prostate cancers depends on androgens and androgen receptor. While inhibition of androgen signalling leads to a temporary regression, prostate cancer commonly relapses, becoming androgen-

independent, followed by metastatic events that allow the cancer to spread to other organs. In recent years, several studies have therefore attempted to characterize the gene expression profiles of early and advanced prostate cancers.

In initial studies, Tomlins and co-workers aimed to profile gene expression patterns in prostate cancer progression. Using laser-capture microdissection to isolate 101 cell populations, prostate cancer progression from benign epithelium to metastatic disease was determined and profiled (247). In collaboration with Dr. Zeyad Nassar (Adelaide Medical School, University of Adelaide, SA, Australia), the publicly available data set from these studies was assessed for an association of ANXA6 expression levels with prostate cancer progression. The complex data set for prostate cancer progression was analyzed using the Molecular Concept Map (MCM), an analytic program that allows to identify associations among all gene sets in the database, enabling the identification and visualization of 'enrichment networks' of linked concepts. However, in this study, ANXA6 expression was comparable in benign, localized and metastatic prostate cancer samples (247) (Figure 2.4A).
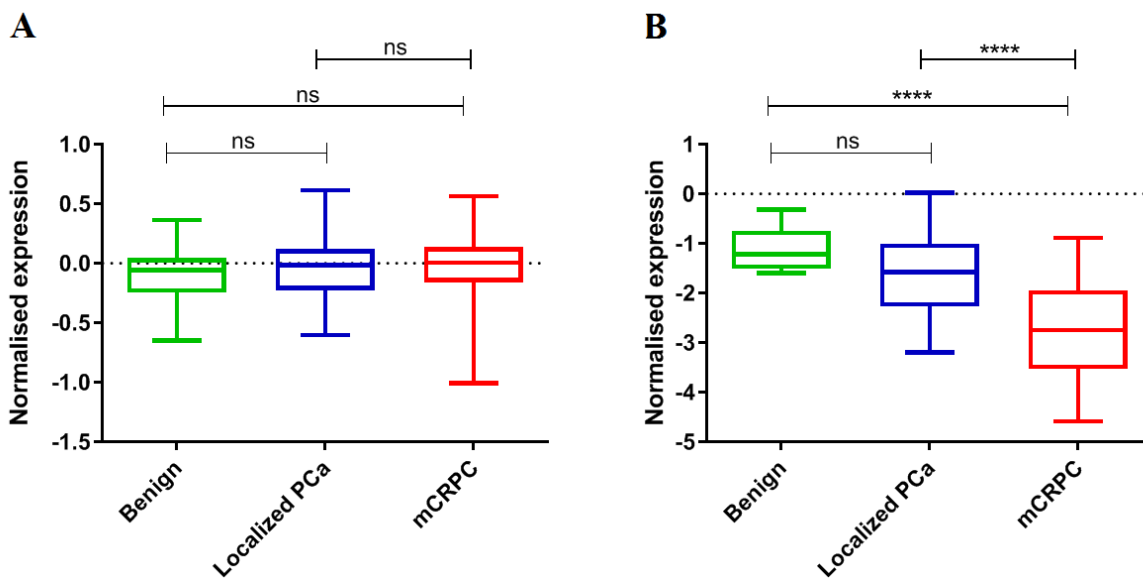
Figure 2.4: **ANXA6 levels in prostate cancer progression. (A)** Relative ANXA6 mRNA levels in cell populations from benign (green), localized (blue) and metastatic (red) prostate cancers. Data analysis is based on 101 cell populations isolated after laser-captured microdissection from benign epithelium to localized and metastatic disease (247). **(B)** Relative ANXA6 mRNA levels in tissue samples from benign (green), treatment-naïve localized (blue) and heavily pre-treated metastatic (red) prostate cancers. Data analysis is based on 50 lethal, heavily pre-treated metastatic castration-resistant prostate cancer obtained after rapid autopsy (246). Three different foci from the same patient were analyzed and then compared to 11 treatment-naïve, high-grade localized prostate cancers and normal tissue specimens from men who died of lethal castrate-resistant metastatic disease (248) (****, $p<0.0001$; ns, not significant).

In follow-up studies, to map the mutational landscape of metastatic prostate cancer, Tomlins and co-workers then analyzed the gene expression patterns from 50 lethal, heavily pre-treated metastatic castration-resistant prostate cancer (CRPC) obtained after rapid autopsy (248). The difficulty to interpret and draw conclusions from a single tissue sample from one individual was overcome by the analysis of three different foci from the same patient were analyzed. Expression data was then compared to a cohort of 11 treatment-naïve, high-grade localized prostate cancers and normal tissue specimens from men who died of lethal castrate-resistant metastatic disease (248). Strikingly, within this cohort, ANXA6 expression was highest in the benign tissue, and a continuous and significant downregulation of ANXA6 levels was evident in localized and even more so in metastatic cancer samples (Figure 2.4B). These exciting findings suggest that ANXA6 downregulation may occur during the progression from localized to metastatic prostate cancer.

2.4.3. ANXA6 expression levels and overall cancer survival

As outlined above, ANXA6 expression levels may reflect tumor promoting roles that promote progression and severity in several cancers (reviewed in (76, 210) (see also Table 2.1). Hence, ANXA6 upregulation may characterize the progression of ovarian carcinomas (237), women's thyroid cancer (238), polycystic ovarian syndrome (239), pancreatic cancer (222), oesophageal adenocarcinoma (240). melanoma and squamous cervical cancer progression (235, 236) and allow the detection of acute lymphoblastic leukemia (241).

In contrast, ANXA6 downregulation and tumor suppressor roles were proposed in gastric cancer (232), hepatocellular carcinomas (233) and cervical cancer (234). In breast cancer, reduced ANXA6 levels appear relevant in TNBC rather than non-TNBC subtypes (71, 210). Alike many other proposed biomarkers, these findings are predominantly based on mRNA detection, using RT-PCR, or less frequent, immunohistochemistry and western blotting. Despite the technical limitations of the latter, relying on commercial antibodies, ANXA6 levels might indicate tumor progression and disease outcome.

Given the potential prognostic value of ANXA6 in the various cancers listed above, we next aimed to correlate high and low ANXA6 levels with patient survival, focussing in cholesterol-sensitive cancers including breast, pancreas, colon, liver and prostate cancer (Figures 2.5-2.7). Kaplan-Meier curves are commonly used to estimate the survival time of subgroups within a larger cohort after initial diagnosis or onset of treatment (249).

2.4.3.1. ANXA6 expression levels and overall patient survival in breast cancer

We first analyzed data from 1081 breast cancer patients available from the TCGA (250). A general sense of mortality was obtained by generating overall survival curves, where death from any cause is documented using "survival" package (251) and "survminer" package (252), in two groups with high (n=268) or low (n=813) ANXA6 expression levels (Figure 2.5A). In this analysis, survival probability (%) of both groups was comparable for approximately 4000 days (~ 10 years). Beyond this time point, survival probability of patients with high ANXA6 levels remained unchanged for ~ 3000 days (~ 8 years), but although not significant, continuously declined in the patient group expressing low ANXA6 levels (p=0.61) (Figure 2.5A).

Breast cancer is very heterogeneous with several subtypes characterized by a variety of complex molecular entities. In line with a trend towards reduced overall survival in patients with low ANXA6 levels (Figure 2.5A), Grewal and co-workers previously identified ANXA6 downregulation in EGFR overexpressing and ER-negative breast cancer cells, which was related to increased transformation efficiency (55), and elevated EGFR activity in several triple-negative breast cancer biopsies containing low ANXA6 levels (27). We therefore next compared overall survival in a cohort of 707 breast cancer patients (250) that was divided into human epidermal growth factor receptor-2 (Her2)-positive, luminal (estrogen receptor (ER)-positive) and triple-negative (TNBC; ER-, progesterone receptor (PR)- and Her2-negative) subgroups with high or low/medium ANXA6 levels. Within this cohort, the Her2-positive and triple-negative subgroups with high ANXA6 levels only contained 2 and 8 samples, respectively, and may not be representative to draw conclusions for larger subgroups. Yet, in support of a minor role for ANXA6 in ER-positive cell lines (55), in luminal cancers with high (n=164) or low/medium ANXA6 levels (n=390), overall survival over >4000 days (>10 years) was comparable. Overall survival was slightly reduced in Her2-positive patients compared to other subtypes over >3000 days (>8 years) after diagnosis. In support of a tumor suppressor role of ANXA6 in triple-negative breast cancer, low ANXA6 levels were associated with reduced overall survival at later stages (>3500 days) (p=0.17), which is in line with other reports of reduced ANXA6 expression being allied with poor overall and distant metastasis-free survival of basal-like breast cancer patients (71, 204).
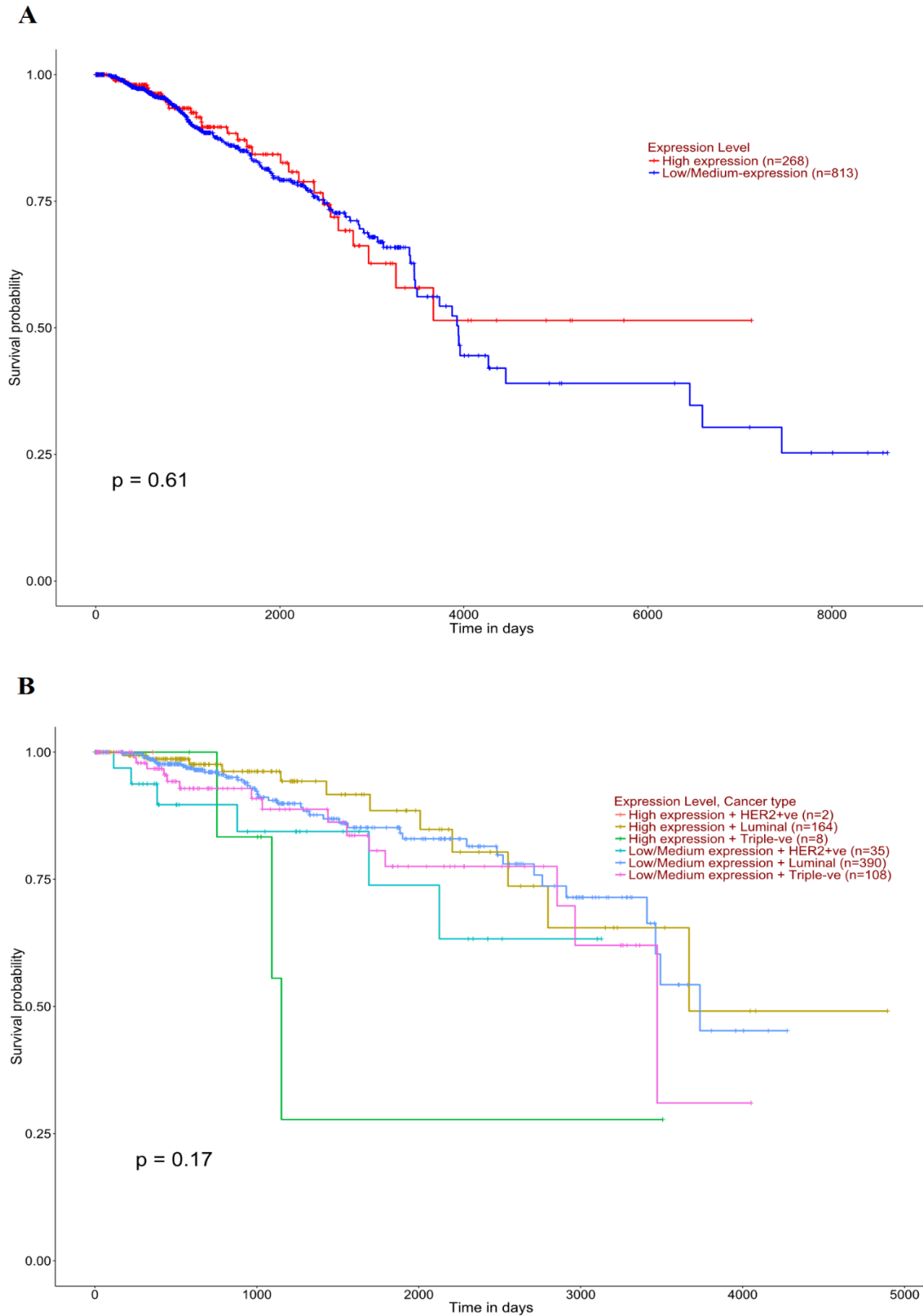
Figure 2.5: Overall survival probability of breast cancer patients with high/low ANXA6 expression levels. (A) breast cancer patients (TCGA) and **(B)** breast cancer patients subdivided into Her2-positive, luminal and triple-negative groups with high and low/medium ANXA6 expression levels (t= 0-5000 days) The number of samples in each subgroup is provided (250) (p=0.17).

2.4.3.2. ANXA6 expression levels and overall patient survival in pancreatic cancer

As outlined above (section 2.1), ANXA6 mRNA levels appeared low in pancreatic tissue while based on the GEPIA database, ANXA6 levels were significantly increased in pancreatic adenocarcinoma (Figure 2.3), an observation that was also reported by others (221, 222). We next examined overall survival of pancreatic cancer patients available from TCGA (n=177) and expressing high (n=132) and low (n=45) ANXA6 levels. Within this cohort, low ANXA6 levels were significantly associated with reduced overall survival compared to patients with high ANXA6 levels at all time points over a period >2000 days (*, p=0.014).

In contrast to these findings, elevated ANXA6 protein levels were linked to shortened survival in other studies (221, 222, 250). Leca and co-workers identified low ANXA6 protein amounts restricted to primary tumor cells, while the surrounding stroma, in particular cancer-associated fibroblasts (CAFs), and extracellular vesicles released from CAFs and isolated from plasma, displayed elevated ANXA6 levels (221, 222, 250). In fact, ANXA6 levels in circulating extracellular vesicles significantly increased with pancreatic cancer grade (grade 1, resectable; grade 2, nonresectable and locally advanced; grade 3, nonresectable and metastatic). O'Sullivan et al. (221) utilized immunohistochemistry to determine ANXA6 levels in a cohort of 57 patients to determine a tendency towards high ANXA6 protein levels being connected with poorer outcome. Hence, the opposite findings reported here and, in the literature, might reflect differences in the experimental design or technical limitations in the analysis of tissue biopsies. While the overall survival data shown in Figure 2.6 is based on mRNA expression, and ANXA6 mRNA and protein levels did not match in normal pancreatic tissues (Chapter 2.1), the abovementioned PDAC-related studies determined ANXA6 protein levels. In addition, both studies (221, 222, 250) proposed extracellular functions of ANXA6 to contribute to pancreatic cancer progression, indicating the need for further research that is able to discriminate for an intracellular role for ANXA6 in LDL-cholesterol related events that support PDAC growth and aggressiveness.
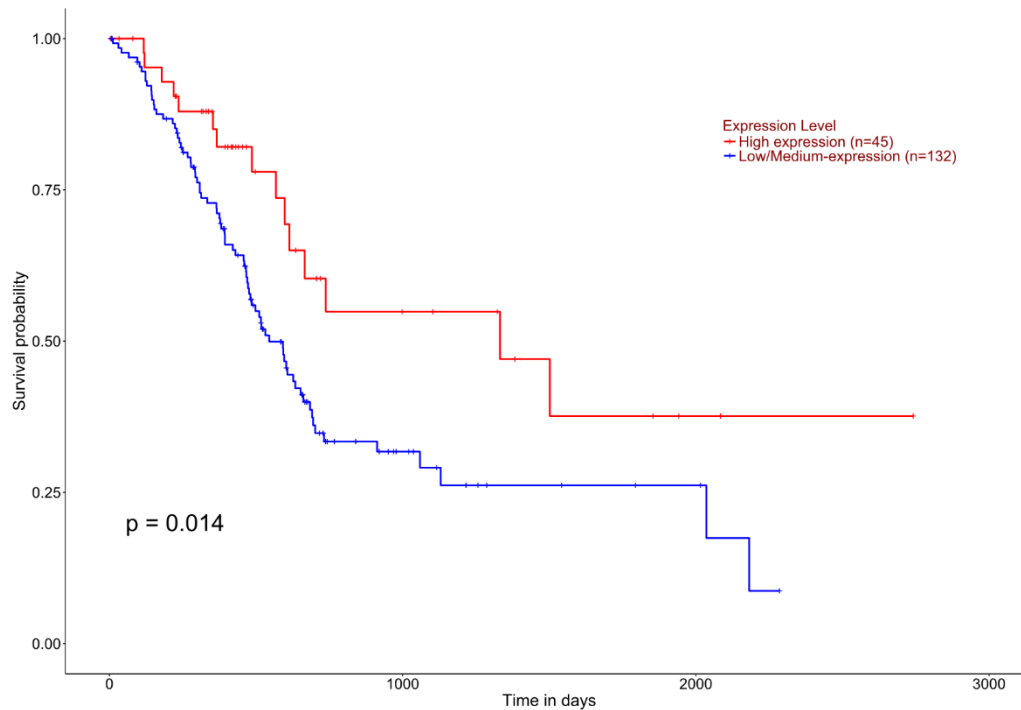
Figure 2.6: Overall survival probability (0-3000 days) of pancreatic ductal adenocarcinoma patients (TCGA) with low/high ANXA6 mRNA levels. The number of samples in each subgroup (n=45, 132) is given (250) (*, p=0.014).

2.4.4. ANXA6 expression levels and overall patient survival in colon, liver and prostate cancer

ANXA6 levels are considered low in colon (147, 209) (Figure 2.1) and were significantly reduced in colon adenocarcinoma (Figure. 2.3). Overall survival of colon cancer patients with high (n=71) and low (n=208) ANXA6 expression levels (TCGA) was comparable, with minor trends towards reduced survival of patients with high ANXA6 levels during two phases over a >3000 day period (Figure 2.7A).

In the liver, ANXA6 mRNA expression is considered very high in rodents (202, 220), but was at medium levels and comparable to other tissues in humans (Figure 2.1). ANXA6 downregulation was previously observed in hepatocellular carcinomas (233), an observation that was not evident in the GEPIA dataset (Figure 2.3). In addition, overall survival of liver cancer patients with high (n=92) and low/medium (n=273) ANXA6 expression levels (TCGA) was comparable, with an insignificant tendency towards reduced survival of patients with low ANXA6 levels over a >3000 day period (Figure 2.7B).

86

In regard to prostate cancer, the GEPIA tool showed slightly decreased ANXA6 levels in prostate carcinoma (Figure 2.3). Also, the comparison of gene expression patterns from metastatic castration-resistant prostate cancer, high-grade localized prostate cancers and normal tissue specimens (248), a continuous and significant downregulation of ANXA6 levels during prostate cancer progression was apparent (Figure 2.4B).

In this patient cohort, survival probability remained almost unchanged for >3000 days for both patients with high and low/medium ANXA6 levels. At later time points, data points on overall patient survival with high ANXA6 levels was not available, while survival of prostate cancer patient expressing low ANXA6 levels dropped substantially at 3500 days. It remains to be determined if the ~ 25% drop in survival probability is linked to low/medium ANXA6 levels.
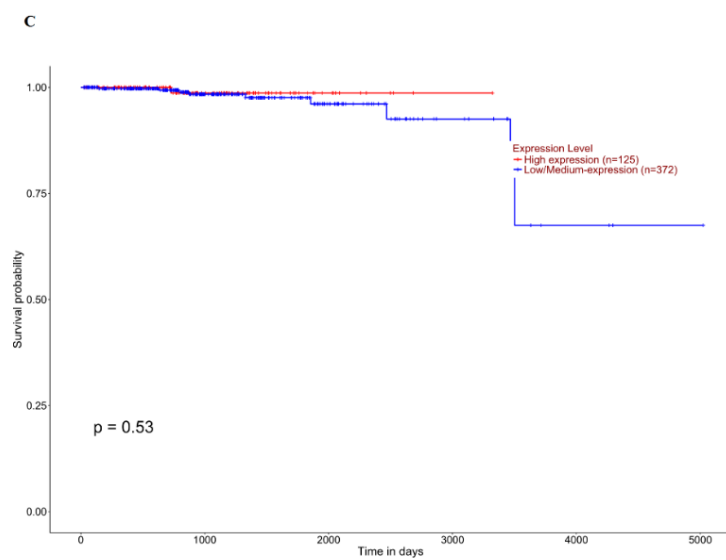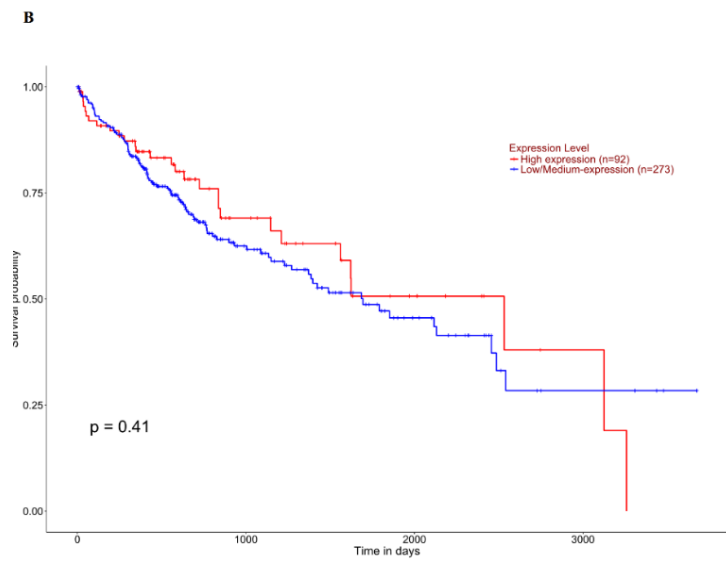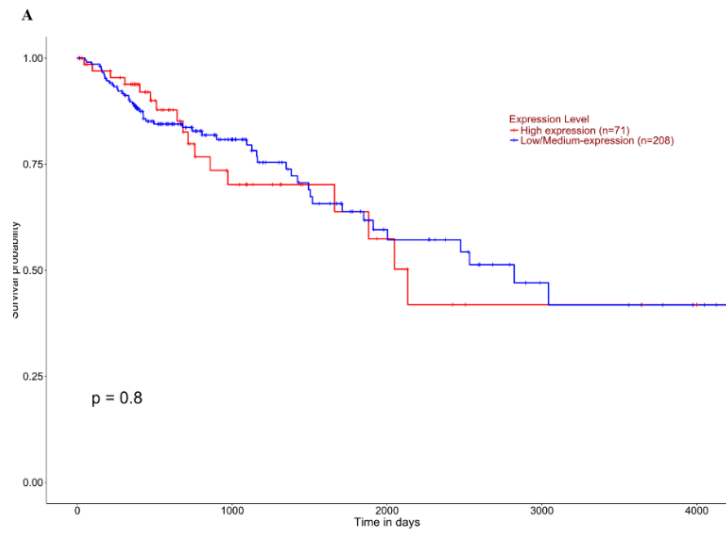
Figure 2.7: Overall survival of (A) colon, (B) liver, and (C) prostate cancer patients with high and low/medium ANXA6 expression levels (TCGA). The number of samples in each subgroup (t= 0-4000 or 5000 days) and p-values (p=0.8, 0.41 and 0.53, respectively) are given (250).

2.5. Discussion

2.5.1. ANXA6 expression patterns in human cancers

A lot of ANXA6 and cancer-related studies performed in cell and models have led to ANXA6 expression levels being considered to reflect tumor suppressor or tumor promoter functions depending on the cancer analyzed. The expression analysis available from the GEPIA dataset (see Figure 2.3) and comparison to current literature is summarized below (Table 2.2).

Cancer type	Tumor Samples	Normal samples	⇑	⇓	p	Reference	Subtypes
Bladder urothelial carcinoma	104	28		x	*, p<0.05		
Breast invasive carcinoma	1085	291				⇓ (73, 74, 201, 204,	⇑ EGFR, ER-negative, TNBC
Cervical SCC and endocervical cancer	306	13		x	*, p<0.05	⇓ (234, 235)	
Colon Adenocarcinoma	275	349		x	*, p<0.05		
Esophageal carcinoma	182	286		(x)			
Head and neck SCC	519	44				⇓ (73, 74)	⇑ EGFR
Liver hepatocellular carcinoma	369	160				⇓ (233)	
Lung adenocarcinoma	483	347		x	*, p<0.05		
Lung SCC	486	338		x			
Ovarian serous cystadenocarcinoma	426	88		x		⇑ (237, 239)	
Pancreatic Adenocarcinoma	179	171	x		*, p<0.05	⇑ (221, 222)	
Prostate adenocarcinoma	492	152		x		⇓ (Fig. 2.4B)	progression (248)
Rectum adenocarcinoma	92	318		x			
Sarcoma	262	2					
Skin cutaneous adenocarcinoma	461	556	(x)			⇓ (72, 230)	A431, ⇓ also in melanoma (236)
Stomac adenocarcinoma	408	211		(x)		⇓ (232)	
Testicular carcinoma	137	165	(x)				
Thymoma	512	337		(x)			

Table 2.2: ANXA6 up- or downregulation in various cancers. The tumor and normal tissue sample numbers, the trends in expression pattern (⇑ , ⇓), significance (*, p<0.05), and comparison to published data and subtypes is provided. Minor and non-significant trends for up- and downregulated ANXA6 levels based on the GEPIA dataset shown in Figure 2.3 are indicated by brackets (x). Abbreviations: EGFR, epidermal growth factor receptor; ER, estrogen receptor, TNBC, triple-negative breast cancer, SCC, squamous cell carcinoma.

As described in 2.4.2.2., for a lot of these tissues, studies addressing the role of ANXA6 in tumor progression are still lacking.

Published expression studies in cervical cancer and pancreatic cancers (221, 222, 234, 235) are in line with significant ANXA6 reduction (cervical) or upregulation (pancreas) in the GEPIA dataset. On the other hand, studies describing ANXA6 upregulation in ovarian cancers (237, 239) differ from our analysis. Also, ANXA6 levels remained unchanged in invasive breast carcinoma, although the Grewal group and others reported ANXA6 downregulation in EGFR overexpressing and ER-negative breast cancer (73, 74, 201, 204, 231), which will be discussed in more detail below (2.6.1.

ANXA6 levels also appeared constant in several other cancer types, including liver hepatocellular carcinoma. However, for liver cancers, the comparison of our data set (Figure 2.3) with published data is difficult. Meier et al (233) analyzed metastatic liver tumors (n=18) derived from colorectal cancers and identified downregulation of ANXA6 protein levels compared to the surrounding non-tumorous tissues in single patients. Interestingly, in these study, ANXA6 mRNA levels in liver tumors were increased, indicating the involvement of post-translational regulatory mechanisms. In contrast, the origin of liver cancers from the TCGA used in the GEPIA analysis (Figure 2.3) is less well defined and based on mRNA expression analysis comparing tumor vs. normal tissues from different patients, altogether making it difficult to directly compare the two data sets.

In regard to prostate cancer, the GEPIA data displayed reduced ANXA6 expression levels, although not significant. However, the dissection of expression patterns into (i) treatment naïve, high-grade localized prostate cancers and (ii) heavily pre-treated metastatic and castration-resistant prostate cancer samples available from Tomlins and co-workers (248) identified a highly significant downregulation of ANXA6 expression (Fig. 2.4.B). These exciting findings suggest that ANXA6 downregulation may occur during the progression from localized to metastatic prostate cancer. As ANXA6 downregulation is associated with upregulated growth factor receptor and Ras/MAPK signalling, which both contribute to prostate cancer aggressiveness and progression (253-255), one can envisage a tumor suppressor role for ANXA6, adding to aberrant signal activities in prostate cancer metastasis. In addition, as elevated LDL-cholesterol levels contribute to prostate progression (138, 163), we speculate that low ANXA6 levels in advanced prostate cancers may also be linked to an improved cellular distribution of internalized LDL

cholesterol (147), which would favour metastatic events (152). Based on our recent studies (147, 152), a potential stimulatory impact of ANXA6 downregulation on prostate cancer cell motility would be favoured by differential changes in the expression patterns of ANXA6 interaction partners in the late endosomal compartment, including Niemann-Pick type C1 (NPC1), TBC1D15, RAB7 and StAR related lipid transfer domain containing 3 (STARD3), which will be described in more detail in Chapter 3.

In summary, ANXA6 expression levels vary in distinct cancers from different tissues, stages and database sources. While the remainder of this thesis will focus on the link between cholesterol homeostasis and ANXA6 expression and function in the LE/Lys compartment with cancer growth and progression, it appears likely that the differential ANXA6 expression patterns do not reflect a universal role for ANXA6 in cholesterol homeostasis that impacts on cancer progression and patient survival. Besides various cancers employing a variety of functional networks that require different gene expression levels, epigenetic regulation appears a likely and major contributor to explain varied ANXA6 expression levels in different tumor tissues and cells. Environmental factors (e.g. diet) and cancer-specific mutations will trigger activation of epigenetic pathways that impact on ANXA6 expression. Along these lines, earlier studies from the Grewal group identified ANXA6 downregulation and a highly methylated region in the CpG-rich ANXA6 promoter in breast cancer cells with aberrant EGFR levels or lacking ER (75). This epigenetic silencing of ANXA6 via promoter methylation was also observed by others in gastric cancer (256, 257).

These findings might reflect a plethora of epigenetic mechanisms that have in recent years increasingly been identified to regulate metabolic pathways and cancer properties. For instance, several miRNAs have been shown to modulate lipid, cholesterol and glucose metabolism in oncogenic settings via lowering the expression of their multiple target genes (258-261)

2.5.2. Association of ANXA6 expression levels with overall patient survival probability

The results comparing overall patient survival probability with high, or low ANXA6 expression levels is summarized in Table 2.3.

Cancer type	⇑	⇓	Reference	Subtypes	Overall patient survival (published)	Overall patient survival probability (High vs. low ANXA6 le
Breast invasive carcinoma					ANXA6 levels not associated (13, 29)	0-3000 days: comparable >3500 days: reduced survival with low ANXA6 levels
Breast, ER-positive (luminal)					ANXA6 levels not associated (13, 29)	0-4000 days: comparable
Breast, TNBC (basal)		⇓ (73, 74, 201, 204, 231)		⇑ EGFR, ER-negative, TNBC	Reduced with low ANXA6 (13, 29)	>3500 days: TNBC, reduced with low ANXA6 levels
Pancreatic Adenocarcinoma	x	⇑ (221, 222)				0-3500 days: Reduced with low ANXA6 levels, p=0.014
Prostate adenocarcinoma		x	⇓ (Fig. 2.3-2.4)	Progression Localized to metastatic (248)		0-4000 days: comparable
Colon Adenocarcinoma		x				0-4000 days: comparable
Liver hepatocellular carcinoma				⇓ (233)		0-4000 days: comparable

Table 2.3: Association of ANXA6 levels with overall patient survival probability. The trends in expression pattern (⇑ , ⇓), and comparison of published data with data retrieved from TCGA (see Kaplan-Meier curves in 2.5-2.7) on high/low ANXA6 expression levels and overall patient survival in breast cancer subtypes, pancreatic, prostate, colon and liver cancers is provided.

The Sawke group recently followed up on cell-based findings based on ANXA6 downregulation in EGFR overexpressing and ER-negative breast cancer cell lines and compared ANXA6 expression with breast cancer patient survival. Using data available from approximately 3000 breast cancer patients (262), ANXA6 levels were found not accompanied with the overall, relapse-free or distant metastasis-free survival of all breast cancer patients. However, reduced ANXA6 expression was associated with poor overall and distant metastasis-free survival of basal-like breast cancer patients, which often represent the aggressive TNBC cancers (71, 204). Alike these findings, analysis of TCGA data (Figure 2.5A-B), showed comparable survival probabilities for total and luminal (ER-positive) cancers with high or low/medium ANXA6 levels (Figure 2.5A).

Furthermore, supporting the tumor suppressor role of ANXA6 in TNBC, and survival analysis of Sawke et al. (71, 204, 262), low ANXA6 levels were related to reduced overall survival at later stages in TNBC (>3500 days).

In regard to pancreatic cancers, overall survival was strongly and significantly (p=0.014) reduced in patients with low ANXA6 levels (Figure 2.6). These findings are somewhat unexpected as expression levels in pancreatic cancers were elevated in the GEPIA dataset (Figure 2.3) and associated with shortened survival in previous studies by others (221, 222, 250).. These opposite findings could be due to different ANXA6 amounts in primary tumor cells and the surrounding stroma in the tumor samples analyzed (221, 222, 250). It should also be noted that the overall survival data (Figure 2.6) is based on mRNA expression, that ANXA6 mRNA and protein levels varied in normal pancreatic tissues (Figure 2.2 and that PDAC-related survival studies was based on ANXA6 protein levels (221, 222, 250).. Hence, further research will be needed to clarify which cell type and environmental changes can provide clues on the potential role prognostic value of ANXA6 levels in pancreatic patient survival.

Finally, despite downregulation of ANXA6 expression levels being observed in prostate carcinoma progression (Figure 2.4), colon cancers (Figure 2.3), and hepatocellular carcinoma (233), high and low ANXA6 expression levels were not coupled with altered patient survival probability for any of these three cancers (Figure 2.7). As observed from the strikingly different findings on ANX6 during prostate progression (Figure 2.4) when comparing pooled cell populations vs. multiple foci (247, 248) from a single tumor or patient, future studies with improved techniques to better differentiate cancer subtypes and cell populations might deliver new findings.

2.5.3. ANXA6 expression levels and the complexity of molecular entities in breast cancer subtypes

Breast cancer is often associated with de-regulated cholesterol homeostasis (152, 210) or a lipid- and/or adipose-rich microenvironment that promotes breast cancer growth and progression (263). In addition, oncogenic breast cancer signalling commonly involves signalling complexes regulated by ANXA6 (67, 199, 205). ANXA6 up- or downregulation impacts on cholesterol homeostasis and/or cell signalling (55, 67, 72-74, 82, 83, 147, 199, 204, 205, 264), yet as outlined above, ANXA6 levels appeared rather unchanged when comparing all breast cancers (Figure 2.3), which initially questioned a potential role of ANXA6 as a tumor suppressor in this tissue. Yet, on

closer inspection and mentioned above (2.6.1-2.6.2), changes in ANXA6 expression levels appear relevant only in certain cancer subtypes. This is well reflected in breast cancer, which are classified as luminal A, luminal B, Her2-enriched, basal-like, and TNBC (210). Basal-like breast cancers are often TNBCs, lacking or expressing low levels of the ER, PR and Her2. Moreover, gene expression profiling of TNBC tumors identified at least four molecular subtypes, with 60–80% of these cancers expressing elevated levels of EGFR (210).

The Grewal group initially screened a panel of 20 breast cancer cell (BCC) lines (74), identifying that ANXA6 protein levels differed significantly when comparing ER-positive and ER-negative BCCs. While BCCs with deregulated ErbB2/3 and all ER-positive BCCs expressed high ANXA6 levels (∼3–5 pg per cell; for quantification of total ANXA6 amounts see (83)), 6 out of 12 ER-negative lines displayed low ANXA6 level [<1 pg per cell (83)], several of those (BT20, MDA-MB-468) with high EGFR levels comparable to the EGFR overexpressing A431 epithelial cell line that lacks endogenous ANXA6. In follow-up studies, the Grewal group then identified ANXA6-related tumor suppressor activities in EGFR overexpressing A431, but also breast as well as head and neck cancer cell lines (73).

This ability of ANXA6 to reduce tumor growth is based on ANXA6 promoting protein kinase C (PKC)-mediated EGFR phosphorylation and inactivation (73). When Grewal and co-workers examined the expression profiles from grade 3 carcinomas (n=8 per group) of luminal (ER+, PR+, Her2−), Her2-positive (ER−, PR−) and basal (triple negative: ER−, PR−, Her2−) breast cancers, only several samples exhibited high ANXA6 levels that correlated with high amounts of PKC-phosphorylated EGFR. Hence, the study was unable to observe a direct correlation between ANXA6 and the PKC-dependent phosphorylation pattern of EGFR.

Interestingly, expression patterns that could contribute to ANXA6-related impacts on breast cancer growth and progression include an inverse correlation between the levels of ANXA6 and a Ras protein specific guanine nucleotide exchange factor, RasGRF2 (201).-RasGRF2 activates Ras proteins to promote cell proliferation and inhibits Rho GTPases to reduce cell motility and invasiveness. Hence, the reciprocal expression of these two proteins may influence the invasiveness and/or rapid growth of TNBC cells (201, 210). Taken together, the heterogeneous and complex molecular entities of breast cancer subtypes might only identify correlations of ANXA6 levels with PKC-dependent EGFR phosphorylation status, GRF2 expression within small groups of certain subtypes and would require correlation studies using larger cohorts.

Chapter 3

Expression patterns of the late endosomal/lysosomal ANXA6 interactome in cancer

3.1. Introduction

As outlined in Chapter 1, increased uptake of dietary and LDL-derived cholesterol promotes cancer growth, progression, and aggressiveness (3, 152, 162). After LDL receptor-mediated endocytosis, the late endosomal/lysosomal compartment represents the central hub for the distribution of LDL-derived cholesterol to other cellular compartments. Cholesterol export from late endosomes/lysosomes (LE/Lys) requires NPC1 or other cholesterol transporters and we demonstrated (56, 147) that blocking cholesterol export from LE/Lys reduced cancer growth, migration and invasion, employing pharmacological NPC1 inhibition or shRNA-mediated NPC1 depletion (see also Chapter 1).

In addition, upregulation of ANXA6, which controls LDL endocytosis and LDL-cholesterol distribution, also caused late endosomal cholesterol accumulation (55, 67, 68). Similar to loss of NPC1 function, this led to a cellular cholesterol imbalance characterized by cholesterol depletion at the plasma membrane, Golgi apparatus and recycling endosomes. Consequently, at these locations, several cholesterol-sensitive SNAREs including Stx4, Stx6, and caveolin-1 lost their ability to control the cell surface delivery of integrins, and the secretion of fibronectin, inhibiting migratory and invasive cell behaviour (85-87, 147)

Over the years, Grewal and co-workers unravelled the underlying mechanisms that enable ANXA6 to interfere with cholesterol export from LE/Lys. ANXA6 generally binds to membranes in a Ca^{2+}-dependent manner, but LDL loading or NPC1 inhibition led to ANXA6 binding to cholesterol-rich LE/Lys (77, 80, 265). At this location, ANXA6 recruits TBC1D15, a RAB7-GTPase activating protein (RAB7-GAP), which downregulates RAB7, a key regulator of LE/Lys function (266). Indeed. ANXA6 overexpression downregulated RAB7 activity in a TBC1D15-dependent manner, which was accompanied by strongly reduced egress of cholesterol from late

endosomes (55). Vice versa, ANXA6 depletion in NPC1 mutant cells upregulated RAB7 activity, rescuing cholesterol export from LE/Lys via transport routes involving the STARD3 protein (55).

The latter findings coincide with restoration of cholesterol delivery to focal adhesions and improved cell migration and invasion of ANXA6-depleted NPC1 mutant cells (56). Importantly, TBC1D15 and STARD3 knockdown experiments revealed that their presence was essential in order for high/low ANXA6 levels to impact on late endosomal cholesterol transport (55). Hence, for ANXA6 levels to influence cancer growth and progression in a cholesterol-dependent manner, the amounts of ANXA6 interaction partners within the LE/Lys compartment appears important.

Therefore, based on published data and several unpublished findings from the Grewal and Enrich laboratories, the 'ANXA6 interactome' in LE/Lys, listing the network of protein-protein interactions and functional relationships (Figure 3.1) was developed. In this Figure, cholesterol-binding proteins identified in a genome-wide screening assay (81) are also indicated. For further information on the proteins (and lipids: lysobisphosphatidic acid, LBPA) listed here and physical and functional links to ANXA6, we recommend recent review articles from Grewal and colleagues (147, 202). Most relevant, proteins reported to interact with ANXA6 (NPC1, RAB7, TBC1D15), including TBC1D5 (Grewal et al., unpublished), or those impacted by ANXA6 and being involved in cholesterol uptake and distribution from the late endosomal compartment in an ANXA6-dependent manner (LDLR, STARD3), are highlighted in blue.

Annexin A6 interactome in late endosomes

AnxA11 — ALG-2[7,12] — dynactin/dynein[13]
ALG-2[7,12] — TRPML1[8]
AnxA2 *   AnxA7   Src
AnxA8[16]   LBPA[11]
ALIX* — Tsg101[7] — Hrs[9]
ALIX* — Chmp4[7]
LDLR[#,25]   14-3-3
StARD3[#15,25]   actin   α-actinin/cortactin   14-3-3   StARD3[#15,25]
VAP-A[#]   spectrin[24]   14-3-3   SLC38A9[21]   ORP5[14]
AnxA6[#]   NPC1[#4]   mTORc1
S100A   Lamp2[#5]
ORP1L[#]   TPD52[1] — PLIN2[6]
TBC1D15*[25]   14-3-3   StARD3[#15,25]
LC3[10]   TBC1D5*   Stx7[#*]   TPC1/2[3]   #
ATPaseH+V0a2[2]   PKCα[26]
Rab7[#25] — mTORc1[23]
Kinesin-1   Protrudin[17]   LC3[22]
FYCO1
RILP[18] — dynactin/dynein

* Grewal et al., unpublished
# Cholesterol binding (Hulce et al., 2013)

Figure 3.1: The ANXA6 interactome in the late endosomal/lysosomal compartment. The network of ANXA6-binding proteins and its interaction partners in late endosomes/lysosomes (LE/Lys) is shown. The proteins directly interacting with ANXA6 and/or being involved in cholesterol uptake and distribution from LE/Lys in an ANXA6-dependent manner are indicated in blue. Cholesterol-binding proteins recognized in a genome-wide screening assays (81) are listed (#). Unpublished (e.g. TBC1D5) interactions of ANXA6 with LE/Lys proteins identified by Grewal and colleagues and based on yeast-two-hybrid, pulldown and co-immunoprecipitation assays are indicated (*). Interactions labelled with 15, 24-26 (RAB7, STARD3, TBC1D15, LDLR, spectrin, PKCα) reflect previous research from Grewal et al (55, 73, 77, 79). Numbers 1-14, 16-23 represent other ANXA6-protein interactions or functional relationships published by others (23, 24, 38, 42, 83, 100, 239, 267-279). With kind permission from T. Grewal and C. Enrich (unpublished).

3.2. Aims

Over the last two decades it has become clear that not only the expression of a single gene, but rather gene networks determine functional outcome in physiological conditions related to health and disease. Bioinformatic approaches revealed distinct patterns of coordinated co-expression of genes when analyzed within a cohort of biological samples (280-282). This observation is also relevant in cancer settings, with a substantial number of studies identifying expression patterns of

gene networks, implicating relationships with functional significance for cancer growth and progression (138, 253, 283, 284). In this context, utilizing unbiased network and module analysis has become more common, often identifying novel gene correlation patterns and functional links that are not obvious when considering direct protein interactions and/or close proximity in a certain cellular location.

Given the prominent and cholesterol-related role of ANXA6 in LE/Lys, rather than performing unbiased network expression analysis, we decided to examine expression patterns focussing on a defined set of genes based on the ANXA6 interactome (Figure 3.1) in the late endsosomal/lysosomal compartment. Hence, the aim of this Chapter was to identify potential associations and correlations in the expression levels of ANXA6 with late endosomal/lysosomal proteins (NPC1, RAB7, TBC1D15, TBC1D5) or proteins impacted by ANXA6 and being involved in cholesterol uptake and distribution from the late endosomal compartment in an ANXA6-dependent manner (LDLR, STARD3). This approach could possibly identify ANXA6-related functional links to cancer aggressiveness, progression, and treatment outcome (74, 76, 147, 210, 222).

3.3. Methods

3.3.1. ANXA6 interactome expression patterns using cBioPortal

Several platforms, including TCGA, CANCERTOOL, the MET500 cohort (285), *Clinical Proteomic Tumor Analysis Consortium* (*CPTAC*), GEPIA, HPA, GTEx, and cBioPortal provide access to data sets and tools to analyse not only the expression pattern of a single gene, but also to link the expression patterns of two or more genes within a cancer cohort. Correlation of the expression levels of ANXA6 with interaction partners (NPC1, RAB7, TBC1D15, TBC1D5) or proteins modulated by ANXA6 (LDLR, STARD3) was first performed using cBioPortal, and in the following chapter, CANCERTOOL (see Chapter 3.3.2).

The cBioPortal for Cancer Genomics is an open-access resource that enables exploration of genomics and expression data from complex cancer datasets (e.g. TCGA Firehose Legacy), developed originally at Memorial Sloan Kettering Cancer Center (USA). Each of these data sets contain the relative expression levels of individual genes in each tumor sample compared to its expression levels in the whole population of samples. For each gene, mRNA expression was analyzed, with z-scores relative to all samples reflecting the deviation from the mean. A z-score threshold of ±2 was selected, and expression data were then used to obtain gene correlations. The Spearman coefficient was used as a correlation coefficient and correlation plots were retrieved and accessed in generic R data frames as described (286, 287).

Gene correlations comparing the mRNA levels of ANXA6 with NPC1, LDLR, RAB7A, STARD3, TBC1D5 and TBC1D15 were investigated in data sets available for breast, colorectal, liver, pancreas and prostate cancers as shown in the following (Tables 3.1 -3.5). Its relation to RAB7, RAB7A and RAB7B isoforms with only 50% identity exist. While RAB7A is ubiquitously expressed and considered the master regulator of LE/Lys function, RAB7B is exclusively found in cells with monocyte and myeloid origin, and only controls endosome to Golgi transport (288). Hence, our correlation analysis only included the RAB7A isoform, hereafter also referred as RAB7.

3.3.2. ANXA6 interactome expression patterns using CANCERTOOL

Based on the expression analysis obtained from cBioPortal described above, some, but not all cohorts, showed mostly weak tendencies of an association between ANXA6 mRNA levels and

expression levels of one or more genes (NPC1, LDLR, RAB7A, TBC1D5 and TBC1D15). Yet, a strikingly common feature of the gene correlation analysis in cBioPortal revealed a positive correlation, some of those considered strong (e.g. colon, prostate), of ANXA6 with STARD3 expression levels in breast, colon/colorectal, pancreatic, and prostate cohorts (Table 3.1-3.5).

This was addressed further using an alternative to cBioPortal, CANCERTOOL provides access to gene expression data from well-annotated cancer datasets and allows gene-to-gene correlations in individual tumor samples in multiple datasets. cBioPortal enabled correlations based on the mean of relative expression levels of individual genes in each tumor sample compared to its expression levels in the whole population of cohort samples. Importantly, besides gene-to-gene correlations, CANCERTOOL also allowed the generation of graphs showing the relative expression of gene pairs of individual tumors. For the development of this freely accessible tool, data from GEO, cBioPortal (for METABRIC, cbioportal.org), TCGA and several other comprehensive and published datasets (n=21) was used. The data presented in this thesis were based on data retrieval from the first and current version, which contains data from breast, colorectal, lung and prostate cancers (289).
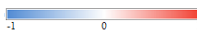
3.4. Results

3.4.1. ANXA6 interactome expression patterns in breast cancer

ANXA6 is downregulated in EGFR overexpressing and ER-negative breast cancer cells (27, 205, 210) and there was a development towards reduced overall survival in patients with low ANXA6 levels (Figure 2.5A), including Her2-positive and triple-negative breast cancer patients at later stages after diagnosis, which supported poor overall and distant metastasis-free survival of basal-like breast cancer patients reported recently (204, 210).

In Table 3.1 the correlation between the mRNA expression of ANXA6 with NPC1, LDLR, RAB7A, STARD3, TBC1D5 and TBC1D15 in 4 different breast cancer data sets (286, 287, 290-293) is shown. In the TCGA data sets, ANXA6 expression negatively correlated with most selected genes, in particular NPC1, but not STARD3. Yet, this rather weak leaning was not observed in two smaller data sets, where positive correlations between ANXA6 and all other genes, ranging from R=0.15 – 0.62, were found. Interestingly, the data set that contained the strongest positive correlation between ANXA6 and NPC1 was from a Korean breast cancer cohort (168 primary tumors), which was reported to harbor more Her2+ and luminal B subtypes compared to the cohort selected from the TCGA. The fourth data set consisted of 146 metastatic cancers (290), and alike the Korean cohort listed above, might differ from the subtype composition of the tumors listed in the TCGA cohorts. In both of these data sets, elevated ANXA6 levels interconnected with upregulation of TBC1D15 and TBC1D5, which could indicate an ability to effectively downregulate RAB7 activity. This could be counteracted by increased expression of LDLR and NPC1, ensuring LDL-uptake and distribution despite ANXA6, TBC1D15 and possibly TBC1D5 contributing to downregulate RAB7-dependent cholesterol egress from LE/Lys.

Data Set	Samples	NPC1	LDLR	RAB7A	STARD3	TBC1D5	TBC1D15
TCGA, Firehose Legacy (291)	1100	-0.25	-0.02	-0.04	0.19	-0.03	0.05
TCGA, 2015 (292)	816	-0.25	-0.01	-0.02	0.19	-0.01	0.05
Breast Cancer (SMC 2018) (293)	168	0.62	0.23	0.33	0.19	0.32	0.35
TMBCP (Provisional, 2020) (290)	146	0.15	0.15	0.41	0.19	0.26	0.19

Table 3.1 Correlation between the mRNA expression of ANXA6 and NPC1, LDLR, RAB7A, STARD3, TBC1D5 and TBC1D15 in four breast cancer data sets. z-scores are relative to all samples with a threshold ± 2. The positive (red) and negative (blue) correlations ranging from +1 to -1 are indicated. Abbreviations: TCGA, The Cancer Genome Atlas; TMBCP, The Metastatic Breast Cancer Project. Colour code

Of note, STARD3 levels correlated positively with ANXA6 expression in all four breast cancer data sets. Hence, despite the variation in cancer subtypes that build these data banks, this might indicate a common co-regulation and association of ANXA6 and STARD3 expression levels that is not restricted to certain breast cancer subtypes and cancer stages (primary vs metastatic).

3.4.2. ANXA6 interactome expression patterns in colon, colorectal and liver cancers

In the GEPIA datasets, ANXA6 levels in adenocarcinoma of colon cancers were significantly reduced compared to controls (Figure 2.3). On the other hand, there was a minor development towards reduced survival of patients with high ANXA6 levels during two phases over a >3000-day period (Figure 2.7A), yet overall, significant correlation between high or low/medium ANXA6 expression levels and overall survival in colon cancer was lacking (Figure 2.7).

In Table 3.2, the correlation between the mRNA expressions of ANXA6 with NPC1, LDLR, RAB7A, STARD3, TBC1D5 and TBC1D15 in 3 different colorectal and colon cancer cohorts with 382, 244 and 106 patient samples were analyzed (286, 287). In the study by the Cancer Genome Atlas Network (TGCA), expression patterns and genetic composition of ≥244 human colorectal carcinomas consisting of colon and rectum cancers were examined (294). Vasaikar and colleagues compared proteogenomic data from tumour and adjacent normal tissue in a colon cancer cohort (n=106;) (295), which did not contain any rectum cancers. In all three cohorts, a clear trend for a positive or negative correlation of ANXA6 with NPC1, RAB7 and TBC1D15 was lacking. ANXA6 expression levels negatively related to LDLR expression in all three cohorts (R=-0.08, -0.12, -0.31, indicating that low ANXA6 levels could be accompanied by elevated LDLR expression (and vice versa), which would allow effective LDL endocytosis. Furthermore, ANXA6 expression positively correlated with STARD3 and TBC1D5 expression in all three cohorts, indicating the possibility of coordinated ANXA6, STARD3 and/or TBC1D5 expression.

Data Set	Samples	NPC1	LDLR	RAB7A	STARD3	TBC1D5	TBC1D15
TCGA, Firehose Legacy (291)	382	0.17	-0.12	0.05	0.29	0.33	-0.02
TCGA, 2012 (294)	244	N/A	-0.08	0.21	0.16	0.11	-0.04
CPTAC-2 Prospective (295)	106	-0.01	-0.31	0.05	0.17	0.07	0.1

Table 3.2 Correlation between the mRNA expressions of ANXA6 and NPC1, LDLR, RAB7A, STARD3, TBC1D5 and TBC1D15 in colorectal and colon cancers in three different data sets. The positive (red) and negative (blue) correlations ranging from +1 to -1 are indicated. Abbreviations: TCGA, The Cancer Genome Atlas; CPTAC, *Clinical Proteomic Tumor Analysis Consortium*. Colour code

Hepatic ANXA6 mRNA expression levels are very high in rodents (202, 220), but at medium levels in humans and comparable to many other tissues (Figure 2.1). ANXA6 downregulation in hepatocellular carcinomas (233) was not evident in the GEPIA dataset (Figure 2.3) and overall survival of liver cancer patients did not significantly relate to high or low/medium ANXA6 expression levels (Figure 2.7). A strong correlation between the mRNA expression of ANXA6 with NPC1, LDLR, RAB7A, STARD3, TBC1D5 or TBC1D15 in a liver cancer cohort with 373 patient samples (286, 287, 291) (Table 3.3) was not evident, indicating that ANXA6 levels in liver cancers are not coordinated with other proteins handling cholesterol in the LE/Lys compartment.

Data Set	Samples	NPC1	LDLR	RAB7A	STARD3	TBC1D5	TBC1D15
TCGA, Firehose Legacy (291)	373	-0.13	0.05	0.08	0.01	0.02	0.01
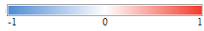
Table 3.3 Correlation between the mRNA expression of ANXA6 and NPC1, LDLR, RAB7A, STARD3, TBC1D5 and TBC1D15 in a cohort of liver cancers (n=373) from TCGA. The positive (red) and negative (blue) correlation ranging from +1 to -1 is indicated. Abbreviations: TCGA, The Cancer Genome Atlas. Colour code

3.4.3. ANXA6 interactome expression patterns in pancreatic cancers

ANXA6 levels were significantly increased in pancreatic adenocarcinoma (Figure 2.3), which is in line with other reports (221, 222). Yet, low ANXA6 levels were associated with reduced overall survival (Figure 2.6). The correlation of ANXA6 levels with NPC1, LDLR, RAB7A, STARD3, TBC1D5 and TBC1D15 from 2 cohorts with 179 and 96 patient samples is shown in Table 3.4. The cohort available from the TCGA contained 179 samples, while expression data from 96 tumours with high epithelial content from pancreatic ductal adenocarcinomas (296) are listed in the second cohort in Table 3.4.

Data Set	Samples	NPC1	LDLR	RAB7A	STARD3	TBC1D5	TBC1D15
TCGA, PanCancer Atlas (297)	179	-0.04	-0.43	0.07	0.16	0.29	0.09
QCMG, 2016 (296)	96	-0.02	-0.14	0.08	0.04	0.18	0.05

Table 3.4 Correlation of ANXA6 mRNA expression with NPC1, LDLR, RAB7A, STARD3, TBC1D5 and TBC1D15 in two cohorts from pancreatic cancers. The positive (red) and negative (blue) correlation ranging from +1 to -1 is indicated. Abbreviations: TCGA, The Cancer Genome Atlas; QCMG, Queensland Centre for Medical Genomics). Colour code -1 0 1

Interestingly, ANXA6 levels showed a trend towards negative association with LDLR expression levels in both cohorts. Levels of NPC1, RAB7A and TBC1D15 lacked a strong association with ANXA6 levels, while STARD3 and TBC1D5 levels positively correlated with ANXA6 in one or both cohort cohorts, respectively. Hence, low ANXA6 levels might favour increased LDL uptake in pancreatic cancers, which in some patients could be associated with increased LDL-cholesterol distribution via STARD3.

3.4.4. ANXA6 interactome expression patterns in prostate cancers

Although ANXA6 levels were slightly increased in prostate carcinoma (Figure 2.3), ANXA6 downregulation was observed during the progression from localized to metastatic prostate cancer (Figure 2.4B), with the survival of prostate cancer patients expressing low ANXA6 levels dropping substantially at later stages (Figure 2.7C). To assess any correlation of ANXA6 expression levels with the ANXA6 interactome, we compared the mRNA expression of ANXA6 and NPC1, LDLR, RAB7A, STARD3, TBC1D5 and TBC1D15 in prostate cancer in eight different data sets (Table 3.5) (298-302). This included three cohorts with advanced, metastatic and castration-resistant tumours (298, 299, 301), one cohort with both primary and metastatic cancers (302), as well as two sample collections from predominantly treatment-naïve American and Australian or Chinese prostate cancer patients (300, 303), both with a rather wide range of grades, stages, and risk of recurrence.

Data Set	Samples	NPC1	LDLR	RAB7A	STARD3	TBC1D5	TBC1D15
TCGA, Firehose Legacy (291)	498	0.13	-0.12	0.01	0.09	0	-0.36
TCGA, 2015 (292)	333	0.15	-0.07	-0.02	0.04	0.06	-0.36
SU2C/PCF Dream Team (298)	208	0.03	0.01	0	0.15	-0.15	-0.17
NPC (Multi-Institute) (299)	49	0.38	-0.16	0.5	0.64	0.05	0.47
Broad/Cornell, 2012 (300)	20	N/A	0.04	0.1	0.48	-0.1	-0.22
Fred Hutchinson CRC (301)	171	-0.19	-0.02	0.4	0.34	0.07	-0.05
MSKCC - PCOG, 2010 (302)	150	-0.49	0.37	0.41	0.02	0.04	0.01
SMMU, Eur Urol 2017 (303)	65	N/A	-0.11	0.16	0.37	0.29	-0.18

Table 3.5 Correlation of ANXA6 mRNA expression with NPC1, LDLR, RAB7A, STARD3, TBC1D5 and TBC1D15 mRNA levels in eight prostate cancer cohorts. The positive (red) and negative (blue) correlation ranging from +1 to -1 is indicated. Abbreviations: TCGA, The Cancer Genome Atlas; NPC, Neuroendocrine Prostate Cancer; Su2C/PCF, Stand Up to Cancer Prostate/Prostate Cancer Foundation; MSKCC – PCOG: Memorial Sloan Kettering Cancer Center - Prostate Cancer Oncogenome Group; SMMU, Second Military Medical University). Colour code

-1   0   1

Several cohorts (n=3) showed a positive correlation between ANXA6 and NPC1 expression levels, which coincided with negatively correlated LDLR levels, indicating that elevated LDLR levels are not associated with upregulation of NPC1. Yet, similar to several other cancer cohorts listed above (Table 3.1, 3.2 and 3.4 for breast, colon, and pancreas, respectively), there was a trend of weak (n=4), but also strong (n=4) positive correlations of ANXA6 with STARD3 levels in all prostate cancer cohorts. Several of those also displayed a positive correlation of ANXA6 with RAB7 levels, which could point at high/low ANXA6 levels influencing the contribution of RAB7-dependent and STARD3-mediated cholesterol export from LE/Lys. Strong association of ANXA6 levels with both RAB7 and STARD3 were found in cohorts of castration-resistant neuroendocrine prostate cancer (299) and metastatic prostate cancer (301), supporting an increasingly important contribution of cholesterol export from LE/Lys at later stages.

3.4.5. ANXA6 interactome expression patterns in breast cancer

For the correlation of ANXA6 mRNA levels with those from LDLR, NPC1, RAB7A, STARD3, TBC1D5 and TBC1D15 in breast cancer subtypes, data sets from multiple cohorts (289, 291, 304-307) were available and analyzed using CANCERTOOL (see Table 3.6).

All these cohorts varied in sample numbers for breast cancer subtypes and included ER-negative, ER-positive, Her2-enriched, basal-like, and luminal tumors. Two cohorts (289, 291, 306) also provided control data from normal-like tissues. The different cohort sizes and diversity of breast cancer subtypes for each study group are listed (Table 3.6).

Study	Cohort size	ER-negative	ER-positive	Her2-enriched	Basal	Luminal (A+B)	Null	Normal
Ivshina (304)	289	34	211				40	
Lu (305)	129	53	76	31	32	61	5	
Pawaitan (306)	159			15	25	39+23	20	37
Wang (307)	286	77	209					
TCGA (289, 291)	1093	237	806	58	97	237+127	48, 572	8

Table 3.6: Sample size and breast cancer subtypes in several cohorts (289, 291, 304-307) available for gene correlation analysis in CANCERTOOL. Tumors that lack subtype determination (Null) are listed. 'Normal' represents 'normal-like' tissue.

For the statistical analyses of gene-to-gene correlations, the Pearson correlation coefficient was calculated for each pair of genes, and the statistical significance (p) and 'coherence' (R) are provided. The latter estimated the strength of the correlation when more than 50% of the datasets showed unidirectional and significant correlation with greater than 0.2 or lower than -0.2 for direct or inverse correlations, respectively.

In the following, relative mRNA expression of ANXA6 was correlated with relative mRNA levels of NPC1, LDLR, RAB7A, STARD3, TBC1D5 and TBC1D15 in the breast cancer subtypes listed above from the various studies. Individual data points represent the relative expression of gene pairs in a single tumor. The correlations and significance (R, p) are shown.

The Grewal group initially identified ANXA6 downregulation in ER-negative breast cancer cell lines, and together with ANXA6 tumor suppressor functions in TNBC (27, 205, 210), we therefore first correlated ANXA6 expression levels with LDLR, NPC1, RAB7A, STARD3, TBC1D5 and TBC1D15 in ER-negative breast cancers (Figure 3.2). Interestingly, in all data sets, there was a trend for a negative correlation of ANXA6 and LDLR levels ranging from R=-0.05 to R=-0.19.

A

ER-negative
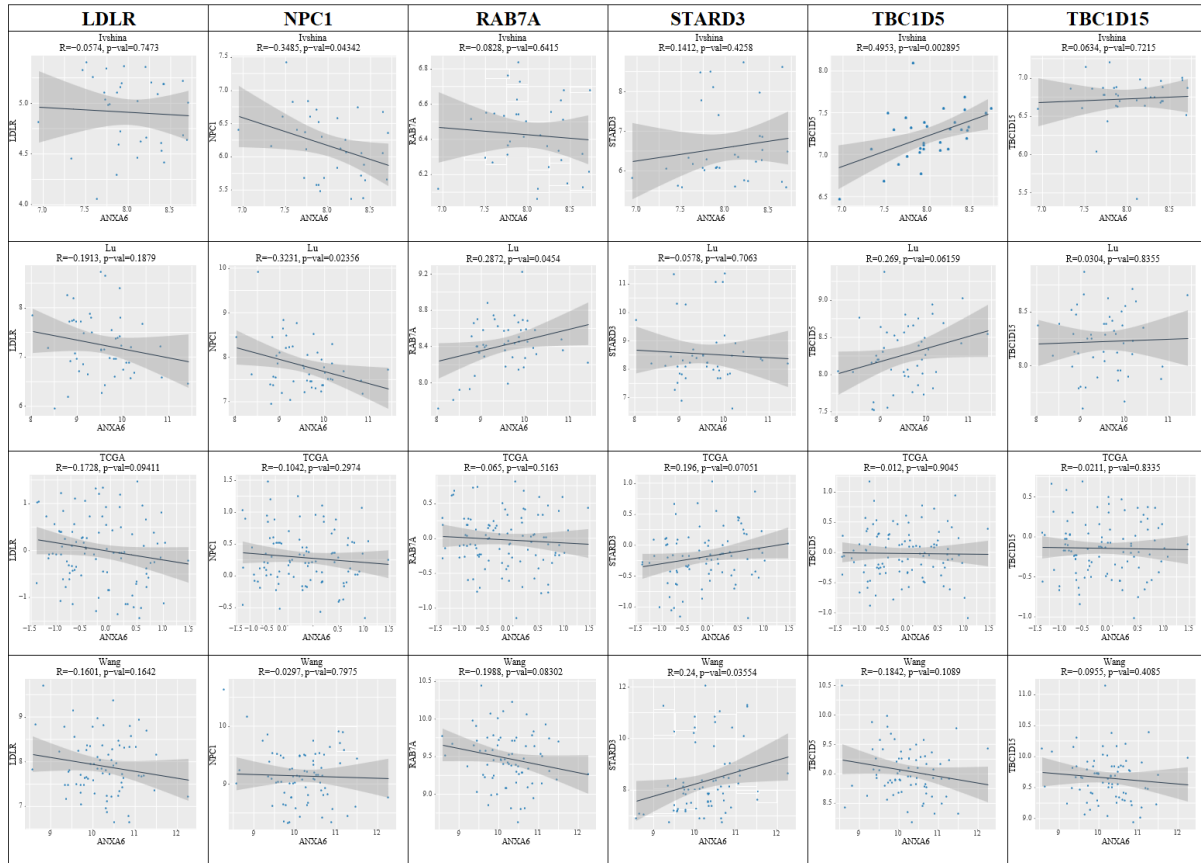
B **ER-negative**

Figure 3.2: A. Correlation of relative mRNA expression of ANXA6 and LDLR, NPC1, RAB7A, STARD3, TBC1D5 and TBC1D15 in ER-negative breast cancers. The origin of the four different data sets (289, 291, 304, 305, 307) are indicated. Each data point represents relative mRNA expression of ANXA6 (X-axis) and LDLR, NPC1, RAB7A, STARD3, TBC1D5 and TBC1D15 (Y-axis) in a single tumor, respectively. **B. Heatmap with the overall significance (p) and the Pearson coefficient (R) for each correlation analysis is given.** The positive (red) and negative (blue) correlation is indicated.

A

ER-positive

B

ER-positive

Figure 3.3: A. Correlation of relative mRNA expression of ANXA6 and LDLR, NPC1, RAB7A, STARD3, TBC1D5 and TBC1D15 in ER-positive breast cancers. The origin of the four different data sets is indicated (289, 291, 304, 305, 307). Each data point represents relative mRNA expression of ANXA6 (X-axis) and LDLR, NPC1, RAB7A, STARD3, TBC1D5 and TBC1D15 (Y-axis) in a single tumor, respectively. **B. Heatmap with the overall significance (p) and the Pearson coefficient (R) for each correlation analysis is given in a heatmap.** The positive (red) and negative (blue) correlation is indicated.

Likewise, ANXA6 levels negatively correlated with NPC1 levels in all four studies, with two data sets (289, 291, 304, 305, 307) derived from 34 and 53 ER-negative tumor samples, respectively, showing a strong negative correlation (R=-0.34 and R=-0.32) and significant p-values (0.04 and 0.02), respectively. It should

be noted that these observations were not apparent from the correlation analysis of breast cancer cohorts using cBioPortal (Table 3.1), probably because these data sets did not discriminate between different breast cancer subtypes.

Furthermore, these findings coincide with three from four studies pointing at a positive correlation between ANXA6 and STARD3 levels, one of those (307) with 77 samples showing a strong relationship between these two genes (R=0.24). These findings are in line with the trend observed in the breast cancer expression analysis using cBioPortal (Table 3.1) and may indicate that depending on high/low ANXA6 expression levels, ER-negative breast cancer cells may preferentially utilize either NPC1 or STARD3 for LDL-cholesterol export from late endosomes. While RAB7A and TBC1D15 did not reveal a consistent expression pattern in relation to ANXA6, two ER-negative cohorts (304, 305) showed a strong positive correlation between ANXA6 and TBC1D5 (R=0.49 and 0.26, respectively). Hence, one can envisage that high ANXA6 levels in ER-negative breast cancers may be associated not only with low LDLR and NPC1 levels, but also with an increased TBC1D5-mediated downregulation of RAB7-GTPase activity. In contrast to TBC1D15-mediated RAB7 inactivation reducing cellular distribution of LDL-cholesterol export from LE/Lys to the ER, lipid droplets and the plasma membrane (ref 15), it has yet to be determined if elevated TBC1D5 levels downregulating RAB7-GTP levels would have similar effects on LDL-cholesterol homeostasis and its role in tumor growth and progression in these cancers.

We next correlated ANXA6 expression with LDLR, NPC1, RAB7A, STARD3, TBC1D5 and TBC1D15 levels in ER-positive breast cancers (Figure 3.3). In striking difference to ER-negative cancers, trends indicating an association of ANXA6 expression levels with LDLR, NPC1, RAB7A, TBC1D5 and TBC1D15 were lacking in ER-positive tumors. In addition to the lack of previous evidence linking ANXA6 levels with ER-positive breast cancers (27, 205, 210), these findings might also reflect a reduced ability of LDL to influence growth and progression of ER-positive tumors. Indeed, in earlier studies only ER-negative breast cancer cells showed increased proliferation and migration upon LDL exposure (106, 308).

We then examined ANXA6 and LDLR, NPC1, RAB7A, STARD3, TBC1D5 and TBC1D15 expression levels in Her2-enriched breast cancers (Figure 3.4). Strikingly, alike ER-negative breast cancers, there were negative correlations of relative ANXA6 amounts with both LDLR and NPC1 levels, some of those revealing strong relationships (305) (R=-0.44, p=0.006 for ANXA6/LDLR

and R=-0.34 and p= 0.05 for ANXA6/NPC1). As observed in the other breast cancer subtypes, Her2-enriched breast cancers lacked a clear association of ANXA6 with RAB7A and TBC1D15.

A   **HER2-enriched**
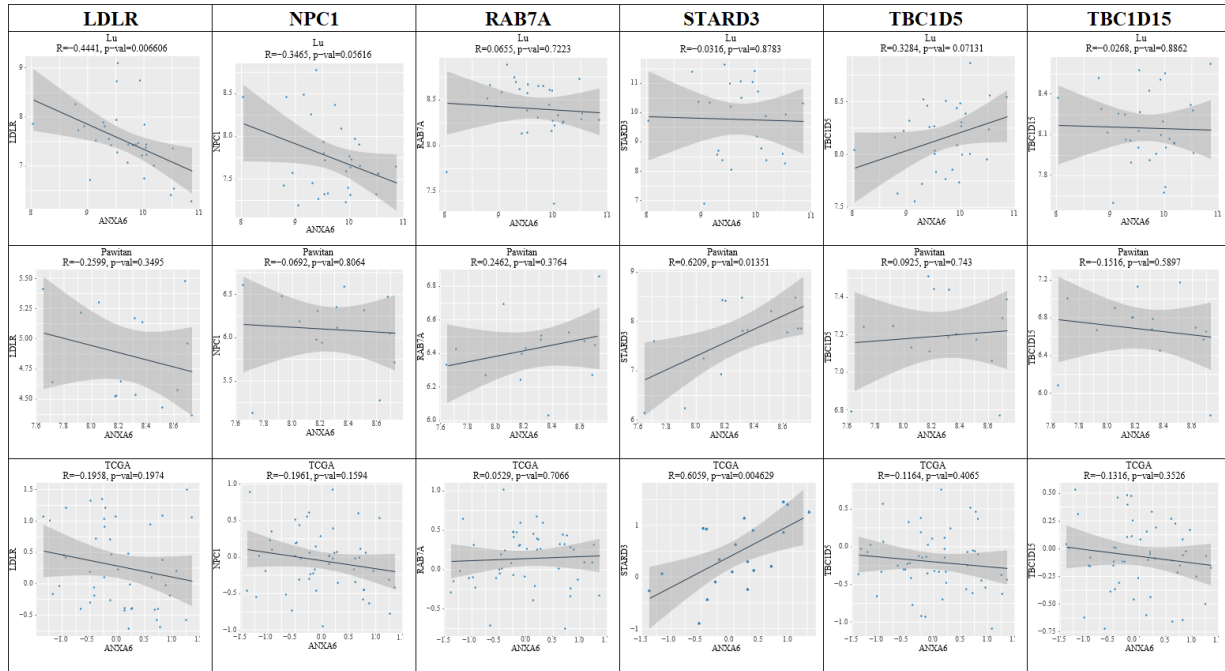
B **HER2-enriched**
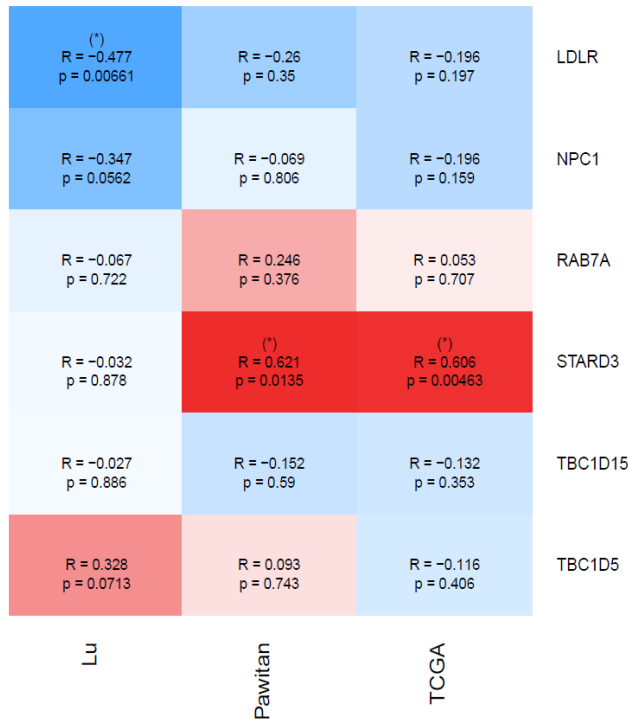
Figure 3.4: A. Correlation of relative mRNA expression of ANXA6 and LDLR, NPC1, RAB7A, STARD3, TBC1D5 and TBC1D15 in Her2-enriched breast cancers. The origin of the three different data sets is indicated (289, 291, 305, 306). Each data point represents relative mRNA expression of ANXA6 (X-axis) and LDLR, NPC1, RAB7A, STARD3, TBC1D5 and TBC1D15 (Y-axis) in a single tumor, respectively. **B. Heatmap with the overall significance (p) and the Pearson coefficient (R) for each correlation analysis is given.** The positive (red) and negative (blue) correlation is indicated.

Yet, alike ER-negative breast cancers, two data sets showed strong positive correlations between ANXA6 and STARD3 expression levels (306) (R=0.6 and p=0.01; TCGA: R=0.6 and p=0.004). Thus, in Her2-enriched and ER-negative breast cancer cells, low ANXA6

expression levels may be associated with increased LDL-cholesterol uptake and distribution via LDLR and NPC1. Interestingly, loss of 5q31-35, which contains the ANXA6 locus, is common in ER-negative breast tumors that carry *Her2* gene amplifications (309, 310) which may also contribute to upregulated LDL-cholesterol uptake and distribution via LDLR and NPC1. On the other hand, Her2-enriched cancers with high ANXA6 and concomitant high STARD3 levels may also exist. The latter might indicate that ANXA6 upregulation is associated with the common co-amplification and overexpression of STARD3 and Her2 in breast cancer (311).

Elevated STARD3 levels may contribute to increased cholesterol delivery from LE/Lys to mitochondria, the latter being highly dependent on cholesterol to promote cancer growth and progression. STARD3 has been linked to cholesterol overload in mitochondria in NPC1 deficiency (32) and ANXA6 may contribute to STARD3 facilitating transport of LDL-derived cholesterol to mitochondria in Her2-enriched breast cancers for mitochondrial well-being and energy production, all anti-apoptotic properties in cancer settings (32). Moreover, these findings may link LDL-cholesterol and upregulated ANXA6 levels in Her2-related breast cancers with the ability of elevated STARD3 expression to promote cell migration and invasion (312) (reviewed in (11)).

Next, we examined basal-like tumors, which predominantly consist of TNBCs lacking estrogen, progesterone and Her2 receptors (Figure 3.5). Moreover, reduced ANXA6 expression were associated with poor overall and distant metastasis-free survival of basal-like breast cancer patients (71, 204). Somewhat like the gene patterns observed in ER-negative cancers (Figure 3.2), and with the exception of a strong, but not significant, positive correlation of ANXA6 and LDLR levels in one study (306) (R=0.24, p=0.24), we observed a trend towards negative correlations of ANXA6 amounts with LDLR and NPC1 levels in all cohorts.

Furthermore, all cohorts showed positive correlations for ANXA6 and STARD3 levels. Although these trends lacked statistical significance, this also paralleled findings for ANXA6 levels being linked to STARD3 expression in ER-negative breast cancers (Figure 3.2). Alike most other breast cancer subtypes analyzed above, ANXA6 correlations with RAB7, and the RAB7-GTPase activating proteins TBC1D5 and TBC1D15 only showed a strong positive (insignificant) correlation in one of the three cohorts (305) and were generally not prominent and did not reveal common trends.

Taken together, in line with the correlation analysis in ER-negative breast cancer cells (Figure 3.2), depending on high/low ANXA6 expression levels, basal-like tumors may either utilize NPC1 or STARD3 for LDL-cholesterol export from late endosomes.

Luminal breast cancer subtypes are ER-positive and either PR-positive, Her2-negative (luminal A), or PR-negative, Her2-positive (luminal B). Given these differences to cancer subtypes

A   **Basal-like**
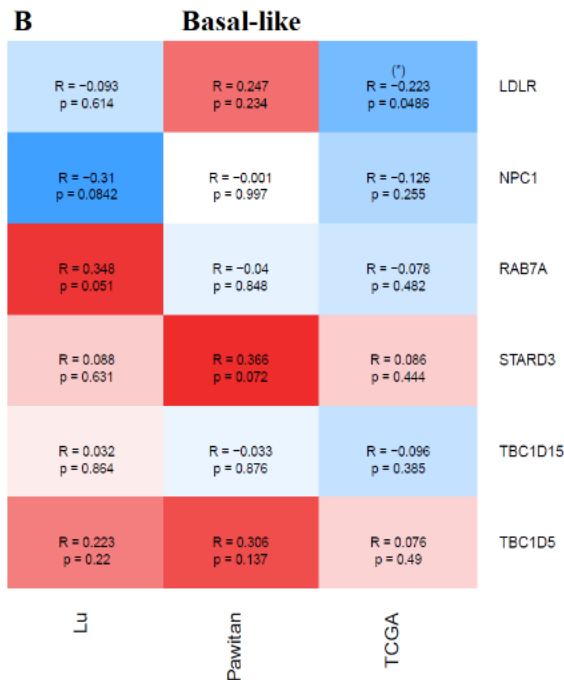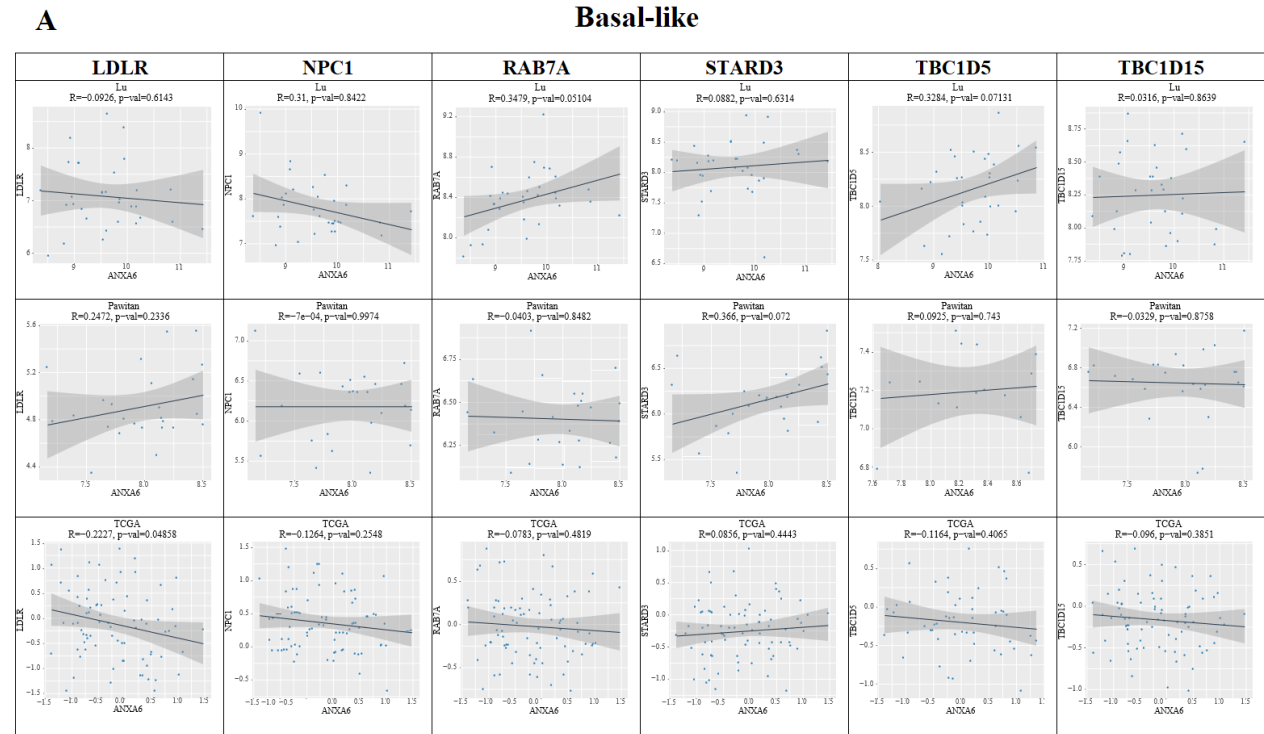
B   **Basal-like**

Figure 3.5: A. Correlation of relative mRNA expression of ANXA6 and LDLR, NPC1, RAB7A, STARD3, TBC1D5 and TBC1D15 in basal-like breast cancers. The origin of the three different data sets is indicated (289, 291, 305, 306). Each data point represents relative mRNA expression of ANXA6 (X-axis) and LDLR, NPC1, RAB7A, STARD3, TBC1D5 and TBC1D15 (Y-axis) in a single tumor, respectively. **B. Heatmap with the overall significance (p) and the Pearson coefficient (R) for each correlation analysis is given.** The positive (red) and negative (blue) correlation is indicated.

categorized solely on ER or Her2 (Figures 3.2-3.4), we also performed gene-to-gene correlations of ANXA6 with LDLR, NPC1, RAB7A, STARD3, TBC1D5 and TBC1D15 in luminal breast cancer subtypes from 3 cohorts (289, 291, 305, 306). Alike

the weak correlations observed in the TCGA. cohort when analyzing ER-positive cancers (Figure 3.3), ANXA6 expression showed only weak association with LDLR, NPC1, RAB7A, TBC1D5 and TBC1D15 With the exception of RAB7A being negatively associated with ANXA6 levels in the Pawitan cohort (306) (39 luminal A and 23 luminal B tumor samples; R=-0.26, p=0.03),

A   **Luminal**
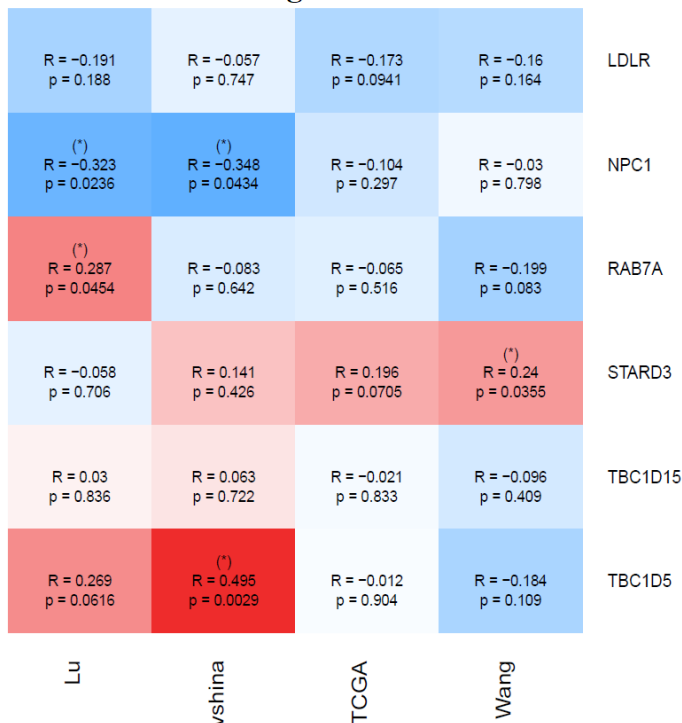

B   **Luminal-like**

Figure 3.6: A. Correlation of relative mRNA expression of ANXA6 and LDLR, NPC1, RAB7A, STARD3, TBC1D5 and TBC1D15 in luminal breast cancers. The origin of the three different data sets is indicated (289, 291, 305, 306). Each data point represents relative mRNA expression of ANXA6 (X-axis) and LDLR, NPC1, RAB7A, STARD3, TBC1D5 and TBC1D15 (Y-axis) in a single tumor, respectively. **B. Heatmap with the overall significance (p) and the Pearson coefficient (R) for each correlation analysis is given.** The positive (red) and negative (blue) correlation is indicated.

RAB7A, TBC1D5 and TBC1D15 expression did not reveal a prominent link to ANXA6 expression levels in the other two cohorts.

The other two cohorts showed several strong positive correlations between ANXA6 and LDLR

as well as NPC1, an observation that was not apparent in the other breast cancer subtypes. Yet, similar to 3/4 ER-negative, 2/4 ER-positive, 2/3 Her2-enriched and 3/3 basal-like breast cancer subgroups (Figure 3.2-3.5), relative ANXA6 amounts showed a strong (2/3) and positive correlation with STARD3 levels in all 3 cohorts that reached significance (R=0.36, p=0.04; R=0.31, p=0.01; R=0.13, p=0.02).

In order to assess if certain expression signatures observed in the various breast cancer subtypes would remain visible within more complex data sets, we performed gene-to-gene correlations of ANXA6 with LDLR, NPC1, RAB7A, STARD3, TBC1D5 and TBC1D15 in all tumors. Indeed, negative correlations for ANXA6 with LDLR and NPC1 observed in 4/4 ER-negative breast cancers (Figure 3.2), 3/4 ER-positive cohorts (Figure 3.3) and 3/3 Her2-enriched tumors (Figure 3.4) were also detected when analyzing all tumors.

A   **All tumors**
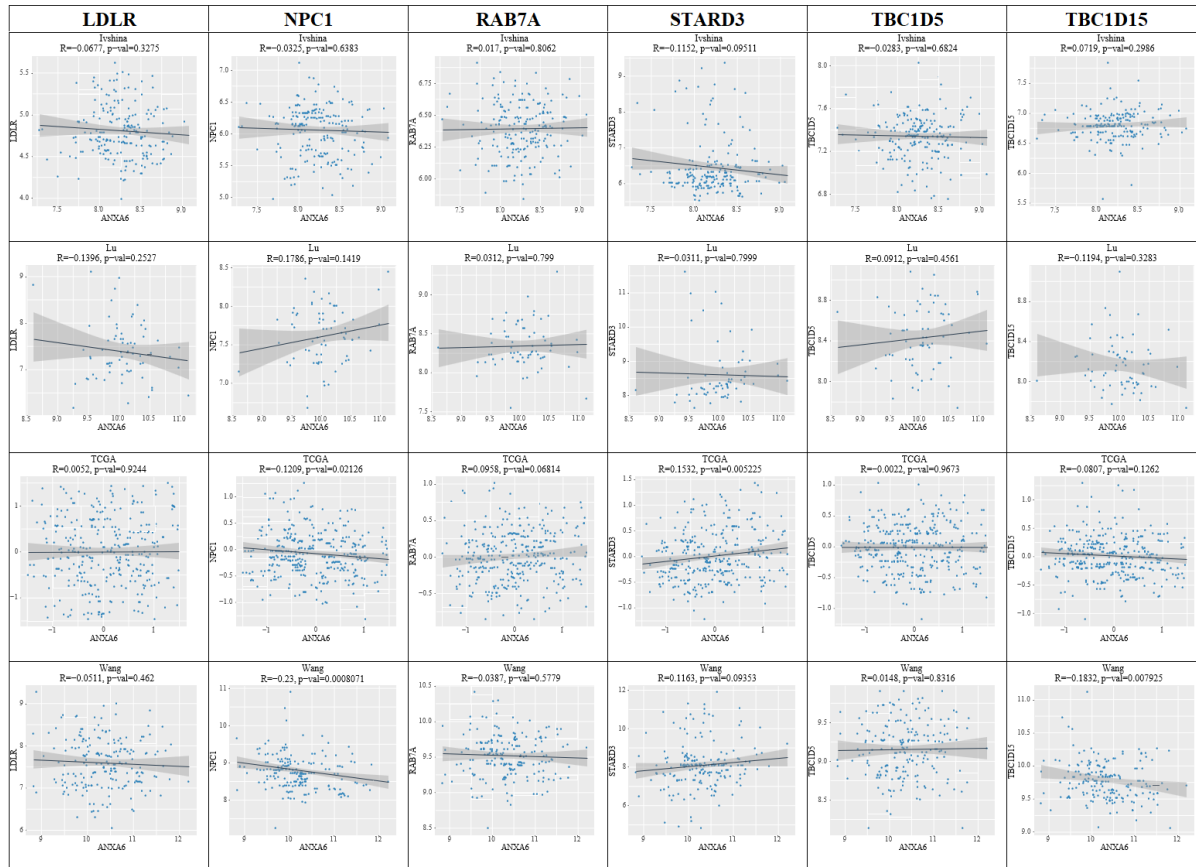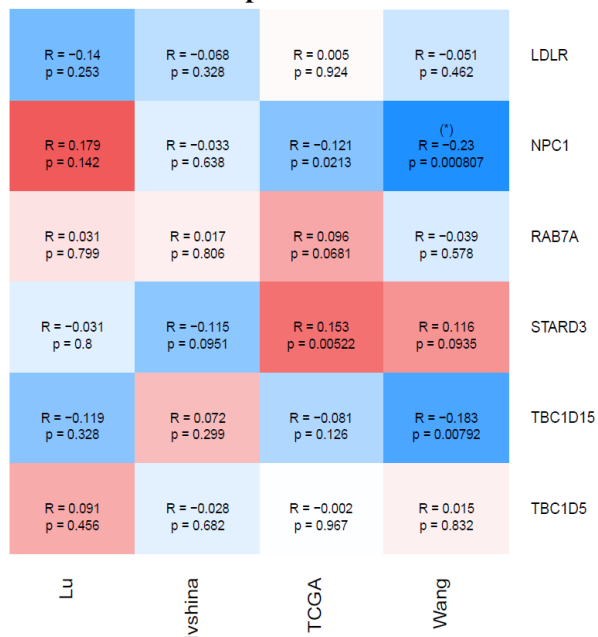

B   **All tumors**

Figure 3.7: **A. Correlation of relative mRNA expression of ANXA6 and LDLR, NPC1, RAB7A, STARD3, TBC1D5 and TBC1D15 in all breast cancers.** The origin of the five different data sets (Lu, Ivshina, Pawitan, TCGA, Wang) are indicated (289, 291, 304-307). Each data point represents relative mRNA expression of ANXA6 (X-axis) and LDLR, NPC1, RAB7A, STARD3, TBC1D5 and TBC1D15 (Y-axis) in a single tumor, respectively. **B. Heatmap with the overall significance (p) and the Pearson coefficient (R) for each correlation analysis is given.** The positive (red) and negative (blue) correlation is indicated.

While overall the strength of these correlations was weak, we found significant negative correlations for ANXA6 and NPC1 expression for several cohorts (Lu,

p=0.01; Ivshina, p=0.08; TCGA, p=0.001 and Wang, p=0.0007) (289, 291, 304-307). This could indicate that irrespective of ER and Her2 status, ANXA6 downregulation might be associated with elevated NPC1 expression in breast cancers.

Furthermore, the positive association of ANXA6 with STARD3 identified in 3/4 ER-negative, 2/4 ER-positive, 2/3 Her2-enriched, 3/3 basal-like and 3/3 luminal breast cancer subtypes (Figures 3.2-3.6) was also significant in 3/5 cohorts when all tumor samples were analyzed (Pawitan, R=0.31, p=4×10^{-5}; TCGA, R=0.17, p=0.0004; Wang, R=0.14, p=0.01) (289, 291, 304-307). Hence, not only in Her-2 positive breast cancers, which often show Her2 and STARD3 co-amplification (32), but also in breast cancers with high ANXA6 levels, elevated STARD3 levels may contribute to increased cholesterol delivery from LE/Lys to other organelles to promote cancer growth and progression (32, 312) (reviewed in (11).

A **Normal**

B **Normal**

Figure 3.8: A. Correlation of relative mRNA expression of ANXA6 and LDLR, NPC1, RAB7A, STARD3, TBC1D5 and TBC1D15 in normal-like tissues. The origin of the two different data sets (289, 291, 306) are indicated. Each data point represents relative mRNA expression of ANXA6 (X-axis) and LDLR, NPC1, RAB7A, STARD3, TBC1D5 and TBC1D15 (Y-axis) in a single tumor, respectively. **B. Heatmap with the overall significance (p) and the Pearson coefficient (R) for each correlation analysis is given.** The positive (red) and negative (blue) correlation is indicated.

Finally, to address if the transformation of normal to cancerous tissue would be accompanied with changes in gene-to-gene correlations related to ANXA6, we determined the gene expression patterns of ANXA6 and LDLR, NPC1, RAB7A, STARD3, TBC1D5 and TBC1D15 in 37 normal-like tissue samples from the Pawitan

cohort, and 8 samples from the TCGA cohort (289, 291, 306). Interestingly, in contrast to the negative correlation of ANXA6 and LDLR in ER-negative, ER-positive, and Her2-enriched breast cancer subtypes, ANXA6 levels showed a strong positive correlation with LDLR in control tissues. Opposite to strong negative correlations of ANXA6 and NPC1 in some ER-negative and HER2-enriched cohorts, ANXA6 and NPC1 expression were not strongly associated in the control groups. Taken together, although the sample numbers in this control groups were limited, this may indicate that ANXA6 differentially contributes to LDLR-mediated endocytosis and NPC1-dependent LDL-cholesterol distribution in normal vs. breast cancer tissues.

A strong positive correlation of ANXA6 and STARD3 was found in the Pawitan cohort (306) with 37 samples (R=0.3, p=0.05). Although this might indicate an association of ANXA6 and STARD3 also in normal tissues, an opposite result was obtained from the small TCGA cohort (8 samples). In addition, negative correlations of ANXA6 with RAB7 and TBC1D15, although not significant, were not apparent in the two control cohorts. Further studies will be needed to address the relationship of ANXA6 with STARD3 as well as the RAB7 and its regulators in **non**-cancerous settings, which might be altered by yet to be identified oncogenic events in certain breast cancer subtypes.

3.4.6. ANXA6 interactome expression patterns in colon cancers

In the colon, ANXA6 is expressed at lower levels compared to other tissues (203, 209) (Figure 2.1) and in colon adenocarcinoma, ANXA6 levels were significantly reduced (Figure 2.3). However, reduced ANXA6 levels in these tumors did not manifest in overall patient survival, which was comparable to colon cancer patients with high ANXA6 expression levels (TCGA) (Figure 2.7A).

We next analyzed the gene-to-gene relationship of ANXA6 with LDLR, NPC1, RAB7A, STARD3, TBC1D5 and TBC1D15 in seven cohorts available in CANCERTOOL (Table 3.7). These sample collections consisted of primary tumors, with two cohorts also providing information on normal adjacent and normal colon tissues (289, 313). Cohort sizes ranged from 150 – 585 samples from predominantly Stage II-III colon cancers, which had spread up to the outer layer of the colon (or rectum) (Stage II) or even up to lymph nodes in the vicinity (Stage III).

Interestingly, in six out of seven data sets from primary tumors cohorts (286, 289, 291, 313-317), there was a trend for a negative correlation of ANXA6 and LDLR levels ranging from R=-

0.08 to R=-0.27 (Figure 3.9). Four of these data sets also showed significance for in part strong correlations (Colonomics: R=-0.27, p=0.006; Laibe: R=-0.25, p=0.03; Marisa R=-0.12, p=0.001; TCGA: R=-0.12, p=0.01). It should be noted that similar trends for the ANXA6/LDLR gene relationship were also noted in the correlation analysis of all three cancer cohorts using cBioPortal (Table 3.2). This relationship was not apparent for ANXA6/NPC1 gene pairs, but alike trends in several breast cancer subtypes (Figure 3.2-3.4), low ANXA6 levels in colon cancers seem associated with elevated LDLR levels, which would favour increased uptake of LDL-derived cholesterol to promote cancer growth and progression.

Study	Colonomics (318-325)	Jorissen (314)	Kemper (315)	Laibe (316)	Marisa (313)	Roepman (317)	TCGA (286, 287, 289)
Primary tumors	98	290	90	130	566	188	376
Normal adjacent	98						
Normal	50		16		16		
Cohort size	246	290	209	130	585	188	376
Other	Stage II	Stage I-IV (n=44,95,93,61) incl. 40 rectum	Stage II	Stage II-III (n=73,57) No rectum	Stage I-IV II-III >80%	Stage II-III	

Table 3.7: Sample size comparison of seven colon cancer cohorts (286, 287, 289, 313-325). The number of samples from primary tumors, normal adjacent and normal tissue samples are listed and were utilized for gene correlation analysis in CANCERTOOL.

Furthermore, in the abovementioned six cohorts (286, 287, 289, 313-325), a positive association of relative ANXA6 amounts with STARD3 levels was also noticeable. Moreover, in three of these cohorts that showed a negative correlation between ANXA6 and LDLR (see above), the strong positive correlation between ANXA6 and STARD3 levels was significant (Kemper: R=0.27, p=0.008; Marisa: R=0.22, p=$3x10^{-8}$; TCGA: R=0.2, p=$4x10^{-5}$). Hence, in colon cancers with high ANXA6 levels, elevated STARD3 levels may enhance cholesterol export from late endosomes/lysosomes to other organelles. This positive gene-to-gene relationship of ANXA6 with STARD3 was also observed in several breast cancer subtypes (Figures 3.2-3.5) and might point at a therapeutic potential of these gene expression patterns, as the recently developed STARD3

inhibitor VS1, which promotes STARD3 degradation, reduced cell viability of both breast and colon cancer cell lines (11, 326).

A   **Primary tumours**

B   **Primary tumors**

	Colonomics	Jorissen	Kemper	Laibe	Marisa	Roepman	TCGA	
	(*) R = −0.274 p = 0.00625	R = 0.049 p = 0.402	R = −0.141 p = 0.187	(*) R = −0.254 p = 0.00351	R = −0.13 p = 0.00199	R = −0.083 p = 0.256	R = −0.126 p = 0.0149	LDLR
	R = 0.043 p = 0.673	(*) R = 0.218 p = 0.000177	R = −0.04 p = 0.707	R = 0.12 p = 0.175	R = 0.003 p = 0.95	R = −0.003 p = 0.963	R = 0.185 p = 0.000322	NPC1
	(*) R = 0.278 p = 0.0056	R = −0.13 p = 0.0266	R = 0.028 p = 0.795	R = −0.129 p = 0.144	R = −0.018 p = 0.67	R = 0.172 p = 0.018	R = 0.05 p = 0.339	RAB7A
	R = 0.15 p = 0.14	R = −0.238 p = 4.12e−05	(*) R = 0.276 p = 0.00838	R = 0.115 p = 0.191	(*) R = 0.229 p = 3.48e−08	R = 0.07 p = 0.339	(*) R = 0.21 p = 4.36e−05	STARD3
	R = −0.107 p = 0.292	R = 0.16 p = 0.00637	R = −0.178 p = 0.0937	R = −0.063 p = 0.478	(*) R = −0.256 p = 6.26e−10	(*) R = −0.279 p = 0.000105	R = −0.028 p = 0.594	TBC1D15
	R = 0.096 p = 0.347	R = −0.078 p = 0.183	(*) R = 0.221 p = 0.0362	R = 0.079 p = 0.373	R = 0.014 p = 0.742	(*) R = 0.226 p = 0.00183	(*) R = 0.324 p = 1.45e−10	TBC1D5

Figure 3.9: A. Correlation of relative mRNA expression of ANXA6 and LDLR, NPC1, RAB7A, STARD3, TBC1D5 and TBC1D15 in seven colon cancer cohorts (see also Table 3.7). The origin of the seven different data sets (Colonomics, Jorissen, Kemper, Laibe, Marisa, Roepman, TCGA) are indicated (286, 287, 289, 313-325). Each data point represents relative mRNA expression of ANXA6 (X-axis) and LDLR, NPC1, RAB7A, STARD3, TBC1D5 and TBC1D15 (Y-axis) in a single tumor, respectively. **B. Heatmap with the overall significance (p) and the Pearson coefficient (R) for each correlation analysis is given.** The positive (red) and negative (blue) correlation is indicated.

Remarkably, alike the majority of colon cancer data sets (Figure 3.9), there was a strong negative correlation of ANXA6 and LDLR levels in normal adjacent (Colonomics: R=-0.39, p=$6x10^{-5}$) and one cohort with control tissue samples (Marisa: R=-0.36, p=0.12) (Figure 3.10). Furthermore, a negative relationship was apparent for ANXA6 in combination with NPC1, RAB7A and STARD3, several of those showing strong and significant associations (e.g. for NPC1 in Colonomics R=-0.24, p=0.01; RAB7 in Colonomics: R=-0.48, p=$3.7x10^{-7}$; Marisa: R=-0.61, p=0.005; for STARD3 in Colonomics: R=-0.32,p=0.001 in both normal adjacent and normal) (Figure 3.10). Hence, low ANXA6 levels in colon may be associated with high LDLR and NPC1 levels, but also RAB7 and STARD3 levels. Together with low TBC1D5 and TBC1D15 levels, this could facilitate very effective LDL-cholesterol uptake and distribution in normal colon tissue. Overall, the negative (LDLR, NPC1, RAB7A, STARD3) and positive (TBC1D5, TBC1D15) associations of ANXA6 with these genes appeared stronger in normal adjacent and normal tissue samples, indicating that transformation might be associated with the loss of these strong gene relationships in colon cancer tissue.

While several reports found blood lipids, including cholesterol, not to be associated with the risk of colon or rectal cancer (327, 328), a recent study identified that pharmacological inhibition of proprotein convertase subtilisin/kexin type 9 (PCSK9), which effectively lowers plasma LDL-cholesterol levels, to modestly reduce tumor growth, and improve lifespan and survival in a mouse model of colon adenocarcinoma (329). The underlying mechanism have yet to be determined.

PCSK9 inhibition leads to increased LDLR expression and LDL-cholesterol uptake and *in vivo*, this enables the liver to effectively clear the plasma from LDL lipoproteins.

Figure 3.10: A. Correlation of relative mRNA expression of ANXA6 and LDLR, NPC1, RAB7A, STARD3, TBC1D5 and TBC1D15 in normal-adjacent and normal tissues from colon cancer cohorts (see also Table 3.7). The origin of the two different data sets (Colonomics, Marisa) are indicated **(313, 318-325)**. Each data point represents relative mRNA expression of ANXA6 (X-axis) and LDLR, NPC1, RAB7A, STARD3, TBC1D5 and TBC1D15 (Y-axis) in a single tumor, respectively. **B. Heatmap with the overall significance (p) and the Pearson coefficient (R) for each correlation analysis is given.** The positive (red) and negative (blue) correlation is indicated.

Hence, one can envisage this to reduce availability of LDL-cholesterol for cancer cells in other tissues, which might contribute to the anti-tumor effects in studies utilizing PCSK9 inhibitors (330).

3.4.7. ANXA6 interactome expression patterns in prostate cancers

Decreased ANXA6 levels in prostate carcinoma (Figure 2.3) and during progression from localized to metastatic stages (Fig. 2.4). Although this did not correlate with reduced ANXA6 levels affecting overall survival (Figure 2.7), this could indicate improved cholesterol handling in advanced prostate cancers. In partial support of this, the gene correlation analysis using cBioportal (3.3.1.4.) showed a trend towards negative association of ANXA6 with LDLR. Yet, STARD3 and TBC1D5 levels positively correlated with ANXA6 levels.

Study	Tomlins (247)	Grasso (248)	Taylor (302)	Glinsky (331)	Lapointe (332)	Varambally (333)	TCGA (291)
Primary tumors	32	49	131		13	7	497
Metastatic	20	27	19		4	6	
Normal, normal adjacent, benign	23	12	29		9	6	
Cohort size	104	88	183	79	26	19	497
Other	29		4	37 Recurrent and 42 non-recurrent			

Table 3.8: The number of samples from primary tumors, normal adjacent, normal tissue samples, benign and metastatic tumors of seven prostate cancer cohorts (247, 248, 291, 302, 331-333). are listed and were utilized for gene correlation analysis in CANCERTOOL.

The correlation of ANXA6 and its interactome expression patterns again showed a trend towards a negative association of ANXA6 with LDLR in 4 from 6 primary prostate tumour sample collections. The Taylor cohort with 37 primary tumors displayed a strong positive association of ANXA6 with LDLR, NPC1, RAB7 and TBC1D5, all of which significant (p=0.0007, 1.2×10^{-8}, 1.7×10^{-7}, 0.0005, respectively), a relationship that was not evident in such a prominent manner in any of the other cohorts. Only the Glinsky cohort (331) showed a significant association of ANXA6 with NPC1 (p=0.0009). In contrast, a significant negative association of ANXA6 with RAB7 (p=0.01) was observed in the Glinsky cohort (331), and similar trends, although not significant, were also seen in 3 other cohorts. TBC1D5 was positively associated with ANXA6 in 3 cohorts, 5 out of 6 cohorts showed a negative association between ANXA6 and TBC1D15, which was significant in the Glinksy cohort (p=0.01) (331), but not observed in cBioportal (3.3.1.4.).

A **Primary tumors**
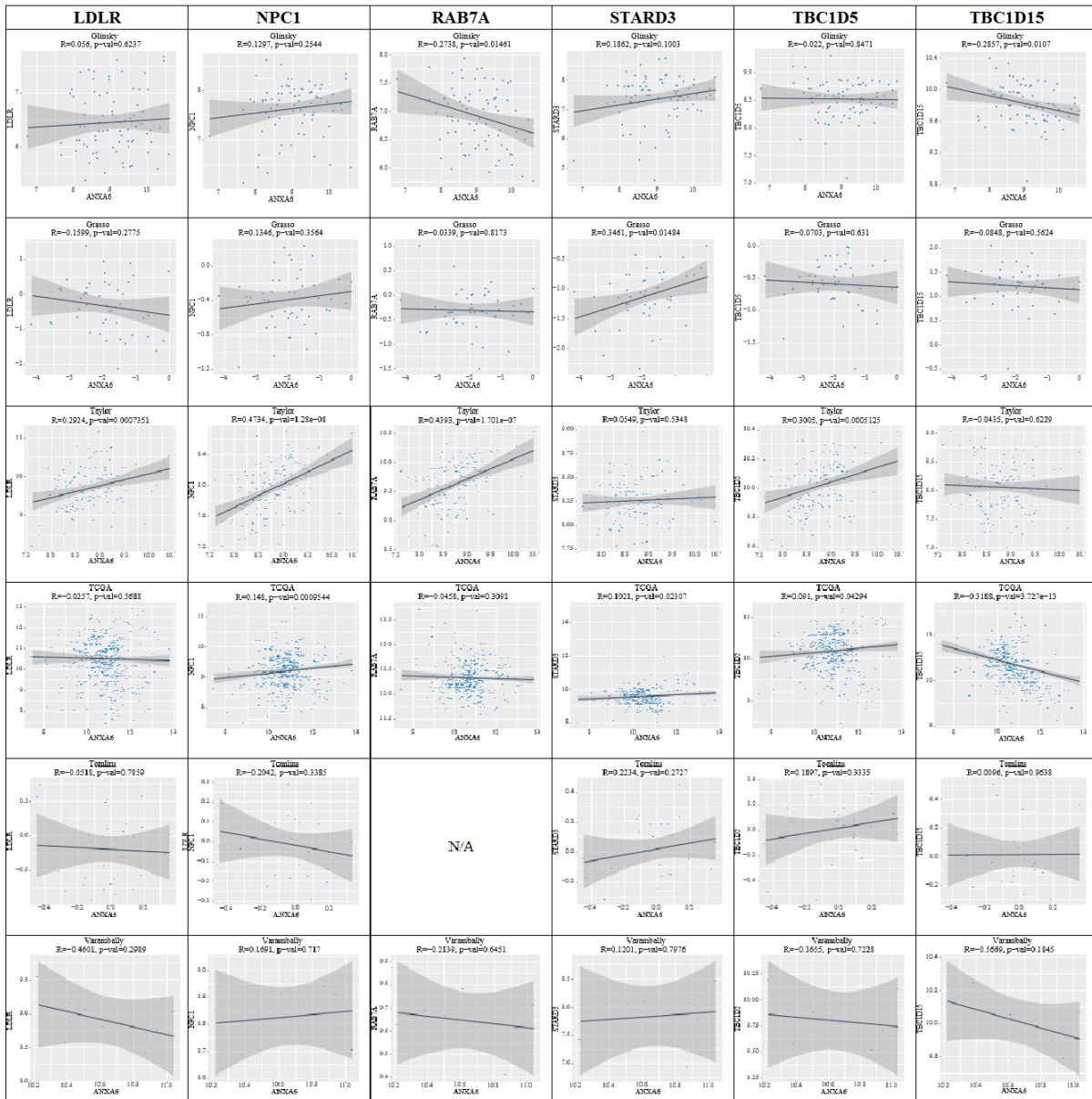
Figure 3.11: A. Correlation of relative mRNA expression of ANXA6 and LDLR, NPC1, RAB7A, STARD3, TBC1D5 and TBC1D15 in primary prostate cancer cohorts. The origins of the different data sets are indicated (247, 248, 291, 302, 331-333). Each data point represents relative mRNA expression of ANXA6 (X-axis) and LDLR, NPC1, RAB7A, STARD3, TBC1D5 and TBC1D15 (Y-axis) in a single tumor, respectively. **B. Heatmap showing the overall significance (p) and the Pearson coefficient (R) for each correlation analysis.** The positive (red) and negative (blue) correlation is indicated.

B   **Primary tumors**

R = 0.13 p = 0.254	R = 0.135 p = 0.356	(*) R = 0.473 p = 1.28e−08	R = 0.148 p = 0.000954	R = −0.204 p = 0.339	R = 0.169 p = 0.717	NPC1
R = 0.056 p = 0.624	R = −0.16 p = 0.278	(*) R = 0.292 p = 0.000735	R = −0.026 p = 0.569	R = −0.052 p = 0.786	R = −0.46 p = 0.299	LDLR
(*) R = −0.274 p = 0.0146	R = −0.034 p = 0.817	(*) R = 0.439 p = 1.7e−07	R = −0.046 p = 0.309	NA	R = −0.214 p = 0.645	RAB7A
R = 0.186 p = 0.1	(*) R = 0.346 p = 0.0148	R = 0.055 p = 0.535	R = 0.102 p = 0.0231	R = 0.223 p = 0.273	R = 0.12 p = 0.798	STARD3
R = −0.022 p = 0.847	R = −0.07 p = 0.631	(*) R = 0.301 p = 0.000512	R = 0.091 p = 0.0429	R = 0.19 p = 0.334	R = −0.166 p = 0.723	TBC1D5
(*) R = −0.286 p = 0.0107	R = −0.085 p = 0.562	R = −0.044 p = 0.623	(*) R = −0.319 p = 3.73e−13	R = 0.01 p = 0.964	R = −0.567 p = 0.184	TBC1D15
Glinsky	Grasso	Taylor	TCGA	Tomlins	Varambally	

Furthermore, and in contrast to the cBioportal correlation analysis, all cohorts revealed trends towards or strong positive association between ANXA6 and STARD3.

A
Metastatic

B
Metastatic

Figure 3.12: A. Correlation of relative mRNA expression of ANXA6 and LDLR, NPC1, RAB7A, STARD3, TBC1D5 and TBC1D15 in metastatic prostate cancer cohorts. The origin of the different data sets is indicated (247, 248, 302, 333). Each data point represents relative mRNA expression of ANXA6 (X-axis) and LDLR, NPC1, RAB7A, STARD3, TBC1D5 and TBC1D15 (Y-axis) in a single tumor, respectively. **B. Heatmap showing the overall significance (p) and the Pearson coefficient (R) for each correlation analysis is given.** The positive (red) and negative (blue) correlation is indicated.

When performing the correlation analysis of ANXA6 with its interactome in metastatic prostate cancers, similar relationships were observed. The Grasso cohort (248) revealed a positive, but not significant association of ANXA6 with RAB7A and TBC1D15. Alike primary tumors, the Taylor cohort (302) showed positive, in part significant associations of ANXA6 with

LDLR, NPC1, RAB7A (p=0.04), TBC1D5 and TBC1D15. The Tomlins sample collection (247) for metastatic tumors also revealed positive and negative associations of ANXA6 with NPC1 and STARD3, respectively. Overall, only the correlation of ANXA6 with STARD3 showed similar trends over 3 different cohorts in metastatic prostate cancers, an observation that was also observed for 5 out 6 primary prostate cancer sample collections. When analyzing all tumor samples (primary + metastatic), the correlation analysis in the Taylor cohort (302) of LDLR, NPC1, RAB7A and TBC1D5 remained significantly associated with ANXA6 (p=7.4x10-8, 5.4x10-7, 0.4x10-8, 0.0008, respectively). Similar trends for NPC1, LDLR and TBC1D5 were observed in 2-3 other cohorts. 4 cohorts remained to display trends towards a negative association of ANXA6 with STARD3, an observation that was significant in the Grasso cohort (p=0.01) and similar to the trends seen in primary and metastatic cohorts (Figure 3.11-3.12). 3 of the 6 cohorts showed a negative and in part significant association of ANXA6 with TBC1D15 (p=0.01, 3.73x10-13 for Glinsky and TCGA cohorts, respectively). This was similar to the correlation data sets obtained from primary, but only to a minor extent to the metastatic sample collections. Interestingly, ANXA6 levels were negatively associated with LDLR in all cohorts with normal prostate tissues (Figure 3.14), which might indicate a change in gene relationships when transformation in prostate tissue occurs. Overall, even though gene correlations differed within cohorts, each cohort appeared to display patterns of gene pair correlations for ANXA6 and its interaction partners that were similar in primary, metastatic and all tumors.
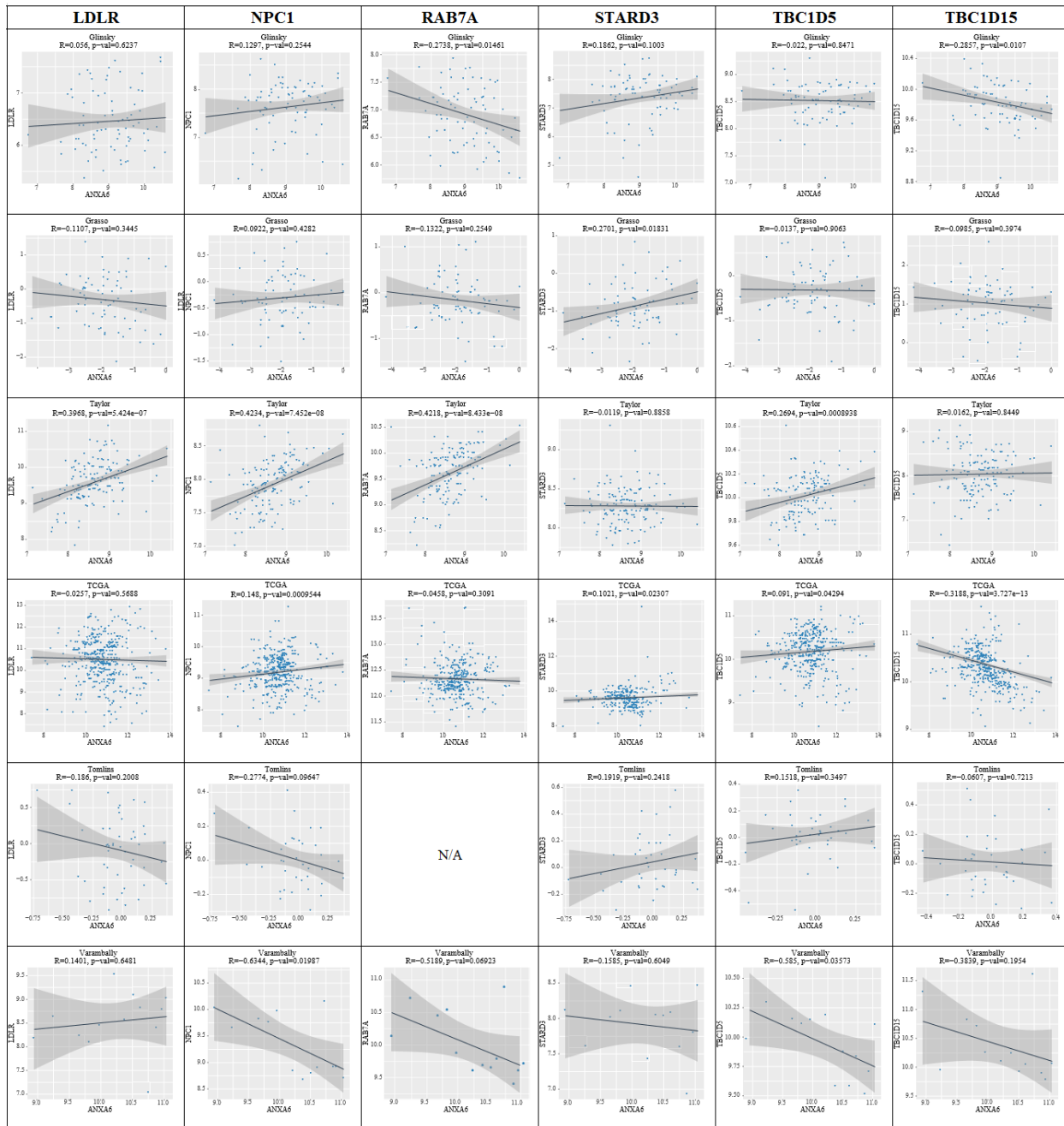
Figure 3.13: A. Correlation of relative mRNA expression of ANXA6 and LDLR, NPC1, RAB7A, STARD3, TBC1D5 and TBC1D15 in cohorts for all prostate tumors. The origins of the different data sets (247, 248, 291, 302, 331-333) are indicated. Each data point represents relative mRNA expression of ANXA6 (X-axis) and LDLR, NPC1, RAB7A, STARD3, TBC1D5 and TBC1D15 (Y-axis) in a single tumor, respectively. **B. Heatmap showing the overall significance (p) and the Pearson coefficient (R) for each correlation analysis is given.** The positive (red) and negative (blue) correlation is indicated.

B   **All tumors**

	Glinsky	Grasso	Taylor	TCGA	Tomlins	Varambally	
	R = 0.13 p = 0.254	R = 0.092 p = 0.428	(*) R = 0.423 p = 7.45e−08	R = 0.148 p = 0.000954	R = −0.277 p = 0.0965	(*) R = −0.634 p = 0.0199	NPC1
	R = 0.056 p = 0.624	R = −0.111 p = 0.345	(*) R = 0.397 p = 5.42e−07	R = −0.026 p = 0.569	R = −0.186 p = 0.201	R = 0.14 p = 0.648	LDLR
	(*) R = −0.274 p = 0.0146	R = −0.132 p = 0.255	(*) R = 0.422 p = 8.43e−08	R = −0.046 p = 0.309	NA	R = −0.519 p = 0.0692	RAB7A
	R = 0.186 p = 0.1	(*) R = 0.27 p = 0.0183	R = −0.012 p = 0.886	R = 0.102 p = 0.0231	R = 0.192 p = 0.242	R = −0.159 p = 0.605	STARD3
	R = −0.022 p = 0.847	R = −0.014 p = 0.906	(*) R = 0.269 p = 0.000894	R = 0.091 p = 0.0429	R = 0.152 p = 0.35	(*) R = −0.585 p = 0.0357	TBC1D5
	(*) R = −0.286 p = 0.0107	R = −0.098 p = 0.397	R = 0.016 p = 0.845	(*) R = −0.319 p = 3.73e−13	R = −0.061 p = 0.721	R = −0.384 p = 0.195	TBC1D15

A **Normal**

B **Normal**

Figure 3.14: A. Correlation of relative mRNA expression of ANXA6 and LDLR, NPC1, RAB7A, STARD3, TBC1D5 and TBC1D15 cohorts of normal prostate tissue samples. The origins of the different data sets are indicated (247, 248, 302, 333). Each data point represents relative mRNA expression of ANXA6 (X-axis) and LDLR, NPC1, RAB7A, STARD3, TBC1D5 and TBC1D15 (Y-axis) in a single tumor, respectively. **B. Heatmap showing the overall significance (p) and the Pearson coefficient (R) for each correlation analysis.** The positive (red) and negative (blue) correlation is indicated.
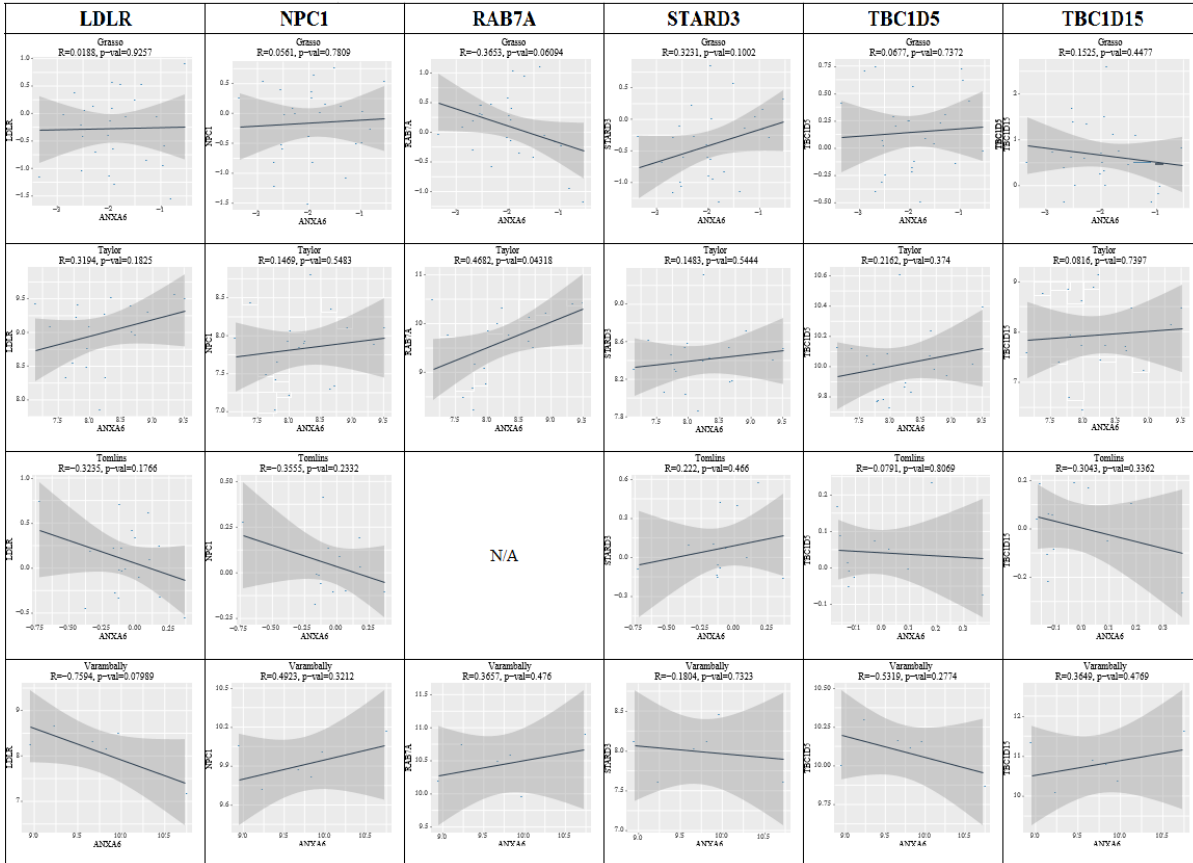
3.5. Discussion

3.5.1. ANXA6 and late endosomal/lysosomal cholesterol transporters expression profiles in cancer

3.5.1.1. The association of ANXA6 and LDLR expression patterns

As outlined in Chapter 1.1.4., upregulated LDLR-mediated endocytosis is common in many cancer cells, driving oncogenic behaviour and adaptations to utilize LDL-derived cholesterol for tumor growth and progression and chemoresistance (2, 92, 93, 97, 101). Yet, for efficient cellular distribution of LDL-derived cholesterol from LE/Lys, a plethora of proteins that coordinate lysosomal targeting of LDL and subsequent LDL-cholesterol export from LE/Lys is required. This includes the gatekeeper function of ANXA6, and previous research from Grewal and coworkers identified ANXA6 depletion to improve delivery of LDL-cholesterol from LE/Lys to the plasma membrane and lipid droplets (see Chapter 2.1.). On the other hand, high ANXA6 expression levels led to an NPC1-mutant-like phenotype and an accumulation of LDL-derived cholesterol in LE/Lys, reducing migratory and invasive behaviour of cancer cells (55, 68, 82, 83, 202).

In this chapter, we therefore aimed to investigate if cholesterol-sensitive cancers display a coordinated expression of ANXA6 and LDLR, which might indicate a functional significance for cancer growth and progression in breast, prostate, colon, pancreatic and liver cancers.

LDLR	Levels	Tumor growth and metastatic behaviour	Prognosis	Drug resistance	ANXA6 levels	ANXA6/LDLR cBioportal	ANXA6/LDLR (Cancertool)
Breast	⇑	⇑	⇓	⇑	⇓ (TNBC, ER-neg.)	Positive (2/4) (Her2+, ER+)	Negative: 5/5 (ER-), 3/4 (ER+), 3/3 (Her2+)
Prostate		⇑	⇓		⇓ (local-advanced)	Negative (5/8)	Negative (2/4) metastatic
Colon	⇑	⇑			⇓	Negative (3/3)	Negative (6/7)
Pancreas	⇑	⇑	⇓	⇑	⇑	Negative (2/2)	N.A.
Liver	⇑				⇓	Positive (1/1)	N.A.

Table 3.9: Up- (⇑) or downregulated (⇓) LDLR and ANXA6 expression levels and association with tumor growth, metastatic behaviour, prognosis, and drug resistance in breast, prostate, colon, pancreatic and liver cancers (see Chapters 1.1.4. and 2.1. for further details). The overall trends (and number of cohorts) in ANXA6/LDLR gene pair association studies using expression data from cBioportal and CANCERTOOL are given. Abbreviations: TNBC, triple-negative breast cancer; ER, estrogen receptor; Her2, human epidermal growth factor receptor 2 (Erbb2); N.A., not available.

LDLR upregulation and enhanced LDL uptake has been reported for breast cancer (106, 107), colorectal carcinoma (69, 111), hepatocellular carcinoma (HCC) (108), and PDAC (104, 105), which correlates with increased aggressiveness, poor prognosis and development of drug resistance as summarized in Table 3.9 for breast, prostate, colon and pancreatic cancers, respectively (for details see Chapter 1.1.4.).

ANXA6 downregulation and potential tumor suppressor function has been described in TNBC overexpressing EGFR and ER-negative breast cancer cell lines (73, 74, 201, 204, 231), hepatocellular carcinomas (233), and during prostate cancer progression (Figure 2.4). On the other hand, elevated ANXA6 levels were reported in pancreatic cancer (221, 222).
Gene correlation analysis using cBioportal found a positive correlation between ANXA6 and LDLR levels in Her2+ and ER-positive cancers (2/4), both breast cancer subtypes that up to date have not yet been linked with de-regulated LDL uptake or ANXA6 cancer-related functions. Likewise, trends towards negative and positive correlation of the ANXA6/LDLR gene pair in pancreas and liver, respectively, did not support published findings of ANXA6 expression in these cancers (221, 222, 233). Yet, a negative correlation between ANXA6 and LDLR in prostate (5/8) and colon (3/3) cancer cohorts was observed, which matches proposed ANXA6 tumor suppressor functions in these cancers.

Strikingly, gene correlation analysis using CANCERTOOL found trends for negative correlations between ANXA6 and LDLR levels in ER-negative cancers (5/5), metastatic prostate cancers (2/4) and colon cancers (6/7). These findings support published reports on either the downregulation of ANXA6 or the upregulated LDLR levels in these cancers. Hence, this gene pair expression pattern could support a cancer-promoting model of increased LDL uptake being accompanied by an efficient distribution of LDL-cholesterol from LE/Lys via NPC1-dependent and NPC1-independent (and ANXA6-regulated) routes to other cellular organelles.

3.5.1.2. The association of ANXA6 and NPC1 expression patterns

Elevated NPC1 levels were found in metastatic ER-negative breast cancer cells and were associated with poor prognosis (165). Although NPC1 upregulation correlates with increased cancer risk, poor prognosis, and drug resistance in several cancers (see Chapter 1.4.2 for details), reports on NPC1 expression levels in prostate, colon and pancreatic cancers and their potential impact on aggressiveness, survival and treatment outcome are still limited. Yet, pharmacological

inhibition of NPC1 has been proposed as a therapeutic target in prostate and pancreatic cancers (175, 176, 178). On the other hand, cholesterol accumulation in LE/Lys during acute or chronic liver dysfunction increases the risk of fibrosis and cirrhosis, which can lead to the development of HCC (171). Furthermore, elevated NPC1 levels may support drug efflux and undermine chemotherapies (168, 169).

While ANXA6 depletion could overcome NPC1 deficiency to restore cholesterol export from LE/Lys, ANXA6 overexpression caused cholesterol accumulation in LE/Lys, even in cells expressing NPC1, indicating that elevated ANXA6 interfere with NPC1-dependent cholesterol transport even in normal cells (55, 68, 82, 83, 202).

Strikingly, in TNBC and ER-negative breast cancers, NPC1 upregulation and associated poorer prognosis and possible drug resistance as well as reduced ANXA6 expression has been reported. These observations from independent studies are supported by the negative correlation of ANXA6 and NPC1 in 2/4 breast cancer cohorts analyzed in cBioportal, and 4/4 (ER-), 3/4 (ER+) and 3/3 (Her2+) cohorts examined using CANCERTOOL. On the other hand, both cBioportal and CANCERTOOL identified positive ANXA6/NPC1 gene pair associations mainly in Her2+ and ER-positive breast cancers, an observation that was also made for the ANXA6/LDLR gene pair (see 3.4.1.1.). Nevertheless, a substantial number of expression data from various breast cancer cohorts suggest that the combination of high NPC1 and low ANXA6 levels promote an efficient cellular distribution of incoming LDL-cholesterol to promote breast cancer growth and progression, leading to poorer prognosis and treatment response.

NPC1	Levels	Prognosis	Drug target	Drug resistance	ANXA6 levels	ANXA6/NPC1 cBioportal	ANXA6/NPC1 (Cancertool)
Breast	⇑	⇓		⇑?	⇓ (TNBC, ER-neg.)	Negative (2/4) Positive (2/4; Her2+, ER-positive)	Negative: 4/4 (ER-), 3/4 (ER+), 3/3 (Her2+), 3/3 (basal), Positive: 2/3 (luminal)
Prostate			Yes		⇓ (local-advanced)	Positive (4/8)	Positive: 5/6 (primary), 3/4 (metastatic)
Colon					⇓	Negative (3/3)	Positive (5/7)
Pancreas			Yes		⇑	Negative (2/2)	N.A.
Liver		⇓?			⇓	Negative (1/1)	N.A.

Table 3.10: Up- (⇑) or downregulated (⇓) NPC1 and ANXA6 expression levels and association with prognosis, drug target potential and drug resistance in breast, prostate, colon, pancreatic and liver cancers (see Chapters 1.4.2. and 2.1. for further details). The overall trends (and number of cohorts) in ANXA6/NPC1 gene pair association studies using expression data from cBioportal and CANCERTOOL are given. Abbreviations: TNBC, triple-negative breast cancer; ER, estrogen receptor; Her2, human epidermal growth factor receptor 2 (Erbb2); N.A., not available.

Both cBioportal and CANCERTOOL identified several prostate cancer cohorts with positive ANXA6/NPC1 gene pair associations, indicating high ANXA6 together with high NPC1 levels to provide cancer cells with growth and progression advantages. This trend was also observed in metastatic prostate cancer cohorts using CANCERTOOL, although expression analysis of primary and metastatic prostate cancers indicated downregulation of ANXA6 during prostate cancer progression (Figure 2.4).

Negative association of ANXA6 with NPC1 using cBioportal in all colon, pancreatic and liver cohorts could indicate an effective distribution of internalized LDL-cholesterol in these cancers, although this was not supported by the trend of a positive association of the ANXA6/NPC1 gene pair in 5/7 colon cancer cohorts using CANCERTOOL. Yet, alike observation made for the ANXA6/LDLR pair, a trend towards a negative association of ANXA6 and NPC1 was observed in many cohorts, indicating that many cancers may develop gene-regulatory or post-translational strategies to downregulate ANXA6 levels in order to ensure efficient LDL uptake and its subsequent distribution to other organelles.

3.5.1.3. The association of ANXA6 and RAB7 expression patterns

Tumorigenic and anti-tumorigenic activities related to RAB7 influence cell growth and motility (334, 335). Elevated RAB7 was reported in ovarian, thyroid, and peritoneal serous carcinoma (336, 337). In mice lacking lysosomal lipase, metabolic reprogramming led to RAB7-dependent endothelial tumor growth and metastasis (338). RAB7 has also been linked to oncogenic signal transduction induced by lipids, mTORC1 or Rac1 GTPase and associated with migration, and anti-apoptotic signaling in lung and breast cancer (338-341). Vice versa, migration and invasion of cervical and fibrosarcoma cell lines was blocked by a dominant-negative RAB7 mutant (342).

RAB7 and tumor outcomes	Cancer types
Tumor promoter	A431 squamous carcinoma (56, 341), lung cancer (340), breast cancer (341), cervical carcinoma (342), ovarian cancer (337), peritoneal serous carcinoma (337), thyroid cancer (336)
Tumor suppressor	A549 lung cancer (343), glioblastoma (170), thyroid cancer (344)
Oncojanus	inflammatory breast cancer (345), melanoma (346)
Chemoresistance	Cisplatin: cervical cancer (266)

Table 3.11: Roles of RAB7 in the various cancer types. Adapted from (11).

Yet, RAB7 deficiency promoted metastatic properties in prostate cancer and glioblastoma (170, 347), supported oncogenic EGFR activity and cancer progression in thyroid cancers (344) and A549 lung cancer xenografts (343). RAB7 downregulation correlated with cisplatin resistance in cervical cancer cell lines (266). Hence, tumor promoter and suppressor roles for RAB7 in different cancers exist, and some cancers display changes in RAB7 levels during progression (346) and inflammation (345).

RAB7	Levels	Prognosis	Drug target	Drug resistance	ANXA6 levels	ANXA6/RAB7 cBioportal	ANXA6/RAB7 (Cancertool)
Breast	⇑		Yes?		⇓ (TNBC, ER-neg.)	Negative (2/4) Positive (2/4; Her2+, ER-positive)	Negative: 3/4 (ER-), Positive: 3/4 (ER+), 2/3 (Her2+), 2/3 (basal), 2/3 (luminal)
Prostate					⇓ (local-advanced)	Positive (6/8)	Negative: 2/6 (primary), Positive: 2/4 (metastatic)
Colon					⇓	Positive (2/3)	Positive (5/7)
Pancreas					⇑	Positive (2/2)	N.A.
Liver					⇓	Positive (1/1)	N.A.

Table 3.12: Up- (⇑) or downregulated (⇓) RAB7 and ANXA6 expression levels in breast, prostate, colon, pancreatic and liver cancers. RAB7 expression levels and association with prognosis, drug target potential and drug resistance in breast, prostate, colon, pancreas, and liver cancers are lacking. Based on anticancer activity of RAB7 inhibition in other models (see text for details), RAB7 might have potential as a drug target in breast cancer. The overall trends (and number of cohorts) in ANXA6/RAB7 gene pair association studies using expression data from cBioportal and CANCERTOOL are given. Abbreviations: TNBC, triple-negative breast cancer; ER, estrogen receptor; Her2, human epidermal growth factor receptor 2 (Erbb2); N.A., not available.

Alike the prominent negative association of ANXA6 with LDLR and NPC1 in many ER-negative cohorts (Tables 3.9 and 3.10), ANXA6/RAB7 gene pairs showed a trend towards negative association in 2/4 (cBioportal) breast cancer cohorts and 3/4 ER-negative breast cancer groups (CANCERTOOL). This correlates with RAB7 overexpression (338-341) and ANXA6 downregulation observed in TNBC and ER-negative breast cancers in other studies (73, 74, 201, 204, 231). Taken together, this supports a scenario in ER-negative and TNBC breast cancers of low ANXA6 levels ensuring upregulated LDL-uptake and distribution due to high LDLR, NPC1 and RAB7 expression levels. On the other hand, trends towards positive associations of ANXA6 with RAB7 in a large number of prostate, colon, pancreas and liver cohorts from cBioportal and CANCERTOOL was observed. In prostate, colon, and liver, where low ANXA6 has been reported, this might reflect tumor suppressor activities of RAB7. However, it remains to be determined if the association of ANXA6/RAB7 gene pairs in these cancer types reflects alterations in cholesterol homeostasis.

3.5.1.4. The association of ANXA6 and STARD3 expression patterns

The STARD3 gene is located on chromosome 17 within 50 kilobases from the Her2 (Erbb2) locus [164] and in many breast carcinomas (~25%), STARD3 and Her2 are co-amplified and highly expressed (311, 348-352). This correlates with lower drug efficacy (trastuzumab) (350, 353, 354) and poor overall survival, disease metastasis-free survival and relapse-free survival in Her2-positive breast cancer (311, 312, 350). However, highlighting the differential contribution of this cholesterol transporter to breast cancer progression, in ER-positive and TNBC's low STARD3 levels are common and associated with poor prognosis and reduced overall survival (350). These opposite findings within breast cancer subtypes might reflect different roles for STARD3 in the direction of cholesterol transfer to and from LE/Lys (see also Chapter 1.1.3.2.). Elevated STARD3-mediated delivery of cholesterol to mitochondria has been proposed to contribute to intratumoral steroid production in estrogen-responsive tumors, promoting breast cancer cell migration and invasion (312, 355-357). In Her2-positive breast cancer, STARD3 deficiency decreased tumor cell propagation (358, 359). Alternatively, STARD3 might contribute to tumor growth and migratory/invasive behaviour via delivering cholesterol from LE/Lys to focal adhesions and lipid droplets, in particular in cells that express low levels of ANXA6 (55, 56).

STARD3 expression and cancer	Cancer types
Tumor risk	breast cancer (350), gastric cancer (360, 361), ovarian cancer (362)
Prognosis	breast cancer (312), ER-positive and triple-negative breast cancer (350), gastric cancer (360), prostate cancer (363)
Chemotherapy response	breast cancer (312, 364)
Therapeutic target	compound VS1: breast and colon cancer (326)

Table 3.13: Roles of STARD3 in various cancers. Adapted from (11).

Elevated STARD3 has also been documented in ovarian cancer (362). Alike some breast carcinoma, STARD3 was co-amplified with Her2 in gastric cancer (360, 361), correlated with poor prognosis (360) and was proposed to stimulate cholesterol transfer to mitochondria for improved mitochondrial homeostasis, steroidogenesis and cancer cell survival (361), (365). In >20% primary human gastric cancers, fusion of the STARD3 gene with protein phosphatase 1 regulatory inhibitor subunit 1B has been considered to promote signal transduction pathways that promote cell proliferation (366). Furthermore, elevated STARD3 was associated with increased risk of

pancreatic cancer (367) and short relapse-free time in prostate cancer (363). These many studies linking STARD3 upregulation with cancer progression and poor outcome prompted efforts to develop STARD3 inhibitor VS1, which induced STARD3 degradation and reduced cell viability of breast and colon cancer cell lines (326). In addition, lapatinib treatment in STARD3-depleted breast cancer cells promoted apoptotic events to reduce survival and proliferation (359).

STARD 3	Levels	Prognosis	Drug efficacy	Drug target	ANXA6 levels	ANXA6/STARD3 cBioportal	ANXA6/STARD3 (Cancertool)
Breast (Her2+)	⇑	⇓	⇓ (trastuz-umab)	VS1		Positive (4/4; 2/4: Her2+)	Strong Positive: 2/3 (Her2+), p=0.01, 0.004
Breast (TNBC, ER+)	⇓	⇓			⇓ (TNBC, ER-neg.)	Positive (4/4; 2/4 ER-+)	Positive: 2/4 (ER+) Positive: 3/4 (ER-), Positive: 3/3 (basal) Positive: 3/3 (luminal) Negative: 2/4 (ER+)
Prostate	⇑	⇓			⇓ (local-advanced)	Positive (8/8)	Positive: 6/6 primary 3/4 (metastatic)
Colon				VS1	⇓	Positive (3/3)	Positive (5/6)
Pancreas	⇑				⇑	Positive (2/2)	N.A.
Liver					⇓	Positive (1/1)	N.A.

Table 3.14: Up- (⇑) or downregulated (⇓) STARD3 and ANXA6 expression levels and association with poor prognosis, and drug efficacy in breast, prostate, colon, pancreatic and liver cancers. VS1 might have therapeutic potential in breast and colon cancers with high STARD3 levels. The overall trends (and number of cohorts) in ANXA6/STARD3 gene pair association studies using expression data from cBioportal and CANCERTOOL are given. Abbreviations: TNBC, triple-negative breast cancer; ER, estrogen receptor; Her2, human epidermal growth factor receptor 2 (Erbb2); N.A., not available.

STARD3 facilitated cholesterol transfer from LE/Lys to the ER in ANXA6-depleted NPC1 mutant cells, followed by ACAT-dependent cholesterol esterification and cholesteryl ester storage in lipid droplets (55). siRNA-mediated STARD3 knockdown led to the loss of this NPC1-independent cholesterol transport route in ANXA6-depleted NPC1 mutant cells. Hence, in this NPC1 mutant cell model, an increased involvement of STARD3 in cholesterol export from LE/Lys to the ER was only observed in the absence of ANXA6. These observations would implicate low ANXA6 levels to promote the involvement of STARD3 in cholesterol distribution in cells. On the other hand, high ANXA6 levels would probably restrict the involvement of STARD3 in cholesterol

transfer from the LE/Lys compartment to the ER. Strikingly, the gene correlation of the ANXA6/STARD3 gene pair in cBioportal revealed a positive correlation in all cancer cohorts, including breast, prostate, colon, pancreas, and liver (Table 3.14). Likewise, the majority of cancer cohorts analyzed with CANCERTOOL revealed a positive association of ANXA6 and STARD3.

This may indicate that the expression of these genes is coordinated and that ANXA6 might indeed be a gatekeeper that controls the involvement of STARD3-mediated cholesterol transfer from LE/Lys to the ER. For example, both low ANXA6 and low STARD3 levels have been reported in TNBC, and in both cases, been associated with poor prognosis and reduced overall survival (71, 76, 350). It is tempting to speculate that ANXA6 might regulate the cholesterol transfer directions mediated by STARD3. In NPC1 mutant cells, cholesterol accumulation in LE/Lys triggers transfer of increased amounts of cholesterol into mitochondria (368). Cholesterol accumulation in LE/Lys also occurs in cells expressing high ANXA6 levels (83). This could promote STARD3-mediated delivery of cholesterol to mitochondria for energy and steroid production in estrogen-responsive breast tumors (312, 355-357), but also androgen-responsive prostate cancers.

3.5.1.5. The association of ANXA6 and TBC1D15 expression patterns

Rab effectors, in particular Rab guanine nucleotide exchange factors (Rab-GEFs) and Rab-GTPase activating proteins (Rab-GAPs) are critical regulators of Rab activity, balancing the amount of active (GTP-bound) and inactive (GDP-bound) Rab-GTPases. Three members of the Tre2-Bub2-Cdc16 (TBC) domain-containing family of Rab-GAPs (Armus, TBC1D5, TBC1D15) promote RAB7 inactivation (369). However, little is yet known about the contribution of RAB7-GAPs in cancer. Out of the three RAB7-GAPs, Armus has been reported to promote E-cadherin degradation, which controls cell-cell adhesion, a critical feature that when de-regulated, contributes to epithelial tumorigenesis (370). In addition, many tumors overexpress the miRNA-17-92 cluster (also called oncomir-1), which also targets Armus and thereby affects RAB7-dependent endocytic trafficking (371). Armus is also overexpressed in some breast and colon cells, connecting RAB7-dependent autophagy with cell plasticity and oncogenesis.

Reports linking TB1D5 or TBC1D15 with cancer growth and progression are still lacking. In pulldown assays, ANXA6 interacted with TBC1D15 (55) and TBC1D5 (Grewal and Enrich, unpublished), but not Armus. Also, only TBC1D15, but not TBC1D5 or Armus, translocated to

LE/Lys upon ANXA6 overexpression (55). The functional relevance of ANXA6/TBC1D5 protein-protein interaction has still to be clarified. Yet, the ANXA6-mediated recruitment of TBC1D15 to LE/Lys, promoting LDL-cholesterol delivery from LE/Lys to focal adhesions and lipid droplets, could be relevant for metastatic behaviour of cancer cells (11). Hence, the proposed roles for RAB7 as a tumor promoter and suppressor (334-342) could be influenced by TBC1D15 and the other two RAB7-specific GAPs.

TBCs	ANXA6 levels	Prognosis	ANXA6/ TBC1D5 cBioportal	ANXA6/ TBC1D5 Cancertool	ANXA6/ TBC1D15 cBioportal	ANXA6/ TBC1D15 Cancertool
Breast	⇓ (TNBC, ER-neg.)	⇓	Positive (2/4, ER+)	Positive (2/4 ER-, 2/3 Her2+, 3/3 basal)	Positive 4/4	Positive (2/4 ER-) Negative (3/4 ER-, 2/3 Her2+, 2/3 luminal, 2/2 normal)
Prostate	⇓ (local-advanced)	⇓	Positive (5/8 primary, 2/4 metastatic) Negative (2/4 metastatic)	Positive (3/6) Negative (3/6)	Negative (6/8)	Positive (2/4 metastatic) Negative (4/6 primary, 2/4 metastatic)
Colon	⇓		Positive (3/3)	Positive (5/7 primary, 3/3 normal, adjacent)	[Negative (2/3)]	Negative (5/7) Positive (2/3 normal, adjacent)
Pancreas	⇑		Positive (2/2)	N.A.	[Positive (2/2)]	N.A.
Liver	⇓		[Positive (1/1)]	N.A.	[Positive (1/1)]	N.A.

Table 3.15: Up- (⇑) or downregulated (⇓) ANXA6 expression levels and association with poor prognosis in breast, prostate, colon, pancreatic and liver cancers. The overall trends (and number of cohorts) in ANXA6/TBC1D5 and ANXA6/TBC1D15 gene pair association studies using expression data from cBioPortal and CANCERTOOL are given. Abbreviations: TNBC, triple-negative breast cancer; ER, estrogen receptor; Her2, human epidermal growth factor receptor 2 (Erbb2); N.A., not available.

The gene correlation of the ANXA6/TBC1D5 gene pair in cBioPortal showed a (sometimes weak) positive correlation in breast, prostate, colon, pancreas, and liver cancers (Table 3.15). Interestingly, a negative correlation between ANXA6 and TBC1D5 was found in 2/4 metastatic prostate cancer cohorts, Similarly, the ANXA6/TBC1D15 gene pair showed negative association in 6/8 cohorts in cBioPortal, and in 4/6 and 2/4 primary and metastatic prostate cancer cohorts, respectively. Likewise, in 3/4 ER-negative cancer cohorts, as well as Her2+ (2/3) and luminal (2/3) cancers, ANXA6 was negatively associated with TBC1D15. Hence, low ANXA6 levels may

not accommodate for an effective recruitment of highly expressed TBC1D5 and TBC1D15 proteins to downregulate RAB7 activity. Future experiments in prostate and breast cancer cell models determining TBC1D5 and TBC1D15 membrane association and RAB7 activity may clarify if ANXA6/TBC1D5 and ANXA6/TBC1D15 gene association studies reflect RAB7-dependent biological activities relevant for cancer cell growth and motility.

Chapter 4

Expression patterns of the endo-lysosomal ANXA6 interactome and overall patient survival in different cancers

4.1. Introduction

As described in Chapter 3, gene networks determine biological outcome, and the coordinated expression of genes have functional significance for cancer growth and progression (253, 283, 284, 372). In support of this concept, the analysis of ANXA6 expression patterns in combination with interaction partners of the ANXA6 interactome (LDLR, NPC1, RAB7, STARD3, TBC1D15, TBC1D5) identified several gene pair correlations that could reflect ANXA6 to modulate cellular distribution of LDL-cholesterol, thereby contributing to cancer aggressiveness, progression, and treatment outcome.

Indeed, some observations support a tumor suppressor function for ANXA6 that is related to increased LDL uptake and LDL-cholesterol distribution. For instance, gene correlation analysis using CANCERTOOL found trends for negative correlations between ANXA6 and LDLR levels in ER-negative cancers (5/5 cohorts), metastatic prostate cancers (2/4) and colon cancers (6/7). In this scenario, elevated LDLR would enable increased LDL uptake, and low ANXA6 levels would ensure efficient distribution of LDL-cholesterol from LE/Lys to other cellular organelles (see Chapter 3.3.2.).

Likewise, a negative association of ANXA6 with NPC1 using cBioportal in all colon, pancreatic and liver cohorts could indicate an effective distribution of internalized LDL-cholesterol in these cancers, and in CANCERTOOL a trend towards a negative association of ANXA6 and NPC1 was observed in many cohorts, indicating cancers to downregulate ANXA6 levels in order to allow for effective cellular distribution of LDL-cholesterol.

Interestingly, in line with a scenario in ER-negative and TNBC breast cancers of low ANXA6 levels ensuring upregulated LDL uptake and LDL-cholesterol distribution due to high LDLR and NPC1 expression levels, ANXA6/RAB7 gene pairs also showed trends towards a negative association in breast cancer, including ER-negative breast cancer cohorts analyzed in cBioportal and CANCERTOOL (Chapter 3.3.2.). This is an attractive hypothesis, and findings related to the

ANXA6/RAB7 gene pair could indicate increased activity of NPC1-dependent as well as -independent cholesterol export routes from LE/Lys. In addition, the gene pair analysis of ANXA6 and TBC1D15 or TBC1D5 did not reveal strong positive correlations indicative of cancers downregulating ANXA6-mediated recruitment of TBCs to increase potentially oncogenic RAB7 activity (Chapter 3.3.2).

Yet, the ANXA6/STARD3 gene pair often showed a positive correlation in all cancer cohorts, including breast, prostate, colon, pancreas, and liver in cBioportal and CANCERTOOL (Table 3.14), which may indicate ANXA6 to control the involvement of STARD3-mediated cholesterol transfer from LE/Lys to the ER.

In this chapter, we aimed to extend these findings by analyzing overall survival of gene pairs to possibly identify ANXA6-related functional links to cancer aggressiveness, progression, and prognosis.

4.2. Aims

In addition to analyzing the potential association of gene pair expression patterns, the expression levels of gene pairs also provide insights on disease outcome and prognosis. Well known examples include the accumulation of oncogenic mutations, such as EGFR amplification together with the loss of tumor suppressor phosphatase and tensin homolog deleted on chromosome 10 (PTEN) or p53 in glioma, colorectal and other cancers (373, 374).

Gene pair associations also exist in cellular metabolism related to cholesterol homeostasis. For instance, elevated levels of the cholesterol-binding protein caveolin-1, which is a critical scaffold for the formation of cholesterol-rich caveolae at the cell surface, structures believed to act as signalling hubs controlling cancer growth and progression, were positively associated with genes responsible for lipid scavenging and metabolism in prostate cancer (375). Similarly, upregulation of multiple genes driving increased cholesterol synthesis in hepatocellular carcinoma contributes to cancer progression (376).

Hence, based on the ANXA6-related gene correlations described above (see also Chapter 3), together with current literature pointing at the need for changes in gene networks to cause metabolic changes that support cancer growth and progression, we hypothesized that analysis of ANXA6 expression levels in combination with LDLR, NPC1, RAB7, STARD3, TBC1D5 and TBC1D15 could provide insights into cancer prognosis. As described in detail in the previous

chapters, high ANXA6 levels cause LDL-cholesterol accumulation characterized by NPC1 inhibition and low RAB7 activity, which correlates with reduced cancer cell growth and migratory behaviour. Hence, we hypothesized that high ANXA6 levels in combination with low NPC1, RAB7A or STARD3 or high TBC1D15 expression levels would display reduced cholesterol export from LE/Lys. This would ultimately lower cholesterol availability for cancer growth and progression. Furthermore, if cholesterol export from LE/Lys affects cancer outcome, these gene pair associations could be reflected in improved overall patient survival. On the other hand, low ANXA6 level promote NPC1-independent cholesterol efflux routes via STARD3 in a RAB7-dependent manner, which correlates with increased metastatic potential (55, 56, 83, 86, 87, 152). Thus, the combination of low ANXA6 levels together with high NPC1, Rab7, StARD3 or low TBC1D15 expression levels would provide a scenario of increased cholesterol availability for cancer cells to grow and metastasize, which could be manifested in a reduced overall patient survival. In this chapter, therefore we aimed to extend our analysis on ANXA6 and its interactome, analyzing the probability of overall patient survival in gene pairs that relate to the role of ANXA6 in the LE/Lys compartment.

4.3. Methods

4.3.1. Analysis of overall patient survival probability with high/low ANXA6 and ANXA6 interactome partners expression levels using cBioPortal

As outlined in Chapter 3.3.1., the cBioportal platform provides access to data sets and tools that enable analysis of expression pattern of single genes, as well as gene pairs within a cancer cohort. In addition to gene pair expression patterns shown in Chapter 3, cBioportal also allows the correlation of patient survival probability for selected gene pairs. The cancer datasets from TCGA Firehose Legacy (286, 287, 291) contain the relative expression levels of individual genes in each tumor sample compared to its expression levels in the whole population of samples with relatively high (EXP>1) and low (EXP<1) mRNA expression for LDLR, NPC1, RAB7A, STARD3, TBC1D5 and TBC1D15 were selected, and within these subgroups, samples with high/low ANXA6 expression levels were identified. Overall patient survival probability (%) was plotted for high/low levels of individual genes (Panels A) and then survival was plotted for subgroups that contained high LDLR, NPC1, RAB7A, STARD3, TBC1D5 and TBC1D15 in combination with high/low ANXA6 (Panels B). Then survival was plotted for low LDLR, NPC1, RAB7A, STARD3, TBC1D5 and TBC1D15 in combination with high/low ANXA6. The sample number for each subgroup is provided and the statistical significance was calculated.

4.3.2. Expression pattern of individual breast and prostate cancer samples

The cBioportal platform also allows the display of multiple genes for each tumor sample. ER-negative and EGFR overexpressing cancer samples from a cohort of invasive breast carcinoma samples (n>1000) (286, 287, 291) as well as 50 lethal, heavily pre-treated metastatic castration-resistant prostate cancer obtained after rapid autopsy (248). were analyzed. Individual tumor samples with high/low expression levels of ANXA1, LDLR, NPC1, RAB7A, STARD3, TBC1D5 and TBC1D15 were identified (red: EXP>1; blue: EXP<1); grey: mean expression) and plotted.

4.4. Results

4.4.1. Expression patterns of the endo-lysosomal ANXA6 interactome and overall patient survival in breast cancer

To analyze the potential impact of gene pair associations within the ANXA6 interactome for overall breast cancer patient survival probability, we utilized cBioportal and examined a cohort of breast cancer carcinoma (TCGA, Firehose legacy; 1100 samples (286, 287, 291). Within this cohort, approx. 50-100 samples displayed either high/low LDLR, NPC1, RAB7, STARD3, TBC1D5 or TBC1D15 expression levels. Within these high/low expression groups of ANXA6 interactome proteins, approximately 5-25 samples showed high/low ANXA6 expression levels. Gene pairs in patient samples with relatively high (EXP>1) and low (EXP<1) expression levels of ANXA6 and LDLR (Fig. 4.1), ANXA6 and NPC1 (Fig. 4.2), ANXA6 and RAB7 (Fig. 4.3), ANXA6 and STARD3 (Fig. 4.4), ANXA6 and TBC1D5 (Fig. 4.5), ANXA6 and TBC1D15 (Fig. 4.6) were selected. We first plotted the overall patient survival probability (%) of patients with high/low levels of single genes (ANXA6, LDLR in Fig. 4.1A; ANXA6, NPC1 in Fig. 4.2A; ANXA6, RAB7 in Fig. 4.3A etc.) as shown in Panels A of Figures 4.1-4.6. In Panel B of each of these figures (Fig. 4.2-4.6), the overall survival probability of breast cancer patients with high LDLR, NPC1, RAB7, STARD3, TBC1D5 and TBC1D15 expression levels in combination with high/low ANXA6 levels are provided, respectively. In Panel C of each of these figures (Fig. 4.2-4.6), the overall survival probability of breast cancer patients with low LDLR, NPC1, RAB7, STARD3, TBC1D5 and TBC1D15 expression levels in combination with high/low ANXA6 levels are shown, respectively.

When single genes were analyzed, overall survival probability was comparable for cancers with high/low LDLR, NPC1, RAB7 and TBC1D15 levels for approximately 120 months (Panels A in Fig. 4.1-4.3, 4.6). High STARD3 and TBC1D5 levels showed reduced survival probability from 20-50 months onwards, respectively, compared to patients with low STARD3 and TBC1D5 levels (Fig. 4.4A, 4.5A). Please note that high/low ANXA6 levels displayed differential overall survival curves depending on the gene pair selected. However, overall high/low ANXA6 levels showed comparable patient survival probability when plotted for samples co-analyzed for high/low LDLR, NPC1, RAB7, TBC1D5 and TBC1D15 (Fig. 4.1A-4.3A, 4.5A-4.6A). Interestingly, the breast cancer patient samples co-analyzed for high/low STARD3 levels showed 15-25% reduced patient survival probability for 0-120 months with low ANXA6 levels compared to those

expressing high ANXA6 levels. This could indicate a functional relationship between these two proteins that is further supported by the gene pair analysis in Fig. 4.4B-C (see below).

Given the extensive gene pair analysis in this cohort of breast carcinoma samples, providing large amounts of data shown in Panels B-C of Figures 4.1-4.6, we have summarized the main features of these datasets in Table 4.1.
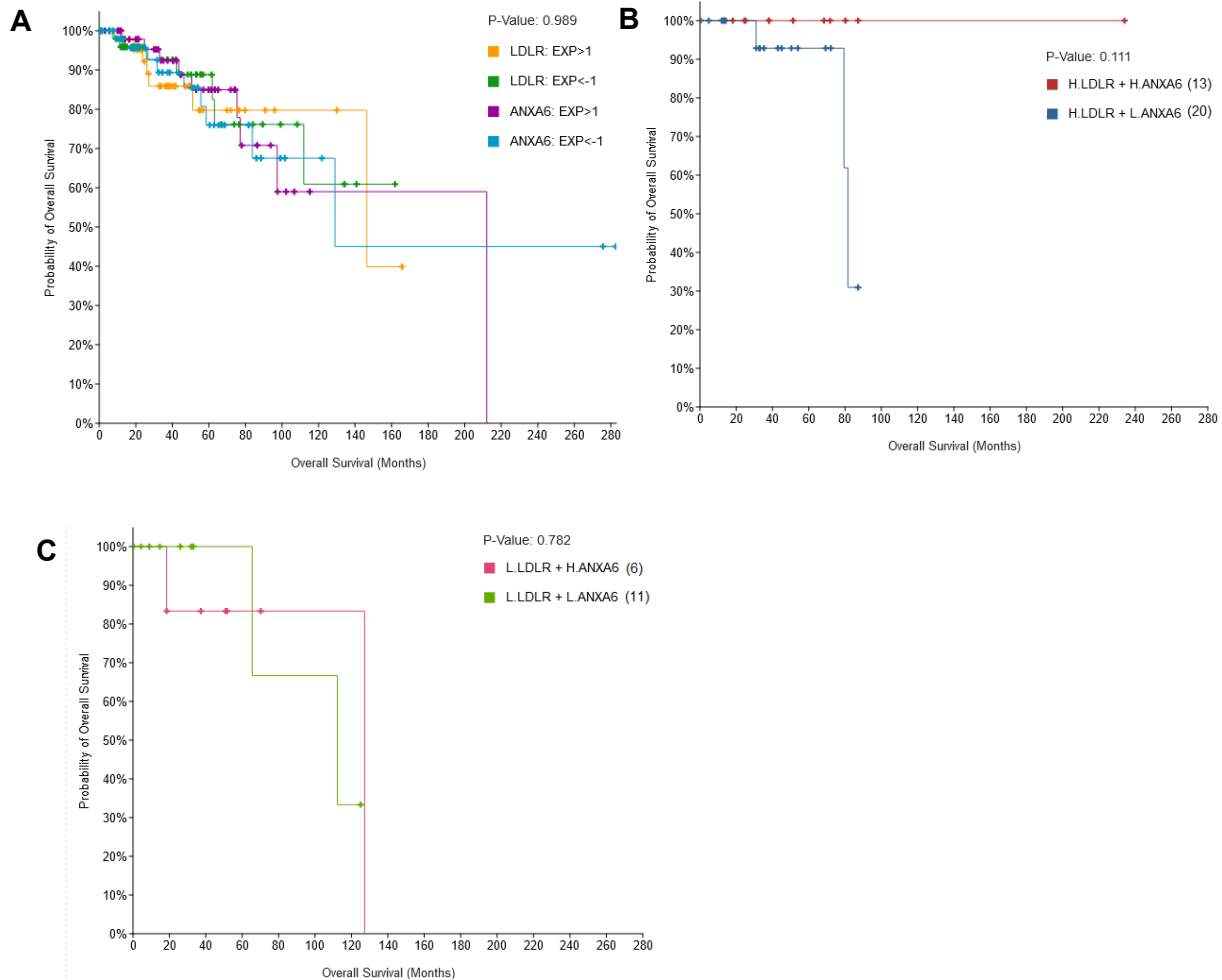
Figure 4.1: A. Probability (%) of overall patient survival (months) from breast invasive carcinoma (TCGA, Firehose Legacy) with high (EXP>1) and low (EXP<1) LDLR (n=90, 68) and ANXA6 (73, 94) expression levels. B-C. Probability (%) of overall patient survival with high (EXP>1) and low (EXP<1) LDLR in combination with high/low ANXA6 expression levels as indicated. The number of samples with high/low LDLR and ANXA6 levels are given, and the significance was calculated.
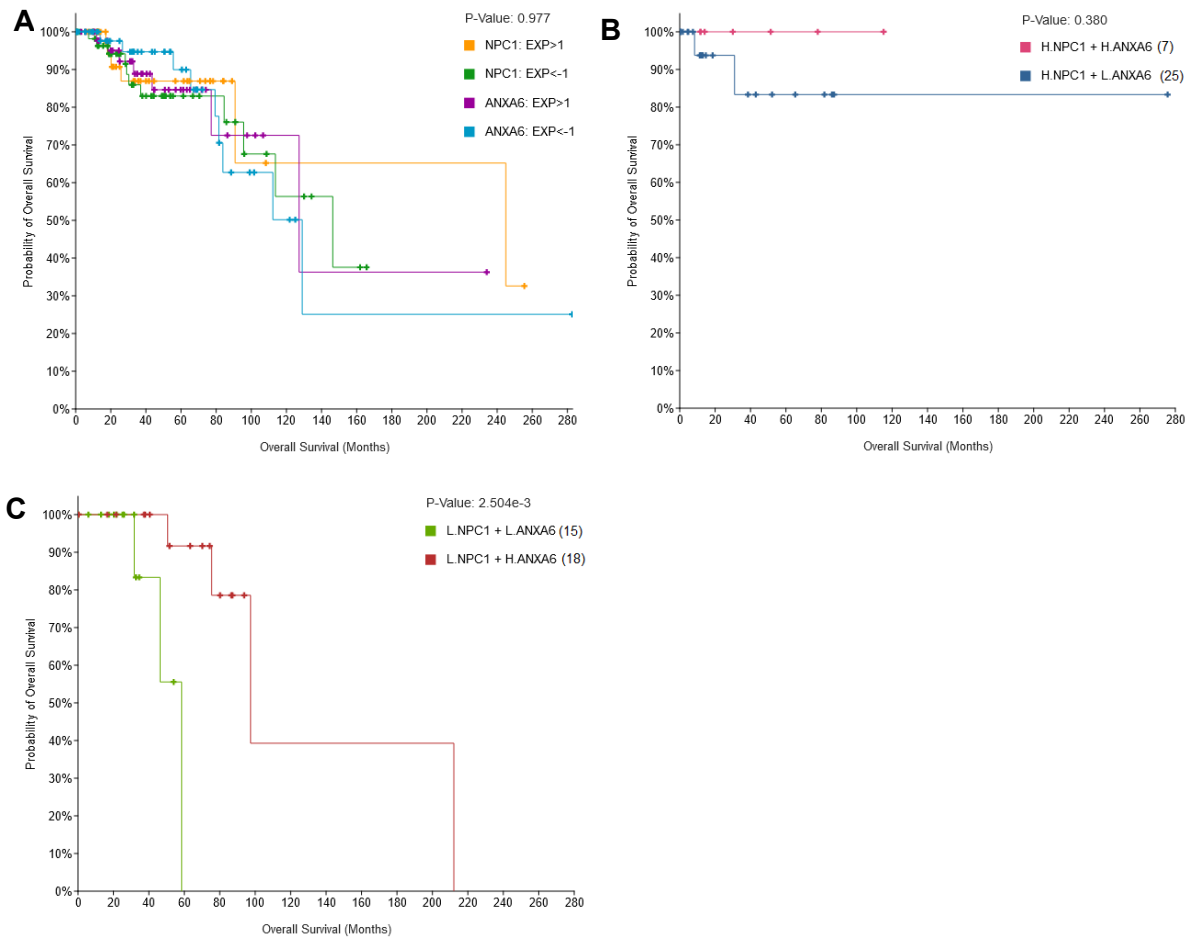
Figure 4.2: A. Probability (%) of overall patient survival (months) from breast invasive carcinoma (TCGA, Firehose Legacy) with high (EXP>1) and low (EXP<1) NPC1 (n=84, 92) and ANXA6 (73, 94) expression levels. B-C. Probability (%) of overall patient survival with high (EXP>1) and low (EXP<1) NPC1 in combination with high/low ANXA6 expression levels as indicated. The number of samples with high/low NPC1 and ANXA6 levels are given, and the significance was calculated.
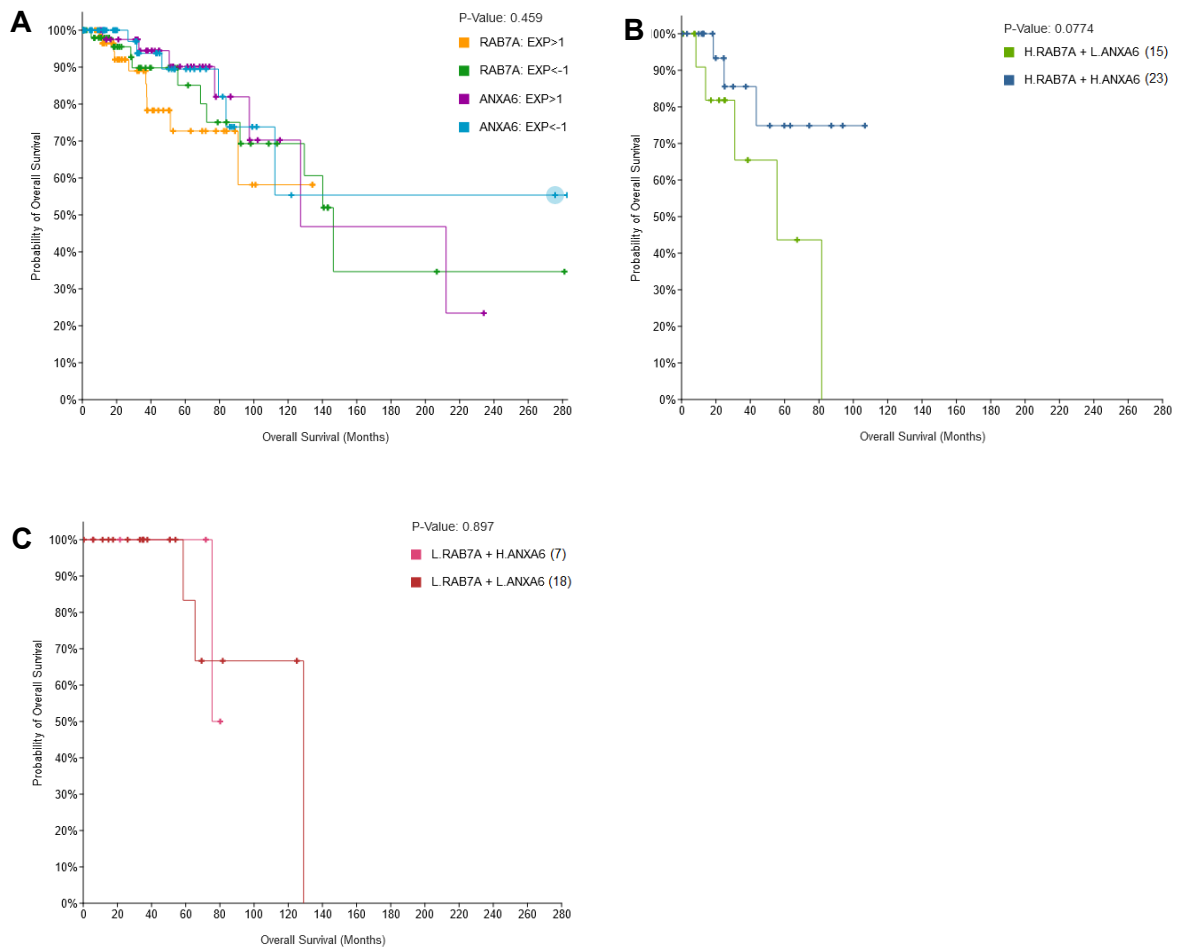
Figure 4.3: A. Probability (%) of overall patient survival (months) from breast invasive carcinoma (TCGA, Firehose Legacy) with high (EXP>1) and low (EXP<1) RAB7A (n=68, 55) and ANXA6 expression levels. B-C. Probability (%) of overall patient survival with high (EXP>1) and low (EXP<1) RAB7A in combination with high/low ANXA6 expression levels as indicated. The number of samples with high/low RAB7 and ANXA6 levels are given, and the significance was calculated.
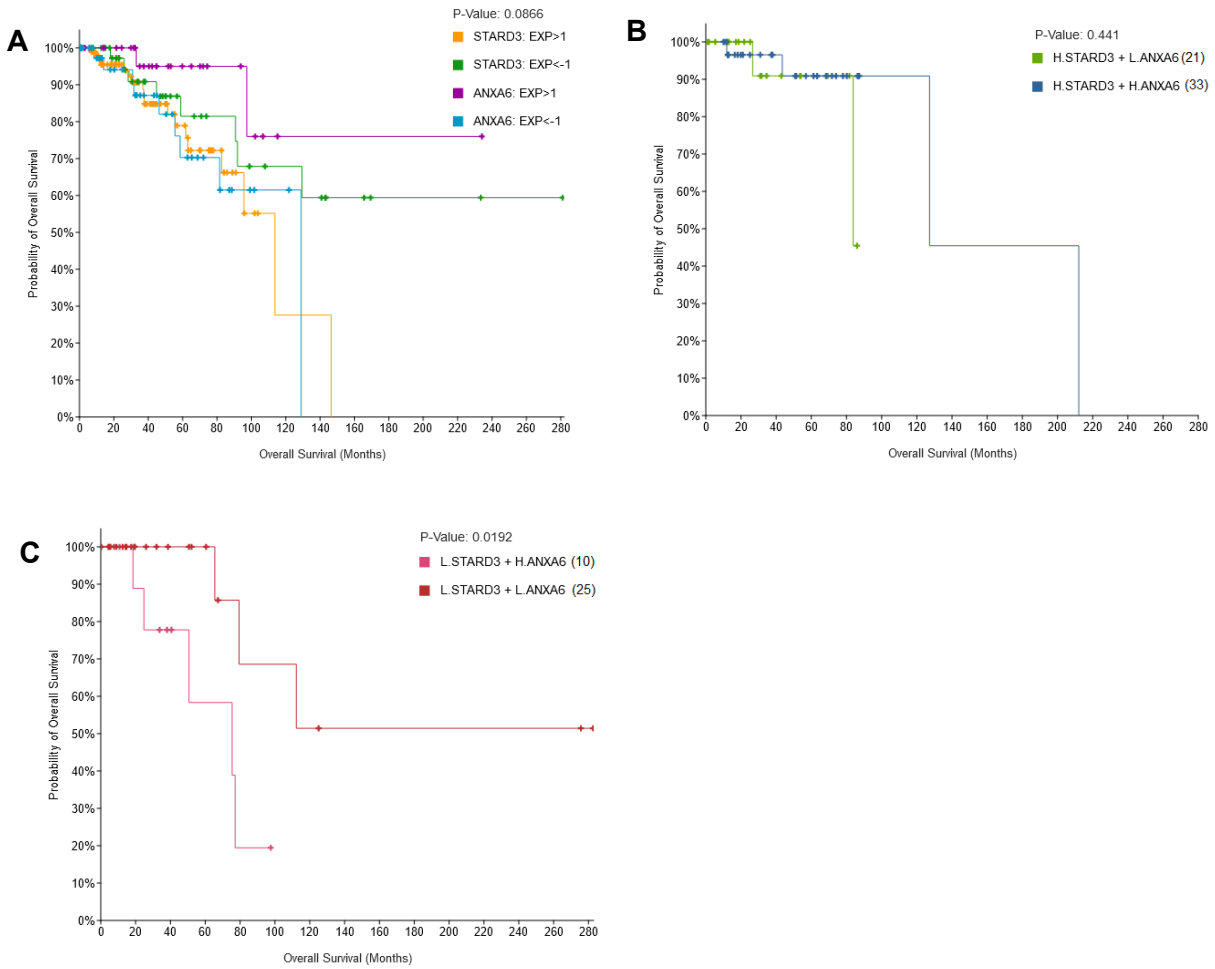
Figure 4.4: A. Probability (%) of overall patient survival (months) from breast invasive carcinoma (TCGA, Firehose Legacy) with high (EXP>1) and low (EXP<1) STARD3 (n=106, 52) and ANXA6 expression levels. B-C. Probability (%) of overall patient survival with high (EXP>1) and low (EXP<1) STARD3 in combination with high/low ANXA6 expression levels as indicated. The number of samples with high/low STARD3 and ANXA6 levels are given, and the significance was calculated.
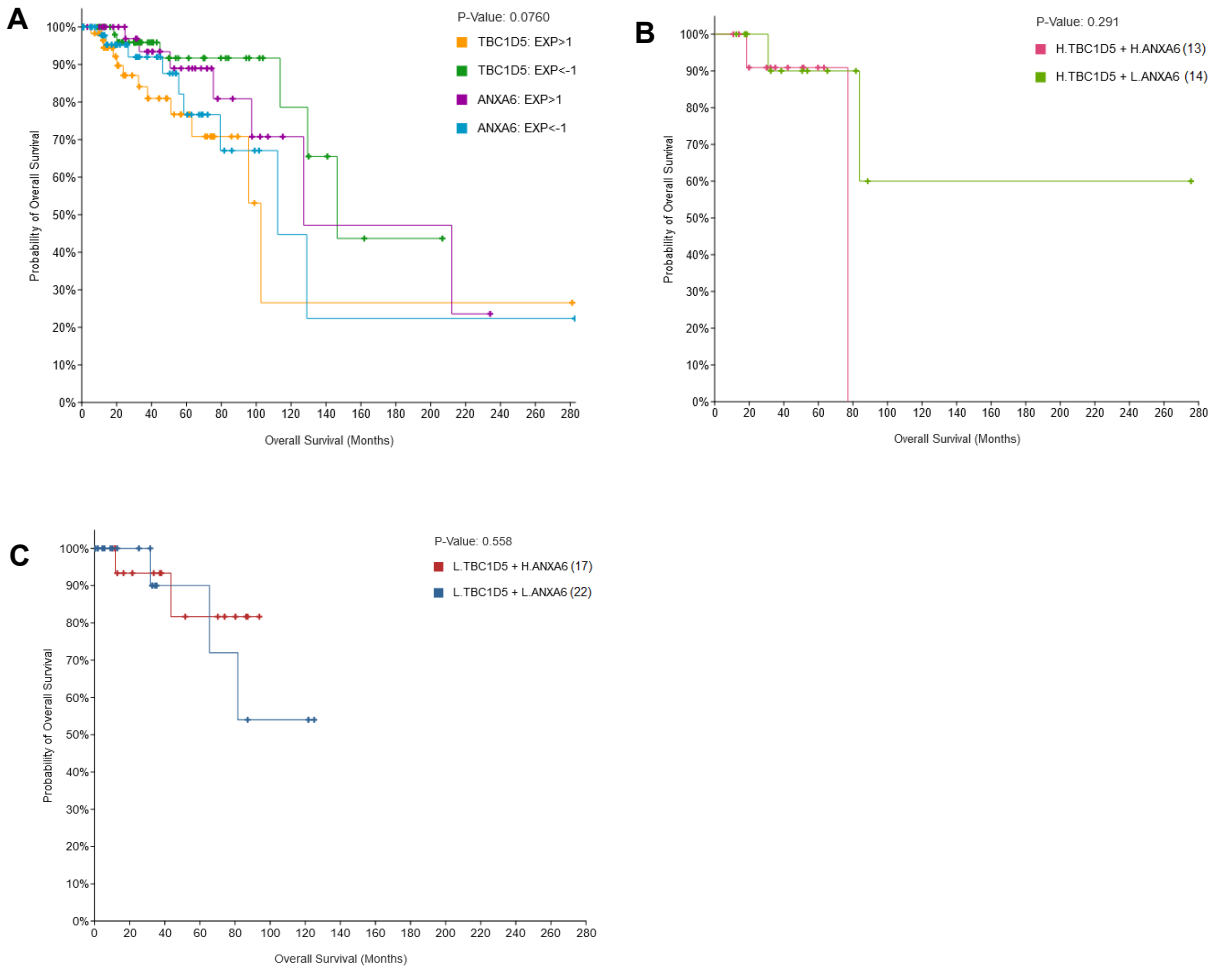
Figure 4.5: A. Probability (%) of overall patient survival (months) from breast invasive carcinoma (TCGA, Firehose Legacy) with high (EXP>1) and low (EXP<1) TBC1D5 (n=62, 64) and ANXA6 expression levels. B-C. Probability (%) of overall patient survival with high (EXP>1) and low (EXP<1) TBC1D5 in combination with high/low ANXA6 expression levels as indicated. The number of samples with high/low TBC1D5 and ANXA6 levels are given, and the significance was calculated.
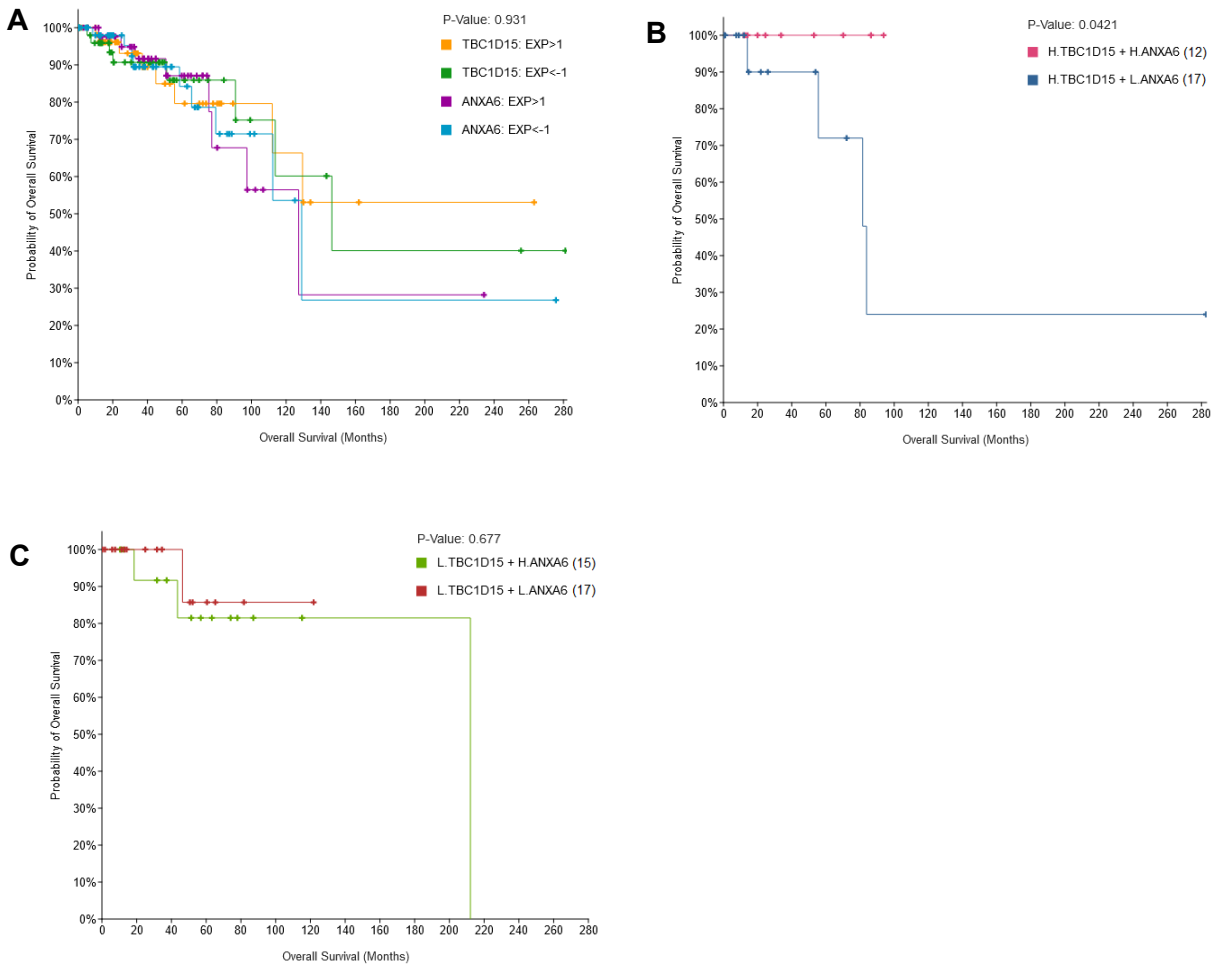
Figure 4.6: A. Probability (%) of overall patient survival (months) from breast invasive carcinoma (TCGA, Firehose Legacy) with high (EXP>1) and low (EXP<1) TBC1D15 (n=65, 53) and ANXA6 expression levels. B-C. Probability (%) of overall patient survival with high (EXP>1) and low (EXP<1) TBC1D15 in combination with high/low ANXA6 expression levels as indicated. The number of samples with high/low TBC1D15 and ANXA6 levels are given, and the significance was calculated.

Table 4.1 summarizes the patient survival probability of high/low ANXA6 levels paired with high/low LDLR, NPC1, RAB7, STARD3, TBC1D5 and TBC1D15. Although some observations were not significant due to low sample numbers, several interesting findings were observed. High ANXA6 levels were associated with longer patient survival probability in breast cancer samples with high/low LDLR and NPC1, high STARD3, RAB7, TBC1D5 and TBC1D15, indicating a potential for elevated ANXA6 levels to limit distribution of LDL-derived cholesterol in breast cancer cells. Vice versa, low ANXA6 levels strongly reduced the survival probability in patients with high LDLR (Fig. 4.1B), high RAB7 (Fig. 4.3B) and STARD3 (Fig. 4.4B) levels, altogether suggesting that low ANXA6 levels might favour efficient distribution via RAB7- and STARD3-dependent cholesterol routes in breast cancer settings where elevated LDLR activity allows

152

ANXA6	LDLR ⇑	LDLR ⇓	NPC1 ⇑	NPC1 ⇓	RAB7 ⇑	RAB7 ⇓	STARD3 ⇑	STARD3 ⇓	TBC1D5 ⇑	TBC1D5 ⇓	TBC1D15 ⇑	TBC1D15 ⇓
⇑	>220	>120	>120	100	>100	<80	>120	<80	<80	>100	>100	>210
⇓	80	>100	>260	<80	80	>120	<90	>280	>280	>130	80	120
				** p<0.01				* p<0.05			* p<0.05	

Table 4.1: 50% probability of overall patient survival (months) in breast invasive carcinoma (TCGA). The months of 50% overall patient survival probability for gene pairs with high (⇑) and low (⇓) ANXA6 expression levels in combination with high/low expression levels of LDLR, NPC1, RAB7, STARD3, TBC1D5 and TBC1D15 in breast invasive carcinoma patients (TCGA, Firehose Legacy) are given. Reduced and increased length of overall patient survival probability is indicated in red and green, respectively (* p<0.05, ** p<0.01).

increased uptake of LDL-cholesterol to reach the LE/Lys compartment. Not all observations seem to fit this model, for example low ANXA6 levels and high NPC1 levels showed increased survival probability.

Finally, to map potential ANXA6-related gene networks in individual invasive breast carcinoma, we mapped the expression levels of the ANXA6 interactome in individual patient samples available from a cohort containing invasive breast carcinoma (n>1000) (291). Only breast cancer samples with low estrogen receptor (ESR1; ER-negative) (A) and EGFR (B) overexpression are shown, the latter likely representing predominantly TNBC breast cancers. High (red) and low (blue) relative expression levels of ANXA6, LDLR, NPC1, RAB7A, STARD3, TBC1D5 and TBC1D15 for individual tumors are shown in Fig. 4.7A-B.
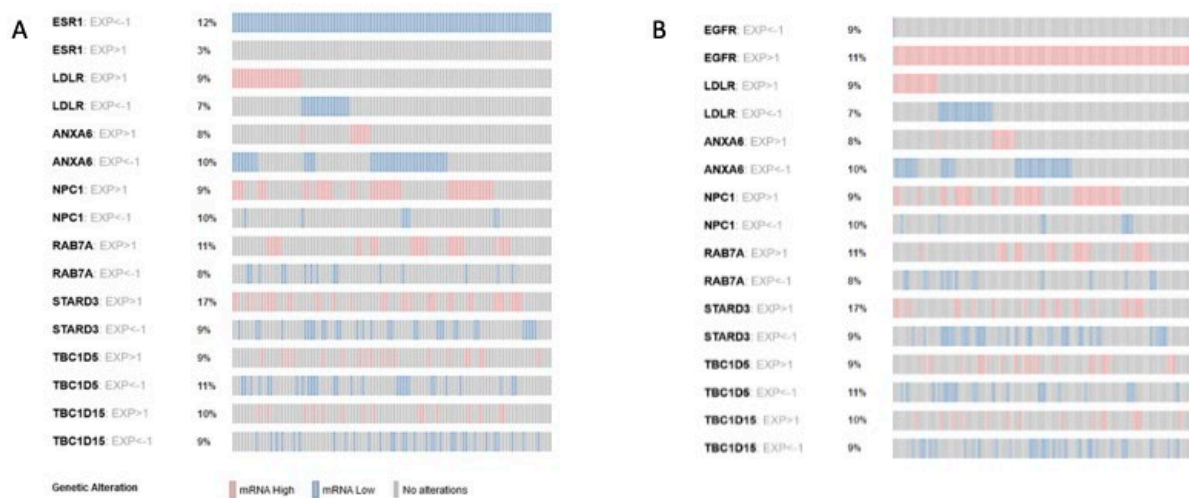
Figure 4.7A-B: High (EXP>1) (red) and low (EXP <1) (blue) gene expression pattern of estrogen receptor (ER or ESR1), epidermal growth factor receptor (EGFR), LDLR, NPC1, RAB7A, STARD3, TBC1D5 and TBC1D15 in individual tumors from a cohort of invasive breast carcinoma with high/low ANXA6 expression levels (TCGA, Firehose legacy) Median expression levels in individual tumor samples are depicted in grey. The percentage of cancers with specific high/low expression levels for each gene within this cohort is given.

Strikingly, within this invasive breast cancer cohort, a substantial number of samples (n~25 ER-negative; n~15 EGFR overexpression) displayed elevated LDLR levels, suggesting elevated LDL uptake in these cancers. Moreover, within these ER-negative and EGFR-related subgroups, approximately 10 samples displayed reduced ANXA6 levels. Several of these cancers were also characterized by high NPC1, RAB7A, STARD3 and low TBC1D15 expression levels. Hence, in ER-negative and EGFR-related breast cancers, subgroups appear to exist that display a gene network expression pattern that favour increased LDL uptake and distribution characterized by

high levels of cholesterol transporters (LDLR, NPC1, StASRD3) and regulatory proteins (ANXA6, RAB7A, TBC1D15) that allow increased membrane contact site formation for cholesterol efflux from LE/Lys.

Hence, these findings support a tumor suppressor role for ANXA6 in ER-negative and TNBC breast cancers (204, 210) that involves increased LDL-cholesterol supply, which has been observed in breast cancer, increasing proliferation and metastatic behaviour, and contributing to poor prognosis and chemoresistance (106, 107, 126, 127, 129).

4.4.2. Expression patterns of the endo-lysosomal ANXA6 interactome and overall patient survival in colorectal adenocarcinoma

We next analyzed the overall survival probability of ANXA6 and ANXA6 interactome gene pairs for colorectal cancers, and examined a cohort of colorectal adenomacarcinoma (TCGA, Firehose legacy; 640 samples (286, 287, 291) through the cBioportal platform. Within this cohort, approx. 20-50 samples displayed either high/low LDLR, NPC1, RAB7, STARD3, TBC1D5 or TBC1D15 expression levels. Within these high/low expression groups of ANXA6 interactome proteins, approximately 3-20 samples showed high/low ANXA6 expression levels. Gene pairs in patient samples with relatively high (EXP>1) and low (EXP<1) expression levels of ANXA6 and LDLR (Fig. 4.8), ANXA6 and NPC1 (Fig. 4.9), ANXA6 and RAB7 (Fig. 4.10), ANXA6 and STARD3 (Fig. 4.11), ANXA6 and TBC1D5 (Fig. 4.12), ANXA6 and TBC1D15 (Fig. 4.13) were selected. and the overall patient survival probability (%) with high/low levels of single genes (ANXA6, LDLR in Fig. 4.8A; ANXA6, NPC1 in Fig. 4.9A; ANXA6, RAB7A in Fig. 4.10 etc.) are shown in Panels A of Figures 4.8-4.13. In Panel B of each of these figures (Fig. 4.8-4.13), the overall survival probability of colorectal adenocarcinoma cancer patients with high LDLR, NPC1, RAB7, STARD3, TBC1D5 and TBC1D15 expression levels in combination with high/low ANXA6 levels are provided, respectively. In Panel C of each of these figures (Fig. 4.8-4.13), the overall survival probability of colorectal cancer patients with low LDLR, NPC1, RAB7, STARD3, TBC1D5 and TBC1D15 expression levels in combination with high/low ANXA6 levels are given, respectively.

Overall survival probability was reduced for single gene analysis with low LDLR, NPC1, and to a minor extend with high TBC1D15 levels (Panel A in Fig. 4.8, 4.9 and 4.13) and comparable for patients with high/low RAB7, STARD3, TBC1D5 levels (Fig. 4.10A, 4.11A, 4.12A). Please

note that high/low ANXA6 levels displayed slightly differential overall survival curves depending on the gene pair selected. Interestingly, high ANXA6 levels showed reduced colorectal patient survival probability when co-analyzed with any of the selected ANXA6 interactome partners: LDLR, NPC1, RAB7, STARD3, TBC1D5 and TBC1D15 (Fig. 4.8A-4.13A). This could indicate an overarching and tumor supporting role for ANXA6 in colorectal adenocarcinoma that might not be related to cholesterol homeostasis.

Alike the previous chapter, we have summarized the large amounts of data shown in Panels B-C in Figures 4.8-4.113, in Table 4.2.
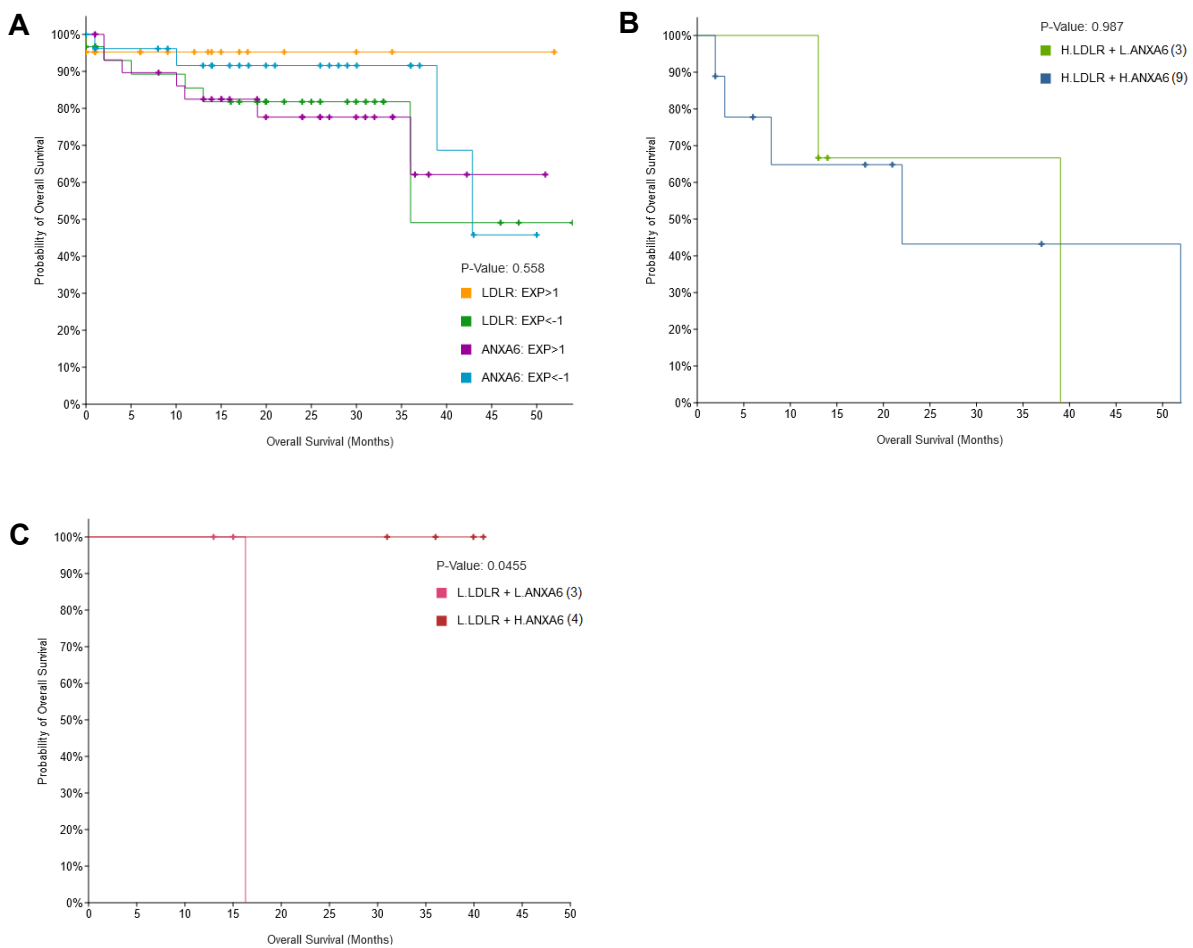
Figure 4.8: A. Probability (%) of overall patient survival (months) from colorectal adenocarcinoma (TCGA, Firehose Legacy) with high (EXP>1) and low (EXP<1) LDLR (n=21, 30) and ANXA6 expression levels. B-C. Probability (%) of overall patient survival with high (EXP>1) and low (EXP<1) LDLR in combination with high/low ANXA6 expression levels as indicated. The number of samples with high/low LDLR and ANXA6 levels are given, and the significance was calculated.
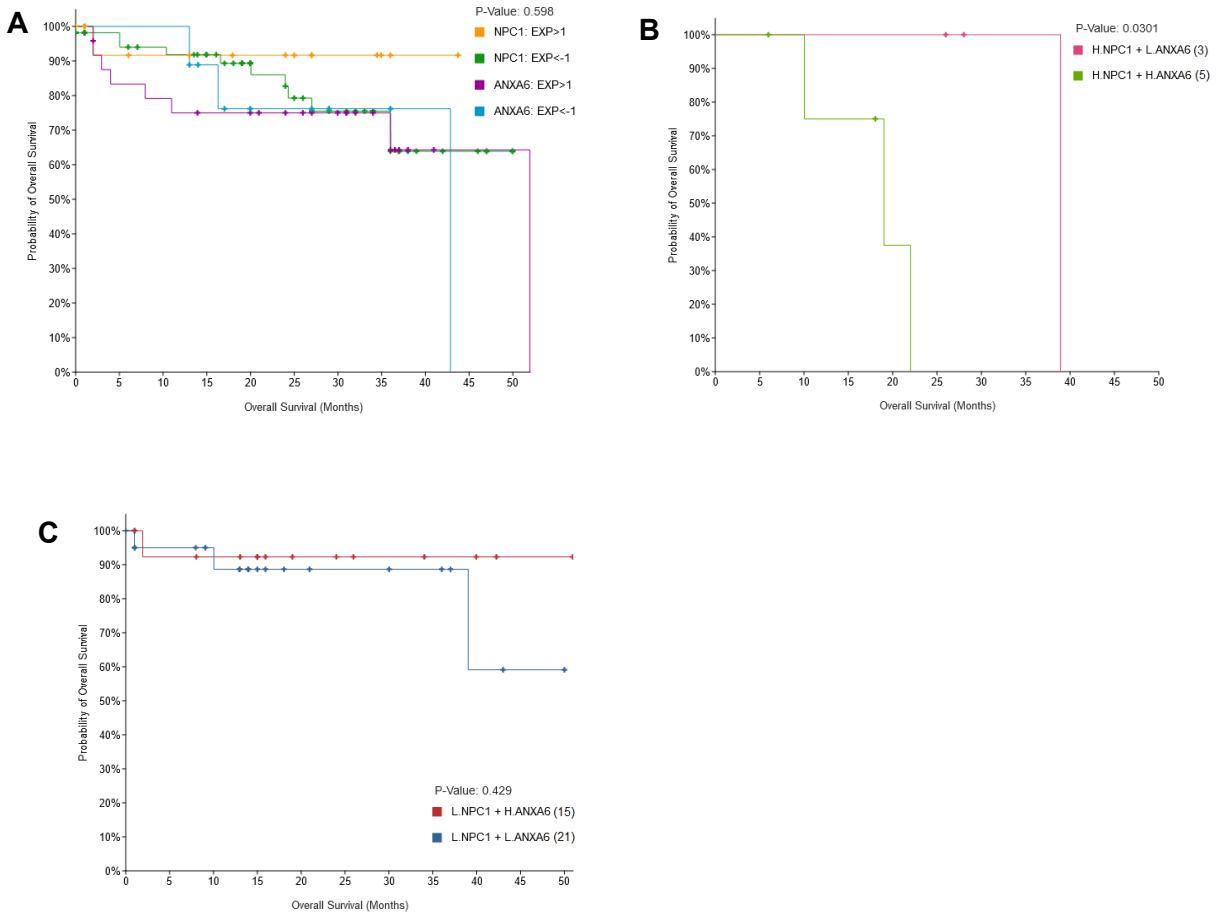
Figure 4.9: A. Probability (%) of overall patient survival (months) from colorectal adenocarcinoma (TCGA, Firehose Legacy) with high (EXP>1) and low (EXP<1) NPC1 (n=17, 55) and ANXA6 expression levels. B-C. Probability (%) of overall patient survival with high (EXP>1) and low (EXP<1) NPC1 in combination with high/low ANXA6 expression levels as indicated. The number of samples with high/low NPC1 and ANXA6 levels are given, and the significance was calculated.
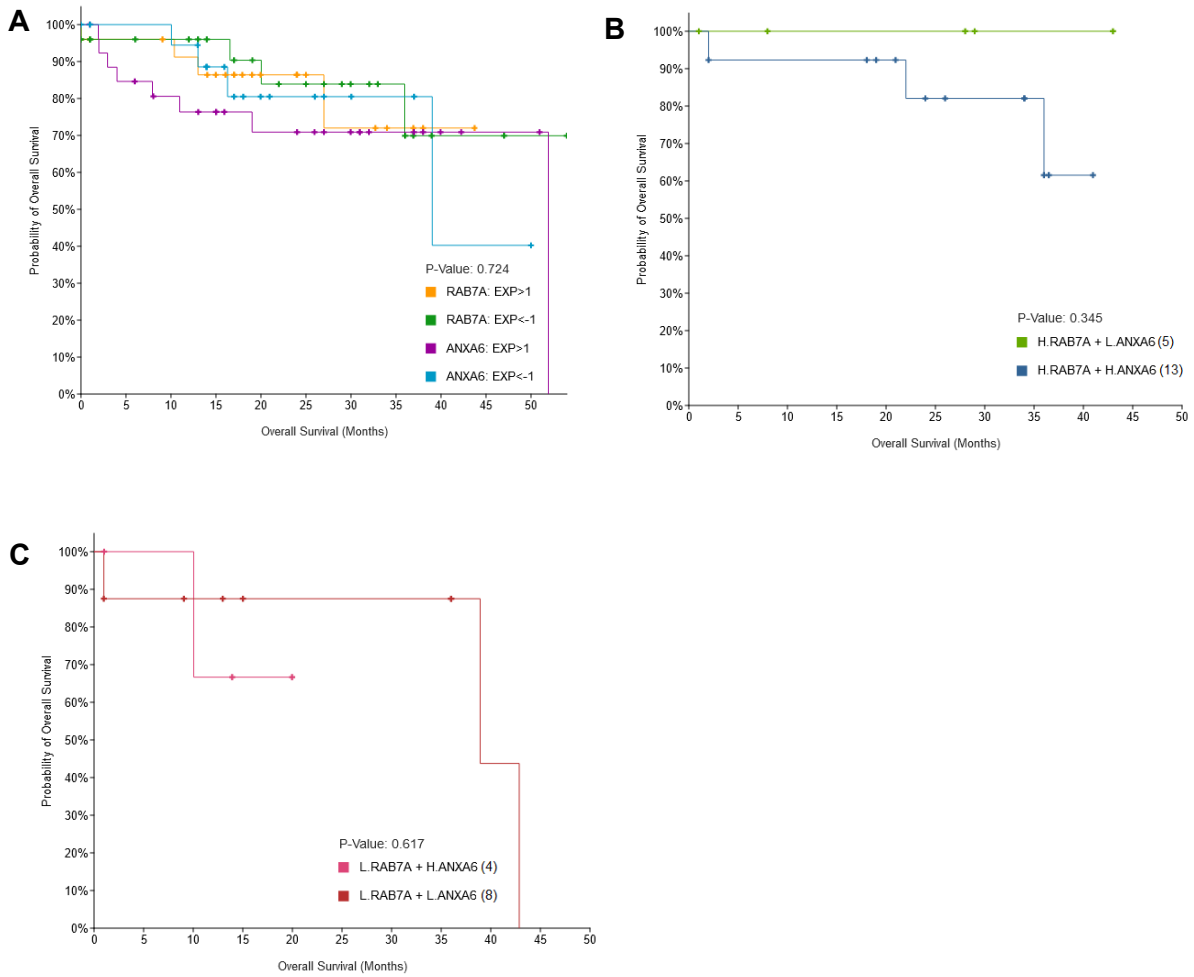
Figure 4.10: A. Probability (%) of overall patient survival (months) from colorectal adenocarcinoma (TCGA, Firehose Legacy) with high (EXP>1) and low (EXP<1) RAB7A (n=25, 25) and ANXA6 expression levels. B-C. Probability (%) of overall patient survival with high (EXP>1) and low (EXP<1) RAB7A in combination with high/low ANXA6 expression levels as indicated. The number of samples with high/low RAB7A and ANXA6 levels are given, and the significance was calculated.

Figure 4.11: A. Probability (%) of overall patient survival (months) from colorectal adenocarcinoma (TCGA, Firehose Legacy) with high (EXP>1) and low (EXP<1) STARD3 (n=24, 20) and ANXA6 expression levels. B-C. Probability (%) of overall patient survival with high (EXP>1) and low (EXP<1) LDLR in combination with high/low ANXA6 expression levels as indicated. The number of samples with high/low STARD3 and ANXA6 levels are given, and the significance was calculated.

Figure 4.12: A. Probability (%) of overall patient survival (months) from colorectal adenocarcinoma (TCGA, Firehose Legacy) with high (EXP>1) and low (EXP<1) TBC1D5 (n=18, 28) and ANXA6 expression levels. B-C. Probability (%) of overall patient survival with high (EXP>1) and low (EXP<1) TBC1D5 in combination with high/low ANXA6 expression levels as indicated. The number of samples with high/low TBC1D5 and ANXA6 levels are given, and the significance was calculated.

Figure 4.13: A. Probability (%) of overall patient survival (months) from colorectal adenocarcinoma (TCGA, Firehose Legacy) with high (EXP>1) and low (EXP<1) TBC1D15 (n=28, 13) and ANXA6 expression levels. B-C. Probability (%) of overall patient survival with high (EXP>1) and low (EXP<1) TBC1D15 in combination with high/low ANXA6 expression levels as indicated. The number of samples with high/low TBC1D15 and ANXA6 levels are given, and the significance was calculated.

The Table 4.2 summarizes the patient survival probability of high/low ANXA6 levels paired with high/low LDLR, NPC1, RAB7, STARD3, TBC1D5 and TBC1D15 in a cohort of colorectal adenocarcinoma. Alike the previous analysis of breast cancer samples, many observations were not significant due to low sample numbers. Furthermore, in line with single gene analysis of patient survival probability (Panels A in Fig. 4.8-4.13), which indicated an alternative, cholesterol-independent role for high ANXA6 levels to lower patient survival in colorectal adenocarcinoma that might not be related to cholesterol homeostasis, a significantly reduced patient survival probability was only observed in samples displaying low ANXA6 levels in combination with low LDLR levels or high ANXA6 with high NPC1 expression levels. The latter could indeed reflect an additional role for ANXA6 in tumor progression unrelated to cholesterol export from LE/Lys. A significant reduction of ANXA6 levels was also observed when comparing normal tissues vs in

ANXA6	LDLR ⇑	LDLR ⇓	NPC1 ⇑	NPC1 ⇓	RAB7 ⇑	RAB7 ⇓	STARD3 ⇑	STARD3 ⇓	TBC1D5 ⇑	TBC1D5 ⇓	TBC1D15 ⇑	TBC1D15 ⇓
⇑	>20	>40	<20	>50	>50	>20	>40	>50	>50	>20	>20	>50
⇓	>35	<20	>35	>50	>50	>40	>35	>50	40	>40	>25	>35

Table 4.2: 50% probability of overall patient survival (months). The months of 50% overall patient survival probability for gene pairs with high (⇑) and low (⇓) ANXA6 expression levels in combination with high/low expression levels of LDLR, NPC1, RAB7, STARD3, TBC1D5 and TBC1D15 in colorectal adenocarcinoma patients (TCGA, Firehose Legacy) are given. Reduced and increased length of overall patient survival probability is indicated in red and green, respectively (* p<0.05).

colon adenocarcinoma (Chapter 2.4.3 – 2.4.5.). Likewise, 50% survival probability of >50 months in patients with high RAB7 as well as low TBC1D15 levels indicate a minor involvement of RAB7 GTPase activation and its regulators in the progression of colorectal cancers.

4.4.3. Expression patterns of the endo-lysosomal ANXA6 interactome and overall patient survival in liver cancer

We next analyzed the overall survival probability of ANXA6 and ANXA6 interactome gene pairs in a cohort of liver hepatocellular carcinoma (TCGA, Firehose Legacy; 379 samples) through the cBioportal platform (286, 287, 291). Within this cohort, approx. 10-50 samples displayed either high/low LDLR, NPC1, RAB7, STARD3, TBC1D5 or TBC1D15 expression levels. Within these high/low expression groups of ANXA6 interactome proteins, approximately 3-10 samples showed high/low ANXA6 expression levels. Gene pairs in patient samples with relatively high (EXP>1) and low (EXP<1) expression levels of ANXA6 and LDLR (Fig. 4.14), ANXA6 and NPC1 (Fig. 4.15), ANXA6 and RAB7 (Fig. 4.16), ANXA6 and STARD3 (Fig. 4.17), ANXA6 and TBC1D5 (Fig. 4.18), ANXA6 and TBC1D15 (Fig. 4.19) were selected and the overall patient survival probability (%) with high/low levels of single genes (ANXA6, LDLR in Fig. 4.14A; ANXA6 and NPC1 in Fig. 4.15A ; ANXA6 and RAB7 in Fig. 4.16 etc) are shown in Panels A of Figures 4.13-4.18. In Panel B of each of these figures (Fig. 4.14-4.19), the overall survival probability of liver hepatocarcinoma patients with high LDLR, NPC1, RAB7, STARD3, TBC1D5 and TBC1D15 expression levels in combination with high/low ANXA6 levels are provided, respectively. In Panel C of each of these figures (Fig. 4.14-4.19), the overall survival probability of liver cancer patients with low LDLR, NPC1, RAB7, STARD3, TBC1D5 and TBC1D15 expression levels in combination with high/low ANXA6 levels are given, respectively.

Overall survival probability was reduced for single gene analysis with low LDLR, high NPC1 and high RAB7 level (Panels A in Fig. 4.14-4.16, while patient survival probability was comparable for patients with high/low STARD3, TBC1D5 and TBC1D15 levels (Fig. 4.17-4.19). Please note that high/low ANXA6 levels displayed slightly differential overall survival curves depending on the gene pair selected. Interestingly, low ANXA6 levels showed reduced liver hepatocarcinoma survival probability when co-analyzed with any of the selected ANXA6 interactome partners: LDLR, NPC1, RAB7, STARD3, TBC1D5 and TBC1D15 (Fig. 4.14A-4.19A). This could indicate a tumor suppressor role for ANXA6 in liver hepatocarcinoma that in

the case of patient samples with high NPC1 and/or RAB7 levels, might not be related to cholesterol homeostasis.

Alike the previous chapter, we have summarized the large amounts of data shown for gene pair associations in Panels B-C of Figures 4.14-4.19, in Table 4.3.
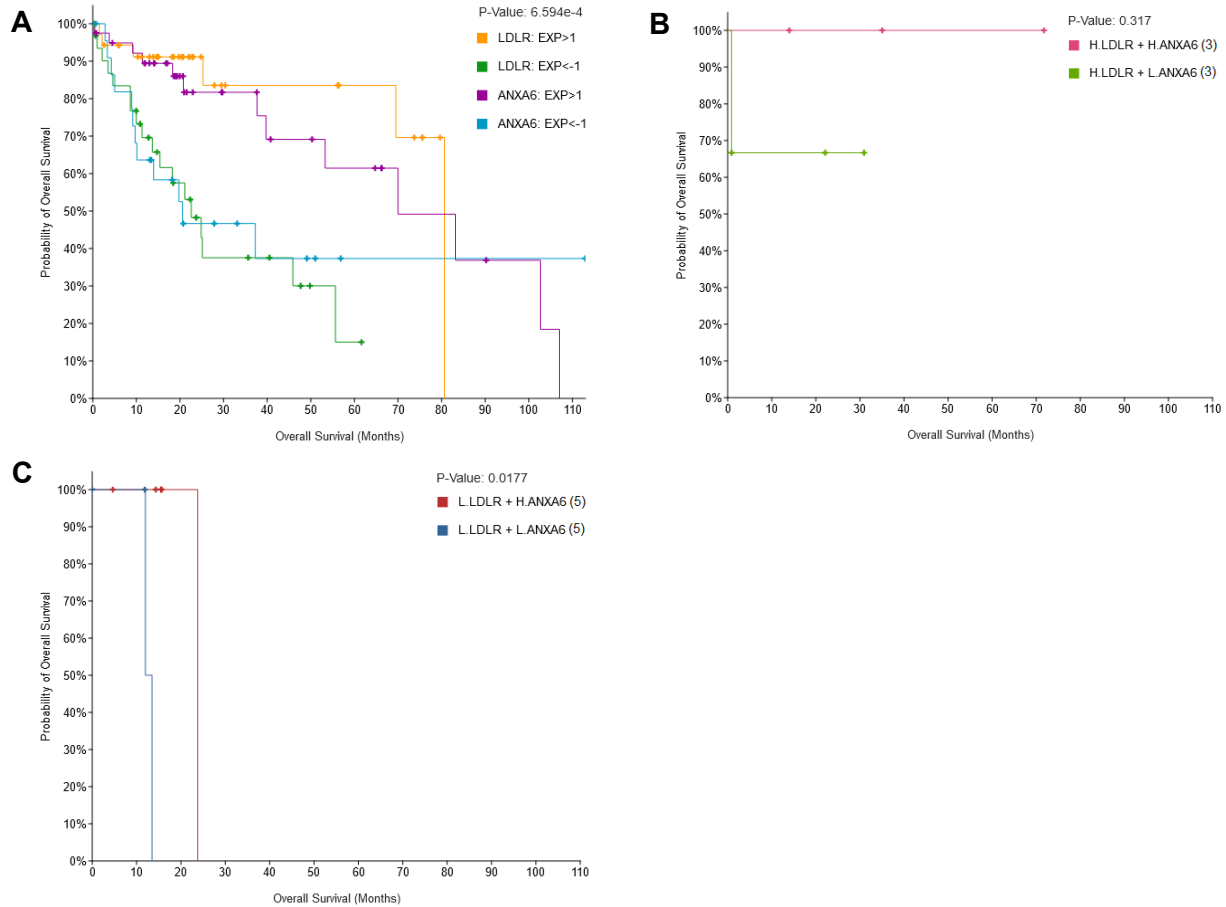
Figure 4.14. A. Probability (%) of overall patient survival (months) from hepatocellular carcinoma (TCGA, Firehose Legacy) with high (EXP>1) and low (EXP<1) LDLR (n=36, 32) and ANXA6 expression levels. B-C. Probability (%) of overall patient survival with high (EXP>1) and low (EXP<1) LDLR in combination with high/low ANXA6 expression levels as indicated. The number of samples with high/low LDLR and ANXA6 levels are given, and the significance was calculated.
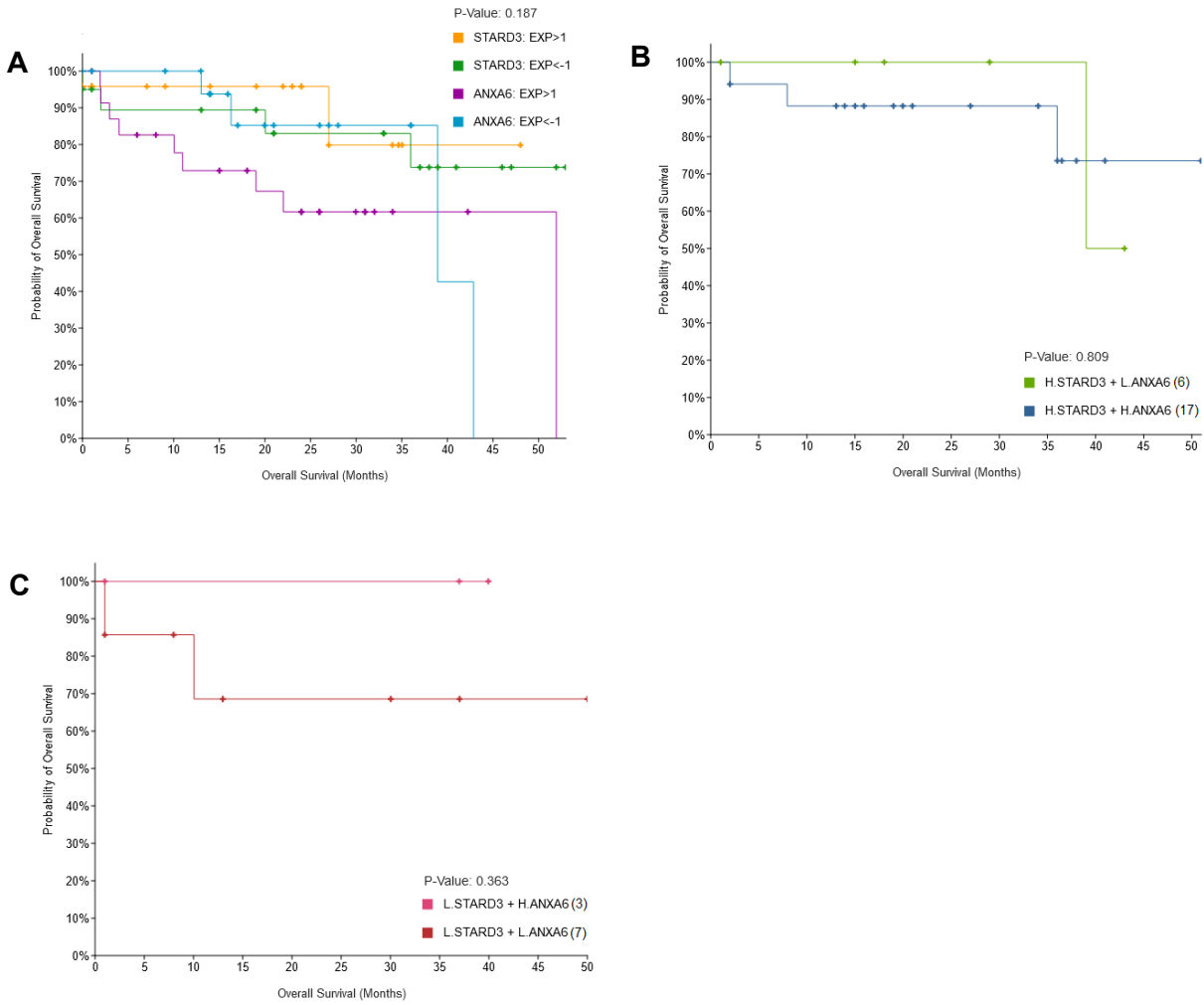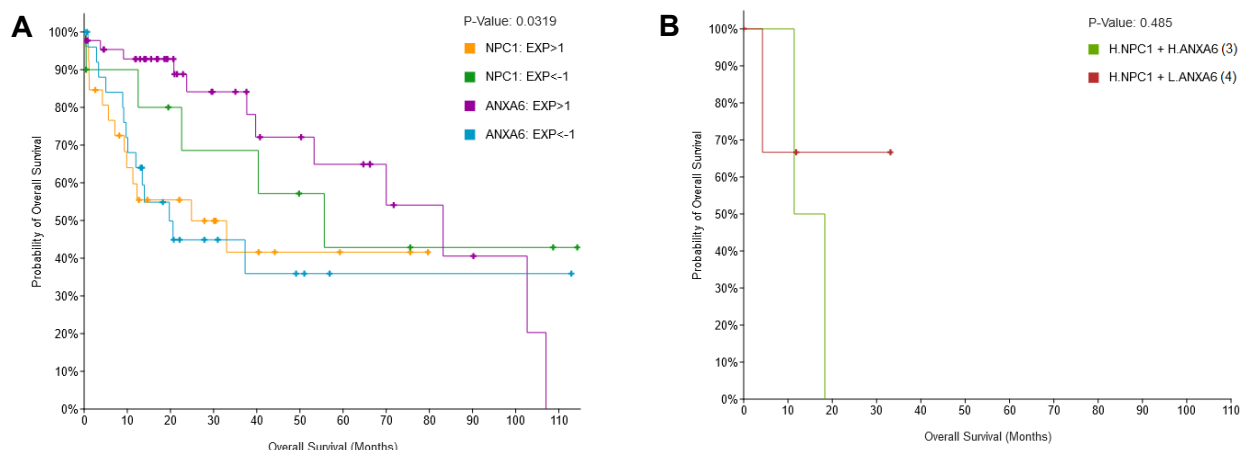
Figure 4.15. A. Probability (%) of overall patient survival (months) from hepatocellular carcinoma (TCGA, Firehose Legacy) with high (EXP>1) and low (EXP<1) NPC1 (n=29, 10) and ANXA6 expression levels. B. Probability (%) of overall patient survival with high (EXP>1) NPC1 in combination with high/low ANXA6 expression levels as indicated. Overall patient probability for samples with low NPC1 in combination with high/low ANXA6 levels was not available. The number of samples with high/low NPC1 and ANXA6 levels are given, and the significance was calculated.
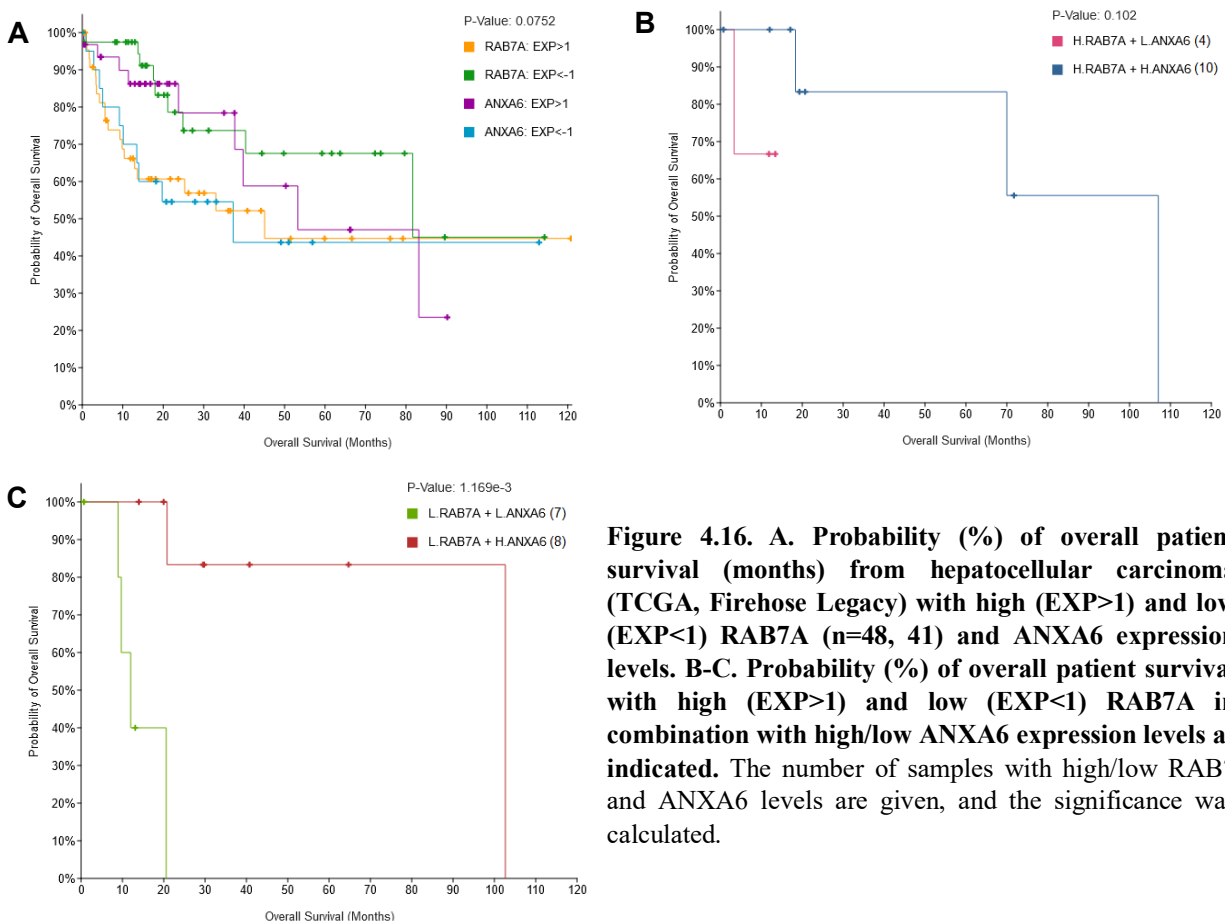
Figure 4.16. A. Probability (%) of overall patient survival (months) from hepatocellular carcinoma (TCGA, Firehose Legacy) with high (EXP>1) and low (EXP<1) RAB7A (n=48, 41) and ANXA6 expression levels. B-C. Probability (%) of overall patient survival with high (EXP>1) and low (EXP<1) RAB7A in combination with high/low ANXA6 expression levels as indicated. The number of samples with high/low RAB7 and ANXA6 levels are given, and the significance was calculated.
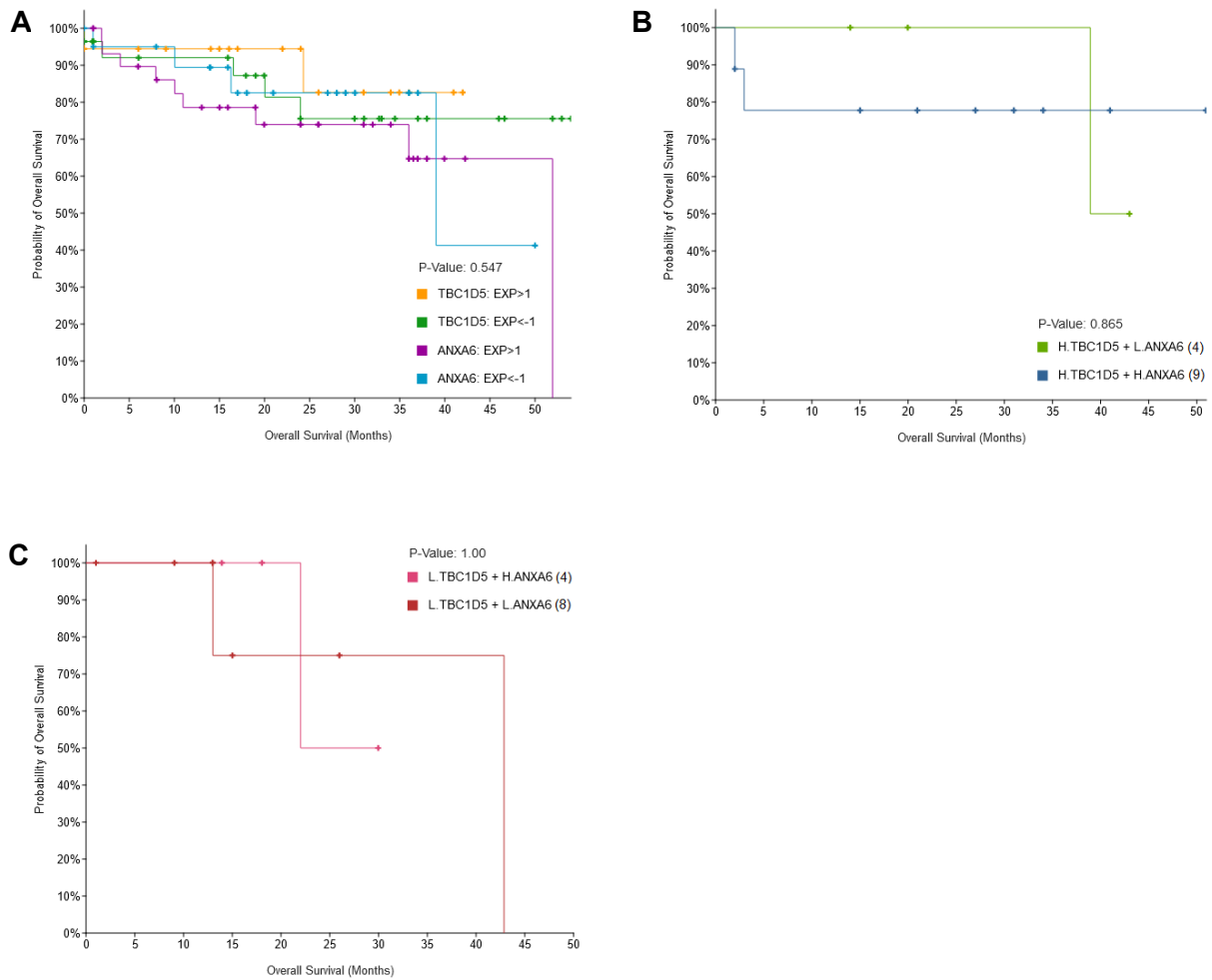
165

Figure 4.17. A. Probability (%) of overall patient survival (months) from hepatocellular carcinoma (TCGA, Firehose Legacy) with high (EXP>1) and low (EXP<1) STARD3 (n=47, 11) and ANXA6 expression levels. B-C. Probability (%) of overall patient survival with high (EXP>1) and low (EXP<1) STARD3 in combination with high/low ANXA6 expression levels as indicated. The number of samples with high/low STARD3 and ANXA6 levels are given, and the significance was calculated.
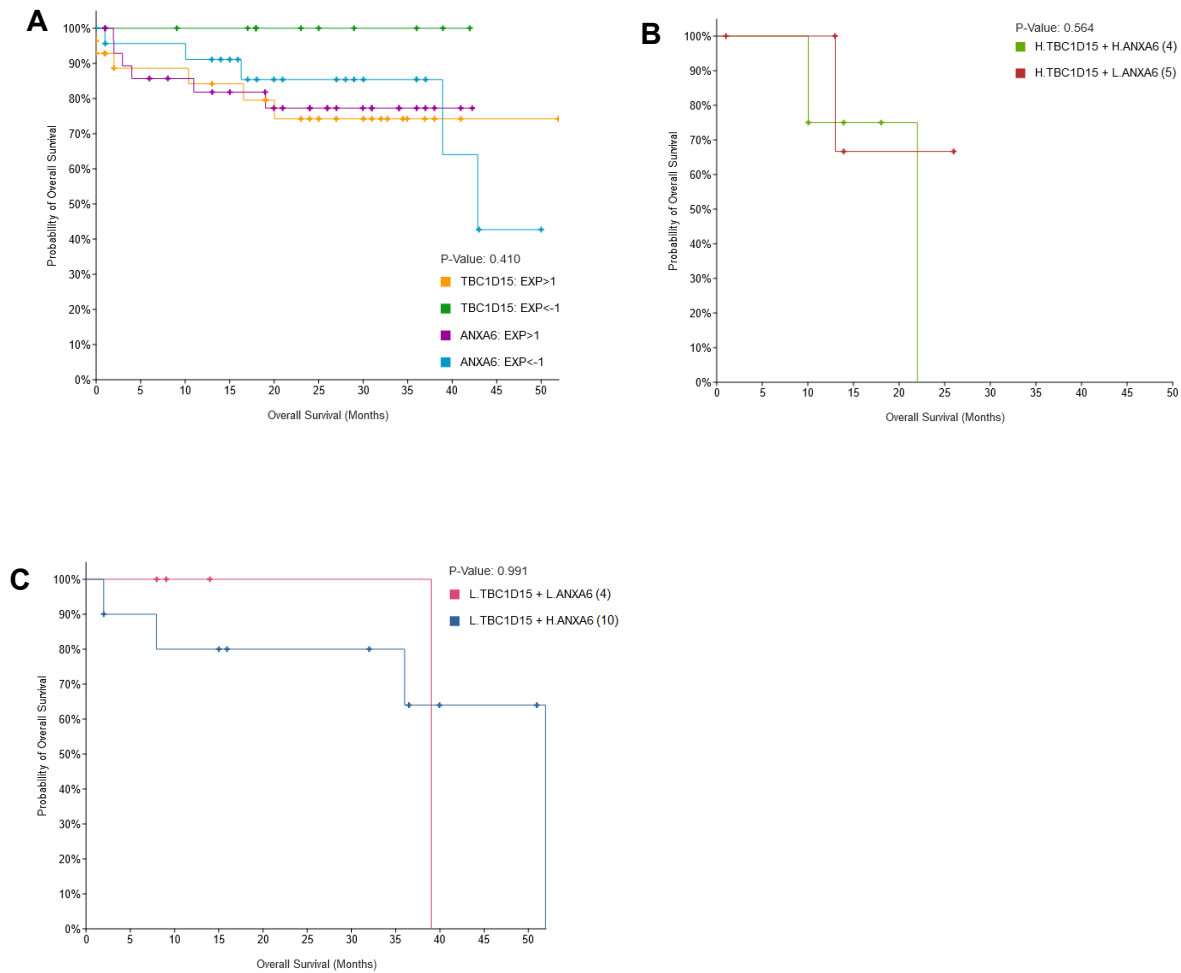
Figure 4.18. A. Probability (%) of overall patient survival (months) from hepatocellular carcinoma (TCGA, Firehose Legacy) with high (EXP>1) and low (EXP<1) TBC1D5 (n=43, 42) and ANXA6 expression levels. B-C. Probability (%) of overall patient survival with high (EXP>1) and low (EXP<1) TBC1D5 in combination with high/low ANXA6 expression levels as indicated. The number of samples with high/low TBC1D5 and ANXA6 levels are given, and the significance was calculated.

Figure 4.19. A. Probability (%) of overall patient survival (months) from hepatocellular carcinoma (TCGA, Firehose Legacy) with high (EXP>1) and low (EXP<1) TBC1D15 (n=49, 37) and ANXA6 expression levels. B-C. Probability (%) of overall patient survival with high (EXP>1) and low (EXP<1) TBC1D15 in combination with high/low ANXA6 expression levels as indicated. The number of samples with high/low TBC1D15 and ANXA6 levels are given, and the significance was calculated.

The Table 4.3 summarizes the patient survival probability of high/low ANXA6 levels paired with high/low LDLR, NPC1, RAB7, STARD3, TBC1D5 and TBC1D15 in a cohort of liver hepatocarcinoma patients. Alike the previous analysis of breast and colorectal cancer samples, many observations were not significant due to low sample numbers. Interestingly, low ANXA6 levels in combination with low LDLR or low RAB7 levels indicated a tumor suppressor role for ANXA6 that might not be related to LDL-cholesterol uptake and distribution (Fig. 4.14C, 4.16C). Low expression levels of the ANXA6/TBC1D5 pair also displayed reduced liver cancer patient survival, and the functional relevance has yet to be identified. Low ANXA6 levels correlating with poorer patient outcome in liver cancers identified here (Fig. 4.14-19, panels A) and in Chapter 2.4.2 (Fig 2.7B), correlates with published data, which identified ANXA6 downregulation in

ANXA6	LDLR ⇑	LDLR ⇓	NPC1 ⇑	NPC1 ⇓	RAB7 ⇑	RAB7 ⇓	STARD3 ⇑	STARD3 ⇓	TBC1D5 ⇑	TBC1D5 ⇓	TBC1D15 ⇑	TBC1D15 ⇓
⇑	>100	<30	<20	N.A.	>100	>100	>100	>30	>80	80	>90	20
⇓	>30	<15	>35	N.A.	>50	>15	<10	>10	>110	10	>30	20
		* p<0.05				** p<0.01				* p<0.05		

Table 4.3: 50% probability of overall patient survival (months). The months of 50% overall patient survival probability for gene pairs with high (⇑) and low (⇓) ANXA6 expression levels in combination with high/low expression levels of LDLR, NPC1, RAB7, STARD3, TBC1D5 and TBC1D15 in liver hepatocellular carcinoma patients (TCGA, Firehose Legacy) are given. Reduced and increased length of overall patient survival probability is indicated in red and green, respectively (* p<0.05, ** p<0.01).

hepatocellular carcinoma (233). Interestingly, low ANXA6 further lowered survival probability of liver cancers with high NPC1 expression levels (Fig. 4.15B). A negative association of ANXA6 with NPC1 using cBioportal was also observed in all liver cohorts (see Chapter 3). None of the other gene pairs analyzed indicated that low ANXA6 levels could promote liver cancer progression via the TBC1D15/RAB7/STARD3 axis. This correlates with the lack of correlations of ANXA6 with LDLR, NPC1, RAB7A, STARD3, TBC1D5 and TBC1D15 in liver cancers (see Chapter 3.3.1.2; Table 3.3). Nevertheless, high NPC1 levels as well as high RAB7 levels reduced patient survival (Fig. 4.15A, 4.16A), which could indicate effective LDL-cholesterol distribution and utilization in these cancers.

4.4.4. Expression patterns of the endo-lysosomal ANXA6 interactome and overall patient survival in pancreatic adenocarcinoma

We next analyzed the overall survival probability of ANXA6 and ANXA6 interactome gene pairs for pancreatic cancers, and examined a cohort of pancreatic adenocarcinoma (TCGA, Firehose legacy; 186 samples through the cBioportal platform (286, 287, 291). Within this cohort, approx. 5-30 samples displayed either high/low LDLR, NPC1, RAB7, STARD3, TBC1D5 or TBC1D15 expression levels. Within these small high/low expression groups of ANXA6 interactome proteins, an even smaller number of samples (n=0-5) displayed high/low ANXA6 expression levels. Hence, a number of gene pairs could not be plotted, as expression data for pancreatic cancer samples with certain gene pair combinations was not available. In Panel B of Figures 4.21, 4.22, 4.23, and 4.25, the overall survival probability of pancreatic adenocarcinoma with high NPC1, RAB7, STARD3, and TBC1D15 expression levels in combination with high/low ANXA6 levels are provided, respectively. In Panel C of Fig. 4.23 and 4.25, the overall survival probability of pancreatic cancer patients with low STARD3 and TBC1D15 expression levels in combination with high/low ANXA6 levels are given, respectively.

In line with significantly reduced survival of pancreatic cancers with low ANXA6 expression patterns observed in Chapter 2.4.2. (See Figure 2.6), gene pairs in patient samples with relatively high (EXP>1) and low (EXP<1) expression levels of ANXA6 in combination with LDLR (Fig. 4.20), NPC1 (Fig. 4.21), RAB7 (Fig. 4.22), STARD3 (Fig. 4.23), TBC1D5 (Fig. 4.24), and TBC1D15 (Fig. 4.25) all showed reduced patient survival probability for low ANXA6 expression levels. Please note that high/low ANXA6 levels displayed slightly differential overall survival

curves depending on the gene pair selected. This could indicate a tumor supporting role for ANXA6 in pancreatic adenocarcinoma that might be linked to cholesterol homeostasis. Alike the previous chapters, we have summarized the data shown in Panels B-C for Figures 4.20-4.25, in Table 4.4.
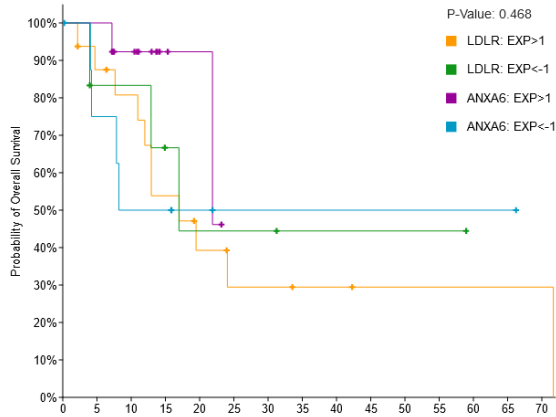
Figure 4.20. Probability (%) of overall patient survival (months) from pancreatic adenocarcinoma (TCGA, Firehose Legacy) with high (EXP>1) and low (EXP<1) LDLR (n=16, 6) and ANXA6 (13. 9) expression levels. The significance was calculated. Overall patient for samples with high/low LDLR in combination with high/low ANXA6 were not available.
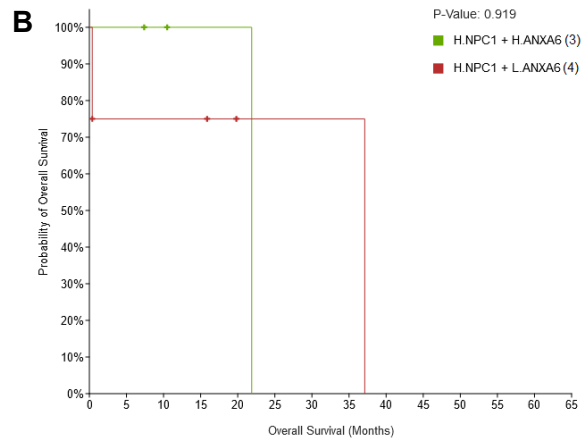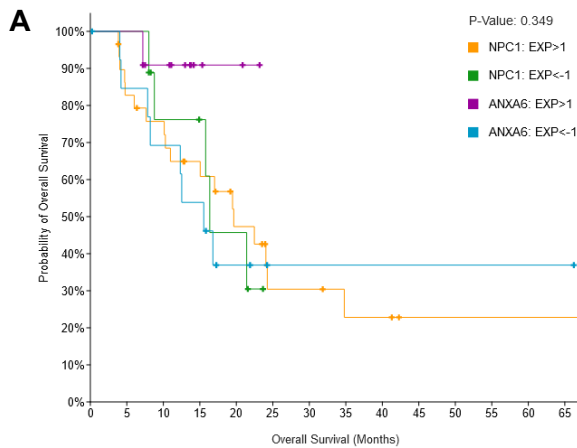
Figure 4.21. A. Probability (%) of overall patient survival (months) from pancreatic adenocarcinoma (TCGA, Firehose Legacy) with high (EXP>1) and low (EXP<1) NPC1 (n=29, 9) and ANXA6 (11. 14) expression levels. B. Probability (%) of overall patient survival with high (EXP>1) NPC1 levels in combination with high/low ANXA6 expression levels as indicated. The number of samples with high/low NPC1 and ANXA6 levels are given, and the significance was calculated. Overall patient for samples with low NPC1 in combination with high/low ANXA6 were not available.
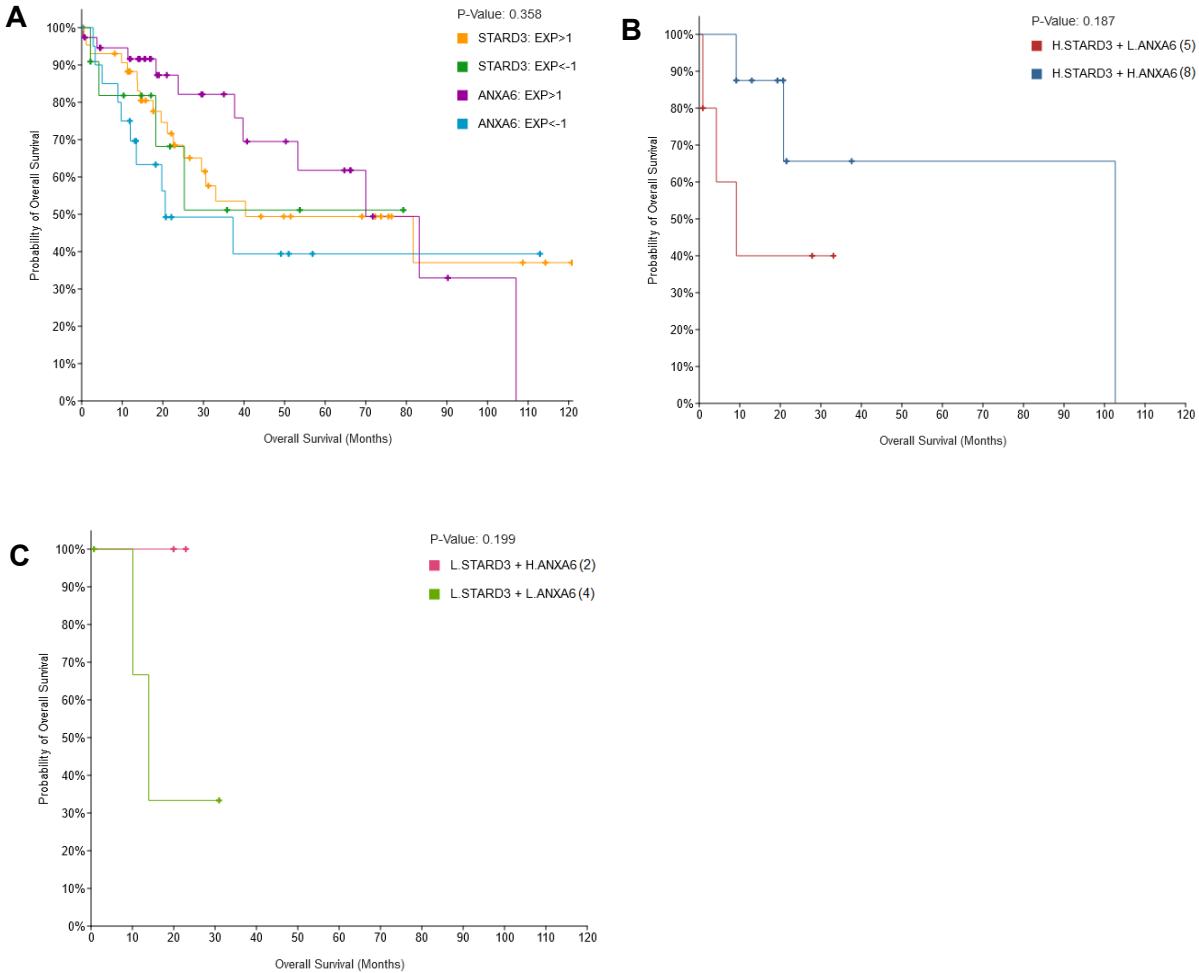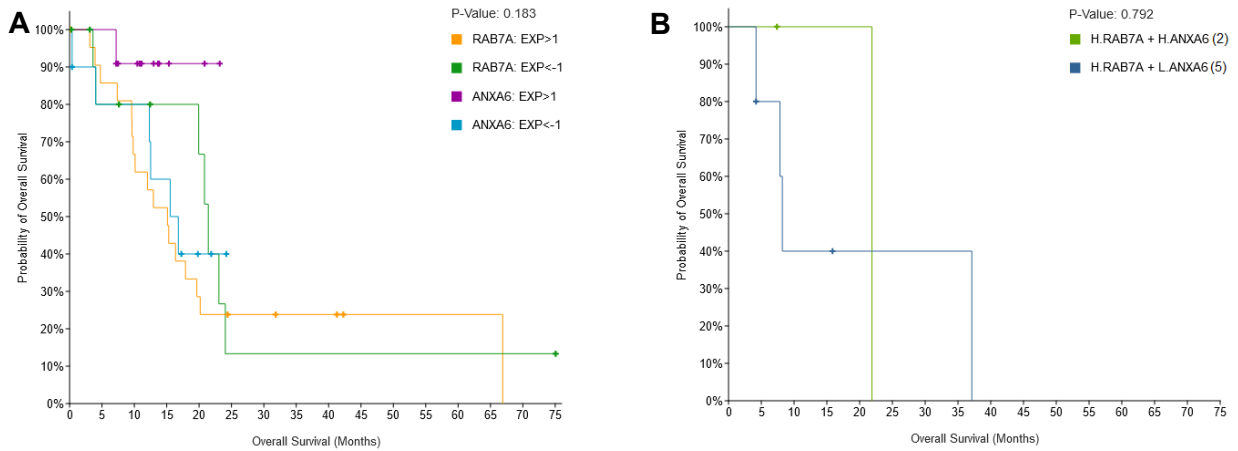
Figure 4.22. A. Probability (%) of overall patient survival (months) from pancreatic adenocarcinoma (TCGA, Firehose Legacy) with high (EXP>1) and low (EXP<1) RAB7A (n=22, 12) and ANXA6 (11. 10) expression levels. B. Probability (%) of overall patient survival with high (EXP>1) RAB7A levels in combination with high/low ANXA6 expression levels as indicated. The number of samples with high/low RAB7A and AN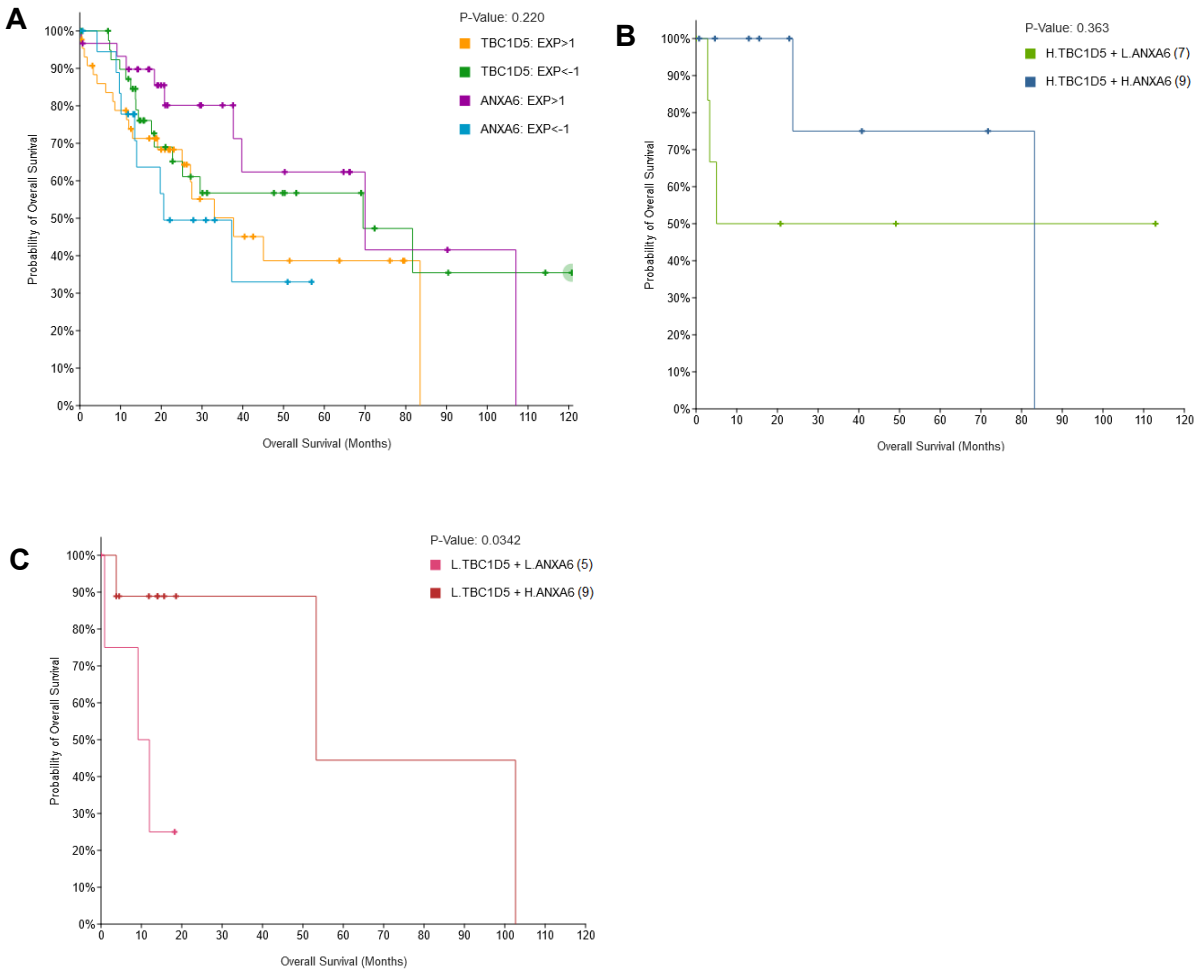XA6 levels are given, and the significance was calculated. Overall patient for samples with low RAB7A in combination with high/low ANXA6 were not available.
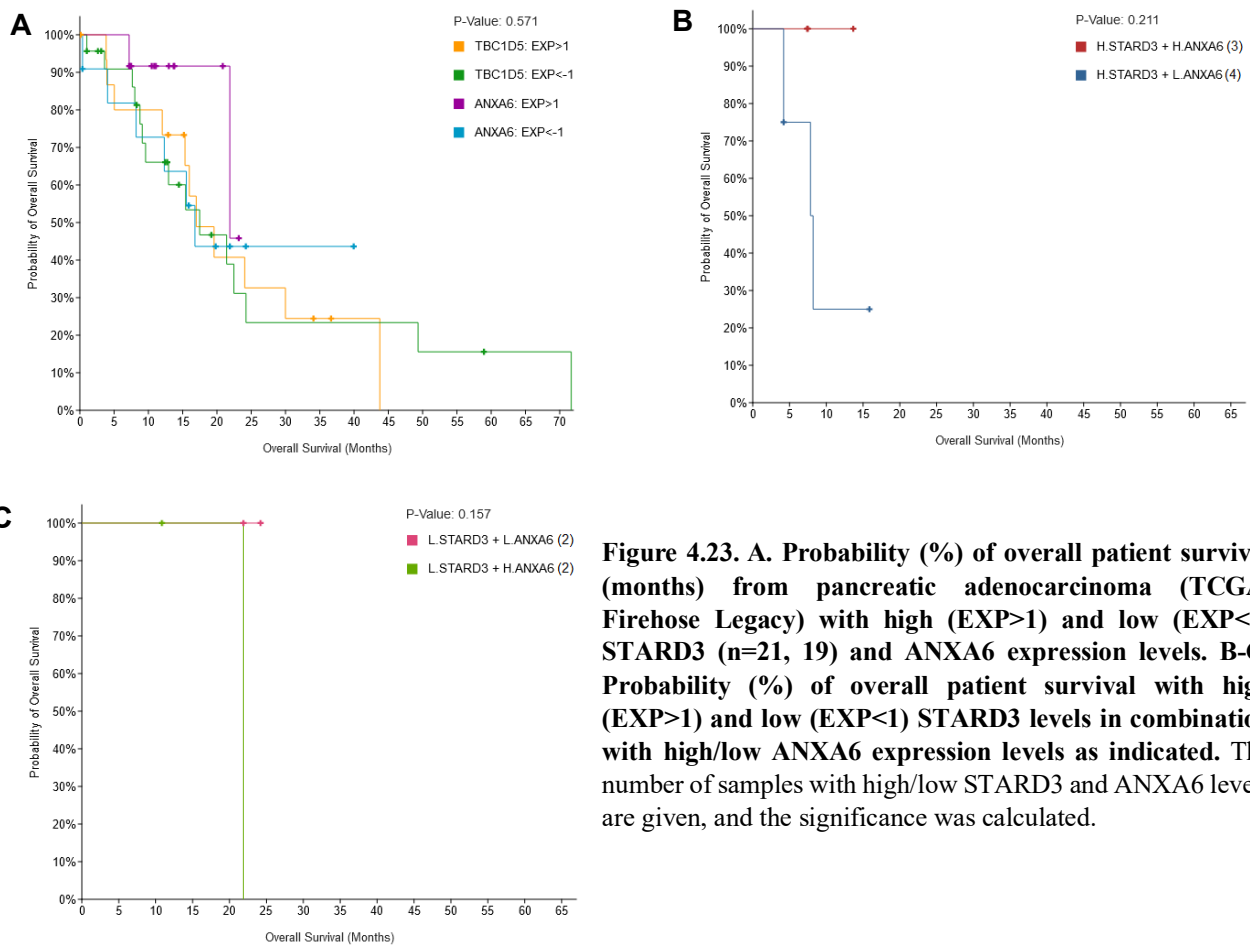
Figure 4.23. A. Probability (%) of overall patient survival (months) from pancreatic adenocarcinoma (TCGA, Firehose Legacy) with high (EXP>1) and low (EXP<1) STARD3 (n=21, 19) and ANXA6 expression levels. B-C. Probability (%) of overall patient survival with high (EXP>1) and low (EXP<1) STARD3 levels in combination with high/low ANXA6 expression levels as indicated. The number of samples with high/low STARD3 and ANXA6 levels are given, and the significance was calculated.
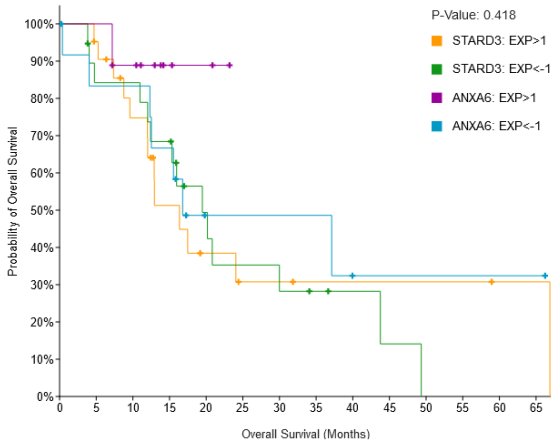
Figure 4.24. Probability (%) of overall patient survival (months) from pancreatic adenocarcinoma (TCGA, Firehose Legacy) with high (EXP>1) and low (EXP<1) TBC1D5 (n=16, 23) and ANXA6 (12. 11) expression levels. The significance was calculated. Overall patient for samples with high/low LDLR in combination with high/low ANXA6 were not available.
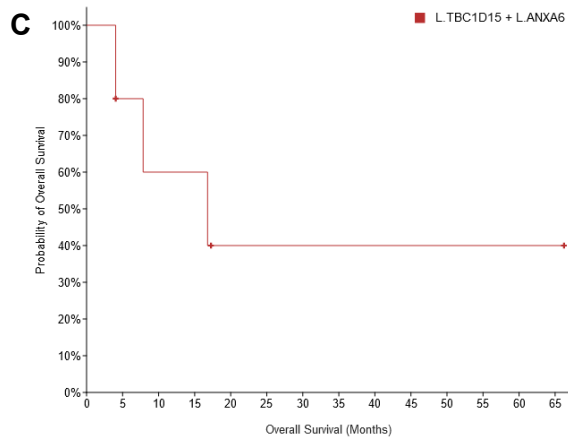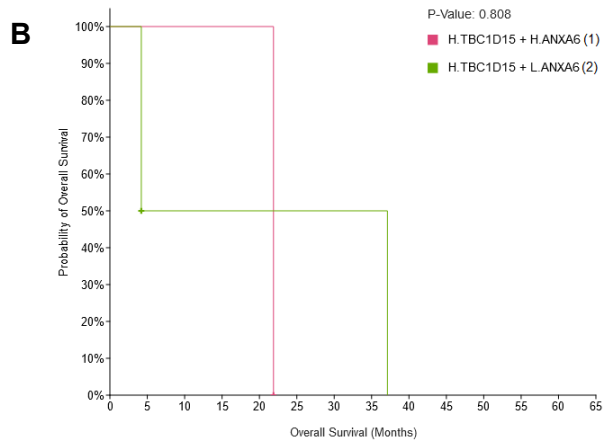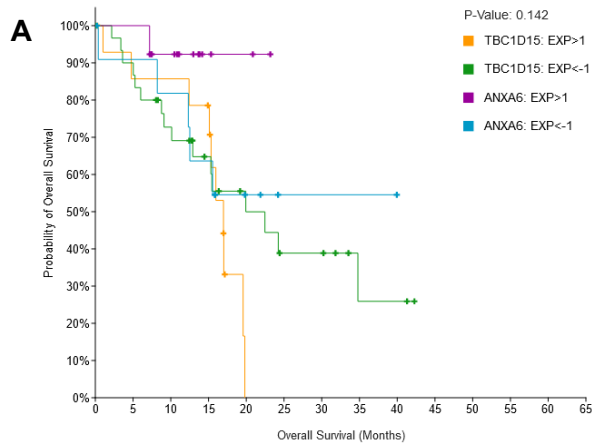
Figure 4.25. A. Probability (%) of overall patient survival (months) from pancreatic adenocarcinoma (TCGA, Firehose Legacy) with high (EXP>1) and low (EXP<1) TBC1D15 (n=15, 31) and ANXA6 expression levels. B-C. Probability (%) of overall patient survival with high (EXP>1) and low (EXP<1) TBC1D15 levels in combination with high/low ANXA6 expression levels as indicated. The number of samples with high/low TBC1D15 and ANXA6 levels are given, and the significance was calculated.
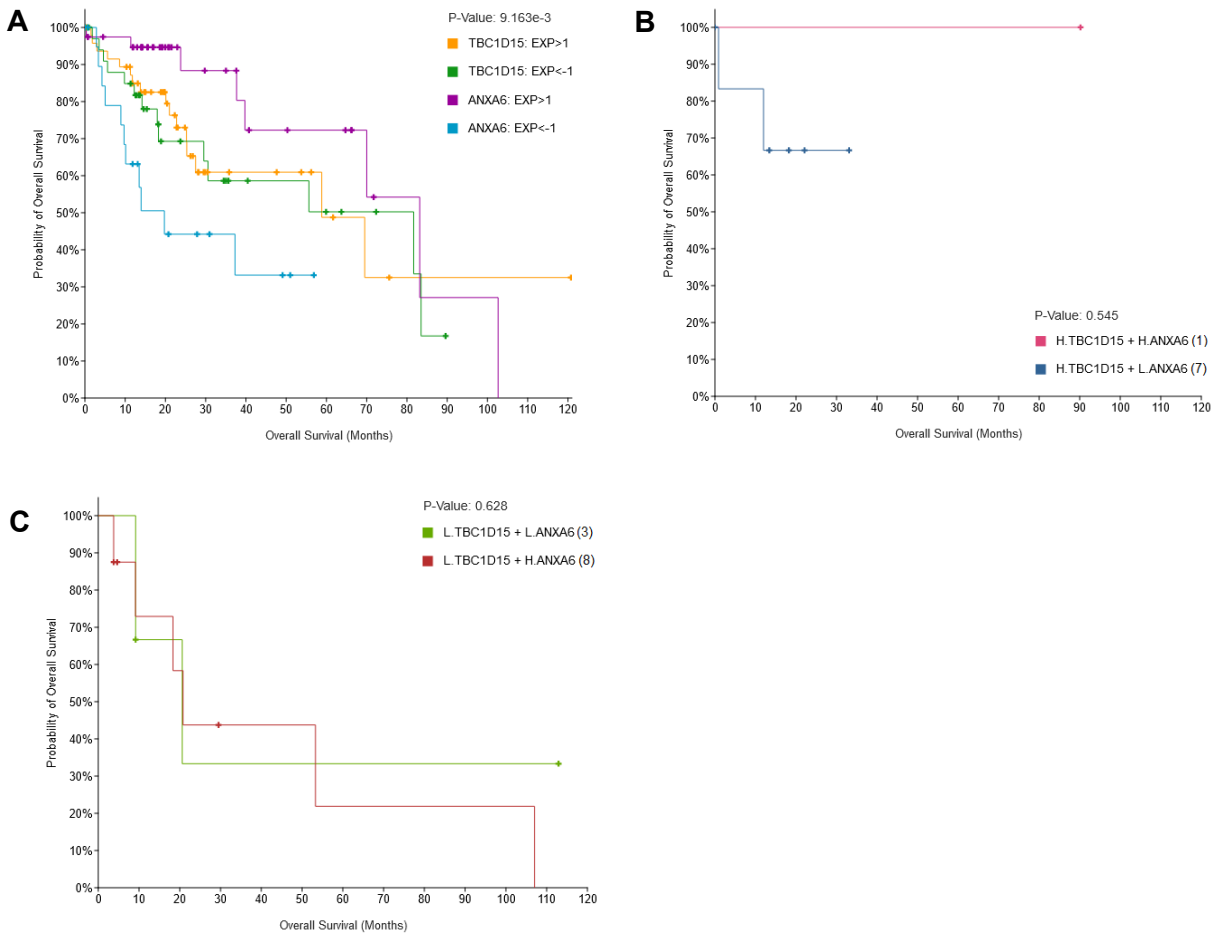
173

The Table 4.4 summarizes the patient survival probability of high/low ANXA6 levels paired with high/low LDLR, NPC1, RAB7, STARD3, TBC1D5 and TBC1D15 in a cohort of pancreatic adenocarcinoma patients. Within this cohort, several gene pair associations were not available, and all gene pairs collections consisted of low sample numbers. Interestingly, despite the low sample numbers, low ANXA6 levels in combination with high RAB7, STARD3 and TBC1D15 displayed a shorter patient survival probability, indicating a role for ANXA6 in the TBC1D15/RAB7A/STARD3 axis possibly related to cholesterol transport in the LE/Lys compartment.

In contrast to these findings, elevated ANXA6 protein levels were associated with shortened survival in other studies (221, 222). Leca *et al*. documented low ANXA6 protein amounts only in primary pancreatic tumor cells, while the tumor environment contained elevated ANXA6 amounts that increased with pancreatic cancer grade (222). O'Sullivan *et al.* (221) also proposed extracellularly high ANXA6 protein levels being associated with poorer outcome. Hence, future experiments that better separate tumor cell-associated vs. extracellular and non-tumor cell-associated ANXA6 amounts will be needed to clarify these opposing findings.

ANXA6	LDLR ⇑	LDLR ⇓	NPC1 ⇑	NPC1 ⇓	RAB7 ⇑	RAB7 ⇓	STARD3 ⇑	STARD3 ⇓	TBC1D5 ⇑	TBC1D5 ⇓	TBC1D15 ⇑	TBC1D15 ⇓
⇑	N/A	N/A	>20	N.A.	>20	N/A	>15	>20	N/A	N/A	>20	N/A
⇓	N/A	N/A	>35	N.A.	<10	N/A	<10	>20	N/A	N/A	<5	>15

Table 4.4: 50% probability of overall patient survival (months). The months of 50% overall patient survival probability for gene pairs with high (⇑) and low (⇓) ANXA6 expression levels in combination with high/low expression levels of LDLR, NPC1, RAB7, STARD3, TBC1D5 and TBC1D15 in pancreatic adenocarcinoma patients (TCGA, Firehose Legacy) are given. Reduced and increased length of overall patient survival probability is indicated in red and green, respectively. N/A, data not available.

4.4.5. Expression patterns of the endo-lysosomal ANXA6 interactome and overall patient survival in prostate adenocarcinoma

We next analyzed the overall survival probability of ANXA6 and ANXA6 interactome gene pairs in a cohort of prostate adenocarcinoma (TCGA, Firehose legacy; 501 samples through the cBioportal platform (286, 287, 291). Within this cohort, approx. 35-80 samples displayed high/low LDLR, NPC1, RAB7, STARD3, TBC1D5 or TBC1D15 expression levels. Within these sample groups, 25-50 samples showed high/low ANXA6 expression levels. Single genes in patient samples with relatively high (EXP>1) and low (EXP<1) expression levels of ANXA6 in combination with LDLR, NPC1, RAB7A, STARD3, TBC1D5 and TBC1D15 are shown in Fig. 4.26.
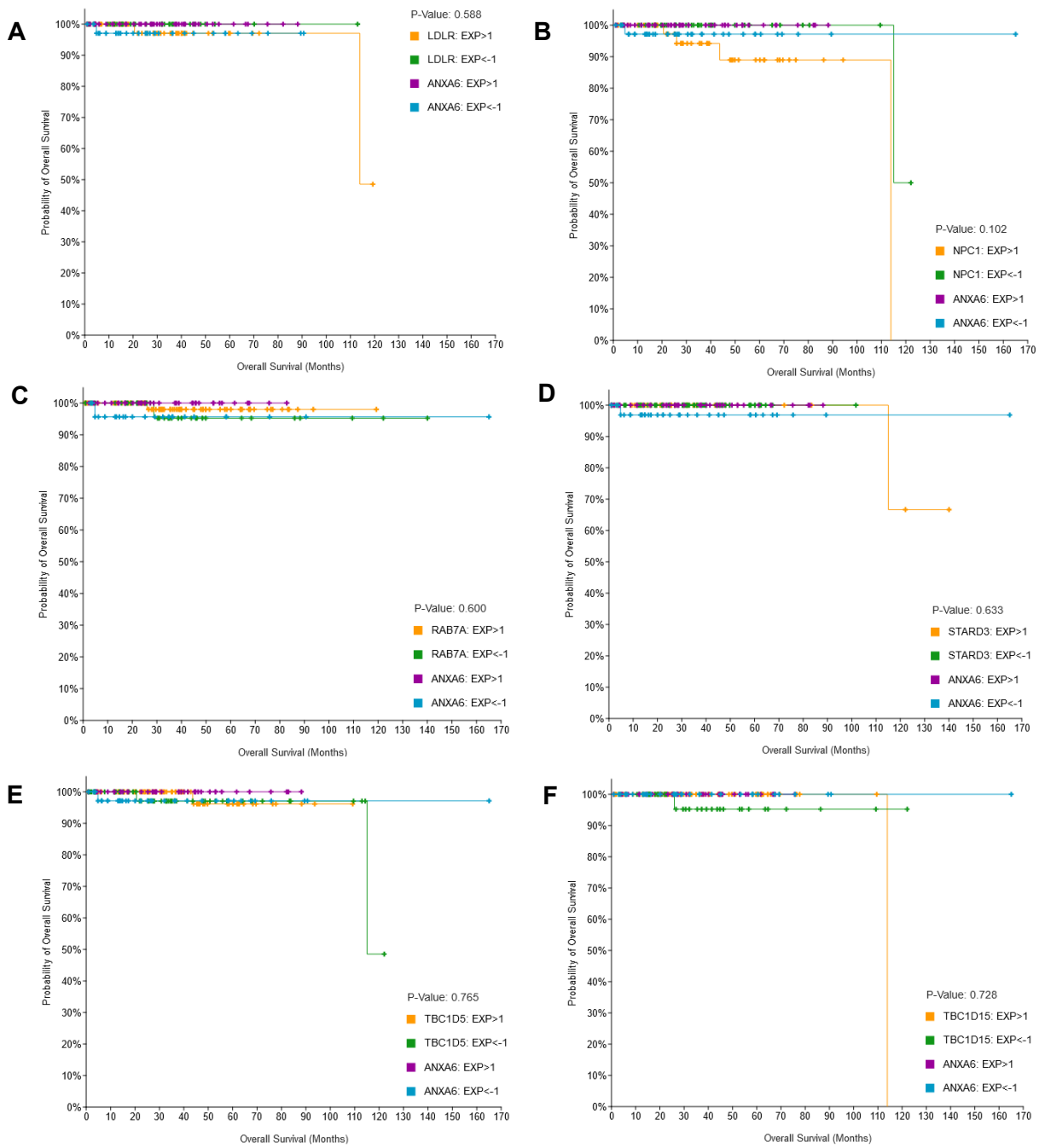
Figure 4.26. A-F. Probability (%) of overall patient survival ((months) from prostate adenocarcinoma (TCGA, Firehose Legacy) with high (EXP>1) and low (EXP<1) LDLR (n=50, 34), NPC1 (n=47, 38), RAB7A (n=70, 40), STARD3 (n=39, 65), TBC1D5 (n=72, 49) and TBC1D15 (n=66, 43) and ANXA6 (n=26-48, respectively) expression levels.

Strikingly and irrespective of high/low expression levels, all ANXA6 interactome genes showed 100% patient survival probability for >90 months. Beyond 90 months, only patient samples with high LDLR, high/low NPC1, high STARD3, high TBC1D5 and high TBC1D15 showed a reduction in survival probability. For all ANXA6 interaction partners, the survival probability remained high irrespective of high/low ANXA6 levels (not shown). These findings indicate that in early stages of prostate cancer, increased cholesterol availability may not be a critical factor that contributes to the outcome of cancer progression and/or treatment response at later stages. This is also in line with the survival probability analyzed in Chapter 2 (Fig. 2.7), which remained almost unchanged for >3000 days (>100 months) for both patients with high and low/medium ANXA6 levels. At later time points, overall patient survival with high ANXA6 levels was not available, while survival of prostate cancers expressing low ANXA6 levels dropped substantially at 3500 days (>115 months). Indeed, the gene expression patterns from 50 lethal, heavily pre-treated metastatic castration-resistant prostate cancer obtained after rapid autopsy (248). identified ANXA6 expression to be highest in the benign tissue, and a continuous and significant downregulation of ANXA6 levels was evident in localized and even more so in metastatic cancer samples (Chapter 2.4.2.3; Figure 2.4B). Hence ANXA6 downregulation may occur during the progression from localized to metastatic prostate cancer and any changes to its functional links with the ANXA6 interactome in the LE/Lys
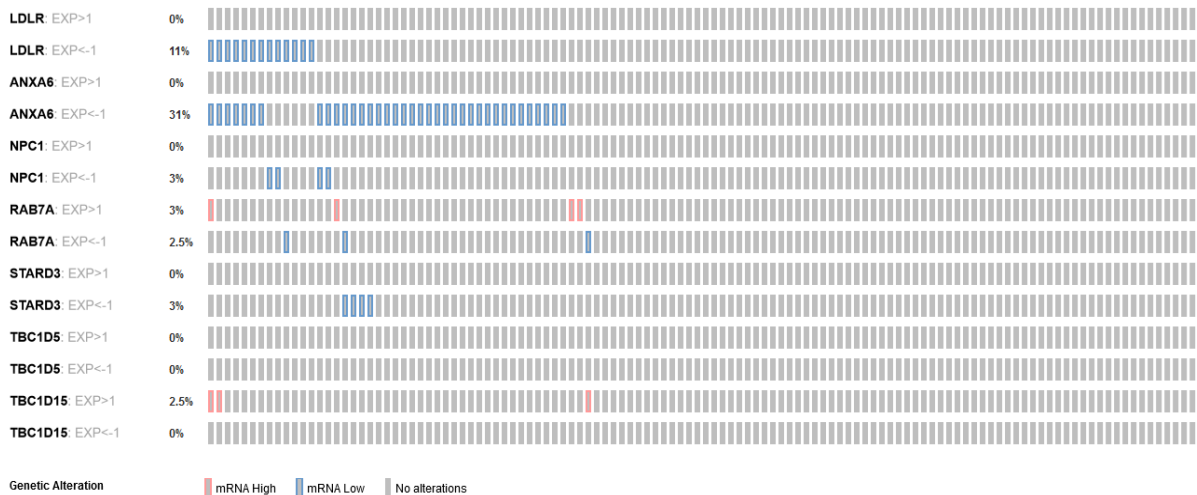
Figure 4.27: High (EXP>1) (red) and low (EXP <1) (blue) gene expression patterns of LDLR, NPC1, RAB7A, STARD3, TBC1D5 and TBC1D15 in a cohort of metastatic prostate adenocarcinoma samples with low ANXA6 expression levels. Median expression levels of all genes in individual tumor samples are depicted in grey (248).

compartment may not impact on the data available within the analyzed time frame for survival probability in the prostate adenocarcinoma cohort analyzed here.

Therefore, to identify potential ANXA6-related gene pair associations in metastatic prostate cancers, we mapped the expression levels of the ANXA6 interactome in individual patient samples available from the Grasso cohort (248). High (red) and low (blue) relative expression levels of ANXA6, LDLR, NPC1, RAB7A, STARD3, TBC1D5 and TBC1D15 for individual tumors are shown in Fig. 4.27. From this metastatic prostate cancer cohort, 37 samples displayed reduced ANXA6 levels. Several of those also expressed low LDLR (n=6), while other tumors displayed low NPC1 (n=2), RAB7A (n=1), STARD3 (n=4) levels. Several tumors contained high RAB7A levels (n=4), two of those in tumors expressing low amounts of ANXA6. Three tumors expressed elevated levels of TBC1D15, one of those also containing high amounts of RAB7A and low ANXA6.

The substantial number of metastatic tumors with low ANXA6 levels could indicate an increased requirement of these tumors for cholesterol, which could be covered by ANXA6 downregulation, increasing efficacy to metabolize and utilize internalized LDL-derived cholesterol. Furthermore, at least in 2 tumors, this could be supported by upregulation of RAB7 expression. These specific expression patterns in selected tumors may indicate gene networks being in place to provide growth and progression advantages. While these networks may only exist in less than 5% of advanced prostate cancers, this still makes a significant contribution to the annual >3500 death from prostate cancer in Australia in 2022 (see canceraustralia.gov.au).

The poor outcome of an increased supply with cholesterol for prostate cancer progression is also exemplified in hypercholesterolemia, which correlates with a more rapid occurrence of castration-resistant prostate cancer after androgen deprivation therapy (95). Likewise, elevated risk of prostate cancer development and progression correlates with elevated plasma cholesterol levels (377-379) . Moreover, cholesteryl ester storage in lipid droplets is increased in advanced and metastatic prostate cancer (138). Also, Grewal and co-workers demonstrated that increased LDL-cholesterol availability stimulated growth of androgen-independent prostate cancer cell lines (89), supporting efficient LDL uptake and export of LDL-derived cholesterol from LE/Lys to other organelles to advance prostate cancer progression.

4.5. Discussion

In the previous Chapter, we identified several gene correlations of ANXA6 and its interactome using cBioportal and CANCERTOOL. In this Chapter, ANXA6-related gene pairs were analyzed on their potential to influence patient survival.

(i) In breast cancer, this analysis showed a positive correlation between ANXA6/LDLR and ANXA6/NPC1 gene pairs in Her2+ and ER-positive cancers (2/4) in both cBioportal and CANCERTOOL platforms. These breast cancer subtypes have not yet been linked with de-regulated LDL uptake or ANXA6 cancer-related functions. Using CANCERTOOL, trends for negative correlations between ANXA6 and LDLR levels in ER-negative cancers (5/5) were observed, which support published reports on ANXA6 downregulation or LDLR upregulation in these cancers (10, 25). Hence, this gene pair expression pattern could support increased LDL uptake and efficient LDL-cholesterol distribution via NPC1-dependent and NPC1-independent (and ANXA6-regulated) routes to cellular sites supporting growth and metastatic behaviour.

This findings coincide with NPC1 upregulation and associated poorer prognosis and possible drug resistance in TNBC and ER-negative breast cancers (380). The negative correlation of ANXA6 and NPC1 in 2/4 breast cancer cohorts in cBioportal, and 4/4 (ER-), 3/4 (ER+) and 3/3 (Her2+) cohorts in CANCERTOOL support these findings. Several breast cancer cohorts suggest high NPC1 in combination with low ANXA6 levels to promote cellular distribution of incoming LDL-cholesterol to promote breast cancer growth and progression, leading to poorer prognosis and treatment response.

The analysis of patient survival probability in this Chapter supports several of these gene correlations listed in Chapter 3. Although some observations were not significant due to low sample numbers, low ANXA6 levels strongly reduced the survival probability in patients with high LDLR (Fig. 4.1B), high RAB7 (Fig. 4.3B) and STARD3 (Fig. 4.4B) levels, supporting the supportive role of ANXA6 for LDL-cholesterol distribution via RAB7- and STARD3-dependent cholesterol routes in breast cancer settings where elevated LDLR activity allows increased uptake of LDL-cholesterol to reach the LE/Lys compartment. On the other hand, high ANXA6 levels were associated with longer patient survival probability in breast cancer samples with high/low LDLR and NPC1, high STARD3, RAB7, TBC1D5 and TBC1D15. This might point at elevated ANXA6 levels to counteract LDL-cholesterol distribution in these breast cancers.

Most interestingly, within the invasive breast cancer cohort from TCGA, a substantial number of samples (n~25 for ER-negative; n~15 for EGFR overexpression) displayed elevated LDLR levels, suggesting increased LDL uptake in these cancers. Moreover, within these ER-negative and EGFR-related subgroups with high LDLR, approximately 10 samples displayed reduced ANXA6 levels. Several of these cancers were also characterized by high NPC1, RAB7A, STARD3 and low TBC1D15 expression levels. Hence, in ER-negative and EGFR-related breast cancers, subgroups appear to exist that display a gene network expression pattern that favour increased LDL uptake and distribution characterized by high levels of cholesterol transporters (LDLR, NPC1, StASRD3) and regulatory proteins (RAB7A, TBC1D15) that allow increased membrane contact site formation for cholesterol efflux from LE/Lys.

These findings support a tumor suppressor role for ANXA6 in ER-negative and TNBC breast cancers (71, 204) that involves increased LDL-cholesterol supply, which has been observed in breast cancer, increasing proliferation and metastatic behaviour, and contributing to poor prognosis and chemoresistance (106, 107, 126, 127, 129). The fact that expression patterns related to ANXA6 and its interactome in LE/Lys might be relevant only in certain breast cancer subgroups indicate that other oncogenic mutations, such as EGFR overexpression, must be present in order for ANXA6-related changes related to cholesterol export from LE/Lys to impact on cancer progression. Furthermore, metabolic reprogramming in these cancers most likely extends beyond cholesterol homeostasis, involving changes in carbohydrate and amino acid metabolism. For example, it is well known that many TNBC cancers are characterized by predominantly aerobic glycolysis, also termed the Warburg effect (381). In addition, increased utilization of amino acids in breast cancer to provide building blocks that support growth is common (382).

Hence, future research will have to identify the master regulators responsible for metabolic reprogramming that involves lipid, but also carbohydrate and amino acid metabolism. Strikingly, the master regulator of cancer cell metabolism, mTORC1 kinase, often de-regulated and hyperactive in many cancers, including prostate, liver, pancreatic and colon cancers discussed below, is located in LE/Lys and activated in a NPC1 and cholesterol-sensitive manner (34, 100).

(ii) In prostate cancers, CANCERTOOL analysis revealed a negative association of ANXA6 and LDLR in metastatic prostate cancers (2/4), which aligns with the proposed tumor suppressor role of ANXA6 in these cancers. Yet, irrespective of high/low ANXA6 expression levels, all ANXA6 interactome genes showed 100% patient survival probability for >90 months in a prostate

adenocarcinoma cohort from TCGA. Only patient samples with high LDLR, high/low NPC1, high STARD3, high TBC1D5 and high TBC1D15 showed a reduction in survival probability after >90 months, altogether indicating that cholesterol availability may not be a decisive factor for late-stage prostate cancer progression and/or treatment response. In line with this, high and low/medium ANXA6 levels showed comparable survival probability (Fig. 2.7) that remained constant for >3000 days (>100 months). Yet, significant ANXA6 downregulation was observed in metastatic and castration-resistant prostate cancer (248).. Within this cohort, 37 samples displayed reduced ANXA6 levels. Several of those also exhibited high RAB7A levels (n=4). This could indicate an increased requirement of these tumors for cholesterol, which could be covered by ANXA6 downregulation and RAB7 upregulation. These patient-specific expression patterns may indicate ANXA6-related gene networks that allow the tumor to become more efficient to metabolize and utilize internalized LDL-derived cholesterol in order to gain growth and progression advantages. If these networks only exist in a small proportion of advanced prostate cancers, this can still be considered significant as annual death from prostate cancer in Australia in 2022 were >3500 (see canceraustralia.gov.au).

In line with this hypothesis, elevated plasma cholesterol levels and increased cholesteryl ester storage are linked to increased risk of prostate cancer development and progression (138, 377-379, 383). Also, hypercholesterolemic patients show a more rapid occurrence of castration-resistant prostate cancer (95), which implicates efficient supply with LDL-cholesterol to advance prostate cancer growth progression (89).

(iii) In liver cancers, gene correlation analysis of ANXA6 and its interactome (see Chapter 3) partially support published findings of ANXA6 expression in liver cancers (233). In fact, low ANXA6 levels correlated with poorer patient outcome in liver cancers (Fig. 2.7B and 4.14-19, panels A), which correlates with ANXA6 downregulation reported by Grewal and colleagues in hepatocellular carcinoma (233). However, in the cohort of liver hepatocarcinoma patients from TCGA, low ANXA6 levels in combination with low LDLR or low RAB7 levels indicated a tumor suppressor role for ANXA6 that might not be related to LDL-cholesterol uptake and distribution (Fig. 4.14C, 4.16C). On the other hand, low ANXA6 lowered survival probability of liver cancers with high NPC1 expression levels (Fig. 4.15B), which coincides with the negative association of ANXA6 with NPC1 using cBioportal in all liver cohorts analyzed (see Chapter 3). Nevertheless, none of the other gene pairs analyzed indicated that low ANXA6 levels could promote liver cancer

progression via the TBC1D15/RAB7/STARD3 axis. Likewise, correlations of ANXA6 with LDLR, NPC1, RAB7A, STARD3, TBC1D5 and TBC1D15 were lacking in liver cancers (see Chapter 3.3.1.2; Table 3.3). Yet, high NPC1 levels as well as high RAB7 levels reduced liver cancer patient survival (Fig. 4.15A, 4.16A), which could indicate effective LDL-cholesterol distribution and utilization in some of these cancers.

(iv) In pancreatic cancers, two studies associated elevated ANXA6 protein levels with reduced survival (221, 222). Both of these studies identified elevated ANXA6 amounts in the tumor stroma and/or extracellular milieu, in contrast to these findings, low ANXA6 levels in combination with high RAB7, STARD3 and TBC1D15 displayed a shorter patient survival probability, indicating the ANXA6-dependent TBC1D15/RAB7A/STARD3 axis to play a role. These opposing findings will need further research to better dissect the role of ANXA6 in tumor cells vs. the surrounding tumor environment.

In colon cancers, a significant reduction of ANXA6 levels was observed in colon adenocarcinoma (Chapter 2.4.3 – 2.4.5.). Both cBioportal and CANCERTOOL showed a negative correlation between ANXA6 and LDLR in the various colon and colorectal cancer cohorts (Chapter 3). However, high ANXA6 levels were characterized by lower patient survival in colorectal adenocarcinoma, indicating a potentially cholesterol-independent role for ANXA6 in these cancers. Low ANXA6 levels in combination with low LDLR levels or high ANXA6 with high NPC1 expression levels showed significantly reduced patient survival probability, which also did not support high/low ANXA6 levels to control tumor progression via cholesterol export from LE/Lys.

Chapter 5
Conclusions and future directions

Besides mutations in proto-oncogenes and loss of tumor suppressors that trigger activation of signalling cascades to promote proliferation, avoidance of apoptosis and ability to metastasize, the substantial reprogramming of cancer cell metabolism has become a well-accepted additional hallmark of oncogenesis. In order to accommodate the increased need for biomolecules and building blocks that support tumor growth and progression, cancer cells develop strategies to alter the activity of metabolic pathways to maintain their growth advantage (384). This is exemplified by the Warburg effect, which describes the upregulation of glucose uptake followed by anaerobic glucose oxidation to produce ATP (385). In addition, cancer cells often show increased utilization of amino acids, such as glutamine, providing building blocks for the synthesis of complex molecules. As cancer cells also need lipids for cell growth and progression, metabolic reprogramming in oncogenesis commonly entails adaptations in the way cancer cells handle lipids (1, 88, 89, 386, 387).
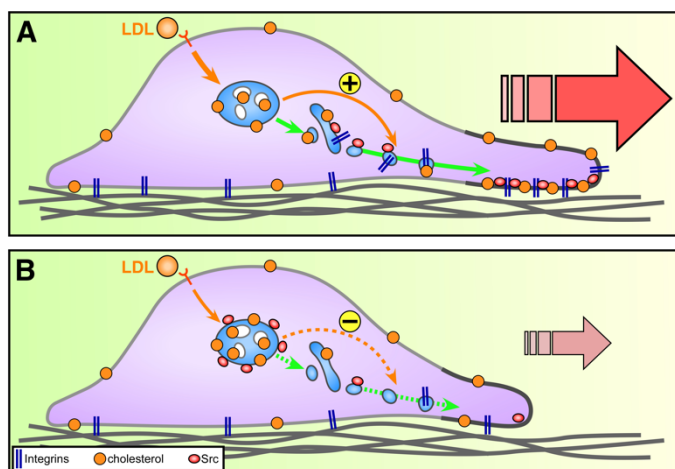
Figure 5.1: LDL internalization by cancer cells and reduction in invasive behaviour by the inhibition of cholesterol export from LE/Lys A. Cancer cells internalize LDL bound to LDL receptors. LDL-derived cholesterol reaches the late endosomal/lysosomal (LE/Lys) compartment and is then delivered to other organelles, such as focal adhesions at the leading edge of cells. Together with an increased delivery of integrins to the leading edge, this promotes migratory and invasive behaviour of cancer cells. **B.** Inhibition of cholesterol export from LE/Lys to the leading edge reduces the invasive behaviour of cancer cells (with kind permission from T. Grewal).

Lipids required for the proper functioning of cell homeostasis represent a complex and diverse group and include fatty acids, triglycerides, phospholipids, sphingo- and glycolipids (387). In addition, cholesterol serves as a precursor for bile acids, steroid hormones and vitamins and is indispensable for membrane integrity, organelle compartmentalization, cell surface receptor

signalling and endocytosis as well as regulation of signal transduction pathways that emanate from the plasma membrane or other intracellular membranes (2, 4, 97).

Besides upregulation of *de novo* cholesterol synthesis, cancer cells often show increased uptake of LDL-derived cholesterol (92, 93) (Figure 5.1). Once endocytosed, LDL-cholesterol is delivered from late endosomes/lysosomes (LE/Lys) to other cellular sites such as the plasma membrane, lipid droplets and mitochondria to promote proliferation and metastatic behaviour. Hence, blocking endocytosis of LDL-derived cholesterol has therapeutic potential, and LDLR depletion or inhibition, as well as pharmacological inhibition of LDL-derived cholesterol esterification inhibited growth and migratory behaviour of cancer cells in multiple settings (105, 130, 132, 138, 152, 386) and in ovarian and pancreatic cancer models, sensitized cancer cells to anticancer therapy (93, 137).

It has yet to be determined if the pharmacological manipulation of cholesterol homeostasis described here and below for itraconazole and other drugs targeting cholesterol transport in LE/Lys (171-185) can become an effective and selective approach to limit cancer progression. It is evident from a plethora of other studies that many cancers often prefer to upregulate glucose uptake or enhance amino acid metabolism to gain a growth advantage (374-376). Rather identifying the subgroups of cancer patients that will benefit the most from therapeutic interventions blocking cholesterol uptake and utilization, most likely in combination with current anticancer drugs, that could become a strategy to develop further in the future.

In line with this, the Grewal group and colleagues identified several LDL-cholesterol sensitive mechanisms driving cell motility that could be targeted by genetic or pharmacological inhibition of cholesterol export from LE/Lys. For instance, pharmacological NPC1 inhibitors or ANXA6 overexpression, which caused an NPC1-mutant like phenotype, compromised membrane transport regulated by cholesterol-sensitive SNARE and Rab proteins responsible for integrin recycling, fibronectin secretion (85-87), focal adhesion assembly (44, 56, 57) and caveolae formation (83), as well as cholesteryl ester storage in lipid droplets (55, 89) (Figure 5.2).
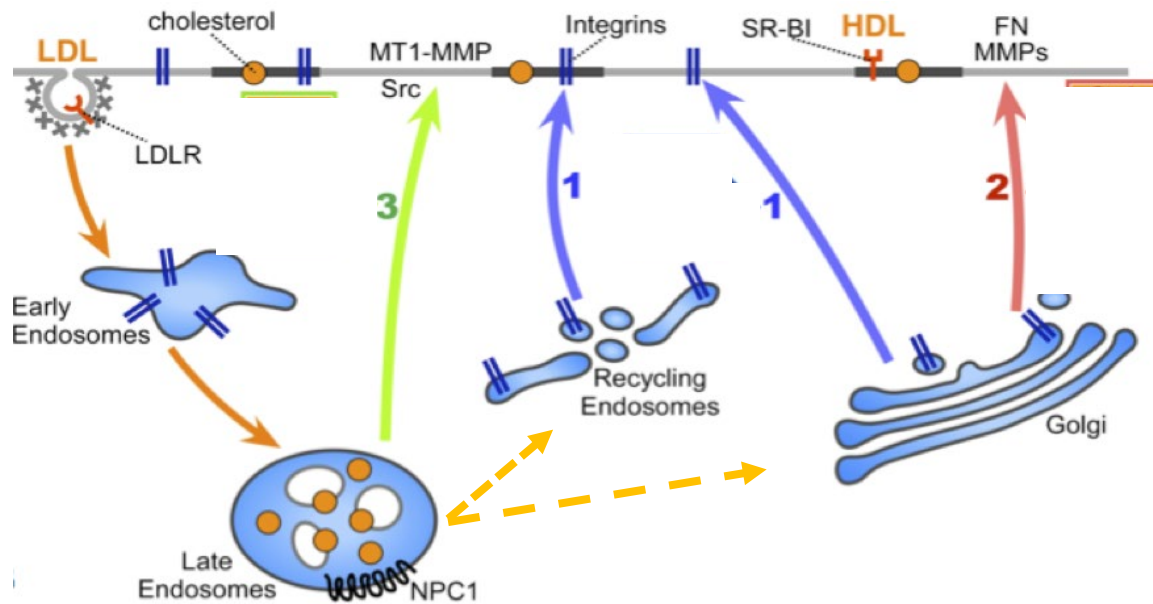
Figure 5.2: LDL-derived cholesterol transportation and contribution to the invasive and metastatic behaviour. LDL-derived cholesterol reaches the late endosomal/lysosomal (LE/Lys) compartment and cholesterol transporters such as Niemann Pick Type C1 (NPC1) then deliver cholesterol to the Golgi, recycling endosomes and plasma membrane to support molecular events that drive invasive behaviour and metastasis (1, 384, 385), including formation of caveolae, delivery of metalloproteases (MMPs, MT1-MMP), integrins, extracellular matrix (fibronectin, FN) to the cell surface, including focal adhesions at the leading edge of cells (see text for further details; with kind permission from T. Grewal).

Most of the findings described above were derived from fibroblast cell lines, and there is still limited knowledge if cellular distribution of internalized LDL-cholesterol has any role for cancer cell motility. Chapter 1 of this thesis provides the proof-of-principle, showing that depletion of the cholesterol transporter NPC1 in a well-established and aggressive cancer cell line significantly reduced cell migration not only in 2-dimensional wound healing assays (56), but also compromised the ability of these cancer cells to adhere and invade secondary organs *in vivo*. This identifies NPC1 as a therapeutic target in cancer, and while pharmacological NPC1 inhibitors exist (U18666A), their side-effects up to date limited further drug development. Alternatively, the antifungal agent itraconazole also inhibits NPC1-mediated cholesterol export and showed potential for cancer therapy (173, 176, 181, 182). These anticancer properties of itraconazole also improved cisplatin efficacy and have resulted in Phase I and II trials in non-small cell lung cancer, basal cell carcinoma, metastatic prostate, and pancreatic cancer.

Likewise, cholesterol accumulation in LE/Lys triggered by the alkaloid cepharanthine, the antihistamine astemizole and the lysosomotropic compound leelamine correlate with improved anticancer drug efficacy, lowering of adverse effects after chemotherapy and downregulation of oncogenic signal transduction pathways (173-180, 184).

In addition, a better understanding of cholesterol export from LE/Lys and the role of other cholesterol transport routes in this compartment could provide alternative therapeutic opportunities. Along these lines, in previous work from the Grewal group, the scaffolding protein ANXA6 was identified as a gatekeeper in LE/Lys, reducing the ability of cholesterol transporters in LE/Lys to export cholesterol to other organelles (55).

Mechanistically, ANXA6 recruits the RAB7-GTPase activating protein TBC1D15 to cholesterol-rich LE/Lys. This leads to TBC1D15/RAB7 complex formation, followed by inhibition of RAB7 activity and lowering of RAB7-GTP levels. Vice versa, ANXA6 depletion and the concomitant loss of TBC1D15 membrane targeting elevated RAB7-GTP levels, enabling cholesterol export from LE/Lys via the cholesterol transporter STARD3 to the ER, followed by cholesterol esterification and storage in lipid droplets. Rather than being exported from LE/Lys via vesicular or non-vesicular transport, ANXA6-regulated cholesterol transfer exiting LE/Lys occurs through the formation of membrane contact sites (MCS), which is depicted in Figure 5.3. In addition, ANXA6 depletion also increased delivery of LDL-derived cholesterol to focal adhesions, indicating that low ANXA6 levels can contribute to cancer aggressiveness in cancers that are known to respond to increased supply with dietary cholesterol.

It should be noted that TBC1D15/RAB7 assembly is also relevant for communication between LE/Lys and mitochondria. MCS formation between these two organelles is inhibited by TBC1D15-mediated RAB7-GTP hydrolysis. This mechanism has yet only been described to disrupt mitochondrial function in neurological models, such as Parkinson's and Charcot-Marie-Tooth type 2B (CMT2B) (388-391). However, as ANXA6 has also been identified in mitochondria (392), one can envisage that high/low ANXA6 levels also determine the transfer of cholesterol from LE/Lys to mitochondria. In fact, the well-being and ability of mitochondria to support cancer growth and progression greatly depends on an increased delivery of cholesterol to mitochondria (393-395).
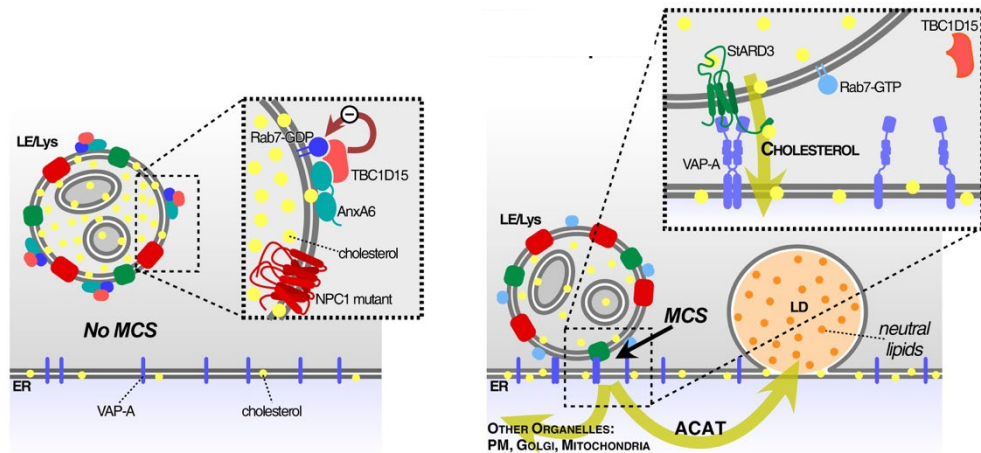
Figure 5.3: ANXA6 controls the formation of membrane contacts sites (MCS) in LE/Lys with the endoplasmic reticulum (ER) and possibly other organelles. Left: High ANXA6 levels recruit the RAB7-GTPase activating protein TBC1D15 to downregulate RAB7 activity and lower RAB7-GTP levels. This blocks the formation of MCS between LE/Lys and the ER (55). **Right:** ANXA6 depletion prevents recruitment of TBC1D15, leading to elevated RAB7-GTP levels. This enables STARD3 to interact with VAMP associated protein-A (VAP-A) in the ER for cholesterol transfer to the ER, followed by acetyl-CoA-acetyltransferase (ACAT) -mediated cholesterol esterification and storage of cholesteryl esters in lipid droplets (55). Other routes of cholesterol from the ER promoted by low ANXA6 levels include the delivery of cholesterol to the plasma membrane (focal adhesions) and mitochondria. Increased cholesterol storage and delivery to focal adhesions promote invasive cancer cell behaviour (56) (with kind permission of T. Grewal).

Hence, high/low ANXA6 levels determining the presence or absence of MCS appear to have consequences for cholesterol transfer between organelles. This may extend to other annexins, such as ANXA1, which acts as a tether to promote MCS formation or ANXA2, which can bridge membranes (reviewed in (396)). Thus, manipulating the levels of regulators of MCS formation offer therapeutic opportunities in chronic disease, such as cancer.

We have addressed this potential tumor suppressor role of ANXA6 related to incoming LDL-cholesterol in Chapter 2-4. Examining cancers linked to de-regulated cholesterol homeostasis or increased responsiveness to oversupply with dietary cholesterol, we found a significant downregulation of ANXA6 expression during the progression from localized to metastatic prostate cancer. Low ANXA6 levels were also associated with reduced overall survival in TNBC breast cancers. Furthermore, ANXA6-related gene network associations seem to exist, as a negative association between ANXA6 and LDLR, NPC1 and RAB7A expression levels was made in several cancers, in particular ER-negative and TNBC breast cancer. This points at an improved LDL-cholesterol utilization when ANXA6 levels are low, and relevant for cancer aggressiveness, progression, and treatment outcome. On the other hand, ANXA6 and STARD3 levels were

positively associated in breast, prostate, colon, pancreas, and liver cohorts, indicating that ANXA6 is indeed a gatekeeper that limits the involvement of STARD3 in cholesterol export from LE/Lys. In further support of cancer cells being able to coordinate the expression of multiple genes involved in cholesterol homeostasis, low ANXA6 levels strongly reduced the survival probability in breast cancer patients with high LDLR or high RAB7A or high STARD3 levels. Indeed, when mapping the expression patterns of all selected genes from the ANXA6 interactome (ANXA6, LDLR, NPC1, RAB7A, STARD3, TBC1D5, TBC1D15) in individual samples, the abovementioned expression patterns were enriched in ER-negative and/or EGFR-related (triple-negative) breast cancers. On the other hand, high ANXA6 levels were associated with longer patient survival probability in breast cancer samples with high/low LDLR and NPC1, high STARD3, RAB7A, TBC1D5 and TBC1D15, suggesting elevated ANXA6 levels to counteract efficient LDL-cholesterol distribution in these breast cancers. Despite the low number of patient samples that displayed these expressions patterns, these findings suggest the existence of expression profiles of ANXA6 and its interactome in LE/Lys that has diagnostic and prognostic value. Results described here implicate blockage of ANXA6 and its interactome (NPC1, RAB7A, STARD3) to inhibit dietary cholesterol supply from LE/Lys as an attractive anticancer approach, yet the limited statistical significance of many of the findings described here due to the low number of samples with certain gene pair combinations requires further analysis of larger cohorts in the future to confirm trends observed here.

Nevertheless, based on the work presented here and studies discussed above, therapeutic targeting of cholesterol homeostasis, in particular the uptake of dietary LDL-cholesterol, could become an attractive alternative or supplement to current anticancer drugs for a variety of cholesterol-sensitive cancers. Also, the combination of drugs interfering with lipid supply together with pharmaceutical approaches that interfere with metabolic pathways supplying cancer cells with glucose and amino acids should be considered (384-386). Our study implicates ANXA6 expression levels to be critical for cancer cells to utilize LDL-derived cholesterol as a growth advantage. Hence, to manipulate ANXA6 expression levels for therapeutic purposes, more insight into the regulation of ANXA6 expression is still needed.

This includes the potential contribution of epigenetic modifications in the ANXA6 gene, but also in genes encoding for the ANXA6 interactome. In previous studies, Grewal and coworkers identified epigenetic silencing of the CpG-rich ANXA6 promoter, which was heavily methylated

in several EGFR overexpressing cancer cells and ER-negative breast cancer cells with low AnxA6 levels (75). Likewise, ANXA6 promoter methylation and downregulation was documented in gastric cancer (257, 362). Along these lines, further insights into the cellular machinery driving histone alkylation and expression of non-coding RNAs to downregulate gene expression should also be considered. The targeting of epigenetic modifiers as an anticancer strategy in breast and prostate cancer includes several miRNAs that modify the expression of multiple genes in lipid, cholesterol, and glucose metabolism (258-261).

Hence, future strategies to block ANXA6-dependent and RAB7A/STARD3-mediated cholesterol export from LE/lys may take advantage of manipulating epigenetic modifications and be beneficial for selected cancer patients in TNBC breast cancers and possibly other tumors (e.g. advanced prostate) that show increased cellular LDL uptake and metabolism.

References

1.   DeBerardinis RJ, Lum JJ, Hatzivassiliou G, Thompson CB. The biology of cancer: metabolic reprogramming fuels cell growth and proliferation. Cell Metab. 2008;7(1):11-20.

2.   Ding X, Zhang W, Li S, Yang H. The role of cholesterol metabolism in cancer. Am J Cancer Res. 2019;9(2):219-27.

3.   Kuzu OF, Noory MA, Robertson GP. The Role of Cholesterol in Cancer. Cancer Res. 2016;76(8):2063-70.

4.   Maxfield FR, van Meer G. Cholesterol, the central lipid of mammalian cells. Curr Opin Cell Biol. 2010;22(4):422-9.

5.   Murai T. Cholesterol lowering: role in cancer prevention and treatment. Biol Chem. 2015;396(1):1-11.

6.   Mehta A, Shapiro MD. Apolipoproteins in vascular biology and atherosclerotic disease. Nat Rev Cardiol. 2022;19(3):168-79.

7.   Kersten S. Physiological regulation of lipoprotein lipase. Biochim Biophys Acta. 2014;1841(7):919-33.

8.   Hegele RA. Plasma lipoproteins: genetic influences and clinical implications. Nat Rev Genet. 2009;10(2):109-21.

9.   Goldstein JL, Brown MS, Anderson RG, Russell DW, Schneider WJ. Receptor-mediated endocytosis: concepts emerging from the LDL receptor system. Annu Rev Cell Biol. 1985;1:1-39.

10.   Ikonen E. Cellular cholesterol trafficking and compartmentalization. Nat Rev Mol Cell Biol. 2008;9(2):125-38.

11.   Nguyen MKL, Jose J, Wahba M, Bernaus-Esqué M, Hoy AJ, Enrich C, Rentero C, Grewal T. Linking Late Endosomal Cholesterol with Cancer Progression and Anticancer Drug Resistance. Int J Mol Sci. 2022;23(13).

12.   Brown MS, Goldstein JL. A receptor-mediated pathway for cholesterol homeostasis. Science. 1986;232(4746):34-47.

13.   Chang TY, Chang CC, Ohgami N, Yamauchi Y. Cholesterol sensing, trafficking, and esterification. Annu Rev Cell Dev Biol. 2006;22:129-57.

14.   Infante RE, Wang ML, Radhakrishnan A, Kwon HJ, Brown MS, Goldstein JL. NPC2 facilitates bidirectional transfer of cholesterol between NPC1 and lipid bilayers, a step in cholesterol egress from lysosomes. Proc Natl Acad Sci U S A. 2008;105(40):15287-92.

15.   Wang ML, Motamed M, Infante RE, Abi-Mosleh L, Kwon HJ, Brown MS, Goldstein JL. Identification of surface residues on Niemann-Pick C2 essential for hydrophobic handoff of cholesterol to NPC1 in lysosomes. Cell Metab. 2010;12(2):166-73.

16.   Enrich C, Rentero C, Grewal T, Futter CE, Eden ER. Cholesterol Overload: Contact Sites to the Rescue! Contact (Thousand Oaks). 2019;2:2515256419893507.

17.   Enrich C, Rentero C, Hierro A, Grewal T. Role of cholesterol in SNARE-mediated trafficking on intracellular membranes. J Cell Sci. 2015;128(6):1071-81.

18.   Ikonen E. Mechanisms of cellular cholesterol compartmentalization: recent insights. Curr Opin Cell Biol. 2018;53:77-83.

19.   Meng Y, Heybrock S, Neculai D, Saftig P. Cholesterol Handling in Lysosomes and Beyond. Trends Cell Biol. 2020;30(6):452-66.

20.   Ikonen E, Holtta-Vuori M. Cellular pathology of Niemann-Pick type C disease. Semin Cell Dev Biol. 2004;15(4):445-54.

21.	Alpy F, Rousseau A, Schwab Y, Legueux F, Stoll I, Wendling C, Spiegelhalter C, Kessler P, Mathelin C, Rio MC, Levine TP, Tomasetto C. STARD3 or STARD3NL and VAP form a novel molecular tether between late endosomes and the ER. J Cell Sci. 2013;126(Pt 23):5500-12.

22.	Alpy F, Stoeckel ME, Dierich A, Escola JM, Wendling C, Chenard MP, Vanier MT, Gruenberg J, Tomasetto C, Rio MC. The steroidogenic acute regulatory protein homolog MLN64, a late endosomal cholesterol-binding protein. J Biol Chem. 2001;276(6):4261-9.

23.	Hölttä-Vuori M, Alpy F, Tanhuanpää K, Jokitalo E, Mutka AL, Ikonen E. MLN64 is involved in actin-mediated dynamics of late endocytic organelles. Mol Biol Cell. 2005;16(8):3873-86.

24.	Liapis A, Chen FW, Davies JP, Wang R, Ioannou YA. MLN64 transport to the late endosome is regulated by binding to 14-3-3 via a non-canonical binding site. PLoS One. 2012;7(4):e34424.

25.	Wilhelm LP, Wendling C, Védie B, Kobayashi T, Chenard MP, Tomasetto C, Drin G, Alpy F. STARD3 mediates endoplasmic reticulum-to-endosome cholesterol transport at membrane contact sites. Embo j. 2017;36(10):1412-33.

26.	Zhang M, Liu P, Dwyer NK, Christenson LK, Fujimoto T, Martinez F, Comly M, Hanover JA, Blanchette-Mackie EJ, Strauss JF, 3rd. MLN64 mediates mobilization of lysosomal cholesterol to steroidogenic mitochondria. J Biol Chem. 2002;277(36):33300-10.

27.	Hoque M, Elmaghrabi YA, Kose M, Beevi SS, Jose J, Meneses-Salas E, Blanco-Munoz P, Conway JRW, Swarbrick A, Timpson P, Tebar F, Enrich C, Rentero C, Grewal T. Annexin A6 improves anti-migratory and anti-invasive properties of tyrosine kinase inhibitors in EGFR overexpressing human squamous epithelial cells. FEBS J. 2020.

28.	Borthwick F, Allen AM, Taylor JM, Graham A. Overexpression of STARD3 in human monocyte/macrophages induces an anti-atherogenic lipid phenotype. Clin Sci (Lond). 2010;119(7):265-72.

29.	Balboa E, Castro J, Pinochet MJ, Cancino GI, Matías N, Sáez PJ, Martínez A, Álvarez AR, Garcia-Ruiz C, Fernandez-Checa JC, Zanlungo S. MLN64 induces mitochondrial dysfunction associated with increased mitochondrial cholesterol content. Redox Biol. 2017;12:274-84.

30.	Höglinger D, Burgoyne T, Sanchez-Heras E, Hartwig P, Colaco A, Newton J, Futter CE, Spiegel S, Platt FM, Eden ER. NPC1 regulates ER contacts with endocytic organelles to mediate cholesterol egress. Nat Commun. 2019;10(1):4276.

31.	Charman M, Kennedy BE, Osborne N, Karten B. MLN64 mediates egress of cholesterol from endosomes to mitochondria in the absence of functional Niemann-Pick Type C1 protein. J Lipid Res. 2010;51(5):1023-34.

32.	Vassilev B, Sihto H, Li S, Holtta-Vuori M, Ilola J, Lundin J, Isola J, Kellokumpu-Lehtinen PL, Joensuu H, Ikonen E. Elevated levels of StAR-related lipid transfer protein 3 alter cholesterol balance and adhesiveness of breast cancer cells: potential mechanisms contributing to progression of HER2-positive breast cancers. Am J Pathol. 2015;185(4):987-1000.

33.	Olkkonen VM, Ikonen E. Cholesterol transport in the late endocytic pathway: Roles of ORP family proteins. J Steroid Biochem Mol Biol. 2022;216:106040.

34.	Lim CY, Davis OB, Shin HR, Zhang J, Berdan CA, Jiang X, Counihan JL, Ory DS, Nomura DK, Zoncu R. ER-lysosome contacts enable cholesterol sensing by mTORC1 and drive aberrant growth signalling in Niemann-Pick type C. Nat Cell Biol. 2019;21(10):1206-18.

35.	Johansson M, Lehto M, Tanhuanpää K, Cover TL, Olkkonen VM. The oxysterol-binding protein homologue ORP1L interacts with Rab7 and alters functional properties of late endocytic compartments. Mol Biol Cell. 2005;16(12):5480-92.

36.	Johansson M, Rocha N, Zwart W, Jordens I, Janssen L, Kuijl C, Olkkonen VM, Neefjes J. Activation of endosomal dynein motors by stepwise assembly of Rab7-RILP-p150Glued, ORP1L, and the receptor betalll spectrin. J Cell Biol. 2007;176(4):459-71.

37.	van der Kant R, Fish A, Janssen L, Janssen H, Krom S, Ho N, Brummelkamp T, Carette J, Rocha N, Neefjes J. Late endosomal transport and tethering are coupled processes controlled by RILP and the cholesterol sensor ORP1L. J Cell Sci. 2013;126(Pt 15):3462-74.

38.	Rocha N, Kuijl C, van der Kant R, Janssen L, Houben D, Janssen H, Zwart W, Neefjes J. Cholesterol sensor ORP1L contacts the ER protein VAP to control Rab7-RILP-p150 Glued and late endosome positioning. J Cell Biol. 2009;185(7):1209-25.

39.	Wijdeven RH, Janssen H, Nahidiazar L, Janssen L, Jalink K, Berlin I, Neefjes J. Cholesterol and ORP1L-mediated ER contact sites control autophagosome transport and fusion with the endocytic pathway. Nat Commun. 2016;7:11808.

40.	Eden ER, Sanchez-Heras E, Tsapara A, Sobota A, Levine TP, Futter CE. Annexin A1 Tethers Membrane Contact Sites that Mediate ER to Endosome Cholesterol Transport. Dev Cell. 2016;37(5):473-83.

41.	Kobuna H, Inoue T, Shibata M, Gengyo-Ando K, Yamamoto A, Mitani S, Arai H. Multivesicular body formation requires OSBP-related proteins and cholesterol. PLoS Genet. 2010;6(8).

42.	Zhao K, Ridgway ND. Oxysterol-Binding Protein-Related Protein 1L Regulates Cholesterol Egress from the Endo-Lysosomal System. Cell Rep. 2017;19(9):1807-18.

43.	Cianciola NL, Greene DJ, Morton RE, Carlin CR. Adenovirus RIDalpha uncovers a novel pathway requiring ORP1L for lipid droplet formation independent of NPC1. Mol Biol Cell. 2013;24(21):3309-25.

44.	Takahashi K, Kanerva K, Vanharanta L, Almeida-Souza L, Lietha D, Olkkonen VM, Ikonen E. ORP2 couples LDL-cholesterol transport to FAK activation by endosomal cholesterol/PI(4,5)P(2) exchange. Embo j. 2021;40(14):e106871.

45.	Kentala H, Koponen A, Kivela AM, Andrews R, Li C, Zhou Y, Olkkonen VM. Analysis of ORP2-knockout hepatocytes uncovers a novel function in actin cytoskeletal regulation. FASEB J. 2018;32(3):1281-95.

46.	Du X, Kumar J, Ferguson C, Schulz TA, Ong YS, Hong W, Prinz WA, Parton RG, Brown AJ, Yang H. A role for oxysterol-binding protein-related protein 5 in endosomal cholesterol trafficking. J Cell Biol. 2011;192(1):121-35.

47.	Trinh MN, Brown MS, Goldstein JL, Han J, Vale G, McDonald JG, Seemann J, Mendell JT, Lu F. Last step in the path of LDL cholesterol from lysosome to plasma membrane to ER is governed by phosphatidylserine. Proc Natl Acad Sci U S A. 2020;117(31):18521-9.

48.	Eskelinen EL, Schmidt CK, Neu S, Willenborg M, Fuertes G, Salvador N, Tanaka Y, Lullmann-Rauch R, Hartmann D, Heeren J, von Figura K, Knecht E, Saftig P. Disturbed cholesterol traffic but normal proteolytic function in LAMP-1/LAMP-2 double-deficient fibroblasts. Mol Biol Cell. 2004;15(7):3132-45.

49.	Heybrock S, Kanerva K, Meng Y, Ing C, Liang A, Xiong ZJ, Weng X, Ah Kim Y, Collins R, Trimble W, Pomes R, Prive GG, Annaert W, Schwake M, Heeren J, Lullmann-Rauch R, Grinstein S, Ikonen E, Saftig P, Neculai D. Lysosomal integral membrane protein-2 (LIMP-2/SCARB2) is involved in lysosomal cholesterol export. Nat Commun. 2019;10(1):3521.

50.	Hubert V, Weiss S, Rees AJ, Kain R. Modulating Chaperone-Mediated Autophagy and Its Clinical Applications in Cancer. Cells. 2022;11(16).

51.	Pfeffer SR. Rab GTPases: master regulators that establish the secretory and endocytic pathways. Mol Biol Cell. 2017;28(6):712-5.

52.	Lebrand C, Corti M, Goodson H, Cosson P, Cavalli V, Mayran N, Faure J, Gruenberg J. Late endosome motility depends on lipids via the small GTPase Rab7. EMBO J. 2002;21(6):1289-300.

53.	Rink J, Ghigo E, Kalaidzidis Y, Zerial M. Rab conversion as a mechanism of progression from early to late endosomes. Cell. 2005;122(5):735-49.

54.	van den Boomen DJH, Sienkiewicz A, Berlin I, Jongsma MLM, van Elsland DM, Luzio JP, Neefjes JJC, Lehner PJ. A trimeric Rab7 GEF controls NPC1-dependent lysosomal cholesterol export. Nat Commun. 2020;11(1):5559.

55.	Meneses-Salas E, García-Melero A, Kanerva K, Blanco-Muñoz P, Morales-Paytuvi F, Bonjoch J, Casas J, Egert A, Beevi SS, Jose J, Llorente-Cortés V, Rye KA, Heeren J, Lu A, Pol A, Tebar F, Ikonen E, Grewal T, Enrich C, Rentero C. Annexin A6 modulates TBC1D15/Rab7/StARD3 axis to control endosomal cholesterol export in NPC1 cells. Cell Mol Life Sci. 2020;77(14):2839-57.

56.	Jose J, Hoque M, Engel J, Beevi SS, Wahba M, Georgieva MI, Murphy KJ, Hughes WE, Cochran BJ, Lu A, Tebar F, Hoy AJ, Timpson P, Rye KA, Enrich C, Rentero C, Grewal T. Annexin A6 and NPC1 regulate LDL-inducible cell migration and distribution of focal adhesions. Sci Rep. 2022;12(1):596.

57.	Kanerva K, Uronen RL, Blom T, Li S, Bittman R, Lappalainen P, Peränen J, Raposo G, Ikonen E. LDL cholesterol recycles to the plasma membrane via a Rab8a-Myosin5b-actin-dependent membrane transport route. Dev Cell. 2013;27(3):249-62.

58.	Ganley IG, Pfeffer SR. Cholesterol accumulation sequesters Rab9 and disrupts late endosome function in NPC1-deficient cells. J Biol Chem. 2006;281(26):17890-9.

59.	Walter M, Davies JP, Ioannou YA. Telomerase immortalization upregulates Rab9 expression and restores LDL cholesterol egress from Niemann-Pick C1 late endosomes. J Lipid Res. 2003;44(2):243-53.

60.	Choudhury A, Sharma DK, Marks DL, Pagano RE. Elevated endosomal cholesterol levels in Niemann-Pick cells inhibit rab4 and perturb membrane recycling. Mol Biol Cell. 2004;15(10):4500-11.

61.	Linder MD, Uronen RL, Holtta-Vuori M, van der Sluijs P, Peranen J, Ikonen E. Rab8-dependent recycling promotes endosomal cholesterol removal in normal and sphingolipidosis cells. Mol Biol Cell. 2007;18(1):47-56.

62.	Powelka AM, Sun J, Li J, Gao M, Shaw LM, Sonnenberg A, Hsu VW. Stimulation-dependent recycling of integrin beta1 regulated by ARF6 and Rab11. Traffic. 2004;5(1):20-36.

63.	Holtta-Vuori M, Tanhuanpaa K, Mobius W, Somerharju P, Ikonen E. Modulation of cellular cholesterol transport and homeostasis by Rab11. Mol Biol Cell. 2002;13(9):3107-22.

64.	Ferro E, Bosia C, Campa CC. RAB11-Mediated Trafficking and Human Cancers: An Updated Review. Biology (Basel). 2021;10(1).

65.	Porther N, Barbieri MA. The role of endocytic Rab GTPases in regulation of growth factor signaling and the migration and invasion of tumor cells. Small GTPases. 2015;6(3):135-44.

66.	Tang BL, Ng EL. Rabs and cancer cell motility. Cell Motil Cytoskeleton. 2009;66(7):365-70.

67.   Enrich C, Rentero C, de Muga SV, Reverter M, Mulay V, Wood P, Koese M, Grewal T. Annexin A6-Linking Ca(2+) signaling with cholesterol transport. Biochim Biophys Acta. 2011;1813(5):935-47.

68.   Rentero C, Blanco-Munoz P, Meneses-Salas E, Grewal T, Enrich C. Annexins-Coordinators of Cholesterol Homeostasis in Endocytic Pathways. Int J Mol Sci. 2018;19(5).

69.   Lum DF, McQuaid KR, Gilbertson VL, Hughes-Fulford M. Coordinate up-regulation of low-density lipoprotein receptor and cyclo-oxygenase-2 gene expression in human colorectal cells and in colorectal adenocarcinoma biopsies. Int J Cancer. 1999;83(2):162-6.

70.   Grewal T, Rentero C, Enrich C, Wahba M, Raabe CA, Rescher U. Annexin Animal Models-From Fundamental Principles to Translational Research. Int J Mol Sci. 2021;22(7).

71.   Korolkova OY, Widatalla SE, Williams SD, Whalen DS, Beasley HK, Ochieng J, Grewal T, Sakwe AM. Diverse Roles of Annexin A6 in Triple-Negative Breast Cancer Diagnosis, Prognosis and EGFR-Targeted Therapies. Cells. 2020;9(8).

72.   Grewal T, Evans R, Rentero C, Tebar F, Cubells L, de Diego I, Kirchhoff MF, Hughes WE, Heeren J, Rye KA, Rinninger F, Daly RJ, Pol A, Enrich C. Annexin A6 stimulates the membrane recruitment of p120GAP to modulate Ras and Raf-1 activity. Oncogene. 2005;24(38):5809-20.

73.   Koese M, Rentero C, Kota BP, Hoque M, Cairns R, Wood P, Vila de Muga S, Reverter M, Alvarez-Guaita A, Monastyrskaya K, Hughes WE, Swarbrick A, Tebar F, Daly RJ, Enrich C, Grewal T. Annexin A6 is a scaffold for PKCalpha to promote EGFR inactivation. Oncogene. 2013;32(23):2858-72.

74.   Vilá de Muga S, Timpson P, Cubells L, Evans R, Hayes TE, Rentero C, Hegemann A, Reverter M, Leschner J, Pol A, Tebar F, Daly RJ, Enrich C, Grewal T. Annexin A6 inhibits Ras signalling in breast cancer cells. Oncogene. 2009;28(3):363-77.

75.   Grewal T, Enrich C. Annexins--modulators of EGF receptor signalling and trafficking. Cell Signal. 2009;21(6):847-58.

76.   Qi H, Liu S, Guo C, Wang J, Greenaway FT, Sun MZ. Role of annexin A6 in cancer. Oncol Lett. 2015;10(4):1947-52.

77.   Grewal T, Heeren J, Mewawala D, Schnitgerhans T, Wendt D, Salomon G, Enrich C, Beisiegel U, Jäckle S. Annexin VI stimulates endocytosis and is involved in the trafficking of low density lipoprotein to the prelysosomal compartment. J Biol Chem. 2000;275(43):33806-13.

78.   Kamal A, Ying Y, Anderson RG. Annexin VI-mediated loss of spectrin during coated pit budding is coupled to delivery of LDL to lysosomes. J Cell Biol. 1998;142(4):937-47.

79.   Pons M, Grewal T, Rius E, Schnitgerhans T, Jäckle S, Enrich C. Evidence for the Involvement of annexin 6 in the trafficking between the endocytic compartment and lysosomes. Exp Cell Res. 2001;269(1):13-22.

80.   de Diego I, Schwartz F, Siegfried H, Dauterstedt P, Heeren J, Beisiegel U, Enrich C, Grewal T. Cholesterol modulates the membrane binding and intracellular distribution of annexin 6. J Biol Chem. 2002;277(35):32187-94.

81.   Hulce JJ, Cognetta AB, Niphakis MJ, Tully SE, Cravatt BF. Proteome-wide mapping of cholesterol-interacting proteins in mammalian cells. Nat Methods. 2013;10(3):259-64.

82.   Cubells L, Vila de Muga S, Tebar F, Bonventre JV, Balsinde J, Pol A, Grewal T, Enrich C. Annexin A6-induced inhibition of cytoplasmic phospholipase A2 is linked to caveolin-1 export from the Golgi. J Biol Chem. 2008;283(15):10174-83.

83.   Cubells L, Vilà de Muga S, Tebar F, Wood P, Evans R, Ingelmo-Torres M, Calvo M, Gaus K, Pol A, Grewal T, Enrich C. Annexin A6-induced alterations in cholesterol transport and caveolin export from the Golgi complex. Traffic. 2007;8(11):1568-89.

84.   Ganley IG, Espinosa E, Pfeffer SR. A syntaxin 10-SNARE complex distinguishes two distinct transport routes from endosomes to the trans-Golgi in human cells. J Cell Biol. 2008;180(1):159-72.

85.   Reverter M, Rentero C, de Muga SV, Alvarez-Guaita A, Mulay V, Cairns R, Wood P, Monastyrskaya K, Pol A, Tebar F, Blasi J, Grewal T, Enrich C. Cholesterol transport from late endosomes to the Golgi regulates t-SNARE trafficking, assembly, and function. Mol Biol Cell. 2011;22(21):4108-23.

86.   Reverter M, Rentero C, Garcia-Melero A, Hoque M, Vilà de Muga S, Alvarez-Guaita A, Conway JR, Wood P, Cairns R, Lykopoulou L, Grinberg D, Vilageliu L, Bosch M, Heeren J, Blasi J, Timpson P, Pol A, Tebar F, Murray RZ, Grewal T, Enrich C. Cholesterol regulates Syntaxin 6 trafficking at trans-Golgi network endosomal boundaries. Cell Rep. 2014;7(3):883-97.

87.   García-Melero A, Reverter M, Hoque M, Meneses-Salas E, Koese M, Conway JR, Johnsen CH, Alvarez-Guaita A, Morales-Paytuvi F, Elmaghrabi YA, Pol A, Tebar F, Murray RZ, Timpson P, Enrich C, Grewal T, Rentero C. Annexin A6 and Late Endosomal Cholesterol Modulate Integrin Recycling and Cell Migration. J Biol Chem. 2016;291(3):1320-35.

88.   Hoy AJ, Nagarajan SR, Butler LM. Tumour fatty acid metabolism in the context of therapy resistance and obesity. Nat Rev Cancer. 2021;21(12):753-66.

89.   Raftopulos NL, Washaya TC, Niederprüm A, Egert A, Hakeem-Sanni MF, Varney B, Aishah A, Georgieva ML, Olsson E, Dos Santos DZ, Nassar ZD, Cochran BJ, Nagarajan SR, Kakani MS, Hastings JF, Croucher DR, Rye KA, Butler LM, Grewal T, Hoy AJ. Prostate cancer cell proliferation is influenced by LDL-cholesterol availability and cholesteryl ester turnover. Cancer Metab. 2022;10(1):1.

90.   Yan A, Jia Z, Qiao C, Wang M, Ding X. Cholesterol metabolism in drug-resistant cancer (Review). Int J Oncol. 2020;57(5):1103-15.

91.   Alessandrini F, Pezze L, Ciribilli Y. LAMPs: Shedding light on cancer biology. Semin Oncol. 2017;44(4):239-53.

92.   Huang B, Song BL, Xu C. Cholesterol metabolism in cancer: mechanisms and therapeutic opportunities. Nat Metab. 2020;2(2):132-41.

93.   Xu H, Zhou S, Tang Q, Xia H, Bi F. Cholesterol metabolism: New functions and therapeutic approaches in cancer. Biochim Biophys Acta Rev Cancer. 2020;1874(1):188394.

94.   Johnson KE, Siewert KM, Klarin D, Damrauer SM, Chang KM, Tsao PS, Assimes TL, Maxwell KN, Voight BF. The relationship between circulating lipids and breast cancer risk: A Mendelian randomization study. PLoS Med. 2020;17(9):e1003302.

95.   Jeon JC, Park J, Park S, Moon KH, Cheon SH, Park S. Hypercholesterolemia Is Associated with a Shorter Time to Castration-Resistant Prostate Cancer in Patients Who Have Undergone Androgen Deprivation Therapy. World J Mens Health. 2016;34(1):28-33.

96.   Llaverias G, Danilo C, Mercier I, Daumer K, Capozza F, Williams TM, Sotgia F, Lisanti MP, Frank PG. Role of cholesterol in the development and progression of breast cancer. Am J Pathol. 2011;178(1):402-12.

97.   Gabitova L, Gorin A, Astsaturov I. Molecular pathways: sterols and receptor signaling in cancer. Clin Cancer Res. 2014;20(1):28-34.

98.   Huang P, Nedelcu D, Watanabe M, Jao C, Kim Y, Liu J, Salic A. Cellular Cholesterol Directly Activates Smoothened in Hedgehog Signaling. Cell. 2016;166(5):1176-87 e14.
99.   Sheng R, Chen Y, Yung Gee H, Stec E, Melowic HR, Blatner NR, Tun MP, Kim Y, Kallberg M, Fujiwara TK, Hye Hong J, Pyo Kim K, Lu H, Kusumi A, Goo Lee M, Cho W. Cholesterol modulates cell signaling and protein networking by specifically interacting with PDZ domain-containing scaffold proteins. Nat Commun. 2012;3:1249.
100.   Castellano BM, Thelen AM, Moldavski O, Feltes M, van der Welle RE, Mydock-McGrane L, Jiang X, van Eijkeren RJ, Davis OB, Louie SM, Perera RM, Covey DF, Nomura DK, Ory DS, Zoncu R. Lysosomal cholesterol activates mTORC1 via an SLC38A9-Niemann-Pick C1 signaling complex. Science. 2017;355(6331):1306-11.
101.   Garcia-Ruiz C, Conde de la Rosa L, Ribas V, Fernandez-Checa JC. Mitochondrial Cholesterol and Cancer. Semin Cancer Biol. 2021;73:76-85.
102.   Yen CF, Kalunta CI, Chen FS, Kaptein JS, Lin CK, Lad PM. Regulation of low-density lipoprotein receptors and assessment of their functional role in Burkitt's lymphoma cells. Biochim Biophys Acta. 1995;1257(1):47-57.
103.   Vitols S, Gahrton G, Ost A, Peterson C. Elevated low density lipoprotein receptor activity in leukemic cells with monocytic differentiation. Blood. 1984;63(5):1186-93.
104.   Acier A, Godard M, Gassiot F, Finetti P, Rubis M, Nowak J, Bertucci F, Iovanna JL, Tomasini R, Lecorche P, Jacquot G, Khrestchatisky M, Temsamani J, Malicet C, Vasseur S, Guillaumond F. LDL receptor-peptide conjugate as in vivo tool for specific targeting of pancreatic ductal adenocarcinoma. Commun Biol. 2021;4(1):987.
105.   Guillaumond F, Bidaut G, Ouaissi M, Servais S, Gouirand V, Olivares O, Lac S, Borge L, Roques J, Gayet O, Pinault M, Guimaraes C, Nigri J, Loncle C, Lavaut MN, Garcia S, Tailleux A, Staels B, Calvo E, Tomasini R, Iovanna JL, Vasseur S. Cholesterol uptake disruption, in association with chemotherapy, is a promising combined metabolic therapy for pancreatic adenocarcinoma. Proc Natl Acad Sci U S A. 2015;112(8):2473-8.
106.   Antalis CJ, Uchida A, Buhman KK, Siddiqui RA. Migration of MDA-MB-231 breast cancer cells depends on the availability of exogenous lipids and cholesterol esterification. Clin Exp Metastasis. 2011;28(8):733-41.
107.   Feldt M, Menard J, Rosendahl AH, Lettiero B, Bendahl PO, Belting M, Borgquist S. The effect of statin treatment on intratumoral cholesterol levels and LDL receptor expression: a window-of-opportunity breast cancer trial. Cancer Metab. 2020;8(1):25.
108.   Bhat M, Skill N, Marcus V, Deschenes M, Tan X, Bouteaud J, Negi S, Awan Z, Aikin R, Kwan J, Amre R, Tabaries S, Hassanain M, Seidah NG, Maluccio M, Siegel P, Metrakos P. Decreased PCSK9 expression in human hepatocellular carcinoma. BMC Gastroenterol. 2015;15:176.
109.   Gueddari N, Favre G, Hachem H, Marek E, Le Gaillard F, Soula G. Evidence for up-regulated low density lipoprotein receptor in human lung adenocarcinoma cell line A549. Biochimie. 1993;75(9):811-9.
110.   Vitols S, Peterson C, Larsson O, Holm P, Aberg B. Elevated uptake of low density lipoproteins by human lung cancer tissue in vivo. Cancer Res. 1992;52(22):6244-7.
111.   Niendorf A, Nagele H, Gerding D, Meyer-Pannwitt U, Gebhardt A. Increased LDL receptor mRNA expression in colon cancer is correlated with a rise in plasma cholesterol levels after curative surgery. Int J Cancer. 1995;61(4):461-4.
112.   Daker M, Bhuvanendran S, Ahmad M, Takada K, Khoo AS. Deregulation of lipid metabolism pathway genes in nasopharyngeal carcinoma cells. Mol Med Rep. 2013;7(3):731-41.

113.   Guo D, Reinitz F, Youssef M, Hong C, Nathanson D, Akhavan D, Kuga D, Amzajerdi AN, Soto H, Zhu S, Babic I, Tanaka K, Dang J, Iwanami A, Gini B, Dejesus J, Lisiero DD, Huang TT, Prins RM, Wen PY, Robins HI, Prados MD, Deangelis LM, Mellinghoff IK, Mehta MP, James CD, Chakravarti A, Cloughesy TF, Tontonoz P, Mischel PS. An LXR agonist promotes glioblastoma cell death through inhibition of an EGFR/AKT/SREBP-1/LDLR-dependent pathway. Cancer Discov. 2011;1(5):442-56.

114.   Li F, Guo P, Dong K, Guo P, Wang H, Lv X. Identification of Key Biomarkers and Potential Molecular Mechanisms in Renal Cell Carcinoma by Bioinformatics Analysis. J Comput Biol. 2019;26(11):1278-95.

115.   Alexopoulos CG, Blatsios B, Avgerinos A. Serum lipids and lipoprotein disorders in cancer patients. Cancer. 1987;60(12):3065-70.

116.   Budd D, Ginsberg H. Hypocholesterolemia and acute myelogenous leukemia. Association between disease activity and plasma low-density lipoprotein cholesterol concentrations. Cancer. 1986;58(6):1361-5.

117.   Vitols S, Gahrton G, Björkholm M, Peterson C. Hypocholesterolaemia in malignancy due to elevated low-density-lipoprotein-receptor activity in tumour cells: evidence from studies in patients with leukaemia. Lancet. 1985;2(8465):1150-4.

118.   Hu J, La Vecchia C, Negri E, de Groh M, Morrison H, Mery L, Canadian Cancer Registries Epidemiology Research G. Macronutrient intake and stomach cancer. Cancer Causes Control. 2015;26(6):839-47.

119.   Moon H, Ruelcke JE, Choi E, Sharpe LJ, Nassar ZD, Bielefeldt-Ohmann H, Parat MO, Shah A, Francois M, Inder KL, Brown AJ, Russell PJ, Parton RG, Hill MM. Diet-induced hypercholesterolemia promotes androgen-independent prostate cancer metastasis via IQGAP1 and caveolin-1. Oncotarget. 2015;6(10):7438-53.

120.   Munir R, Usman H, Hasnain S, Smans K, Kalbacher H, Zaidi N. Atypical plasma lipid profile in cancer patients: cause or consequence? Biochimie. 2014;102:9-18.

121.   Henriksson P, Eriksson M, Ericsson S, Rudling M, Stege R, Berglund L, Angelin B. Hypocholesterolaemia and increased elimination of low-density lipoproteins in metastatic cancer of the prostate. Lancet. 1989;2(8673):1178-80.

122.   Chao FC, Efron B, Wolf P. The possible prognostic usefulness of assessing serum proteins and cholesterol in malignancy. Cancer. 1975;35(4):1223-9.

123.   Chen Z, Chen L, Sun B, Liu D, He Y, Qi L, Li G, Han Z, Zhan L, Zhang S, Zhu K, Luo Y, Chen L, Zhang N, Guo H. LDLR inhibition promotes hepatocellular carcinoma proliferation and metastasis by elevating intracellular cholesterol synthesis through the MEK/ERK signaling pathway. Mol Metab. 2021;51:101230.

124.   Stopsack KH, Gerke TA, Andren O, Andersson SO, Giovannucci EL, Mucci LA, Rider JR. Cholesterol uptake and regulation in high-grade and lethal prostate cancers. Carcinogenesis. 2017;38(8):806-11.

125.   Sun Y, Feng Y, Zhang G, Xu Y. The endonuclease APE1 processes miR-92b formation, thereby regulating expression of the tumor suppressor LDLR in cervical cancer cells. Ther Adv Med Oncol. 2019;11:1758835919855859.

126.   Jamalzei B, Karami Tehrani FS, Atri M. Evaluation of LDL receptor and Scavenger Receptor, Class B, Type 1 in the malignant and benign breast tumors: The correlation with the expression of miR-199a-5p, miR-199b-5p and miR-455-5p. Gene. 2020;749:144720.

127.   Pires LA, Hegg R, Freitas FR, Tavares ER, Almeida CP, Baracat EC, Maranhao RC. Effect of neoadjuvant chemotherapy on low-density lipoprotein (LDL) receptor and LDL

receptor-related protein 1 (LRP-1) receptor in locally advanced breast cancer. Braz J Med Biol Res. 2012;45(6):557-64.

128. Ho YK, Smith RG, Brown MS, Goldstein JL. Low-density lipoprotein (LDL) receptor activity in human acute myelogenous leukemia cells. Blood. 1978;52(6):1099-114.

129. Gallagher EJ, Zelenko Z, Neel BA, Antoniou IM, Rajan L, Kase N, LeRoith D. Elevated tumor LDLR expression accelerates LDL cholesterol-mediated breast cancer growth in mouse models of hyperlipidemia. Oncogene. 2017;36(46):6462-71.

130. Furuya Y, Sekine Y, Kato H, Miyazawa Y, Koike H, Suzuki K. Low-density lipoprotein receptors play an important role in the inhibition of prostate cancer cell proliferation by statins. Prostate Int. 2016;4(2):56-60.

131. Hughes-Fulford M, Chen Y, Tjandrawinata RR. Fatty acid regulates gene expression and growth of human prostate cancer PC-3 cells. Carcinogenesis. 2001;22(5):701-7.

132. Sekine Y, Koike H, Nakano T, Nakajima K, Takahashi S, Suzuki K. Remnant lipoproteins induced proliferation of human prostate cancer cell, PC-3 but not LNCaP, via low density lipoprotein receptor. Cancer Epidemiol. 2009;33(1):16-23.

133. Floeth M, Elges S, Gerss J, Schwöppe C, Kessler T, Herold T, Wardelmann E, Berdel WE, Lenz G, Mikesch JH, Hartmann W, Schliemann C, Angenendt L. Low-density lipoprotein receptor (LDLR) is an independent adverse prognostic factor in acute myeloid leukaemia. Br J Haematol. 2021;192(3):494-503.

134. Gonias SL, Karimi-Mostowfi N, Murray SS, Mantuano E, Gilder AS. Expression of LDL receptor-related proteins (LRPs) in common solid malignancies correlates with patient survival. PLoS One. 2017;12(10):e0186649.

135. Rudling MJ, Ståhle L, Peterson CO, Skoog L. Content of low density lipoprotein receptors in breast cancer tissue related to survival of patients. Br Med J (Clin Res Ed). 1986;292(6520):580-2.

136. Chang WC, Wang HC, Cheng WC, Yang JC, Chung WM, Ho YP, Chen L, Hung YC, Ma WL. LDLR-mediated lipidome-transcriptome reprogramming in cisplatin insensitivity. Endocr Relat Cancer. 2020;27(2):81-95.

137. Li J, Qu X, Tian J, Zhang JT, Cheng JX. Cholesterol esterification inhibition and gemcitabine synergistically suppress pancreatic ductal adenocarcinoma proliferation. PLoS One. 2018;13(2):e0193318.

138. Yue S, Li J, Lee SY, Lee HJ, Shao T, Song B, Cheng L, Masterson TA, Liu X, Ratliff TL, Cheng JX. Cholesteryl ester accumulation induced by PTEN loss and PI3K/AKT activation underlies human prostate cancer aggressiveness. Cell Metab. 2014;19(3):393-406.

139. Liscum L, Faust JR. The intracellular transport of low density lipoprotein-derived cholesterol is inhibited in Chinese hamster ovary cells cultured with 3-beta-[2-(diethylamino)ethoxy]androst-5-en-17-one. J Biol Chem. 1989;264(20):11796-806.

140. Cenedella RJ. Cholesterol synthesis inhibitor U18666A and the role of sterol metabolism and trafficking in numerous pathophysiological processes. Lipids. 2009;44(6):477-87.

141. Du X, Zhang Y, Jo SR, Liu X, Qi Y, Osborne B, Byrne FL, Smith GC, Turner N, Hoehn KL, Brown AJ, Yang H. Akt activation increases cellular cholesterol by promoting the proteasomal degradation of Niemann-Pick C1. Biochem J. 2015;471(2):243-53.

142. Adhikary G, Grun D, Kerr C, Balasubramanian S, Rorke EA, Vemuri M, Boucher S, Bickenbach JR, Hornyak T, Xu W, Fisher ML, Eckert RL. Identification of a population of epidermal squamous cell carcinoma cells with enhanced potential for tumor formation. PLoS One. 2013;8(12):e84324.

143.   Theobald J, Hanby A, Patel K, Moss SE. Annexin VI has tumour-suppressor activity in human A431 squamous epithelial carcinoma cells. Br J Cancer. 1995;71(4):786-8.

144.   Giard DJ, Aaronson SA, Todaro GJ, Arnstein P, Kersey JH, Dosik H, Parks WP. In vitro cultivation of human tumors: establishment of cell lines derived from a series of solid tumors. J Natl Cancer Inst. 1973;51(5):1417-23.

145.   Freed-Pastor WA, Mizuno H, Zhao X, Langerod A, Moon SH, Rodriguez-Barrueco R, Barsotti A, Chicas A, Li W, Polotskaia A, Bissell MJ, Osborne TF, Tian B, Lowe SW, Silva JM, Borresen-Dale AL, Levine AJ, Bargonetti J, Prives C. Mutant p53 disrupts mammary tissue architecture via the mevalonate pathway. Cell. 2012;148(1-2):244-58.

146.   Muller PA, Caswell PT, Doyle B, Iwanicki MP, Tan EH, Karim S, Lukashchuk N, Gillespie DA, Ludwig RL, Gosselin P, Cromer A, Brugge JS, Sansom OJ, Norman JC, Vousden KH. Mutant p53 drives invasion by promoting integrin recycling. Cell. 2009;139(7):1327-41.

147.   Grewal T, Hoque M, Conway JRW, Reverter M, Wahba M, Beevi SS, Timpson P, Enrich C, Rentero C. Annexin A6-A multifunctional scaffold in cell motility. Cell Adh Migr. 2017;11(3):288-304.

148.   Sambrook J, Russell DW, Sambrook J. The condensed protocols from Molecular cloning : a laboratory manual. Cold Spring Harbor, N.Y.: Cold Spring Harbor Laboratory Press; 2006. v, 800 p. p.

149.   Lowry OH, Rosebrough NJ, Farr AL, Randall RJ. Protein measurement with the Folin phenol reagent. J Biol Chem. 1951;193(1):265-75.

150.   Brunelle JL, Green R. One-dimensional SDS-polyacrylamide gel electrophoresis (1D SDS-PAGE). Methods Enzymol. 2014;541:151-9.

151.   Goldman A, Ursitti JA, Mozdzanowski J, Speicher DW. Electroblotting from Polyacrylamide Gels. Curr Protoc Protein Sci. 2015;82:10 7 1-6.

152.   Hoque M, Rentero C, Conway JR, Murray RZ, Timpson P, Enrich C, Grewal T. The cross-talk of LDL-cholesterol with cell motility: insights from the Niemann Pick Type C1 mutation and altered integrin trafficking. Cell Adh Migr. 2015;9(5):384-91.

153.   Dahl NK, Reed KL, Daunais MA, Faust JR, Liscum L. Isolation and characterization of Chinese hamster ovary cells defective in the intracellular metabolism of low density lipoprotein-derived cholesterol. J Biol Chem. 1992;267(7):4889-96.

154.   Sun X, Marks DL, Park WD, Wheatley CL, Puri V, O'Brien JF, Kraft DL, Lundquist PA, Patterson MC, Pagano RE, Snow K. Niemann-Pick C variant detection by altered sphingolipid trafficking and correlation with mutations within a specific domain of NPC1. Am J Hum Genet. 2001;68(6):1361-72.

155.   Zeng F, Harris RC. Epidermal growth factor, from gene organization to bedside. Semin Cell Dev Biol. 2014;28:2-11.

156.   Caldieri G, Malabarba MG, Di Fiore PP, Sigismund S. EGFR Trafficking in Physiology and Cancer. Prog Mol Subcell Biol. 2018;57:235-72.

157.   Appert-Collin A, Hubert P, Cremel G, Bennasroune A. Role of ErbB Receptors in Cancer Cell Migration and Invasion. Front Pharmacol. 2015;6:283.

158.   Cruz PM, Mo H, McConathy WJ, Sabnis N, Lacko AG. The role of cholesterol metabolism and cholesterol transport in carcinogenesis: a review of scientific findings, relevant to future cancer therapeutics. Front Pharmacol. 2013;4:119.

159.   Ng KK, Lovell JF, Zheng G. Lipoprotein-inspired nanoparticles for cancer theranostics. Acc Chem Res. 2011;44(10):1105-13.

160.   Beloribi-Djefaflia S, Vasseur S, Guillaumond F. Lipid metabolic reprogramming in cancer cells. Oncogenesis. 2016;5:e189.

161.   Ran FA, Hsu PD, Wright J, Agarwala V, Scott DA, Zhang F. Genome engineering using the CRISPR-Cas9 system. Nat Protoc. 2013;8(11):2281-308.

162.   Silvente-Poirot S, Poirot M. Cancer. Cholesterol and cancer, in the balance. Science. 2014;343(6178):1445-6.

163.   Alfaqih MA, Allott EH, Hamilton RJ, Freeman MR, Freedland SJ. The current evidence on statin use and prostate cancer prevention: are we there yet? Nat Rev Urol. 2017;14(2):107-19.

164.   Vasseur S, Guillaumond F. LDL Receptor: An open route to feed pancreatic tumor cells. Mol Cell Oncol. 2016;3(1):e1033586.

165.   Lund RR, Leth-Larsen R, Caterino TD, Terp MG, Nissen J, Laenkholm AV, Jensen ON, Ditzel HJ. NADH-Cytochrome b5 Reductase 3 Promotes Colonization and Metastasis Formation and Is a Prognostic Marker of Disease-Free and Overall Survival in Estrogen Receptor-Negative Breast Cancer. Mol Cell Proteomics. 2015;14(11):2988-99.

166.   Singh V, Singh LC, Vasudevan M, Chattopadhyay I, Borthakar BB, Rai AK, Phukan RK, Sharma J, Mahanta J, Kataki AC, Kapur S, Saxena S. Esophageal Cancer Epigenomics and Integrome Analysis of Genome-Wide Methylation and Expression in High Risk Northeast Indian Population. OMICS. 2015;19(11):688-99.

167.   Fan Y, Peng X, Li B, Zhao G. Development of Autophagy Signature-Based Prognostic Nomogram for Refined Glioma Survival Prognostication. Biomed Res Int. 2020;2020:1872962.

168.   Gong Y, Duvvuri M, Duncan MB, Liu J, Krise JP. Niemann-Pick C1 protein facilitates the efflux of the anticancer drug daunorubicin from cells according to a novel vesicle-mediated pathway. J Pharmacol Exp Ther. 2006;316(1):242-7.

169.   Naren D, Wu J, Gong Y, Yan T, Wang K, Xu W, Yang X, Shi F, Shi R. Niemann-Pick disease type C1(NPC1) is involved in resistance against imatinib in the imatinib-resistant Ph+ acute lymphoblastic leukemia cell line SUP-B15/RI. Leuk Res. 2016;42:59-67.

170.   Wang Z, Cheng Y, Abraham JM, Yan R, Liu X, Chen W, Ibrahim S, Schroth GP, Ke X, He Y, Meltzer SJ. RNA sequencing of esophageal adenocarcinomas identifies novel fusion transcripts, including NPC1-MELK, arising from a complex chromosomal rearrangement. Cancer. 2017;123(20):3916-24.

171.   Rodriguez-Gil JL, Bianconi SE, Farhat N, Kleiner DE, Nelson M, Porter FD. Hepatocellular carcinoma as a complication of Niemann-Pick disease type C1. Am J Med Genet A. 2021;185(10):3111-7.

172.   Moussay E, Kaoma T, Baginska J, Muller A, Van Moer K, Nicot N, Nazarov PV, Vallar L, Chouaib S, Berchem G, Janji B. The acquisition of resistance to TNFalpha in breast cancer cells is associated with constitutive activation of autophagy as revealed by a transcriptome analysis using a custom microarray. Autophagy. 2011;7(7):760-70.

173.   Kim DJ, Kim J, Spaunhurst K, Montoya J, Khodosh R, Chandra K, Fu T, Gilliam A, Molgo M, Beachy PA, Tang JY. Open-label, exploratory phase II trial of oral itraconazole for the treatment of basal cell carcinoma. J Clin Oncol. 2014;32(8):745-51.

174.   Aftab BT, Dobromilskaya I, Liu JO, Rudin CM. Itraconazole inhibits angiogenesis and tumor growth in non-small cell lung cancer. Cancer Res. 2011;71(21):6764-72.

175.   Tsubamoto H, Sonoda T, Ikuta S, Tani S, Inoue K, Yamanaka N. Combination Chemotherapy with Itraconazole for Treating Metastatic Pancreatic Cancer in the Second-line or Additional Setting. Anticancer Res. 2015;35(7):4191-6.

176. Antonarakis ES, Heath EI, Smith DC, Rathkopf D, Blackford AL, Danila DC, King S, Frost A, Ajiboye AS, Zhao M, Mendonca J, Kachhap SK, Rudek MA, Carducci MA. Repurposing itraconazole as a treatment for advanced prostate cancer: a noncomparative randomized phase II trial in men with metastatic castration-resistant prostate cancer. Oncologist. 2013;18(2):163-73.

177. Shimazu R, Tanaka G, Tomiyama R, Kuratomi Y, Inokuchi A. [Cepharanthin effect on radiation-induced xerostomia and taste disorder in patients with head and neck cancer]. Nihon Jibiinkoka Gakkai Kaiho. 2009;112(9):648-55.

178. Nomoto S, Imada H, Ohguri T, Yahara K, Kato F, Morioka T, Korogi Y. [Effect of Cepharanthin in preventing radiation induced normal tissue damage in prostate cancer]. Gan To Kagaku Ryoho. 2004;31(7):1063-6.

179. Gowda R, Inamdar GS, Kuzu O, Dinavahi SS, Krzeminski J, Battu MB, Voleti SR, Amin S, Robertson GP. Identifying the structure-activity relationship of leelamine necessary for inhibiting intracellular cholesterol transport. Oncotarget. 2017;8(17):28260-77.

180. Kuzu OF, Gowda R, Noory MA, Robertson GP. Modulating cancer cell survival by targeting intracellular cholesterol transport. Br J Cancer. 2017;117(4):513-24.

181. Head SA, Shi WQ, Yang EJ, Nacev BA, Hong SY, Pasunooti KK, Li RJ, Shim JS, Liu JO. Simultaneous Targeting of NPC1 and VDAC1 by Itraconazole Leads to Synergistic Inhibition of mTOR Signaling and Angiogenesis. ACS Chem Biol. 2017;12(1):174-82.

182. Xu J, Dang Y, Ren YR, Liu JO. Cholesterol trafficking is required for mTOR activation in endothelial cells. Proc Natl Acad Sci U S A. 2010;107(10):4764-9.

183. Liu R, Li J, Zhang T, Zou L, Chen Y, Wang K, Lei Y, Yuan K, Li Y, Lan J, Cheng L, Xie N, Xiang R, Nice EC, Huang C, Wei Y. Itraconazole suppresses the growth of glioblastoma through induction of autophagy: involvement of abnormal cholesterol trafficking. Autophagy. 2014;10(7):1241-55.

184. Lyu J, Yang EJ, Head SA, Ai N, Zhang B, Wu C, Li RJ, Liu Y, Chakravarty H, Zhang S, Tam KY, Dang Y, Kwon HJ, Ge W, Liu JO, Shim JS. Astemizole Inhibits mTOR Signaling and Angiogenesis by Blocking Cholesterol Trafficking. Int J Biol Sci. 2018;14(10):1175-85.

185. de Laurentiis A, Donovan L, Arcaro A. Lipid rafts and caveolae in signaling by growth factor receptors. Open Biochem J. 2007;1:12-32.

186. Ringerike T, Blystad FD, Levy FO, Madshus IH, Stang E. Cholesterol is important in control of EGF receptor kinase activity but EGF receptors are not concentrated in caveolae. J Cell Sci. 2002;115(Pt 6):1331-40.

187. Echarri A, Del Pozo MA. Caveolae internalization regulates integrin-dependent signaling pathways. Cell Cycle. 2006;5(19):2179-82.

188. Jelinek D, Heidenreich RA, Orlando RA, Garver WS. The Niemann-Pick C1 and caveolin-1 proteins interact to modulate efflux of low density lipoprotein-derived cholesterol from late endocytic compartments. J Mol Biochem. 2014;3(1):14-26.

189. Riggs KA, Hasan N, Humphrey D, Raleigh C, Nevitt C, Corbin D, Hu C. Regulation of integrin endocytic recycling and chemotactic cell migration by syntaxin 6 and VAMP3 interaction. J Cell Sci. 2012;125(Pt 16):3827-39.

190. Day P, Riggs KA, Hasan N, Corbin D, Humphrey D, Hu C. Syntaxins 3 and 4 mediate vesicular trafficking of alpha5beta1 and alpha3beta1 integrins and cancer cell migration. Int J Oncol. 2011;39(4):863-71.

191.	Williams KC, Coppolino MG. SNARE-dependent interaction of Src, EGFR and beta1 integrin regulates invadopodia formation and tumor cell invasion. J Cell Sci. 2014;127(Pt 8):1712-25.
192.	Conway JR, Carragher NO, Timpson P. Developments in preclinical cancer imaging: innovating the discovery of therapeutics. Nat Rev Cancer. 2014;14(5):314-28.
193.	Follain G, Herrmann D, Harlepp S, Hyenne V, Osmani N, Warren SC, Timpson P, Goetz JG. Fluids and their mechanics in tumour transit: shaping metastasis. Nat Rev Cancer. 2020;20(2):107-24.
194.	Mollinedo F, Gajate C. Lipid rafts as signaling hubs in cancer cell survival/death and invasion: implications in tumor progression and therapy. J Lipid Res. 2020.
195.	Kim HJ, Kwon S, Nam SH, Jung JW, Kang M, Ryu J, Kim JE, Cheong JG, Cho CY, Kim S, Song DG, Kim YN, Kim TY, Jung MK, Lee KM, Pack CG, Lee JW. Dynamic and coordinated single-molecular interactions at TM4SF5-enriched microdomains guide invasive behaviors in 2- and 3-dimensional environments. Faseb j. 2017;31(4):1461-81.
196.	Egeblad M, Werb Z. New functions for the matrix metalloproteinases in cancer progression. Nat Rev Cancer. 2002;2(3):161-74.
197.	Namekawa T, Ikeda K, Horie-Inoue K, Inoue S. Application of Prostate Cancer Models for Preclinical Study: Advantages and Limitations of Cell Lines, Patient-Derived Xenografts, and Three-Dimensional Culture of Patient-Derived Cells. Cells. 2019;8(1).
198.	Conway JRW, Vennin C, Cazet AS, Herrmann D, Murphy KJ, Warren SC, Wullkopf L, Boulghourjian A, Zaratzian A, Da Silva AM, Pajic M, Morton JP, Cox TR, Timpson P. Three-dimensional organotypic matrices from alternative collagen sources as pre-clinical models for cell biology. Sci Rep. 2017;7(1):16887.
199.	Grewal T, Koese M, Rentero C, Enrich C. Annexin A6-regulator of the EGFR/Ras signalling pathway and cholesterol homeostasis. Int J Biochem Cell Biol. 2010;42(5):580-4.
200.	Gerke V, Creutz CE, Moss SE. Annexins: linking Ca2+ signalling to membrane dynamics. Nat Rev Mol Cell Biol. 2005;6(6):449-61.
201.	Whalen DS, Widatalla SE, Korolkova OY, Nangami GS, Beasley HK, Williams SD, Virgous C, Lehmann BD, Ochieng J, Sakwe AM. Implication of calcium activated RasGRF2 in Annexin A6-mediated breast tumor cell growth and motility. Oncotarget. 2019;10(2):133-51.
202.	Enrich C, Rentero C, Meneses-Salas E, Tebar F, Grewal T. Annexins: Ca(2+) Effectors Determining Membrane Trafficking in the Late Endocytic Compartment. Adv Exp Med Biol. 2017;981:351-85.
203.	Grewal T, Wason SJ, Enrich C, Rentero C. Annexins - insights from knockout mice. Biol Chem. 2016;397(10):1031-53.
204.	Koumangoye RB, Nangami GN, Thompson PD, Agboto VK, Ochieng J, Sakwe AM. Reduced annexin A6 expression promotes the degradation of activated epidermal growth factor receptor and sensitizes invasive breast cancer cells to EGFR-targeted tyrosine kinase inhibitors. Mol Cancer. 2013;12(1):167.
205.	Grewal T, Enrich C. Molecular mechanisms involved in Ras inactivation: the annexin A6-p120GAP complex. Bioessays. 2006;28(12):1211-20.
206.	Gerke V, Moss SE. Annexins: from structure to function. Physiol Rev. 2002;82(2):331-71.
207.	Moss SE, Crumpton MJ. Alternative splicing gives rise to two forms of the p68 Ca2(+)-binding protein. FEBS Lett. 1990;261(2):299-302.

208.   Donnelly SR, Moss SE. Functional analysis of the human annexin I and VI gene promoters. Biochem J. 1998;332 (Pt 3):681-7.

209.   Hawkins TE, Roes J, Rees D, Monkhouse J, Moss SE. Immunological development and cardiovascular function are normal in annexin VI null mutant mice. Mol Cell Biol. 1999;19(12):8028-32.

210.   Korolkova OY, Widatalla SE, Whalen DS, Nangami GN, Abimbola A, Williams SD, Beasley HK, Reisenbichler E, Washington MK, Ochieng J, Mayer IA, Lehmann BD, Sakwe AM. Reciprocal expression of Annexin A6 and RasGRF2 discriminates rapidly growing from invasive triple negative breast cancer subsets. PLoS One. 2020;15(4):e0231711.

211.   Human Protein Atlas. Human Protein Atlas 2003 [updated September, 2019; cited 2020 10/07/2020]. Available from: https://www.proteinatlas.org.

212.   Tang Z, Li C, Kang B, Gao G, Li C, Zhang Z. GEPIA: a web server for cancer and normal gene expression profiling and interactive analyses. Nucleic Acids Res. 2017;45(W1):W98-W102.

213.   Chandrashekar DS, Karthikeyan SK, Korla PK, Patel H, Shovon AR, Athar M, Netto GJ, Qin ZS, Kumar S, Manne U, Creighton CJ, Varambally S. UALCAN: An update to the integrated cancer data analysis platform. Neoplasia. 2022;25:18-27.

214.   Tran AN, Dussaq AM, Kennell T, Jr., Willey CD, Hjelmeland AB. HPAanalyze: an R package that facilitates the retrieval and analysis of the Human Protein Atlas data. BMC Bioinformatics. 2019;20(1):463.

215.   Carithers LJ, Ardlie K, Barcus M, Branton PA, Britton A, Buia SA, Compton CC, DeLuca DS, Peter-Demchok J, Gelfand ET, Guan P, Korzeniewski GE, Lockhart NC, Rabiner CA, Rao AK, Robinson KL, Roche NV, Sawyer SJ, Segre AV, Shive CE, Smith AM, Sobin LH, Undale AH, Valentino KM, Vaught J, Young TR, Moore HM, Consortium GT. A Novel Approach to High-Quality Postmortem Tissue Procurement: The GTEx Project. Biopreserv Biobank. 2015;13(5):311-9.

216.   Goldman MJ, Craft B, Hastie M, Repecka K, McDade F, Kamath A, Banerjee A, Luo Y, Rogers D, Brooks AN, Zhu J, Haussler D. Visualizing and interpreting cancer genomics data via the Xena platform. Nat Biotechnol. 2020;38(6):675-8.

217.   Vivian J, Rao AA, Nothaft FA, Ketchum C, Armstrong J, Novak A, Pfeil J, Narkizian J, Deran AD, Musselman-Brown A, Schmidt H, Amstutz P, Craft B, Goldman M, Rosenbloom K, Cline M, O'Connor B, Hanna M, Birger C, Kent WJ, Patterson DA, Joseph AD, Zhu J, Zaranek S, Getz G, Haussler D, Paten B. Toil enables reproducible, open source, big biomedical data analyses. Nat Biotechnol. 2017;35(4):314-6.

218.   Fagerberg L, Hallström BM, Oksvold P, Kampf C, Djureinovic D, Odeberg J, Habuka M, Tahmasebpoor S, Danielsson A, Edlund K, Asplund A, Sjöstedt E, Lundberg E, Szigyarto CA, Skogs M, Takanen JO, Berling H, Tegel H, Mulder J, Nilsson P, Schwenk JM, Lindskog C, Danielsson F, Mardinoglu A, Sivertsson A, von Feilitzen K, Forsberg M, Zwahlen M, Olsson I, Navani S, Huss M, Nielsen J, Ponten F, Uhlén M. Analysis of the human tissue-specific expression by genome-wide integration of transcriptomics and antibody-based proteomics. Mol Cell Proteomics. 2014;13(2):397-406.

219.   Uhlen M, Oksvold P, Fagerberg L, Lundberg E, Jonasson K, Forsberg M, Zwahlen M, Kampf C, Wester K, Hober S, Wernerus H, Bjorling L, Ponten F. Towards a knowledge-based Human Protein Atlas. Nat Biotechnol. 2010;28(12):1248-50.

220.   Tagoe CE, Boustead CM, Higgins SJ, Walker JH. Characterization and immunolocalization of rat liver annexin VI. Biochim Biophys Acta. 1994;1192(2):272-80.

221.   O'Sullivan D, Dowling P, Joyce H, McAuley E, McCann A, Henry M, McGovern B, Barham P, Kelleher FC, Murphy J, Kennedy S, Swan N, Moriarty M, Clynes M, Larkin A. A novel inhibitory anti-invasive MAb isolated using phenotypic screening highlights AnxA6 as a functionally relevant target protein in pancreatic cancer. Br J Cancer. 2017;117(9):1326-35.
222.   Leca J, Martinez S, Lac S, Nigri J, Secq V, Rubis M, Bressy C, Sergé A, Lavaut MN, Dusetti N, Loncle C, Roques J, Pietrasz D, Bousquet C, Garcia S, Granjeaud S, Ouaissi M, Bachet JB, Brun C, Iovanna JL, Zimmermann P, Vasseur S, Tomasini R. Cancer-associated fibroblast-derived annexin A6+ extracellular vesicles support pancreatic cancer aggressiveness. J Clin Invest. 2016;126(11):4140-56.
223.   Ferguson DP, Dangott LJ, Schmitt EE, Vellers HL, Lightfoot JT. Differential skeletal muscle proteome of high- and low-active mice. J Appl Physiol (1985). 2014;116(8):1057-67.
224.   Demonbreun AR, Quattrocelli M, Barefield DY, Allen MV, Swanson KE, McNally EM. An actin-dependent annexin complex mediates plasma membrane repair in muscle. J Cell Biol. 2016;213(6):705-18.
225.   Lizio M, Harshbarger J, Shimoji H, Severin J, Kasukawa T, Sahin S, Abugessaisa I, Fukuda S, Hori F, Ishikawa-Kato S, Mungall CJ, Arner E, Baillie JK, Bertin N, Bono H, de Hoon M, Diehl AD, Dimont E, Freeman TC, Fujieda K, Hide W, Kaliyaperumal R, Katayama T, Lassmann T, Meehan TF, Nishikata K, Ono H, Rehli M, Sandelin A, Schultes EA, t Hoen PA, Tatum Z, Thompson M, Toyoda T, Wright DW, Daub CO, Itoh M, Carninci P, Hayashizaki Y, Forrest AR, Kawaji H, consortium F. Gateways to the FANTOM5 promoter level mammalian expression atlas. Genome Biol. 2015;16:22.
226.   Consortium F, the RP, Clst, Forrest AR, Kawaji H, Rehli M, Baillie JK, de Hoon MJ, Haberle V, Lassmann T, Kulakovskiy IV, Lizio M, Itoh M, Andersson R, Mungall CJ, Meehan TF, Schmeier S, Bertin N, Jorgensen M, Dimont E, Arner E, Schmidl C, Schaefer U, Medvedeva YA, Plessy C, Vitezic M, Severin J, Semple C, Ishizu Y, Young RS, Francescatto M, Alam I, Albanese D, Altschuler GM, Arakawa T, Archer JA, Arner P, Babina M, Rennie S, Balwierz PJ, Beckhouse AG, Pradhan-Bhatt S, Blake JA, Blumenthal A, Bodega B, Bonetti A, Briggs J, Brombacher F, Burroughs AM, Califano A, Cannistraci CV, Carbajo D, Chen Y, Chierici M, Ciani Y, Clevers HC, Dalla E, Davis CA, Detmar M, Diehl AD, Dohi T, Drablos F, Edge AS, Edinger M, Ekwall K, Endoh M, Enomoto H, Fagiolini M, Fairbairn L, Fang H, Farach-Carson MC, Faulkner GJ, Favorov AV, Fisher ME, Frith MC, Fujita R, Fukuda S, Furlanello C, Furino M, Furusawa J, Geijtenbeek TB, Gibson AP, Gingeras T, Goldowitz D, Gough J, Guhl S, Guler R, Gustincich S, Ha TJ, Hamaguchi M, Hara M, Harbers M, Harshbarger J, Hasegawa A, Hasegawa Y, Hashimoto T, Herlyn M, Hitchens KJ, Ho Sui SJ, Hofmann OM, Hoof I, Hori F, Huminiecki L, Iida K, Ikawa T, Jankovic BR, Jia H, Joshi A, Jurman G, Kaczkowski B, Kai C, Kaida K, Kaiho A, Kajiyama K, Kanamori-Katayama M, Kasianov AS, Kasukawa T, Katayama S, Kato S, Kawaguchi S, Kawamoto H, Kawamura YI, Kawashima T, Kempfle JS, Kenna TJ, Kere J, Khachigian LM, Kitamura T, Klinken SP, Knox AJ, Kojima M, Kojima S, Kondo N, Koseki H, Koyasu S, Krampitz S, Kubosaki A, Kwon AT, Laros JF, Lee W, Lennartsson A, Li K, Lilje B, Lipovich L, Mackay-Sim A, Manabe R, Mar JC, Marchand B, Mathelier A, Mejhert N, Meynert A, Mizuno Y, de Lima Morais DA, Morikawa H, Morimoto M, Moro K, Motakis E, Motohashi H, Mummery CL, Murata M, Nagao-Sato S, Nakachi Y, Nakahara F, Nakamura T, Nakamura Y, Nakazato K, van Nimwegen E, Ninomiya N, Nishiyori H, Noma S, Noma S, Noazaki T, Ogishima S, Ohkura N, Ohimiya H, Ohno H, Ohshima M, Okada-Hatakeyama M, Okazaki Y, Orlando V, Ovchinnikov DA, Pain A, Passier R, Patrikakis M, Persson H, Piazza S, Prendergast JG, Rackham OJ, Ramilowski JA, Rashid M, Ravasi T, Rizzu P, Roncador M, Roy

S, Rye MB, Saijyo E, Sajantila A, Saka A, Sakaguchi S, Sakai M, Sato H, Savvi S, Saxena A, Schneider C, Schultes EA, Schulze-Tanzil GG, Schwegmann A, Sengstag T, Sheng G, Shimoji H, Shimoni Y, Shin JW, Simon C, Sugiyama D, Sugiyama T, Suzuki M, Suzuki N, Swoboda RK, t Hoen PA, Tagami M, Takahashi N, Takai J, Tanaka H, Tatsukawa H, Tatum Z, Thompson M, Toyodo H, Toyoda T, Valen E, van de Wetering M, van den Berg LM, Verado R, Vijayan D, Vorontsov IE, Wasserman WW, Watanabe S, Wells CA, Winteringham LN, Wolvetang E, Wood EJ, Yamaguchi Y, Yamamoto M, Yoneda M, Yonekura Y, Yoshida S, Zabierowski SE, Zhang PG, Zhao X, Zucchelli S, Summers KM, Suzuki H, Daub CO, Kawai J, Heutink P, Hide W, Freeman TC, Lenhard B, Bajic VB, Taylor MS, Makeev VJ, Sandelin A, Hume DA, Carninci P, Hayashizaki Y. A promoter-level mammalian expression atlas. Nature. 2014;507(7493):462-70.

227.   Lizio M, Abugessaisa I, Noguchi S, Kondo A, Hasegawa A, Hon CC, de Hoon M, Severin J, Oki S, Hayashizaki Y, Carninci P, Kasukawa T, Kawaji H. Update of the FANTOM web resource: expansion to provide additional transcriptome atlases. Nucleic Acids Res. 2019;47(D1):D752-D8.

228.   Lin Z, Tang Y, Li Z, Li J, Yu C, Yang C, Liu L, Wang Y, Liu Y. miR-24-3p Dominates the Proliferation and Differentiation of Chicken Intramuscular Preadipocytes by Blocking ANXA6 Expression. Genes (Basel). 2022;13(4).

229.   Monastyrskaya K. Functional Association between Regulatory RNAs and the Annexins. Int J Mol Sci. 2018;19(2).

230.   Smythe E, Smith PD, Jacob SM, Theobald J, Moss SE. Endocytosis occurs independently of annexin VI in human A431 cells. J Cell Biol. 1994;124(3):301-6.

231.   Sakwe AM, Koumangoye R, Guillory B, Ochieng J. Annexin A6 contributes to the invasiveness of breast carcinoma cells by influencing the organization and localization of functional focal adhesions. Exp Cell Res. 2011;317(6):823-37.

232.   Wang X, Zhang S, Zhang J, Lam E, Liu X, Sun J, Feng L, Lu H, Yu J, Jin H. Annexin A6 is down-regulated through promoter methylation in gastric cancer. Am J Transl Res. 2013;5(5):555-62.

233.   Meier EM, Rein-Fischboeck L, Pohl R, Wanninger J, Hoy AJ, Grewal T, Eisinger K, Krautbauer S, Liebisch G, Weiss TS, Buechler C. Annexin A6 protein is downregulated in human hepatocellular carcinoma. Mol Cell Biochem. 2016;418(1-2):81-90.

234.   Lomnytska MI, Becker S, Hellman K, Hellstrom AC, Souchelnytskyi S, Mints M, Hellman U, Andersson S, Auer G. Diagnostic protein marker patterns in squamous cervical cancer. Proteomics Clin Appl. 2010;4(1):17-31.

235.   Lomnytska MI, Becker S, Bodin I, Olsson A, Hellman K, Hellstrom AC, Mints M, Hellman U, Auer G, Andersson S. Differential expression of ANXA6, HSP27, PRDX2, NCF2, and TPM4 during uterine cervix carcinogenesis: diagnostic and prognostic value. Br J Cancer. 2011;104(1):110-9.

236.   Francia G, Mitchell SD, Moss SE, Hanby AM, Marshall JF, Hart IR. Identification by differential display of annexin-VI, a gene differentially expressed during melanoma progression. Cancer Res. 1996;56(17):3855-8.

237.   Noreen S, Gardener QA, Fatima I, Sadaf S, Akhtar MW. Up-Regulated Expression of Calcium Dependent Annexin A6: A Potential Biomarker of Ovarian Carcinoma. Proteomics Clinical applications. 2019:e1900078.

238.	Lee HS, Kang Y, Tae K, Bae GU, Park JY, Cho YH, Yang M. Proteomic Biomarkers for Bisphenol A-Early Exposure and Women's Thyroid Cancer. Cancer Res Treat. 2018;50(1):111-7.

239.	Li L, Zhang J, Deng Q, Li J, Li Z, Xiao Y, Hu S, Li T, Tan Q, Li X, Luo B, Mo H. Proteomic Profiling for Identification of Novel Biomarkers Differentially Expressed in Human Ovaries from Polycystic Ovary Syndrome Patients. PLoS One. 2016;11(11):e0164538.

240.	Zaidi AH, Gopalakrishnan V, Kasi PM, Zeng X, Malhotra U, Balasubramanian J, Visweswaran S, Sun M, Flint MS, Davison JM, Hood BL, Conrads TP, Bergman JJ, Bigbee WL, Jobe BA. Evaluation of a 4-protein serum biomarker panel-biglycan, annexin-A6, myeloperoxidase, and protein S100-A9 (B-AMP)-for the detection of esophageal adenocarcinoma. Cancer. 2014;120(24):3902-13.

241.	Chen X, Pan Q, Stow P, Behm FG, Goorha R, Pui CH, Neale GA. Quantification of minimal residual disease in T-lineage acute lymphoblastic leukemia with the TAL-1 deletion using a standardized real-time PCR assay. Leukemia. 2001;15(1):166-70.

242.	Noreen S, Gardner QA, Fatima I, Sadaf S, Akhtar MW. Upregulated Expression of Calcium-Dependent Annexin A6: A Potential Biomarker of Ovarian Carcinoma. Proteomics Clin Appl. 2020;14(2):e1900078.

243.	Twiddy AL, Leon CG, Wasan KM. Cholesterol as a potential target for castration-resistant prostate cancer. Pharm Res. 2011;28(3):423-37.

244.	Pelton K, Freeman MR, Solomon KR. Cholesterol and prostate cancer. Curr Opin Pharmacol. 2012;12(6):751-9.

245.	Schnoeller TJ, Jentzmik F, Schrader AJ, Steinestel J. Influence of serum cholesterol level and statin treatment on prostate cancer aggressiveness. Oncotarget. 2017;8(29):47110-20.

246.	Attard G, Parker C, Eeles RA, Schröder F, Tomlins SA, Tannock I, Drake CG, de Bono JS. Prostate cancer. Lancet. 2016;387(10013):70-82.

247.	Tomlins SA, Mehra R, Rhodes DR, Cao X, Wang L, Dhanasekaran SM, Kalyana-Sundaram S, Wei JT, Rubin MA, Pienta KJ, Shah RB, Chinnaiyan AM. Integrative molecular concept modeling of prostate cancer progression. Nat Genet. 2007;39(1):41-51.

248.	Grasso CS, Wu YM, Robinson DR, Cao X, Dhanasekaran SM, Khan AP, Quist MJ, Jing X, Lonigro RJ, Brenner JC, Asangani IA, Ateeq B, Chun SY, Siddiqui J, Sam L, Anstett M, Mehra R, Prensner JR, Palanisamy N, Ryslik GA, Vandin F, Raphael BJ, Kunju LP, Rhodes DR, Pienta KJ, Chinnaiyan AM, Tomlins SA. The mutational landscape of lethal castration-resistant prostate cancer. Nature. 2012;487(7406):239-43.

249.	Rich JT, Neely JG, Paniello RC, Voelker CC, Nussenbaum B, Wang EW. A practical guide to understanding Kaplan-Meier curves. Otolaryngol Head Neck Surg. 2010;143(3):331-6.

250.	Chandrashekar DS, Bashel B, Balasubramanya SAH, Creighton CJ, Ponce-Rodriguez I, Chakravarthi B, Varambally S. UALCAN: A Portal for Facilitating Tumor Subgroup Gene Expression and Survival Analyses. Neoplasia. 2017;19(8):649-58.

251.	Therneau T. A package for survival analysis in S. R package version 2.37-7. 2014.

252.	Kassambara A, Kosinski M, Biecek P, Fabian S. survminer: Drawing Survival Curves using 'ggplot2'. R package version 03. 2017;1.

253.	Savino A, Provero P, Poli V. Differential Co-Expression Analyses Allow the Identification of Critical Signalling Pathways Altered during Tumour Transformation and Progression. Int J Mol Sci. 2020;21(24).

254.	Miller DR, Ingersoll MA, Lin MF. ErbB-2 signaling in advanced prostate cancer progression and potential therapy. Endocr Relat Cancer. 2019;26(4):R195-R209.

255.   Yu C, Hu K, Nguyen D, Wang ZA. From genomics to functions: preclinical mouse models for understanding oncogenic pathways in prostate cancer. Am J Cancer Res. 2019;9(10):2079-102.

256.   Li Y, Guo S, Zhao Y, Li R, Li Y, Qiu C, Xiao L, Gong K. EZH2 Regulates ANXA6 Expression via H3K27me3 and Is Involved in Angiotensin II-Induced Vascular Smooth Muscle Cell Senescence. Oxid Med Cell Longev. 2022;2022:4838760.

257.   Qi Y, Zhang X, Kang Y, Wu J, Chen J, Li H, Guo Y, Liu B, Shao Z, Zhao X. Genome-wide transcriptional profiling analysis reveals annexin A6 as a novel EZH2 target gene involving gastric cellular proliferation. Mol Biosyst. 2015;11(7):1980-6.

258.   Ortega R, Liu B, Persaud SJ. Effects of miR-33 Deficiency on Metabolic and Cardiovascular Diseases: Implications for Therapeutic Intervention. Int J Mol Sci. 2023;24(13).

259.   Pardo JC, Ruiz de Porras V, Gil J, Font A, Puig-Domingo M, Jorda M. Lipid Metabolism and Epigenetics Crosstalk in Prostate Cancer. Nutrients. 2022;14(4).

260.   Munir MT, Ponce C, Powell CA, Tarafdar K, Yanagita T, Choudhury M, Gollahon LS, Rahman SM. The contribution of cholesterol and epigenetic changes to the pathophysiology of breast cancer. J Steroid Biochem Mol Biol. 2018;183:1-9.

261.   Tovar-Camargo OA, Toden S, Goel A. Exosomal microRNA Biomarkers: Emerging Frontiers in Colorectal and Other Human Cancers. Expert Rev Mol Diagn. 2016;16(5):553-67.

262.   Győrffy B, Benke Z, Lánczky A, Balázs B, Szállási Z, Timár J, Schäfer R. RecurrenceOnline: an online analysis tool to determine breast cancer recurrence and hormone receptor status using microarray data. Breast Cancer Res Treat. 2012;132(3):1025-34.

263.   Balaban S, Shearer RF, Lee LS, van Geldermalsen M, Schreuder M, Shtein HC, Cairns R, Thomas KC, Fazakerley DJ, Grewal T, Holst J, Saunders DN, Hoy AJ. Adipocyte lipolysis links obesity to breast cancer growth: adipocyte-derived fatty acids drive breast cancer cell proliferation and migration. Cancer Metab. 2017;5:1.

264.   Hoque M, Elmaghrabi YA, Kose M, Beevi SS, Jose J, Meneses-Salas E, Blanco-Munoz P, Conway JRW, Swarbrick A, Timpson P, Tebar F, Enrich C, Rentero C, Grewal T. Annexin A6 improves anti-migratory and anti-invasive properties of tyrosine kinase inhibitors in EGFR overexpressing human squamous epithelial cells. FEBS J. 2019;287(14):2961-78.

265.   te Vruchte D, Lloyd-Evans E, Veldman RJ, Neville DC, Dwek RA, Platt FM, van Blitterswijk WJ, Sillence DJ. Accumulation of glycosphingolipids in Niemann-Pick C disease disrupts endosomal transport. J Biol Chem. 2004;279(25):26167-75.

266.   Guerra F, Paiano A, Migoni D, Girolimetti G, Perrone AM, De Iaco P, Fanizzi FP, Gasparre G, Bucci C. Modulation of RAB7A Protein Expression Determines Resistance to Cisplatin through Late Endocytic Pathway Impairment and Extracellular Vesicular Secretion. Cancers (Basel). 2019;11(1).

267.   Thomas DD, Kaspar KM, Taft WB, Weng N, Rodenkirch LA, Groblewski GE. Identification of annexin VI as a Ca2+-sensitive CRHSP-28-binding protein in pancreatic acinar cells. J Biol Chem. 2002;277(38):35496-502.

268.   Huttlin EL, Ting L, Bruckner RJ, Gebreab F, Gygi MP, Szpyt J, Tam S, Zarraga G, Colby G, Baltier K, Dong R, Guarani V, Vaites LP, Ordureau A, Rad R, Erickson BK, Wuhr M, Chick J, Zhai B, Kolippakkam D, Mintseris J, Obar RA, Harris T, Artavanis-Tsakonas S, Sowa ME, De Camilli P, Paulo JA, Harper JW, Gygi SP. The BioPlex Network: A Systematic Exploration of the Human Interactome. Cell. 2015;162(2):425-40.

269.   Lin-Moshier Y, Keebler MV, Hooper R, Boulware MJ, Liu X, Churamani D, Abood ME, Walseth TF, Brailoiu E, Patel S, Marchant JS. The Two-pore channel (TPC) interactome

unmasks isoform-specific roles for TPCs in endolysosomal morphology and cell pigmentation. Proc Natl Acad Sci U S A. 2014;111(36):13087-92.

270.	Kamili A, Roslan N, Frost S, Cantrill LC, Wang D, Della-Franca A, Bright RK, Groblewski GE, Straub BK, Hoy AJ, Chen Y, Byrne JA. TPD52 expression increases neutral lipid storage within cultured cells. J Cell Sci. 2015;128(17):3223-38.

271.	Bissig C, Gruenberg J. ALIX and the multivesicular endosome: ALIX in Wonderland. Trends Cell Biol. 2014;24(1):19-25.

272.	Du X, Kazim AS, Brown AJ, Yang H. An essential role of Hrs/Vps27 in endosomal cholesterol trafficking. Cell Rep. 2012;1(1):29-35.

273.	Yamano K, Fogel AI, Wang C, van der Bliek AM, Youle RJ. Mitochondrial Rab GAPs govern autophagosome biogenesis during mitophagy. Elife. 2014;3:e01612.

274.	Matsuo H, Chevallier J, Mayran N, Le Blanc I, Ferguson C, Faure J, Blanc NS, Matile S, Dubochet J, Sadoul R, Parton RG, Vilbois F, Gruenberg J. Role of LBPA and Alix in multivesicular liposome formation and endosome organization. Science. 2004;303(5657):531-4.

275.	Okumura M, Ichioka F, Kobayashi R, Suzuki H, Yoshida H, Shibata H, Maki M. Penta-EF-hand protein ALG-2 functions as a Ca2+-dependent adaptor that bridges Alix and TSG101. Biochem Biophys Res Commun. 2009;386(1):237-41.

276.	Pridgeon JW, Webber EA, Sha D, Li L, Chin LS. Proteomic analysis reveals Hrs ubiquitin-interacting motif-mediated ubiquitin signaling in multiple cellular processes. FEBS J. 2009;276(1):118-31.

277.	Raiborg C, Wenzel EM, Stenmark H. ER-endosome contact sites: molecular compositions and functions. EMBO J. 2015;34(14):1848-58.

278.	Satoh H, Nakano Y, Shibata H, Maki M. The penta-EF-hand domain of ALG-2 interacts with amino-terminal domains of both annexin VII and annexin XI in a Ca2+-dependent manner. Biochim Biophys Acta. 2002;1600(1-2):61-7.

279.	Pankiv S, Alemu EA, Brech A, Bruun JA, Lamark T, Overvatn A, Bjørkøy G, Johansen T. FYCO1 is a Rab7 effector that binds to LC3 and PI3P to mediate microtubule plus end-directed vesicle transport. J Cell Biol. 2010;188(2):253-69.

280.	Yin W, Mendoza L, Monzon-Sandoval J, Urrutia AO, Gutierrez H. Emergence of co-expression in gene regulatory networks. PLoS One. 2021;16(4):e0247671.

281.	Erola P, Bonnet E, Michoel T. Learning Differential Module Networks Across Multiple Experimental Conditions. Methods Mol Biol. 2019;1883:303-21.

282.	McQueen E, Rebeiz M. On the specificity of gene regulatory networks: How does network co-option affect subsequent evolution? Curr Top Dev Biol. 2020;139:375-405.

283.	Buetti-Dinh A, Herold M, Christel S, El Hajjami M, Delogu F, Ilie O, Bellenberg S, Wilmes P, Poetsch A, Sand W, Vera M, Pivkin IV, Friedman R, Dopson M. Reverse engineering directed gene regulatory networks from transcriptomics and proteomics data of biomining bacterial communities with approximate Bayesian computation and steady-state signalling simulations. BMC Bioinformatics. 2020;21(1):23.

284.	Nam S. Cancer Transcriptome Dataset Analysis: Comparing Methods of Pathway and Gene Regulatory Network-Based Cluster Identification. OMICS. 2017;21(4):217-24.

285.	Robinson DR, Wu YM, Lonigro RJ, Vats P, Cobain E, Everett J, Cao X, Rabban E, Kumar-Sinha C, Raymond V, Schuetze S, Alva A, Siddiqui J, Chugh R, Worden F, Zalupski MM, Innis J, Mody RJ, Tomlins SA, Lucas D, Baker LH, Ramnath N, Schott AF, Hayes DF, Vijai J, Offit K, Stoffel EM, Roberts JS, Smith DC, Kunju LP, Talpaz M, Cieslik M, Chinnaiyan AM. Integrative clinical genomics of metastatic cancer. Nature. 2017;548(7667):297-303.

286.	Cerami E, Gao J, Dogrusoz U, Gross BE, Sumer SO, Aksoy BA, Jacobsen A, Byrne CJ, Heuer ML, Larsson E, Antipin Y, Reva B, Goldberg AP, Sander C, Schultz N. The cBio cancer genomics portal: an open platform for exploring multidimensional cancer genomics data. Cancer Discov. 2012;2(5):401-4.

287.	Gao J, Aksoy BA, Dogrusoz U, Dresdner G, Gross B, Sumer SO, Sun Y, Jacobsen A, Sinha R, Larsson E, Cerami E, Sander C, Schultz N. Integrative analysis of complex cancer genomics and clinical profiles using the cBioPortal. Sci Signal. 2013;6(269):pl1.

288.	Yang M, Chen T, Han C, Li N, Wan T, Cao X. Rab7b, a novel lysosome-associated small GTPase, is involved in monocytic differentiation of human acute promyelocytic leukemia cells. Biochem Biophys Res Commun. 2004;318(3):792-9.

289.	Cortazar AR, Torrano V, Martin-Martin N, Caro-Maldonado A, Camacho L, Hermanova I, Guruceaga E, Lorenzo-Martin LF, Caloto R, Gomis RR, Apaolaza I, Quesada V, Trka J, Gomez-Munoz A, Vincent S, Bustelo XR, Planes FJ, Aransay AM, Carracedo A. CANCERTOOL: A Visualization and Representation Interface to Exploit Cancer Datasets. Cancer Res. 2018;78(21):6320-8.

290.	Nikhil Wagle CP, Max Krevalin, Coyin Oh, Kristin Anderka, Katie Larkin, Niall Lennon, Deborah Dillon, Elizabeth Frank, Eric P. Winer, Eric Lander, Todd Golub; Dana-Farber Cancer Institute, Boston, MA; Broad Institute, Cambridge, MA. The Metastatic Breast Cancer Project: A national direct-to-patient initiative to accelerate genomics research. J Clin Oncol. 2016.

291.	 Broad Institute TCGA Genome Data Analysis Center (2016): Firehose VERSION run. Broad Institute of MIT and Harvard. 2016.

292.	Ciriello G, Gatza ML, Beck AH, Wilkerson MD, Rhie SK, Pastore A, Zhang H, McLellan M, Yau C, Kandoth C, Bowlby R, Shen H, Hayat S, Fieldhouse R, Lester SC, Tse GM, Factor RE, Collins LC, Allison KH, Chen YY, Jensen K, Johnson NB, Oesterreich S, Mills GB, Cherniack AD, Robertson G, Benz C, Sander C, Laird PW, Hoadley KA, King TA, Network TR, Perou CM. Comprehensive Molecular Portraits of Invasive Lobular Breast Cancer. Cell. 2015;163(2):506-19.

293.	Kan Z, Ding Y, Kim J, Jung HH, Chung W, Lal S, Cho S, Fernandez-Banet J, Lee SK, Kim SW, Lee JE, Choi YL, Deng S, Kim JY, Ahn JS, Sha Y, Mu XJ, Nam JY, Im YH, Lee S, Park WY, Nam SJ, Park YH. Multi-omics profiling of younger Asian breast cancers reveals distinctive molecular signatures. Nat Commun. 2018;9(1):1725.

294.	Cancer Genome Atlas N. Comprehensive molecular characterization of human colon and rectal cancer. Nature. 2012;487(7407):330-7.

295.	Vasaikar S, Huang C, Wang X, Petyuk VA, Savage SR, Wen B, Dou Y, Zhang Y, Shi Z, Arshad OA, Gritsenko MA, Zimmerman LJ, McDermott JE, Clauss TR, Moore RJ, Zhao R, Monroe ME, Wang YT, Chambers MC, Slebos RJC, Lau KS, Mo Q, Ding L, Ellis M, Thiagarajan M, Kinsinger CR, Rodriguez H, Smith RD, Rodland KD, Liebler DC, Liu T, Zhang B, Clinical Proteomic Tumor Analysis C. Proteogenomic Analysis of Human Colon Cancer Reveals New Therapeutic Opportunities. Cell. 2019;177(4):1035-49 e19.

296.	Bailey P, Chang DK, Nones K, Johns AL, Patch AM, Gingras MC, Miller DK, Christ AN, Bruxner TJ, Quinn MC, Nourse C, Murtaugh LC, Harliwong I, Idrisoglu S, Manning S, Nourbakhsh E, Wani S, Fink L, Holmes O, Chin V, Anderson MJ, Kazakoff S, Leonard C, Newell F, Waddell N, Wood S, Xu Q, Wilson PJ, Cloonan N, Kassahn KS, Taylor D, Quek K, Robertson A, Pantano L, Mincarelli L, Sanchez LN, Evers L, Wu J, Pinese M, Cowley MJ, Jones MD, Colvin EK, Nagrial AM, Humphrey ES, Chantrill LA, Mawson A, Humphris J, Chou A, Pajic M, Scarlett CJ, Pinho AV, Giry-Laterriere M, Rooman I, Samra JS, Kench JG, Lovell JA,

Merrett ND, Toon CW, Epari K, Nguyen NQ, Barbour A, Zeps N, Moran-Jones K, Jamieson NB, Graham JS, Duthie F, Oien K, Hair J, Grutzmann R, Maitra A, Iacobuzio-Donahue CA, Wolfgang CL, Morgan RA, Lawlor RT, Corbo V, Bassi C, Rusev B, Capelli P, Salvia R, Tortora G, Mukhopadhyay D, Petersen GM, Australian Pancreatic Cancer Genome I, Munzy DM, Fisher WE, Karim SA, Eshleman JR, Hruban RH, Pilarsky C, Morton JP, Sansom OJ, Scarpa A, Musgrove EA, Bailey UM, Hofmann O, Sutherland RL, Wheeler DA, Gill AJ, Gibbs RA, Pearson JV, Waddell N, Biankin AV, Grimmond SM. Genomic analyses identify molecular subtypes of pancreatic cancer. Nature. 2016;531(7592):47-52.
297.   Hoadley KA, Yau C, Hinoue T, Wolf DM, Lazar AJ, Drill E, Shen R, Taylor AM, Cherniack AD, Thorsson V, Akbani R, Bowlby R, Wong CK, Wiznerowicz M, Sanchez-Vega F, Robertson AG, Schneider BG, Lawrence MS, Noushmehr H, Malta TM, Cancer Genome Atlas N, Stuart JM, Benz CC, Laird PW. Cell-of-Origin Patterns Dominate the Molecular Classification of 10,000 Tumors from 33 Types of Cancer. Cell. 2018;173(2):291-304 e6.
298.   Abida W, Cyrta J, Heller G, Prandi D, Armenia J, Coleman I, Cieslik M, Benelli M, Robinson D, Van Allen EM, Sboner A, Fedrizzi T, Mosquera JM, Robinson BD, De Sarkar N, Kunju LP, Tomlins S, Wu YM, Nava Rodrigues D, Loda M, Gopalan A, Reuter VE, Pritchard CC, Mateo J, Bianchini D, Miranda S, Carreira S, Rescigno P, Filipenko J, Vinson J, Montgomery RB, Beltran H, Heath EI, Scher HI, Kantoff PW, Taplin ME, Schultz N, deBono JS, Demichelis F, Nelson PS, Rubin MA, Chinnaiyan AM, Sawyers CL. Genomic correlates of clinical outcome in advanced prostate cancer. Proc Natl Acad Sci U S A. 2019;116(23):11428-36.
299.   Beltran H, Prandi D, Mosquera JM, Benelli M, Puca L, Cyrta J, Marotz C, Giannopoulou E, Chakravarthi BV, Varambally S, Tomlins SA, Nanus DM, Tagawa ST, Van Allen EM, Elemento O, Sboner A, Garraway LA, Rubin MA, Demichelis F. Divergent clonal evolution of castration-resistant neuroendocrine prostate cancer. Nat Med. 2016;22(3):298-305.
300.   Barbieri CE, Baca SC, Lawrence MS, Demichelis F, Blattner M, Theurillat JP, White TA, Stojanov P, Van Allen E, Stransky N, Nickerson E, Chae SS, Boysen G, Auclair D, Onofrio RC, Park K, Kitabayashi N, MacDonald TY, Sheikh K, Vuong T, Guiducci C, Cibulskis K, Sivachenko A, Carter SL, Saksena G, Voet D, Hussain WM, Ramos AH, Winckler W, Redman MC, Ardlie K, Tewari AK, Mosquera JM, Rupp N, Wild PJ, Moch H, Morrissey C, Nelson PS, Kantoff PW, Gabriel SB, Golub TR, Meyerson M, Lander ES, Getz G, Rubin MA, Garraway LA. Exome sequencing identifies recurrent SPOP, FOXA1 and MED12 mutations in prostate cancer. Nat Genet. 2012;44(6):685-9.
301.   Kumar A, Coleman I, Morrissey C, Zhang X, True LD, Gulati R, Etzioni R, Bolouri H, Montgomery B, White T, Lucas JM, Brown LG, Dumpit RF, DeSarkar N, Higano C, Yu EY, Coleman R, Schultz N, Fang M, Lange PH, Shendure J, Vessella RL, Nelson PS. Substantial interindividual and limited intraindividual genomic diversity among tumors from men with metastatic prostate cancer. Nat Med. 2016;22(4):369-78.
302.   Taylor BS, Schultz N, Hieronymus H, Gopalan A, Xiao Y, Carver BS, Arora VK, Kaushik P, Cerami E, Reva B, Antipin Y, Mitsiades N, Landers T, Dolgalev I, Major JE, Wilson M, Socci ND, Lash AE, Heguy A, Eastham JA, Scher HI, Reuter VE, Scardino PT, Sander C, Sawyers CL, Gerald WL. Integrative genomic profiling of human prostate cancer. Cancer Cell. 2010;18(1):11-22.
303.   Ren S, Wei GH, Liu D, Wang L, Hou Y, Zhu S, Peng L, Zhang Q, Cheng Y, Su H, Zhou X, Zhang J, Li F, Zheng H, Zhao Z, Yin C, He Z, Gao X, Zhau HE, Chu CY, Wu JB, Collins C, Volik SV, Bell R, Huang J, Wu K, Xu D, Ye D, Yu Y, Zhu L, Qiao M, Lee HM, Yang Y, Zhu

Y, Shi X, Chen R, Wang Y, Xu W, Cheng Y, Xu C, Gao X, Zhou T, Yang B, Hou J, Liu L, Zhang Z, Zhu Y, Qin C, Shao P, Pang J, Chung LWK, Xu J, Wu CL, Zhong W, Xu X, Li Y, Zhang X, Wang J, Yang H, Wang J, Huang H, Sun Y. Whole-genome and Transcriptome Sequencing of Prostate Cancer Identify New Genetic Alterations Driving Disease Progression. Eur Urol. 2018;73(3):322-39.

304.   Ivshina AV, George J, Senko O, Mow B, Putti TC, Smeds J, Lindahl T, Pawitan Y, Hall P, Nordgren H, Wong JE, Liu ET, Bergh J, Kuznetsov VA, Miller LD. Genetic reclassification of histologic grade delineates new clinical subtypes of breast cancer. Cancer Res. 2006;66(21):10292-301.

305.   Lu X, Lu X, Wang ZC, Iglehart JD, Zhang X, Richardson AL. Predicting features of breast cancer with gene expression patterns. Breast Cancer Res Treat. 2008;108(2):191-201.

306.   Pawitan Y, Bjohle J, Amler L, Borg AL, Egyhazi S, Hall P, Han X, Holmberg L, Huang F, Klaar S, Liu ET, Miller L, Nordgren H, Ploner A, Sandelin K, Shaw PM, Smeds J, Skoog L, Wedren S, Bergh J. Gene expression profiling spares early breast cancer patients from adjuvant therapy: derived and validated in two population-based cohorts. Breast Cancer Res. 2005;7(6):R953-64.

307.   Wang Y, Klijn JG, Zhang Y, Sieuwerts AM, Look MP, Yang F, Talantov D, Timmermans M, Meijer-van Gelder ME, Yu J, Jatkoe T, Berns EM, Atkins D, Foekens JA. Gene-expression profiles to predict distant metastasis of lymph-node-negative primary breast cancer. Lancet. 2005;365(9460):671-9.

308.   Antalis CJ, Arnold T, Rasool T, Lee B, Buhman KK, Siddiqui RA. High ACAT1 expression in estrogen receptor negative basal-like breast cancer cells is associated with LDL-induced proliferation. Breast Cancer Res Treat. 2010;122(3):661-70.

309.   Johannsdottir HK, Jonsson G, Johannesdottir G, Agnarsson BA, Eerola H, Arason A, Heikkila P, Egilsson V, Olsson H, Johannsson OT, Nevanlinna H, Borg A, Barkardottir RB. Chromosome 5 imbalance mapping in breast tumors from BRCA1 and BRCA2 mutation carriers and sporadic breast tumors. Int J Cancer. 2006;119(5):1052-60.

310.   Pierga JY, Reis-Filho JS, Cleator SJ, Dexter T, Mackay A, Simpson P, Fenwick K, Iravani M, Salter J, Hills M, Jones C, Ashworth A, Smith IE, Powles T, Dowsett M. Microarray-based comparative genomic hybridisation of breast cancer patients receiving neoadjuvant chemotherapy. Br J Cancer. 2007;96(2):341-51.

311.   Alpy F, Boulay A, Moog-Lutz C, Andarawewa KL, Degot S, Stoll I, Rio MC, Tomasetto C. Metastatic lymph node 64 (MLN64), a gene overexpressed in breast cancers, is regulated by Sp/KLF transcription factors. Oncogene. 2003;22(24):3770-80.

312.   Cai W, Ye L, Sun J, Mansel RE, Jiang WG. Expression of MLN64 influences cellular matrix adhesion of breast cancer cells, the role for focal adhesion kinase. Int J Mol Med. 2010;25(4):573-80.

313.   Marisa L, de Reyniès A, Duval A, Selves J, Gaub MP, Vescovo L, Etienne-Grimaldi MC, Schiappa R, Guenot D, Ayadi M, Kirzin S, Chazal M, Fléjou JF, Benchimol D, Berger A, Lagarde A, Pencreach E, Piard F, Elias D, Parc Y, Olschwang S, Milano G, Laurent-Puig P, Boige V. Gene expression classification of colon cancer into molecular subtypes: characterization, validation, and prognostic value. PLoS Med. 2013;10(5):e1001453.

314.   Jorissen RN, Gibbs P, Christie M, Prakash S, Lipton L, Desai J, Kerr D, Aaltonen LA, Arango D, Kruhoffer M, Orntoft TF, Andersen CL, Gruidl M, Kamath VP, Eschrich S, Yeatman TJ, Sieber OM. Metastasis-Associated Gene Expression Changes Predict Poor Outcomes in Patients with Dukes Stage B and C Colorectal Cancer. Clin Cancer Res. 2009;15(24):7642-51.

315.   Kemper K, Versloot M, Cameron K, Colak S, de Sousa e Melo F, de Jong JH, Bleackley J, Vermeulen L, Versteeg R, Koster J, Medema JP. Mutations in the Ras-Raf Axis underlie the prognostic value of CD133 in colorectal cancer. Clin Cancer Res. 2012;18(11):3132-41.
316.   Laibe S, Lagarde A, Ferrari A, Monges G, Birnbaum D, Olschwang S, Project COL. A seven-gene signature aggregates a subgroup of stage II colon cancers with stage III. OMICS. 2012;16(10):560-5.
317.   Roepman P, Schlicker A, Tabernero J, Majewski I, Tian S, Moreno V, Snel MH, Chresta CM, Rosenberg R, Nitsche U, Macarulla T, Capella G, Salazar R, Orphanides G, Wessels LF, Bernards R, Simon IM. Colorectal cancer intrinsic subtypes predict chemotherapy benefit, deficient mismatch repair and epithelial-to-mesenchymal transition. Int J Cancer. 2014;134(3):552-62.
318.   Solé X, Crous-Bou M, Cordero D, Olivares D, Guinó E, Sanz-Pamplona R, Rodriguez-Moranta F, Sanjuan X, de Oca J, Salazar R, Moreno V. Discovery and validation of new potential biomarkers for early detection of colon cancer. PLoS One. 2014;9(9):e106748.
319.   Cordero D, Sole X, Crous-Bou M, Sanz-Pamplona R, Pare-Brunet L, Guino E, Olivares D, Berenguer A, Santos C, Salazar R, Biondo S, Moreno V. Large differences in global transcriptional regulatory programs of normal and tumor colon cells. BMC Cancer. 2014;14:708.
320.   Sanz-Pamplona R, Berenguer A, Cordero D, Mollevi DG, Crous-Bou M, Sole X, Pare-Brunet L, Guino E, Salazar R, Santos C, de Oca J, Sanjuan X, Rodriguez-Moranta F, Moreno V. Aberrant gene expression in mucosa adjacent to tumor reveals a molecular crosstalk in colon cancer. Mol Cancer. 2014;13:46.
321.   Closa A, Cordero D, Sanz-Pamplona R, Solé X, Crous-Bou M, Paré-Brunet L, Berenguer A, Guino E, Lopez-Doriga A, Guardiola J, Biondo S, Salazar R, Moreno V. Identification of candidate susceptibility genes for colorectal cancer through eQTL analysis. Carcinogenesis. 2014;35(9):2039-46.
322.   Berdiel-Acer M, Sanz-Pamplona R, Calon A, Cuadras D, Berenguer A, Sanjuan X, Paules MJ, Salazar R, Moreno V, Batlle E, Villanueva A, Molleví DG. Differences between CAFs and their paired NCF from adjacent colonic mucosa reveal functional heterogeneity of CAFs, providing prognostic information. Mol Oncol. 2014;8(7):1290-305.
323.   Moreno V, Alonso MH, Closa A, Vallés X, Diez-Villanueva A, Valle L, Castellví-Bel S, Sanz-Pamplona R, Lopez-Doriga A, Cordero D, Solé X. Colon-specific eQTL analysis to inform on functional SNPs. Br J Cancer. 2018;119(8):971-7.
324.   Díez-Villanueva A, Jordà M, Carreras-Torres R, Alonso H, Cordero D, Guinó E, Sanjuan X, Santos C, Salazar R, Sanz-Pamplona R, Moreno V. Identifying causal models between genetically regulated methylation patterns and gene expression in healthy colon tissue. Clin Epigenetics. 2021;13(1):162.
325.   Díez-Villanueva A, Sanz-Pamplona R, Solé X, Cordero D, Crous-Bou M, Guinó E, Lopez-Doriga A, Berenguer A, Aussó S, Paré-Brunet L, Obón-Santacana M, Moratalla-Navarro F, Salazar R, Sanjuan X, Santos C, Biondo S, Diez-Obrero V, Garcia-Serrano A, Alonso MH, Carreras-Torres R, Closa A, Moreno V. COLONOMICS - integrative omics data of one hundred paired normal-tumoral samples from colon cancer patients. Sci Data. 2022;9(1):595.
326.   Lapillo M, Salis B, Palazzolo S, Poli G, Granchi C, Minutolo F, Rotondo R, Caligiuri I, Canzonieri V, Tuccinardi T, Rizzolio F. First-of-its-kind STARD(3) Inhibitor: In Silico Identification and Biological Evaluation as Anticancer Agent. ACS Med Chem Lett. 2019;10(4):475-80.

327.   Luo X, Tu Z, Chen H, Ding J. Blood lipids and risk of colon or rectal cancer: a Mendelian randomization study. J Cancer Res Clin Oncol. 2021;147(12):3591-9.
328.   Fang Z, He M, Song M. Serum lipid profiles and risk of colorectal cancer: a prospective cohort study in the UK Biobank. Br J Cancer. 2021;124(3):663-70.
329.   Momtazi-Borojeni AA, Nik ME, Jaafari MR, Banach M, Sahebkar A. Potential anti-tumor effect of a nanoliposomal antiPCSK9 vaccine in mice bearing colorectal cancer. Arch Med Sci. 2019;15(3):559-69.
330.   Bonaventura A, Vecchié A, Ruscica M, Grossi F, Dentali F. PCSK9 as a New Player in Cancer: New Opportunity or Red Herring? Curr Med Chem. 2022;29(6):960-9.
331.   Glinsky GV, Glinskii AB, Stephenson AJ, Hoffman RM, Gerald WL. Gene expression profiling predicts clinical outcome of prostate cancer. J Clin Invest. 2004;113(6):913-23.
332.   Lapointe J, Li C, Higgins JP, van de Rijn M, Bair E, Montgomery K, Ferrari M, Egevad L, Rayford W, Bergerheim U, Ekman P, DeMarzo AM, Tibshirani R, Botstein D, Brown PO, Brooks JD, Pollack JR. Gene expression profiling identifies clinically relevant subtypes of prostate cancer. Proc Natl Acad Sci U S A. 2004;101(3):811-6.
333.   Varambally S, Yu J, Laxman B, Rhodes DR, Mehra R, Tomlins SA, Shah RB, Chandran U, Monzon FA, Becich MJ, Wei JT, Pienta KJ, Ghosh D, Rubin MA, Chinnaiyan AM. Integrative genomic and proteomic analysis of prostate cancer reveals signatures of metastatic progression. Cancer Cell. 2005;8(5):393-406.
334.   Guerra F, Bucci C. Multiple Roles of the Small GTPase Rab7. Cells. 2016;5(3).
335.   Snider MD. A role for rab7 GTPase in growth factor-regulated cell nutrition and apoptosis. Mol Cell. 2003;12(4):796-7.
336.   Croizet-Berger K, Daumerie C, Couvreur M, Courtoy PJ, van den Hove MF. The endocytic catalysts, Rab5a and Rab7, are tandem regulators of thyroid hormone production. Proc Natl Acad Sci U S A. 2002;99(12):8277-82.
337.   Davidson B, Zhang Z, Kleinberg L, Li M, Florenes VA, Wang TL, Shih Ie M. Gene expression signatures differentiate ovarian/peritoneal serous carcinoma from diffuse malignant peritoneal mesothelioma. Clin Cancer Res. 2006;12(20 Pt 1):5944-50.
338.   Zhao T, Ding X, Yan C, Du H. Endothelial Rab7 GTPase mediates tumor growth and metastasis in lysosomal acid lipase-deficient mice. J Biol Chem. 2017;292(47):19198-208.
339.   Flinn RJ, Yan Y, Goswami S, Parker PJ, Backer JM. The late endosome is essential for mTORC1 signaling. Mol Biol Cell. 2010;21(5):833-41.
340.   Margiotta A, Progida C, Bakke O, Bucci C. Rab7a regulates cell migration through Rac1 and vimentin. Biochim Biophys Acta Mol Cell Res. 2017;1864(2):367-81.
341.   Wang T, Zhang M, Ma Z, Guo K, Tergaonkar V, Zeng Q, Hong W. A role of Rab7 in stabilizing EGFR-Her2 and in sustaining Akt survival signal. J Cell Physiol. 2012;227(6):2788-97.
342.   Williams KC, Coppolino MG. Phosphorylation of membrane type 1-matrix metalloproteinase (MT1-MMP) and its vesicle-associated membrane protein 7 (VAMP7)-dependent trafficking facilitate cell invasion and migration. J Biol Chem. 2011;286(50):43405-16.
343.   Okon IS, Coughlan KA, Zhang C, Moriasi C, Ding Y, Song P, Zhang W, Li G, Zou MH. Protein kinase LKB1 promotes RAB7-mediated neuropilin-1 degradation to inhibit angiogenesis. J Clin Invest. 2014;124(10):4590-602.
344.   Laviolette LA, Mermoud J, Calvo IA, Olson N, Boukhali M, Steinlein OK, Roider E, Sattler EC, Huang D, Teh BT, Motamedi M, Haas W, Iliopoulos O. Negative regulation of

EGFR signalling by the human folliculin tumour suppressor protein. Nat Commun. 2017;8:15866.

345.   Ye Y, Gao JX, Tian H, Yearsley K, Lange AR, Robertson FM, Barsky SH. Early to intermediate steps of tumor embolic formation involve specific proteolytic processing of E-cadherin regulated by Rab7. Mol Cancer Res. 2012;10(6):713-26.

346.   Alonso-Curbelo D, Riveiro-Falkenbach E, Perez-Guijarro E, Cifdaloz M, Karras P, Osterloh L, Megias D, Canon E, Calvo TG, Olmeda D, Gomez-Lopez G, Grana O, Sanchez-Arevalo Lobo VJ, Pisano DG, Wang HW, Ortiz-Romero P, Tormo D, Hoek K, Rodriguez-Peralto JL, Joyce JA, Soengas MS. RAB7 controls melanoma progression by exploiting a lineage-specific wiring of the endolysosomal pathway. Cancer Cell. 2014;26(1):61-76.

347.   Steffan JJ, Dykes SS, Coleman DT, Adams LK, Rogers D, Carroll JL, Williams BJ, Cardelli JA. Supporting a role for the GTPase Rab7 in prostate cancer progression. PLoS One. 2014;9(2):e87882.

348.   Budczies J, Pfarr N, Stenzinger A, Treue D, Endris V, Ismaeel F, Bangemann N, Blohmer JU, Dietel M, Loibl S, Klauschen F, Weichert W, Denkert C. Ioncopy: a novel method for calling copy number alterations in amplicon sequencing data including significance assessment. Oncotarget. 2016;7(11):13236-47.

349.   Dressman MA, Baras A, Malinowski R, Alvis LB, Kwon I, Walz TM, Polymeropoulos MH. Gene expression profiling detects gene amplification and differentiates tumor types in breast cancer. Cancer Res. 2003;63(9):2194-9.

350.   Fararjeh AFS, Al Khader A, Kaddumi E, Obeidat M, Al-Fawares O. Differential Expression and Prognostic Significance of STARD3 Gene in Breast Carcinoma. Int J Mol Cell Med. 2021;10(1):34-41.

351.   Kauraniemi P, Barlund M, Monni O, Kallioniemi A. New amplified and highly expressed genes discovered in the ERBB2 amplicon in breast cancer by cDNA microarrays. Cancer Res. 2001;61(22):8235-40.

352.   Moog-Lutz C, Tomasetto C, Regnier CH, Wendling C, Lutz Y, Muller D, Chenard MP, Basset P, Rio MC. MLN64 exhibits homology with the steroidogenic acute regulatory protein (STAR) and is over-expressed in human breast carcinomas. Int J Cancer. 1997;71(2):183-91.

353.   Peiro G, Ortiz-Martinez F, Gallardo A, Perez-Balaguer A, Sanchez-Paya J, Ponce JJ, Tibau A, Lopez-Vilaro L, Escuin D, Adrover E, Barnadas A, Lerma E. Src, a potential target for overcoming trastuzumab resistance in HER2-positive breast carcinoma. Br J Cancer. 2014;111(4):689-95.

354.   Vu T, Claret FX. Trastuzumab: updated mechanisms of action and resistance in breast cancer. Front Oncol. 2012;2:62.

355.   Asif K, Memeo L, Palazzolo S, Frion-Herrera Y, Parisi S, Caligiuri I, Canzonieri V, Granchi C, Tuccinardi T, Rizzolio F. STARD3: A Prospective Target for Cancer Therapy. Cancers (Basel). 2021;13(18).

356.   Maslyanko M, Harris RD, Mu D. Connecting Cholesterol Efflux Factors to Lung Cancer Biology and Therapeutics. Int J Mol Sci. 2021;22(13).

357.   Wilhelm LP, Tomasetto C, Alpy F. Touche! STARD3 and STARD3NL tether the ER to endosomes. Biochem Soc Trans. 2016;44(2):493-8.

358.   Kao J, Pollack JR. RNA interference-based functional dissection of the 17q12 amplicon in breast cancer reveals contribution of coamplified genes. Genes Chromosomes Cancer. 2006;45(8):761-9.

359.   Sahlberg KK, Hongisto V, Edgren H, Makela R, Hellstrom K, Due EU, Moen Vollan HK, Sahlberg N, Wolf M, Borresen-Dale AL, Perala M, Kallioniemi O. The HER2 amplicon includes several genes required for the growth and survival of HER2 positive breast cancer cells. Mol Oncol. 2013;7(3):392-401.
360.   Kwon MJ, Kim RN, Song K, Jeon S, Jeong HM, Kim JS, Han J, Hong S, Oh E, Choi JS, An J, Pollack JR, Choi YL, Park CK, Shin YK. Genes co-amplified with ERBB2 or MET as novel potential cancer-promoting genes in gastric cancer. Oncotarget. 2017;8(54):92209-26.
361.   Qiu Y, Zhang ZY, Du WD, Ye L, Xu S, Zuo XB, Zhou FS, Chen G, Ma XL, Schneider ME, Xia HZ, Zhou Y, Wu JF, Yuan-Hong X, Zhang XJ. Association analysis of ERBB2 amplicon genetic polymorphisms and STARD3 expression with risk of gastric cancer in the Chinese population. Gene. 2014;535(2):225-32.
362.   De Marco C, Zoppoli P, Rinaldo N, Morganella S, Morello M, Zuccala V, Carriero MV, Malanga D, Chirillo R, Bruni P, Malzoni C, Di Vizio D, Venturella R, Zullo F, Rizzuto A, Ceccarelli M, Ciliberto G, Viglietto G. Genome-wide analysis of copy number alterations led to the characterisation of PDCD10 as oncogene in ovarian cancer. Transl Oncol. 2021;14(3):101013.
363.   Stigliano A, Gandini O, Cerquetti L, Gazzaniga P, Misiti S, Monti S, Gradilone A, Falasca P, Poggi M, Brunetti E, Agliano AM, Toscano V. Increased metastatic lymph node 64 and CYP17 expression are associated with high stage prostate cancer. J Endocrinol. 2007;194(1):55-61.
364.   Vinatzer U, Dampier B, Streubel B, Pacher M, Seewald MJ, Stratowa C, Kaserer K, Schreiber M. Expression of HER2 and the coamplified genes GRB7 and MLN64 in human breast cancer: quantitative real-time reverse transcription-PCR as a diagnostic alternative to immunohistochemistry and fluorescence in situ hybridization. Clin Cancer Res. 2005;11(23):8348-57.
365.   Smith B, Land H. Anticancer activity of the cholesterol exporter ABCA1 gene. Cell Rep. 2012;2(3):580-90.
366.   Yun SM, Yoon K, Lee S, Kim E, Kong SH, Choe J, Kang JM, Han TS, Kim P, Choi Y, Jho S, Yoo H, Bhak J, Yang HK, Kim SJ. PPP1R1B-STARD3 chimeric fusion transcript in human gastric cancer promotes tumorigenesis through activation of PI3K/AKT signaling. Oncogene. 2014;33(46):5341-7.
367.   Liu D, Zhou D, Sun Y, Zhu J, Ghoneim D, Wu C, Yao Q, Gamazon ER, Cox NJ, Wu L. A Transcriptome-Wide Association Study Identifies Candidate Susceptibility Genes for Pancreatic Cancer Risk. Cancer Res. 2020;80(20):4346-54.
368.   Torres S, Matías N, Baulies A, Nuñez S, Alarcon-Vila C, Martinez L, Nuño N, Fernandez A, Caballeria J, Levade T, Gonzalez-Franquesa A, Garcia-Rovés P, Balboa E, Zanlungo S, Fabrías G, Casas J, Enrich C, Garcia-Ruiz C, Fernández-Checa JC. Mitochondrial GSH replenishment as a potential therapeutic approach for Niemann Pick type C disease. Redox Biol. 2017;11:60-72.
369.   Frasa MA, Koessmeier KT, Ahmadian MR, Braga VM. Illuminating the functional and structural repertoire of human TBC/RABGAPs. Nat Rev Mol Cell Biol. 2012;13(2):67-73.
370.   Frasa MA, Maximiano FC, Smolarczyk K, Francis RE, Betson ME, Lozano E, Goldenring J, Seabra MC, Rak A, Ahmadian MR, Braga VM. Armus is a Rac1 effector that inactivates Rab7 and regulates E-cadherin degradation. Curr Biol. 2010;20(3):198-208.

371.   Serva A, Knapp B, Tsai YT, Claas C, Lisauskas T, Matula P, Harder N, Kaderali L, Rohr K, Erfle H, Eils R, Braga V, Starkuviene V. miR-17-5p regulates endocytic trafficking through targeting TBC1D2/Armus. PLoS One. 2012;7(12):e52555.

372.   Yu H, Mitra R, Yang J, Li Y, Zhao Z. Algorithms for network-based identification of differential regulators from transcriptome data: a systematic evaluation. Sci China Life Sci. 2014;57(11):1090-102.

373.   Delgado-Martin B, Medina MA. Advances in the Knowledge of the Molecular Biology of Glioblastoma and Its Impact in Patient Diagnosis, Stratification, and Treatment. Adv Sci (Weinh). 2020;7(9):1902971.

374.   Chandramohan K, Balan DJ, Devi KP, Nabavi SF, Reshadat S, Khayatkashani M, Mahmoodifar S, Filosa R, Amirkhalili N, Pishvaei S, Sargazi-Aval O, Nabavi SM. Short interfering RNA in colorectal cancer: is it wise to shoot the messenger? Eur J Pharmacol. 2023;949:175699.

375.   Vykoukal J, Fahrmann JF, Gregg JR, Tang Z, Basourakos S, Irajizad E, Park S, Yang G, Creighton CJ, Fleury A, Mayo J, Paulucci-Holthauzen A, Dennison JB, Murage E, Peterson CB, Davis JW, Kim J, Hanash S, Thompson TC. Caveolin-1-mediated sphingolipid oncometabolism underlies a metabolic vulnerability of prostate cancer. Nat Commun. 2020;11(1):4279.

376.   Liang JQ, Teoh N, Xu L, Pok S, Li X, Chu ESH, Chiu J, Dong L, Arfianti E, Haigh WG, Yeh MM, Ioannou GN, Sung JJY, Farrell G, Yu J. Dietary cholesterol promotes steatohepatitis related hepatocellular carcinoma through dysregulated metabolism and calcium signaling. Nat Commun. 2018;9(1):4490.

377.   Mondul AM, Clipp SL, Helzlsouer KJ, Platz EA. Association between plasma total cholesterol concentration and incident prostate cancer in the CLUE II cohort. Cancer Causes Control. 2010;21(1):61-8.

378.   Shafique K, McLoone P, Qureshi K, Leung H, Hart C, Morrison DS. Cholesterol and the risk of grade-specific prostate cancer incidence: evidence from two large prospective cohort studies with up to 37 years' follow up. BMC Cancer. 2012;12:25.

379.   Magura L, Blanchard R, Hope B, Beal JR, Schwartz GG, Sahmoun AE. Hypercholesterolemia and prostate cancer: a hospital-based case-control study. Cancer Causes Control. 2008;19(10):1259-66.

380.   O'Neill KI, Kuo LW, Williams MM, Lind H, Crump LS, Hammond NG, Spoelstra NS, Caino MC, Richer JK. NPC1 Confers Metabolic Flexibility in Triple Negative Breast Cancer. Cancers (Basel). 2022;14(14).

381.   Kim S, Kim DH, Jung WH, Koo JS. Metabolic phenotypes in triple-negative breast cancer. Tumour Biol. 2013;34(3):1699-712.

382.   Li S, Zeng H, Fan J, Wang F, Xu C, Li Y, Tu J, Nephew KP, Long X. Glutamine metabolism in breast cancer and possible therapeutic targets. Biochem Pharmacol. 2023;210:115464.

383.   Platz EA, Till C, Goodman PJ, Parnes HL, Figg WD, Albanes D, Neuhouser ML, Klein EA, Thompson IM, Jr., Kristal AR. Men with low serum cholesterol have a lower risk of high-grade prostate cancer in the placebo arm of the prostate cancer prevention trial. Cancer Epidemiol Biomarkers Prev. 2009;18(11):2807-13.

384.   Hanahan D, Weinberg RA. Hallmarks of cancer: the next generation. Cell. 2011;144(5):646-74.

385.   Hirschey MD, DeBerardinis RJ, Diehl AME, Drew JE, Frezza C, Green MF, Jones LW, Ko YH, Le A, Lea MA, Locasale JW, Longo VD, Lyssiotis CA, McDonnell E, Mehrmohamadi

M, Michelotti G, Muralidhar V, Murphy MP, Pedersen PL, Poore B, Raffaghello L, Rathmell JC, Sivanand S, Vander Heiden MG, Wellen KE, Target Validation T. Dysregulated metabolism contributes to oncogenesis. Semin Cancer Biol. 2015;35 Suppl:S129-S50.

386.   Yan A, Jia Z, Qiao C, Wang M, Ding X. Cholesterol metabolism in drugresistant cancer (Review). Int J Oncol. 2020;57(5):1103-15.

387.   Harayama T, Riezman H. Understanding the diversity of membrane lipid composition. Nat Rev Mol Cell Biol. 2018;19(5):281-96.

388.   Wong YC, Peng W, Krainc D. Lysosomal Regulation of Inter-mitochondrial Contact Fate and Motility in Charcot-Marie-Tooth Type 2. Dev Cell. 2019;50(3):339-54.e4.

389.   Kim S, Wong YC, Gao F, Krainc D. Dysregulation of mitochondria-lysosome contacts by GBA1 dysfunction in dopaminergic neuronal models of Parkinson's disease. Nat Commun. 2021;12(1):1807.

390.   Bucci C, De Luca M. Molecular basis of Charcot-Marie-Tooth type 2B disease. Biochem Soc Trans. 2012;40(6):1368-72.

391.   Wong YC, Ysselstein D, Krainc D. Mitochondria-lysosome contacts regulate mitochondrial fission via RAB7 GTP hydrolysis. Nature. 2018;554(7692):382-6.

392.   Chlystun M, Campanella M, Law AL, Duchen MR, Fatimathas L, Levine TP, Gerke V, Moss SE. Regulation of mitochondrial morphogenesis by annexin A6. PLoS One. 2013;8(1):e53774.

393.   Feo F, Canuto RA, Bertone G, Garcea R, Pani P. Cholesterol and phospholipid composition of mitochondria and microsomes isolated from morris hepatoma 5123 and rat liver. FEBS Lett. 1973;33(2):229-32.

394.   Montero J, Morales A, Llacuna L, Lluis JM, Terrones O, Basañez G, Antonsson B, Prieto J, García-Ruiz C, Colell A, Fernández-Checa JC. Mitochondrial cholesterol contributes to chemotherapy resistance in hepatocellular carcinoma. Cancer Res. 2008;68(13):5246-56.

395.   Armandari I, Hamid AR, Verhaegh G, Schalken J. Intratumoral steroidogenesis in castration-resistant prostate cancer: a target for therapy. Prostate Int. 2014;2(3):105-13.

396.   Enrich C, Lu A, Tebar F, Rentero C, Grewal T. Annexins Bridging the Gap: Novel Roles in Membrane Contact Site Formation. Front Cell Dev Biol. 2021;9:797949.